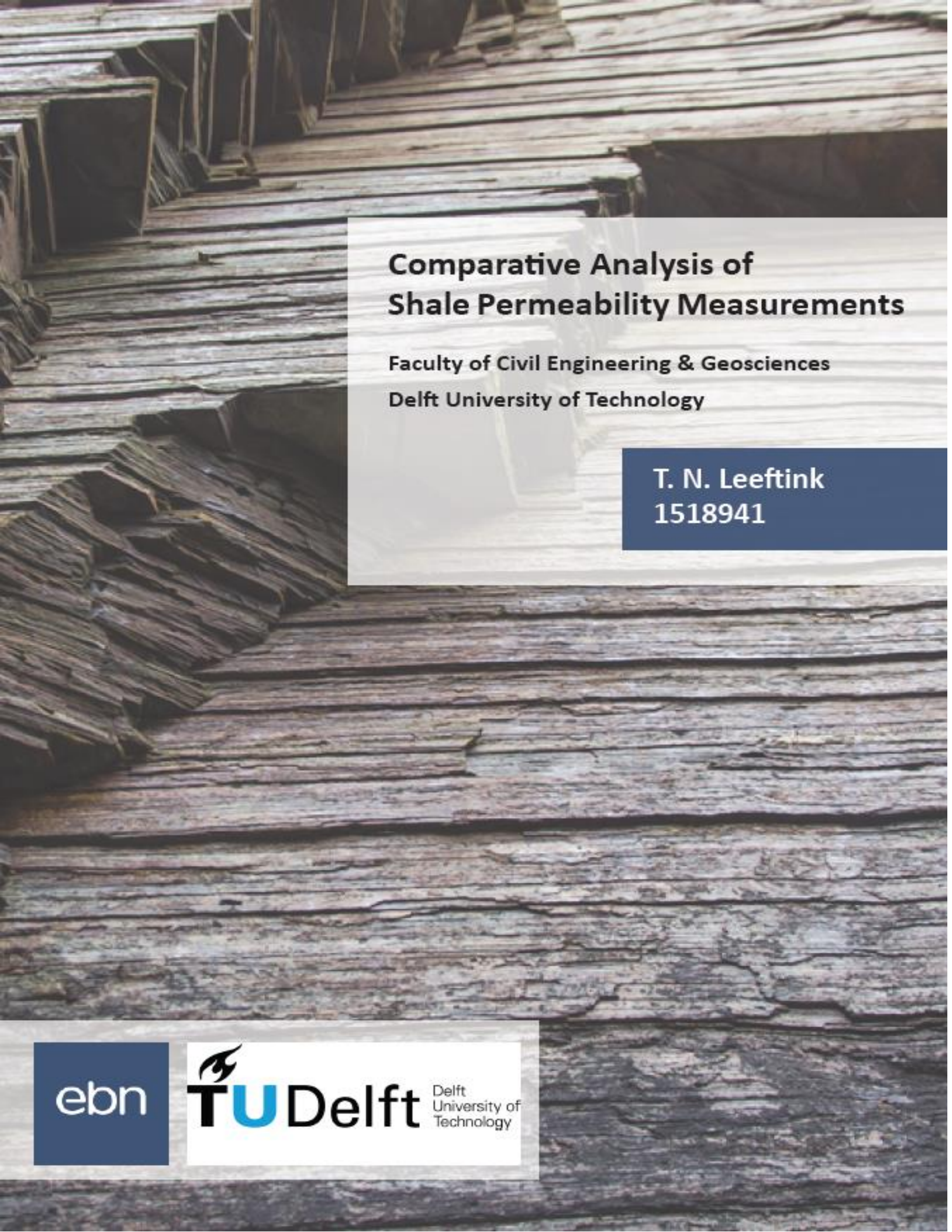

Comparative Analysis of Shale Permeability Measurements

Faculty of Civil Engineering & Geosciences

Delft University of Technology

T. N. Leeftink

1518941

ebn

TU Delft Delft University of Technology

Title	:	Comparative Analysis of Shale Permeability Measurements
Author(s)	:	T.N. Leeftink
Date	:	June 2015
Professor(s)	:	Prof. Dr. S.M. Luthi
Supervisor(s)	:	Prof. Dr. S.M. Luthi Prof. Dr. Q.J. Fisher M. Harings J. Lutgert
Graduation Committee	:	Prof. Dr. S.M. Luthi Prof. Dr. Q.J. Fisher Prof. Dr. G. Bertotti J. Lutgert

Postal Address	:	Section for Applied Geology
		Department of Geoscience & Engineering
		Delft University of Technology
		P.O. Box 5028
		The Netherlands
Telephone	:	(31) 15 2781328 (secretary)
Telefax	:	(31) 15 2781189

Abstract

Gas has proved to be a successful extractable hydrocarbon resource from shale in the United States. In Europe results have so far been disappointing, but with increasing global energy demand a lot of interest remains in the potential of recoverable shale gas reservoirs. However, the way how the economic potential of shale is mapped is insufficient, because there are no industrywide measurement techniques available for measuring the flow properties of these (ultra)low permeable rocks. A proper assessment of the petrophysical properties of the cores from potential areas is therefore very difficult and the results are highly variable.

This study assesses the problems found after evaluating a round robin of experiments on selected samples. The multi-lab experiment was performed on crushed shale to compare the results between different laboratories. The permeability results from the various renowned laboratories were found to differ by multiple orders of magnitude on permeability results. For this study, a selection of core plugs and crushed material from various shale formations was analyzed using a wide spectrum of experiments and history match simulation models. The experiments were performed on the analyzed shales and consist of xenon expansion under a CT scan, as well as helium and methane expansion on linear, radial and crushed core plugs in confined and unconfined sealed core holders for different gas pressures. The measured data was history matched with multiple models including a single and multiple porosity-permeability model, with and without a high-permeability streak (e.g. fracture or silt layer) and the Klinkenberg effect. The combination of all these experiments and simulations resulted in a large dataset. After significant quality control, conclusions could be drawn from this data set, resulting in clearer insights into how porosity and permeability from shale samples can better be computed compared to the current technique that uses simulation results from a crushed GRI experiment.

Xenon flow in shales under a CT scan provided some insights into the permeabilities of the studied sample, but the accuracy is low. Propagation of the expanded gas over time could be monitored when the measured data was extracted from these images. If more information about the flow behavior of the expanded gas could be derived from the CT images of xenon invasion, this would improve the understanding and makes the simulation model more realistic.

The round robin test results for porosity were found to be similar between the laboratories. These experiments were conducted with the noble gas helium. Even though methane has a larger molecule size than helium, the computed porosity from methane expansion is larger due to adsorption on organic matter. Langmuir curve experiment results showed adsorption curves whose maxima positively with the TOC (total organic carbon) of the samples.

A more reliable approach than the round robin test results for permeability is proposed by combining the results of the experiments, such as perform a full core experiment on a radial sample drilled parallel to its lamination in an unconfined set-up, then measure a radial linear sample drilled perpendicular to its lamination in a confined set-up and finally perform a combination of these techniques. The first two of these experiments can be inverted with a single porosity-permeability model and the last one with a multiple porosity-permeability model. The first two results can thus verify the high and low case of the multiple porosity-permeability model, resulting in a more reliable result than obtaining permeability from crushed shale history matches.

Contents

Abstract IV

Table of Figures VII

Table of Tables X

1. Introduction 1

1.1. Research Objectives 1

1.2. Research Outline 1

2. Samples 2

3. Laboratory Methodology and Data Acquisition 5

3.1. Laboratory Methodology 5

3.1.1. Core Material 5

3.1.2. Modified Pulse Decay 7

3.1.3. Gas Research Institute Test (GRI) 9

3.1.3.1. Helium and nitrogen expansion 10

3.1.3.2. Methane expansion 11

3.1.3.3. Xenon expansion under CT scan 13

3.2. Data acquisition 14

3.2.1. Novel inversion of experimental results 16

3.2.1.1. Multiple porosity model 16

3.2.1.2. Methane expansion 18

3.2.1.3. Using porosity as an input parameter 18

4. Results and discussion 19

4.1. Comparison of experimental results with round robin results 19

4.1.1. Round robin results 19

4.1.2. Variations on Leeds' results in round robin test 21

4.1.2.1. Results verification 22

4.1.2.2. Matrix porosity variations 23

4.1.2.1.1. Set-up variation 25

4.1.2.1.2. Lamination effect 26

4.1.2.1.3. Effect of radial drilled core plug 27

4.1.2.1.4. Effect of high permeability streak 28
4.1.2.1.5. Effect of Klinkenberg factor 29
4.1.2.3. Matrix permeability variations 30
4.1.2.3.1. Set-up variation 30
4.1.2.3.2. Lamination effect 31
4.1.2.3.3. Effect of radial drilled core plug 32
4.1.2.3.4. Effect of high permeability streak 33
4.1.2.3.5. Effect of Klinkenberg factor 34
4.2. Xenon expansion 35
4.3. Sorption effects: Methane expansion 38
4.3.1. Crushed results 38
4.3.2. Core plug results 43
5. Evaluation 46
5.1. Crushed shale tests only consistently measure porosity, not permeability 46
5.2. Combination of experiments yield best results 47
5.3. Outcomes of using helium versus methane as expansion gas 50
5.4. The effect of the Klinkenberg factor on matrix permeability 51
6. Conclusions 54
7. Recommendations 56
8. References 59
APPENDIX A: Sample Dimensions and Weight 62
APPENDIX B: Calibration 63
APPENDIX C: History Match Script 65
APPENDIX D: Measured pressure decay curves 78
APPENDIX E: All history matched results 87
APPENDIX F: Images of expanded xenon under a CT scan and results 100
APPENDIX G: Langmuir Sorption Curves 106

Table of Figures

Figure 2.1: Ternary plot containing the mineral composition of the studied samples. 3
Figure 2.2a and b: Ternary plots containing the mineral composition of several shale samples from the Dutch subsurface with the brittle region indicated by a green line in 2.3a. Source: Left: Mezger (2014) based on Rickman, et al. (2008) and right: Bouw & Lutgert (2012). 3
Figure 3.1: Schematic drawing of radial core plug. 6
Figure 3.2a (left): A schematic drawing of the modified pulse decay set-up with the four pressure transducers. 3.3b (right) A photograph of the set-up. 7
Figure 3.4: Further pressure decay after upstream and downstream volumes meet in MPD experiment. Source: SHAPE. 8
Figure 3.5: Multiple successive MPD experiments on sample EBN20 parallel. 9
Figure 3.6a and b: Schematic overview (left) and photograph (right) of the GRI set-up with hydraulic ram. Source: Noordoven (2011). 10
Figure 3.7: Difference in molecule size may prevent flow through small pore throats. Source: Cluff, et al. (2007). 11
Figure 3.8: Difference in molecule size may cause small pore throats to block certain gases. Source: Cluff, et al. (2007). 12
Figure 3.9: The set-up of the xenon expansion experiment under the CT scan (left) and a CT scan, which is a cross section of one of the cores (right). 14
Figure 3.10: Refinement runs on the observed data (red dots with errors bars) (left) result in a best fit history match through the observed data (right). Source: SHAPE, Fisher & Rybalcenko (2014). 15
Figure 3.11: The characterization of a sample for various tests. From left to right: modified pulse decay, crushed GRI, radial full core GRI and a high permeability streak. Source: SHAPE, Fisher & Rybalcenko (2014). 15
Figure 3.12: Different porosity regions in a shale. Source: East (2011). 17
Figure 4.1: As-received Bulk Density results from round robin test. 19
Figure 4.2: Dry grain density results from round robin test. 20
Figure 4.3: Dry matrix porosity results from round robin test. 20
Figure 4.4: Dry matrix permeability results from round robin test. 21
Figure 4.5: A pie chart which shows how the generated data is distributed amongst the different samples. 22
Figure 4.6a and b: The results of a MPD test which is not equilibrated (left) and the results of a MPD test that seem to be equilibrated (right). 23
Figure 4.7a and b: The results of a full core GRI test where temperature effects seem to have taken overhand(left) and the results of a MPD test that seems to be equilibrated (right). 23
Figure 4.8: The overview of the inverted averaged porosity for the different pressure steps for all the different experimental set-ups. 24
Figure 4.9: The dependency of the matrix porosity of the sample OPA2 on a confined or unstressed set-up. 25
Figure 4.10: The effect of the drilled orientation of the plug compared to the lamination on the matrix porosity of the samples EBN20 and OPA2. 26
Figure 4.11: The dependency of the matrix porosity of the sample EBN20 on linear and radial flow, drilled either perpendicular or parallel to the lamination. 27

Figure 4.12: The dependency of the matrix porosity of the Whitehill sample on a high permeability streak. 28
Figure 4.13: The dependency of the matrix porosity of sample EBN20 on the Klinkenberg slippage correction factor. 29
Figure 4.14: The effect of the difference of a confined or a unconfined set-up on the matrix permeability of the sample EBN20........ 30
Figure 4.15: The effect of the drilled orientation of the plug compared to the lamination on the matrix permeability of the sample EBN20. 31
Figure 4.16: The effect of radial flow on the matrix permeability of the sample EBN20. 32
Figure 4.17: The effect of a high permeability streak on the matrix permeability on the sample EBN20. 33
Figure 4.18: The effect of using a Klinkenberg slippage correction factor on matrix permeability for the sample EBN20. 34
Figure 4.19: EBN20 linear core after Xenon flooding 35
Figure 4.20: The OPA2 sample before and after the xenon expansion. The cross section is taken halfway the core plug. 35
Figure 4.21: The Whitehill sample after xenon flooding. 36
Figure 4.22: Two slices from the EBN5 sample, which has a axial hole halfway through the sample. This results in a combination of linear flow and radial flow. 36
Figure 4.23: The radial sample EBN20 processed by subtracting the results after the xenon flooding with the starting scan........ 37
Figure 4.24a (left): Plot of the CT measurements of EBN20 radial, with the results before and after flooding with xenon. 4.25b (right): Plot of the difference after and before the flooding. Both are displayed over the length of the core with the expanded xenon entering on the left hand side of both figures. 37
Figure 4.26: Langmuir curves for methane calibrated with helium of the tested round robin samples. .. 38
Figure 4.27a and b: the Langmuir adsorption and desorption curves for the samples EBN20 and OPB3, both calibrated with helium........ 39
Figure 4.28a and b: Langmuir curve desorption curves for sample OPB2 calibrated with helium (left) and krypton (right). 40
Figure 4.29: The porosity difference between helium and methane in the crushed GRI measurements for the EBN20 sample, calculated using Boyle's law. 41
Figure 4.30: The porosity difference between helium and methane in the crushed GRI measurements for the OPA2 sample, calculated using Boyle's law. 42
Figure 4.31: Pressure decay curve of expanded methane on crushed shale GRI experiment of EBN20 that has not yet reached equilibrium. 42
Figure 4.32: The matrix porosity differences between the full core and crushed experiments for the samples OPA2 and EBN20. 43
Figure 4.33: In full core GRI measurements, the matrix porosity is higher when samples are flooded with methane than with helium. 44
Figure 4.34: In full core GRI measurements, matrix permeability is higher when samples are flooded with methane than with helium. The results depicted are the samples EBN20 and OPA2 with fixed matrix porosities from the crushed GRI tests. 45
Figure 5.1: Matrix permeability measurements of dried crushed shale test on OPA2 with a double and triple porosity-permeability model. Khi, kmid and klo stand for the three regions in the multiple

porosity-permeability model. With a double porosity-permeability model, there is no data for kmid as this second region is combined with the third region. See 3.2.1.1 for more information on what these regions characterize. 46
Figure 5.2: The simulated results with a multiple porosity-permeability model overlap the experimental results for a MPD test on a radial perpendicular drilled core of EBN20 47
Figure 5.3: The multiple porosity-permeability model explained by different experiments on the EBN20 sample. 48
Figure 5.4: A schematic overview of the multiple porosity-permeability model explained by a schematic overview of the different experiments. 48
Figure 5.5a (left): The matrix permeability inversions from the different experiments with a fixed porosity of the EBN20 sample and 5.6b (right): a schematic overview of the order of results in permeability of those experiments 49
Figure 5.7: Relation TOC and adsorption of the tested round robin samples. 50
Figure 5.8: The dependency between b factor and pressure for the samples EBN20 and OPA2. The matrix permeability is increasing with the size of the points. 51
Figure 5.9: A comparison between a set of tight sands modelled with the Klinkenberg gas slippage factor and the experiments conducted in the Wolfson Lab for the purpose of this study. 52
Figure 5.10: A relation between matrix permeability, Klinkenberg correction factor and pressure seems to be the same for multiple samples. 53

Table of Tables

Table 2.1: Overview of the studied samples. 4
Table 3.1: Overview of preparation of the samples. 6
Table 3.2: The molecular sizes of expanded gases. Source: Wolfram Research and Carl W. Kammeyer (1972). 11
Table 3.3: Overview of the selected simulations applied to all the samples. 16
Table 4.1: As-received Bulk Density results from round robin test. 19
Table 4.2: Dry grain density results from round robin test. 20
Table 4.3: Dry matrix porosity results from round robin test. 20
Table 4.4: Dry matrix permeability results from round robin test. 21
Table 4.5: Summary of the experimental results of the Langmuir curve experiment and calculated parameters. 39
Table 4.6: The GRI results for the different gases for the sample EBN20. Source: Rybalcenko & Leeftink (2015 in press.) 40
Table 4.7: The GRI results for the different gases for the sample OPA2. Source: Rybalcenko & Leeftink (2015 in press.) 40
Table 5.1: Relation between TOC and adsorption of the tested round robin samples. 50

1. Introduction

The shale gas boom in the USA brought this highly heterogeneous low-permeability "reservoir rock" to the attention in Europe. A key problem with this greatly varying rock type is identifying its petrophysical properties. A round robin of experiments involving respected service companies gave permeability results that differ by a couple orders of magnitude. That means there is such a great variation in properties from different resource plays between the different service companies that it is not possible to compare results. It also means that modelling is not possible, because properties are not sufficiently well known. Hence this study aims at a better understanding of the petrophysical properties of a series of European shale samples with various experiments. It should contribute to find more successful experimental measuring and history matching methods for determining the porosity and permeability of these formations. This is considered important, because there still is no industry standard to assess the productivity from shales.

This research is part of the SHAPE (SHAle PErmeability) joint industry project and a follow up of earlier theses of Kee (2010), Noordoven (2011) and Mezger (2014). Similar to these studies this thesis is performed under supervision of EBN, the Delft University of Technology and the University of Leeds where the experiments were conducted.

1.1. Research Objectives

The main objective of this study is to enhance the porosity and permeability measurements on shales. This broad research question is tackled in multiple work packages.

These multiple work packages consist a range of experimental techniques, including expanding different gases into core holders filled with core plugs, such as methane and xenon, and use hardware not used before in this field of study, such as a CT scanner. This will significantly contribute to the SHAPE database in new areas such as sorption effects.

Next to the laboratory work, inverting the data using various models may lead to new insights. A goal of these novel inversions of the experimental results is to explain the large differences of the simulated results from major service companies who participated in a round robin experiment. This comparison is broadened by comparing a range of experimental techniques using visualization software.

1.2. Research Outline

This general introduction will be succeeded by chapters that describe, assess and evaluate the problems with the current techniques and new insights will be presented. The second chapter contains information about the used core material. This is followed by an explanation of the experimental set-ups and how the observed data is processed to obtain the petrophysical results in chapter 3. Chapter 4 contains the results of the inverted experimental data and analyses the differences with a base case scenario. The fifth chapter is an evaluation of the key conclusions that can be derived from this large dataset. This is succeeded by the conclusions and recommendations in chapters 6 and 7.

2. Samples

Production of hydrocarbons from shales has a long history, but it was not until the last decade that gas production from shale resource plays contributed significantly to the overall energy resource of any country. Through the development of recent technologies, such as multiple fractures in horizontal wells, these plays have become an interesting field of study for hydrocarbon extraction (Chaudhary, et al., 2011). When shales contain a significant amount of organic matter, their color will usually become dark, giving them their name: black shales. Under the right circumstances natural gas can be extracted from these shales. Natural gas is stored in black shales: by adsorption to the organic matter or as free gas in larger pore spaces and in (micro) fractures (Cluff, et al., 2007).

For the experiments conducted, various plugs from different formations were tested. Their different mineral compositions are plotted below (Figure 2.1). This section provides a brief summary of their origin and properties.

As this project was sponsored by EBN, four of the nine samples that were used and described in this thesis are from the Dutch subsurface. Previous theses (Mezger, 2014; Kee, 2010) described the background of these samples in greater detail, but below a quick overview is given.

As described in literature (Noordoven, 2011), the Netherlands has two potential onshore shale plays: the Lower Jurassic Altena Group which contains the Posidonia and Aalburg shale formations and the older Lower Namurian Geverik formation (Bouw & Lutgert, 2012). The selection of the four EBN samples consists of two from the Geverik formation (EBN5 and EBN9), one from the Posidonia formation (EBN20) and a core plug from the Aalburg formation (EBN33).

Four of the samples tested for the purpose of this experiment were part of a round robin test series conducted in three renowned laboratories as a part of the SHAPE Joint Industry Project.

These samples came from different operators and contained one EBN sample: EBN20. The other round robin samples consist of five European shale samples from two operators. Due to confidentiality, the origin and specifics of these samples have been anonymized. They will be referred to under code names from Operator A and B (OPA1 ,OPA2, OPB1 and OPB2). All samples originated from the US and Europe.

Unfortunately, two of the samples of the round robin test (OPB2&OPB3) failed pressure tests at early stages and could not be tested anymore. They are therefore not part of the new experiments conducted for this thesis. However, some results of them may be used for comparisons. The octet of samples is completed by plugs from the Permian Whitehill formation in the Karoo, South Africa.

This sample is from a quarry and therefore it has not been exposed to substantial weathering. The Whitehill formation has been deposited under anoxic conditions and, although often only about 10-20 meters thick, is considered the potentially most prolific shale gas play in South Africa

These shales contain abundant quartz (Figure 2.1) which makes them brittle. Brittleness is very beneficial for shales as it becomes easier to fracture them and thus extract their resources (Rickman, et al., 2008). The Whitehill has a high TOC and adsorbed methane level (Chere, et al., 2013).

A detailed description of all the samples can be found on the website for the sponsors of the SHAPE project. Only the Whitehill sample is not included in this database. This database also contains all the tests performed on the core plugs and the results from inverting the data. For every sample a series of data and microscopic images (SEM images) is also available. In Table 2.1 a brief summary of the most important data for the purpose of this thesis is listed.

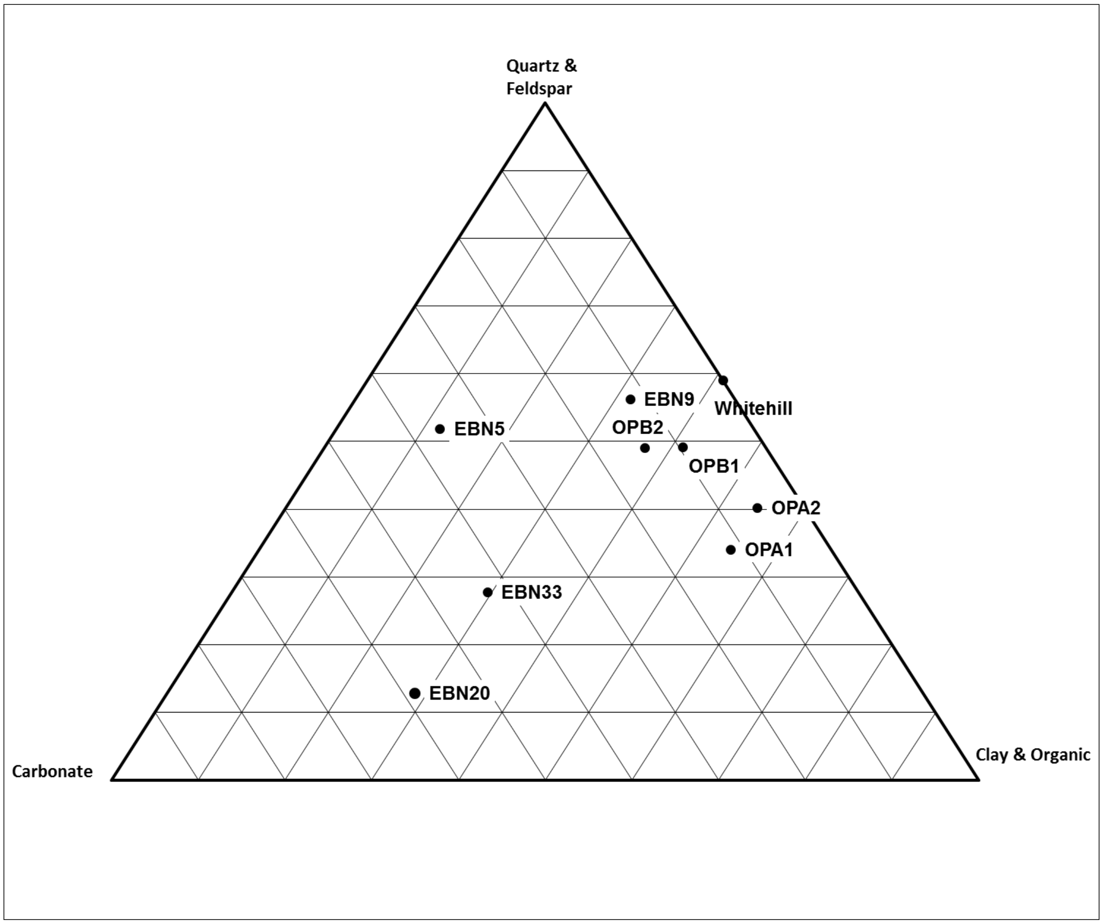

Figure 2.1: Ternary plot containing the mineral composition of the studied samples.

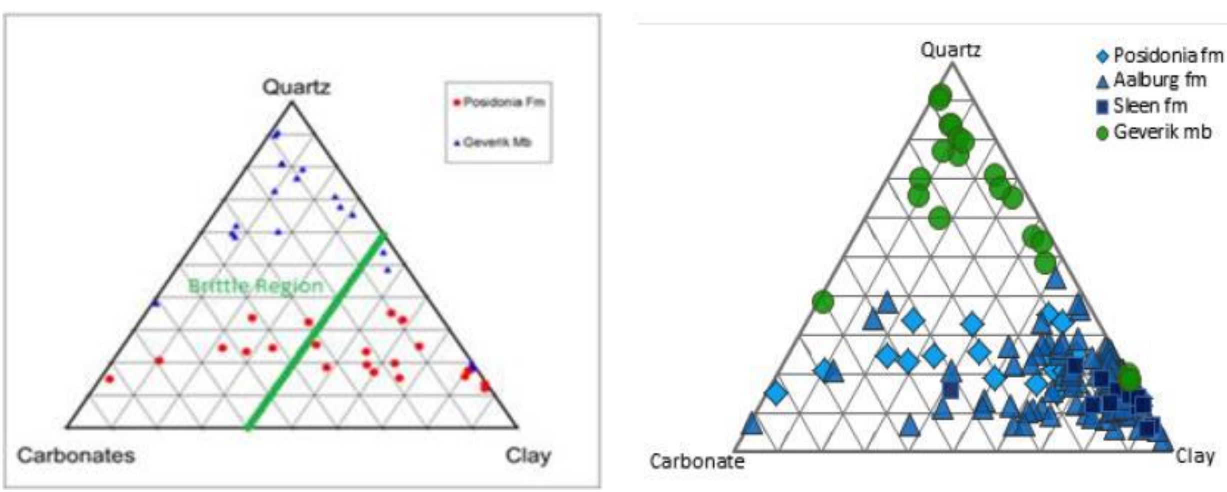

Figure 2.2a and b: Ternary plots containing the mineral composition of several shale samples from the Dutch subsurface with the brittle region indicated by a green line in 2.3a.
Source: Left: Mezger (2014) based on Rickman, et al. (2008) and right: Bouw & Lutgert (2012).

As can be seen from the ternary diagrams (Figure 2.1 and Figure 2.2), the tested samples fit well with the shales from the Dutch subsurface (Bouw & Lutgert, 2012). A focus on the Posidonia (EBN20) and Geverik Formations (EBN5 & EBN9) is chosen here because these fall – at least partly – into the brittle region, making them more likely to be producible with the help of hydraulic stimulation (Rickman, et al., 2008).

Table 2.1: Overview of the studied samples.

	TOC	Well	Location	Formation	Era
EBN5	1.71	GVK-01 at 945m	Netherlands	Geverik	Carboniferous
EBN9	4.33	GVK-01 at 984m	Netherlands	Geverik	Carboniferous
EBN20	5.67	HLM-1 at 1051.5m	Netherlands	Posidonia	Jurassic
EBN33	9.23	ZWE-01 at 1236m	Netherlands	Aalburg	Jurassic
OPA1	2.54	N/A	USA	N/A	Carboniferous
OPA2	4.43	N/A	USA	N/A	Carboniferous
OPB1	3.27	Outcrop	Europe	N/A	Carboniferous
OPB2	3.21	Outcrop	Europe	N/A	Carboniferous
Whitehill	5.56	Outcrop	Karoo, South Africa	Whitehill	Permian

3. Laboratory Methodology and Data Acquisition

Improving the determination of the petrophysical properties of shales will be done by inverting the data measured in the laboratory. In the following section the experimental set-up and the numerical inversion of the data will be described.

3.1. Laboratory Methodology

In this section the core material, the experimental set-up and the procedure will be discussed. Added to that the properties of the different expanded gases will be explained.

All experiments, apart from the CT scan measurements, were performed in a temperature controlled room of 23°C in the Wolfson Laboratory at the University of Leeds, Faculty of Earth and Environment.

This thesis focuses on comparing various experimental measuring techniques. Therefore the experiments were executed in Leeds where new results could be obtained and compared to existing results with greater accuracy because they are performed on the same location using the same set-up on the same samples.

3.1.1. Core Material

At the basis of this study lies the core material that was used in the round robin experiments between three renowned service companies and the University of Leeds. The core material was prepared in various ways. For the full range of experiments full core plugs, perforated plugs and core chips were needed.

Eight different plugs have been examined. These plugs were all about 3.75 cm in diameter while their lengths varied between from just over 2 cm to over 7 cm. Full details of the core plugs can be found in Table 3.1. For every sample, plugged out of a larger piece of the formation, two plugs were made if there was enough material: one plug parallel and another one perpendicular to the lamination of the rock.

When all experiments for the scope of this research were performed on these plugs, a hole of about 3.5 mm was drilled along the central axis of the sample. This is schematically illustrated in Figure 3.1. Subsequently, all experiments were performed again on these perforated samples. From here on, plugs without a hole will be referred to as linear plugs and perforated plugs will be mentioned to as radial plugs. In Table 3.1 an overview can be seen.

Table 3.1: Overview of preparation of the samples.

	Linear Parallel	Linear Perpendicular	Radial Parallel	Radial Perpendicular
	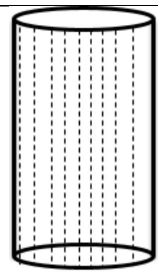	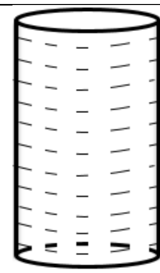	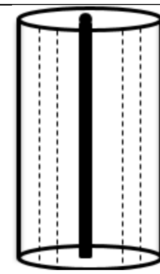	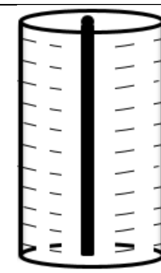
EBN5	No	No	Yes	No
EBN9	Yes	No	No	No
EBN20	Yes	Yes	Yes	Yes
EBN33	Yes	No	Yes	No
OPA1	No	Yes	No	Yes
OPA2	Yes	Yes	Yes	No
OPB1	No	Yes	No	No
OPB2	No	Yes	No	No
Whitehill	No	Yes	No	No

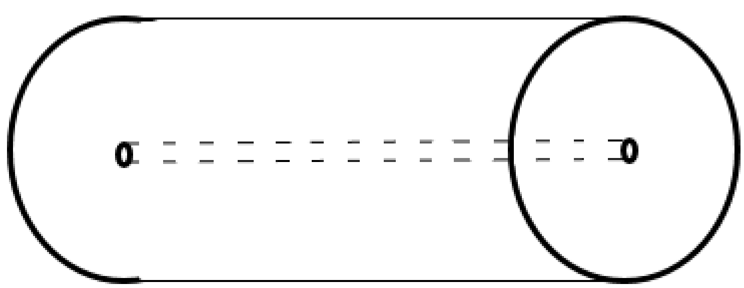

Figure 3.1: Schematic drawing of radial core plug.

From the remains of the material where the plugs were taken, about 200 grams were crushed into chips with particle diameters in the range of 500 < µm < 850. By crushing and sieving the material to the desired size, about half of the weight was lost because the particles were too small, resulting in under 100 grams of prepared chip material. This amount of material is needed according to literature (Luffel, et al., 1993). As these small chip sizes are prone to absorb humidity, the measurements were performed dried and "as-received" (Civan, et al., 2011). The results from the dried samples are most significant and comparable. The reason is that trapped water in the pore space does not influence the petrophysical properties in an unexpected way as with the "as-received" sample (Bustin, et al., 2008).

Preparing the cores is crucial, because the properties of these plugs will be altered when they are cored and brought to surface. Porosity probably increases during core retrieval as a result of the formation of microfractures created due to gas expansion and stress relief when the sample is brought to the surface (Handwerger, et al., 2011). The pore pressure decreases as the gas expands at ambient conditions driving the fluid from the core (East, 2011). Additionally, the coring itself may cause serious core damage. There are some techniques that may prevent such damage, such as freezing the core when it is brought to the surface, or to protect the sample with resin of foam, but these methods are costly and not widely used in the industry.

3.1.2. Modified Pulse Decay

The modified pulse decay set-up is a modification of the pressure transient measurement technique for low permeability plug samples described by Bourbie and Walls (1982) and Brace (1968). Below the major differences between this technique and ours are described.

In this study this set- up was used for experiments on the radial and linear full core plugs, because it has more validity than routine core analysis for measuring low permeability rocks than routine core analysis (Mallon & Swarbrick, 2007). The set-up consists of a core holder with four transducers (Figure 3.2). Two are located on the upstream side, with the first one being used to regulate the upstream pressure ($P_{upstream1}$) and the other to measure the upstream pressure of the sample ($P_{upstream2}$). There is one transducer on the downstream side of the sample which measures the increase in pressure ($P_{downstream}$). This increase is caused by the gas that has penetrated the confined sample. The last transducer regulates the confining pressure by tightening a rubber sleeve around the plug ($P_{confining}$).

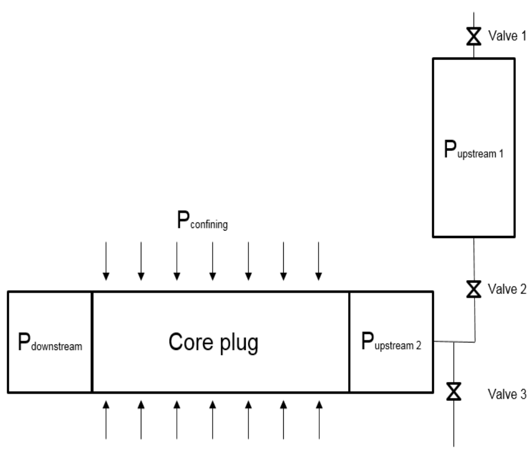

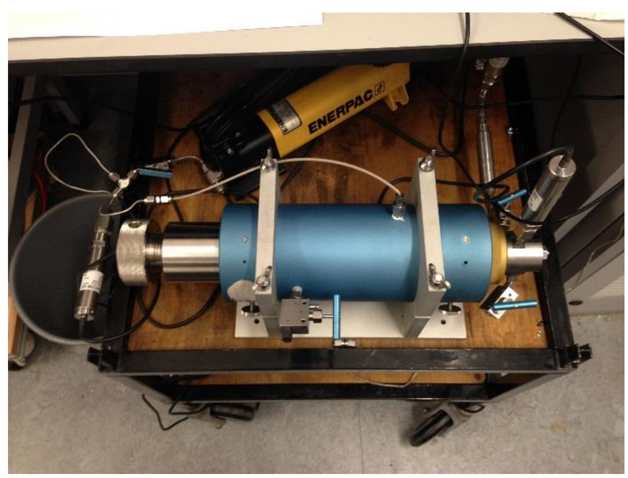

Figure 3.2a (left): A schematic drawing of the modified pulse decay set-up with the four pressure transducers. 3.3b (right) A photograph of the set-up.

Helium gas was used to flood the core plug in all modified pulse decay experiments except for a selection of samples in which Xenon gas under a CT scan was expanded. A description of this technique can be found later on in this chapter.

The main difference with the standard pulse decay set-up is that the pipes between the gas chambers are shortened and calibrated. Therefore the volumes are better calibrated than the generally used pulse decay set-up. This is crucial for these ultra-low permeability shales, because the permeability of the majority of these samples is in the order of nano- to picoDarcy (Mezger, 2014). Small slugs of gas might get trapped or lost in the relatively long connections between the transducers with the original composition of the set-up, which would cause large uncertainties in the porosity and permeability measurements on this scale (Wang, et al., 2010).

A potential problem is that the set-up is not completely leak-free. Calibration results show that about one psi of the upstream volume is lost every 48 hours with a metal plug.

The other key difference of this set-up compared to the generally used one is that in the original pulse-decay experiment the recording stops when the upstream and downstream volumes have reached the same pressure. However, with these shales the trend is that after the upstream and downstream volume reach the same pressure, they tend to decrease further, as can be seen in Figure 3.4. The reason for this is that the gas will first go along the fractures and high permeability streaks, which is the behaviour before the first hour in the plot. After that, the gas goes into the sample. Decay after roughly the first hour until 40 hours of conducting the experiment corresponds with that behaviour. After that an equilibrium is reached in Figure 3.4. Hence, in this modified set-up, the measurement recording has to be stopped manually and can go on for an extended time after the initial pressure equilibration takes place.

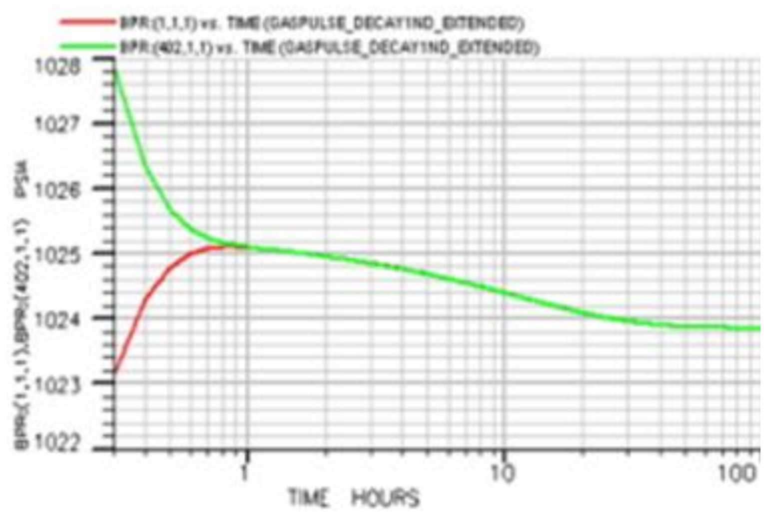

Figure 3.4: Further pressure decay after upstream and downstream volumes meet in MPD experiment. Source: SHAPE.

For the experiments in this study, a confining pressure of 1000 psi (±69 bar) is used. In the case the experiment failed due to leakage, it was redone with a confining pressure of 2000 psi. The full core samples have not been prepared in a special way before the experiments start. Only if the sample was used for another experiment, it was not used for a couple of days for the next experiment. That gave the sample the time to attain ambient conditions again. The experiment starts at a pressure in the first upstream transducer of 200 psi. After this the pressure is increased in steps of 100 psi. This is done three times up to 500 psi. This is followed by a final reverse step, where the upstream pressure was released by quickly opening and closing valve 3 (Figure 3.2), and the stored gas in the sample and downstream volume is ventilated to the upstream transducers.

Subsequent pressure steps are undertaken to narrow down on the unique solutions of porosity and permeability, because the multiple history matches may give the same result for one experiment. By performing multiple pressure steps the number of unique solutions decrease with every pressure step until the correct combination of output parameters is found (Figure 3.5).

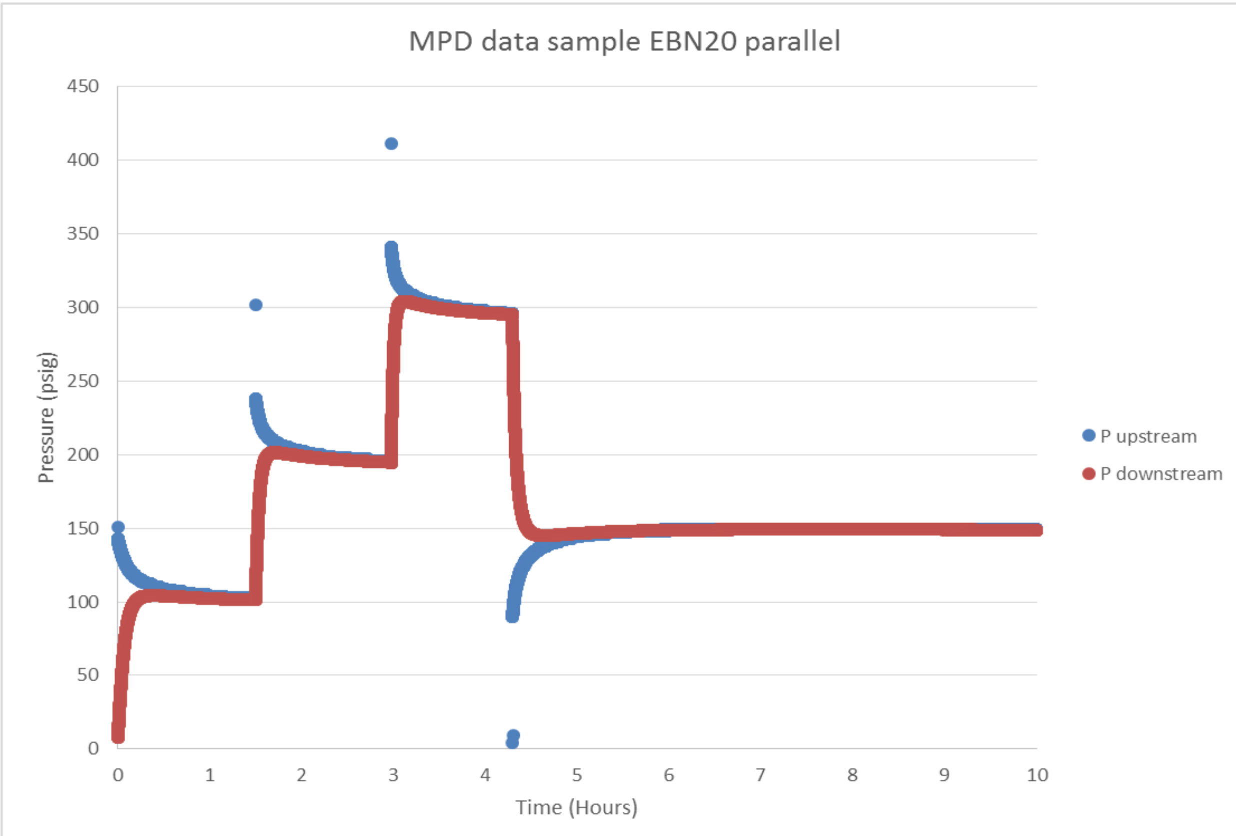

Figure 3.5: Multiple successive MPD experiments on sample EBN20 parallel.

3.1.3. Gas Research Institute Test (GRI)

The GRI tests were performed on the chips and both the linear and radial plugs of all eight samples. The idea of the experiment is more or less equal to the modified pulse decay experiment, but without a confining pressure. Here only two transducers play a role, one connected to the upstream vessel, which regulates the upstream pressure steps, and the other connected to the downstream volume, into which gas is expanded.

Three different experimental set-ups where used for all experiments, all based on the same principle, but with slightly varying volumes in the upstream and downstream vessels. A simplified set-up and a picture of one of the three set-ups is shown in Figure 3.6. Two of these pots have hydraulic rams with a maximum allowed counter-pressure of 250 psi, while the other could cope with a pressure of 500 psi. This varied the measurements slightly, but almost all experiments were executed with pressure steps in the upstream volume of 150 psi to 240 psi in 4 steps. This was followed by a reverse step. The reverse step and multiple pressure steps are as described in the modified pulse decay experiment.

When the sample was loaded in the downstream pot, a maximum of metal calibration balls was added to the pot. This decreases the role free gas plays in experiments where core plugs were analysed. The more free gas expands in the downstream volume, the longer it takes to reach equilibrium during calibration and the more prone the experiments are for temperature effects. This means that the first measurements are inaccurate. In appendix B these calibrations are discussed.

Apart from preparing the samples in different ways, a variation of gases is also used. In the GRI set-up the core plugs will were tested with helium, nitrogen and methane.

All core chips where examined by expanding nitrogen and helium gas, while all full core plugs were tested by expanding helium and methane gas into the sample. Because methane expansion on shale samples is a relatively new principle in this research and the SHAPE project, a full section will describe these experiments later on in this chapter.

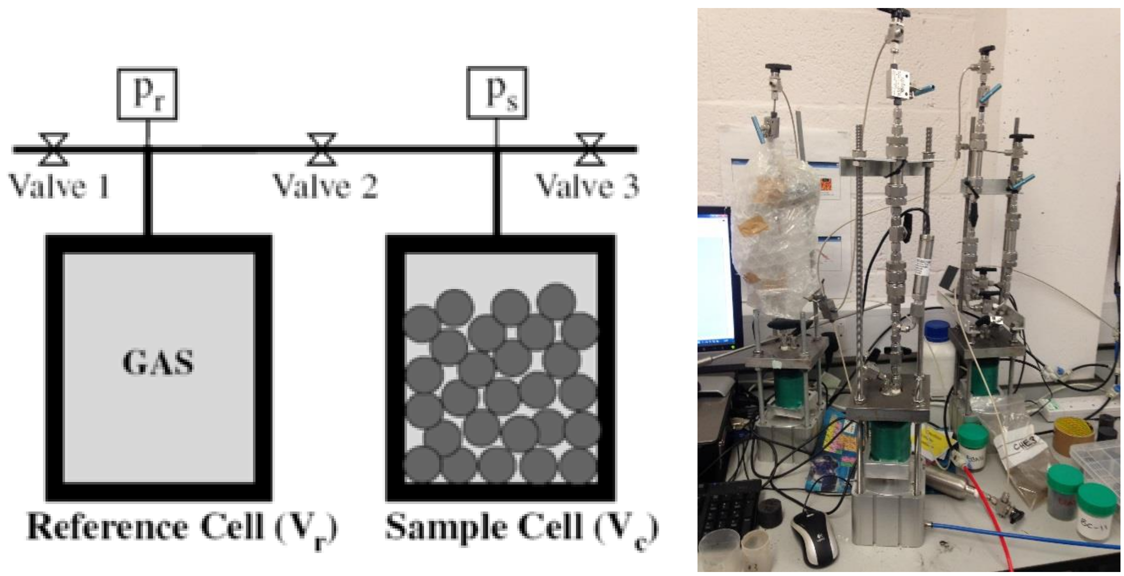

Figure 3.6a and b: Schematic overview (left) and photograph (right) of the GRI set-up with hydraulic ram. Source: Noordoven (2011).

3.1.3.1. Helium and nitrogen expansion

Experiments using different gases, such as helium and nitrogen, are performed to test the dependency of porosity measurements on the variable pore size distribution of the sample (Guarnieri, 2012).

Shales have very small pore throats, so nitrogen and helium are picked to underpin the thought experiment that gases with a larger molecule or Van Der Waal's diameter have less chance of flooding the complete core (Guarnieri, 2012). The molecule diameters of all expanded gases can be found Table 3.2.

Table 3.2: The molecular sizes of expanded gases.
Source: Wolfram Research and Carl W. Kammeyer (1972).

	Van der Waal diameter (Å)	Atomic Radius (Å)
Helium	2.8	0.31
Nitrogen	3.1	0.56
Methane	4.08	N/A
Xenon	4.32	1.08

Larger gas molecules may be blocked out of the numerous very small pore throats shales contain. In Figure 3.7 a schematic illustration of this behaviour is shown. In typical shales, the characteristic throat size of 6 nm corresponds to the largest fraction of pore throats (Sakhaee-Pour & Bryant, 2012).

This means that less gas can be expanded in the downstream volume. This will most likely result in a lower porosity from the data inversion, which will be touched upon in a later stage.

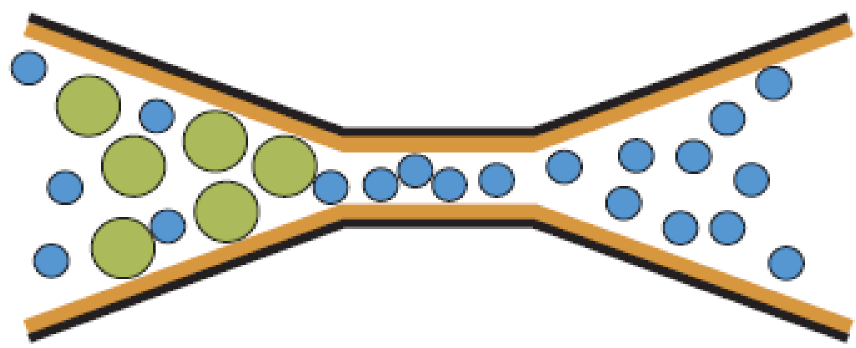

Figure 3.7: Difference in molecule size may prevent flow through small pore throats.
Source: Cluff, et al. (2007).

The crushed GRI tests take the shortest time to reach equilibrium and are therefore less prone to inconsistencies. Additionally, crushed shales have significant more surface area in contact with the gas compared to the full core plugs. This enhances the behaviour of penetration of the gas into the shale matrix. Hence these crushed shale measurements will be primarily used to determine the matrix porosity.

3.1.3.2. Methane expansion

New in this series of experiments is the expansion of methane into shale samples. Until now the database of the SHAPE project only contained experiments performed with either helium or nitrogen as gases.

From Table 3.2 it can be seen that methane has a Van Der Waal's diameter that is almost 1.5 times larger than the molecular diameter of helium. Therefore experiments with helium are expected to yield a porosity that is higher than methane, as methane will be able to penetrate fewer pores due to its larger size, caused by the same effect as described in the previous section. This will most likely cause of an overestimation of matrix porosity when helium is used.

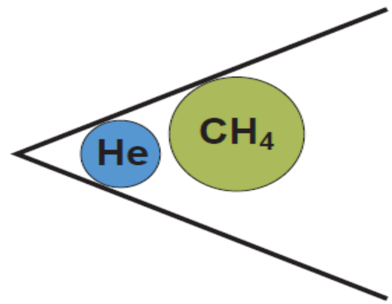

Figure 3.8: Difference in molecule size may cause small pore throats to block certain gases. Source: Cluff, et al. (2007).

On the other hand, helium is a noble gas and nitrogen has a triple bond and is therefore also unlikely to react. Therefore, the expansion of these gases into the core plugs probably causes an underestimation of the absorbed volumes of shale gas, because methane is not a noble gas and will therefore probably react with the organic matter in the sample. This could even cause a larger volume of gas to enter the sample (Sakhaee-Pour & Bryant, 2012).

Adsorption is usually described with adsorption isotherms. These isotherms describe the amount of adsorbed gas as a function of pressure at a fixed temperature (Cui & Bustin, 2009; Civan, et al., 2011):

$$q_a = \frac{q_l p}{p_l + p} \qquad \text{Equation 1}$$

Where q_a is the standard volume of gas adsorbed per mass of shale [m^3/kg], q_l is the Langmuir gas volume [m^3/kg], p is the gas pressure [Pa] and p_l is the Langmuir gas pressure [Pa].

Cui (2009) showed the effect on the shale porosity deriving the following equation for effective shale porosity:

$$\varphi_a = \frac{\rho_s}{V_{std}} \frac{(1-\varphi)}{c_g \rho} \frac{q_l p_l}{(p_l + p)^2} \qquad \text{Equation 2}$$

Where φ_a is the effective porosity of the shale matrix when taking into account adsorption (fraction), ρ_s is the grain density [cm^3/g], V_{std} is the molar volume of gas at standard pressure (101.325 Pa) and temperature (273.15 K) [m^3/kg], φ is the porosity of the shale matrix without adsorption, c_g is the gas compressibility [1/Pa], ρ is the density of the gas [m^3/kg] and other factors are the same as mentioned earlier.

For the Langmuir adsorption experiment, all round robin samples were crushed very fine (<0.44 mm). Matrix void volume for the derivation of adsorption values was calibrated using two types of gasses: helium and krypton. The resulting values were then compared.

After that samples were kept in an environmental chamber for 48 hours to prepare them for the ASTM (American Society for Testing and Materials) moisture equilibration of coal procedure, the samples were directly transferred to the sample cell.

Isotherms were conducted at 30˚C (±0.1°C) and up to ~8500kPa pressure of methane. The tests were performed in 8 to 9 pressure steps with uniform intervals between successive steps.

Experimental adsorption values were first calculated as "excess" sorption and then converted to the corresponding "absolute" values after considering the sorbed phase density of methane of 421 kg/m^3 for each pressure step. Parameters describing the adsorption equation – Langmuir Volume and Pressure (v_l and p_l) – were inverted using the Levenbarg-Martquadt algorithm.

The results of the Langmuir isotherms on the crushed shale will also be the basis of the interpretation of the adsorption in the full core experiments with methane expansion.

3.1.3.3. Xenon expansion under CT scan

Computerized Tomography, better known as CT scan, uses x-rays to make a digital image of what passes through the donut-shaped opening of the machine, where a beam is emitted through the sample and received by a detector on the other side, while rotating quickly and making about 1000 measurements per second. The resulting image is based on the amount of CT units received. This scale describes the density on the Hounsfield attenuation scale, which i.e. how easy electromagnetic radiation, in this case x-rays, pass through the examined medium.

In the experiment performed in the CT room of the Wolfson Laboratory at the University of Leeds, the samples were loaded into the modified pulse decay holder. The set-up was placed on the patient bench of the CT scanner as can be seen in Figure 3.9. First a scan of the sample was taken without the expansion of xenon, so assumed is that the porosity was only filled with air. After this, xenon at 150 psi was allowed to expand in multiple slugs into the sample. The hypothesis of expanding Xenon in shale samples under a CT scan is based on medical research which showed that after inhalation of 50 to 70% non-radioactive Xenon the gray matter in lungs was enhanced by 19 ± 4 Hounsfield Units (HU) and white matter by 24 ± 4 HU (Segawa, et al., 1983). In shales, therefore, the idea is that the flow path of the expanded xenon through the core would light up. This is be done by monitoring the sample before, during and after the expansion.

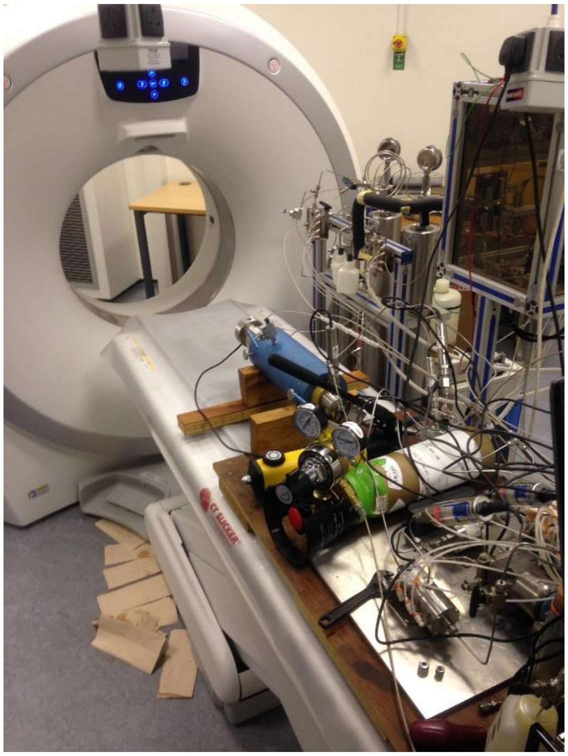

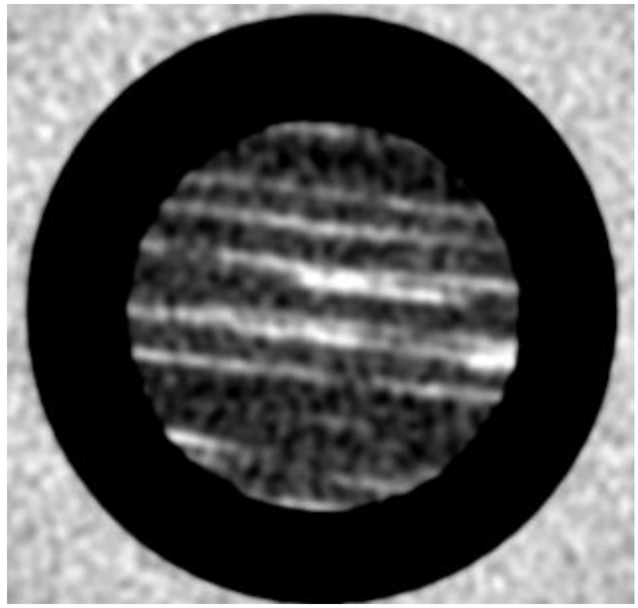

Figure 3.9: The set-up of the xenon expansion experiment under the CT scan (left) and a CT scan, which is a cross section of one of the cores (right).

3.2. Data acquisition

Not only the measurements suffer from inconsistencies in the results, the processing of the data to obtain the petrophysical results can result in errors. Inverting the data is a crucial step in giving reliable results, so this section will describe how the observed data will be processed.

All experiments yield data in the form of pressure versus time. This data will then be inverted using an improved version of the existing finite element method designed for shale-gas permeability (Civan, et al., 2011), with which various parameters can be simulated with the help of Tempest Enable reservoir simulation software. The goal of the history matching is to fit a simulated result as closely as possible to the observed data, as can be seen in Figure 3.10.

The results from all pressure steps done for the same experiment, as is explained in the experimental set-up (Figure 3.5), are performed in two stages. First a wide spectrum around a most-likely value for each parameter bounded by a maximum and minimum value will give a number of “scoping runs”. Now the observed data from the experiments is uploaded and a wide range of results around the data is visible. To approach the data as closely as possible, error bars are placed around the observed data at certain time steps. The software uses an Eclipse back-end simulator with a nearest neighbourhood algorithm to approach a solution between these error bars, the so-called “refinement runs” (Fisher & Rybalcenko, 2014).

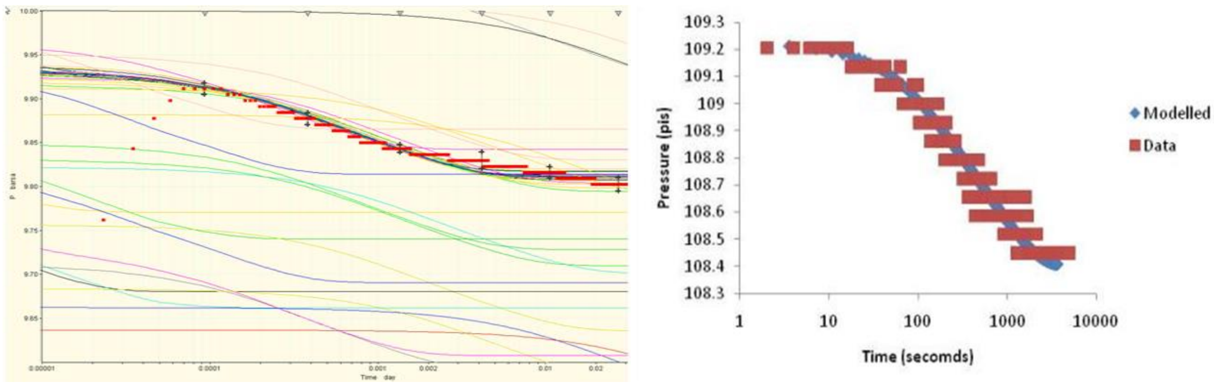

Figure 3.10: Refinement runs on the observed data (red dots with errors bars) (left) result in a best fit history match through the observed data (right).
Source: SHAPE, Fisher & Rybalcenko (2014).

For the different tests and varying sizes of the samples, different numerical models are needed, of which a selection can be seen in Figure 3.11. Hence, every core plug has a uniquely designed representative model. The full core plugs have an amount of cells dependent on their length, the radial core plugs have a 1-celled hole through the middle and the crushed material is characterized as fragments.

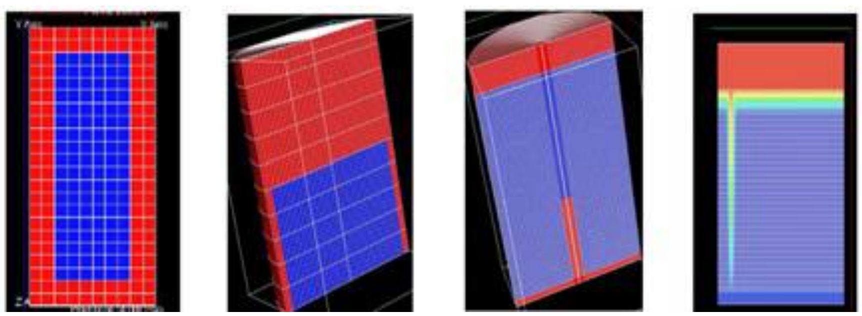

Figure 3.11: The characterization of a sample for various tests. From left to right: modified pulse decay, crushed GRI, radial full core GRI and a high permeability streak.
Source: SHAPE, Fisher & Rybalcenko (2014).

The assumptions and set-up of the code is based on earlier papers (Lorinczi, et al., 2013; Fisher & Rybalcenko, 2014; Crook, 2014), and this section will touch upon the variations used for the experiments conducted. Below an explanation is given on how the data was inverted.

All the full core experiments were inverted in multiple ways for each pressure step. This is done to approach different effects taking place in the shales. Four standard ways of simulating each pressure step were conducted, as can be seen in Table 3.3. Later the improvements of the code will be discussed in the section describing the novel inversion of experimental results.

The base script models a homogeneous representation of the core plug. Added to that is the option to include a higher permeability streak through the middle of the core, such as a (micro)fracture or another conduit, e.g. calcite or sand vein (see the right most panel of Figure 3.9).

Another option is to include a correction for the Klinkenberg slippage factor. These (ultra)low permeability rocks have very small pore throats. For shales, the pore radius of the nanopores of these samples can be as low as 0.01µm (Mezger, 2014). This results that the natural gas is in the transitional flow behaviour with a Knudsen number in the range of 0.1-10. That means that the mean free path of the gas is almost equal to the pore space. This results in a decrease in the permeability depending on the pressure, expressed as the Klinkenberg effect, which is characterized as the b-factor (Florence, et al., 2007; Christou, et al., 2015). With this option a numerical script is included based on equation 3. In the APPENDIX, the eclipse script can be found.

$$\frac{b_k}{\hat{p}} = \left(\frac{k_{app}}{k_{abs}} - 1\right) \qquad \text{Equation 4}$$

Table 3.3: Overview of the selected simulations applied to all the samples.

	Without a Klinkenberg gas slippage correction	With a Klinkenberg gas slippage correction
With no high permeability streak	No fracture no b	No fracture + b
With a high permeability streak	Fracture no b	Fracture + b

3.2.1. Novel inversion of experimental results

3.2.1.1. Multiple porosity model

Recent history matches use a single porosity system to fit the model to the observed data. However, literature (Handwerger, et al., 2011) refers to multiple porosity systems for shales (Hudson, et al., 2012). East (2011) even mentions six effective porosity regions according to the number of liquids in the rock (Figure 3.12).

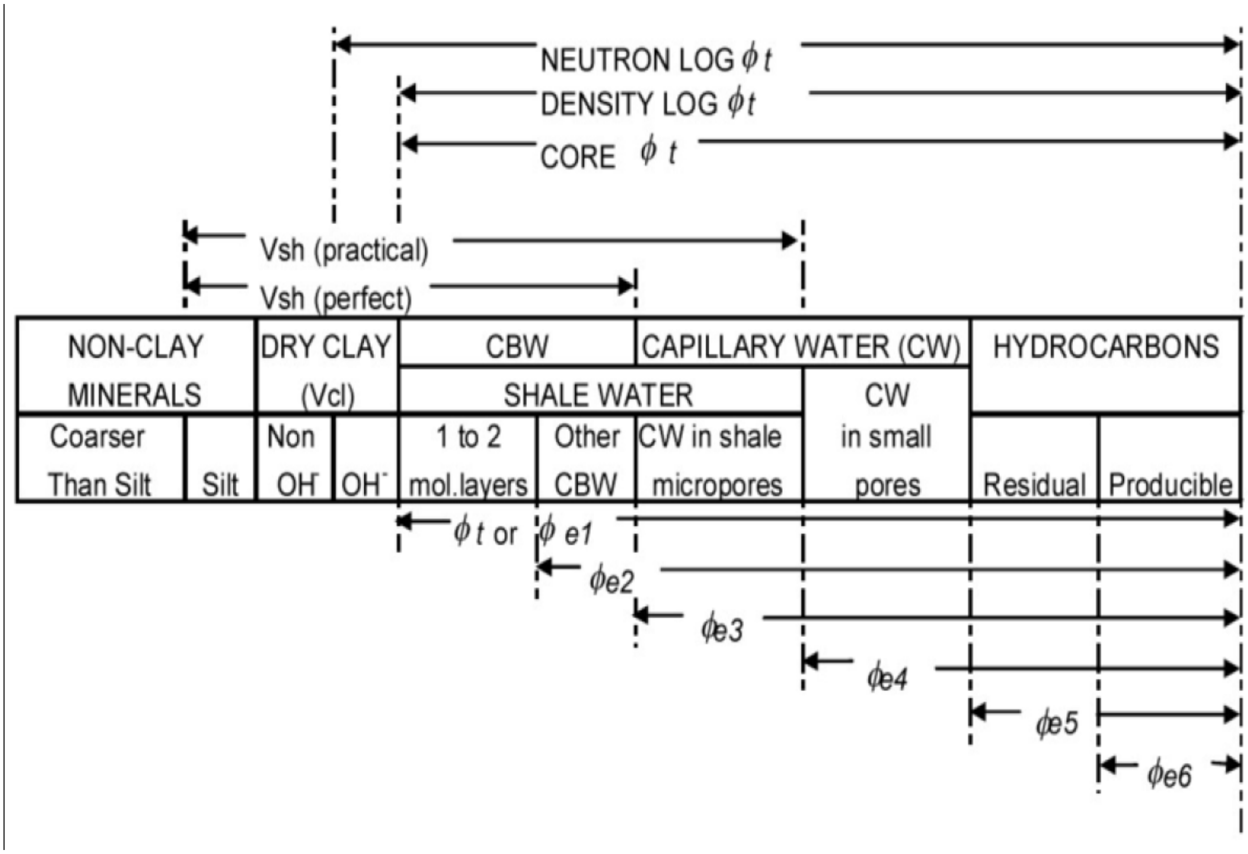

Figure 3.12: Different porosity regions in a shale.
Source: East (2011).

Within the SHAPE project a dual and triple porosity system has been established (Lorinczi, et al., 2013; Crook, 2014). It is used to determine the various steps of expanding gas into crushed shale samples.

The triple porosity assumption comprises the following stages, an example of the accompanying permeability results can be seen in Figure 5.1. The first one, *hi*, corresponds to the major drop of the measured pressure, which is the gas that penetrates the pore space and is referred to as free or compression gas. The second stage, *mid*, corresponds to the adsorbed gas on clays and kerogen, and this smaller pressure drop can be observed in the data. The third stage, *low*, is the adsorbed and absorbed gas which penetrates the matrix of the tested shale (Loucks, et al., 2009). Depending on the properties of the gas the amount of porosity measured in each stage differs according to their amount of sorption. A dual porosity system was developed where the last two porosity regions, the adsorbed and absorbed porosity region, have been combined into one porosity region, because most experiments were conducted with gases that have a low tendency to react with the rock.

These multiple porosity models have been created in the newest version of Tempest (version 7.1.1). The main improvement of this new version is that the material balance is not altered by a fictive well as in the previous version of Tempest. In the old version, a fictive well had to be inserted for the purpose of the in- and outlet regulation. This disturbed the material balance and caused that the upstream and downstream volume became input parameters that had to be calibrated according to the numerical code (Fisher & Rybalcenko, 2014).

3.2.1.2. Methane expansion

The PVT settings in the code for the expanded gas have to be altered for methane, because every gas has different properties. In the history matches, no account was taken of the amount of sorption and therefore no other ways of flow than free gas flow are incorporated in the model. This neglects the important aspect of boundary controlled flow. Therefore, in the future different options could be looked into. For example inserting the Langmuir adsorption curves in the model or look into the Coal Bed Methane (CBM) option of Eclipse.

3.2.1.3. Using porosity as an input parameter

The shorter the experiments take to reach equilibrium, the more chance there is that the data does not become distorted due to inconsistencies in the measurements (Profice, et al., 2011). Therefore the novel system proposed to determine the porosity and permeability from these samples is twofold. First, porosity is determined from the crushed GRI tests with the multiple porosity system described above. The permeability of the crushed GRI tests has large spread and seems unreliable (Soeder, 1988; Guidry, et al., 1995). This is known from previous measurements and results discussed later in this thesis. Therefore only the matrix porosity model will be implemented as an input value in the full core experiments inversion. Now Tempest Enable will only use permeability, at least in the base case, as the variable parameter. This should give a more reliable match as the history matching is based on fewer parameters.

4. Results and discussion

This section describes and gives a brief discussion of the results of the experiments and the inversion of experimental data. All results will be depicted in three large sections. First, the round robin results from the different labs will be compared to the petrophysical results inverted from the performed experiments in the Wolfson Laboratory in Leeds. This is followed by a section about the xenon expansion experiment under a CT scan. The last section describes the effects of adsorption and absorption of the shale samples when methane is used.

4.1. Comparison of experimental results with round robin results

A round robin test has been performed between three different renowned laboratories and the University of Leeds to test and compare different petrophysical properties of a selection of shale core plugs. From all conducted experiments in the Wolfson Laboratory in Leeds, this section will only focus on the experiments done with helium to give a fair comparison with the results from the round robin results of the service companies, who used helium as expansion gas.

4.1.1. Round robin results

In this section, the most imported tested parameters will be plotted in the section below: bulk density, grain density, matrix porosity and matrix permeability.

Subsequently, additions and variations on experiments and simulations will be discussed.

Table 4.1: As-received Bulk Density results from round robin test.

	Leeds [g/cm^3]	Lab A [g/cm^3]	Lab B [g/cm^3]	Lab C [g/cm^3]
OPA1	2.50	2.51	2.50	2.51
OPA2	2.40	2.39	2.37	2.40
EBN20	2.41	2.53	2.55	2.50
OPB1	2.48	2.48	2.38	2.51
OPB2	2.48	2.48	2.46	2.49
OPB3	2.49	2.51	2.50	2.51

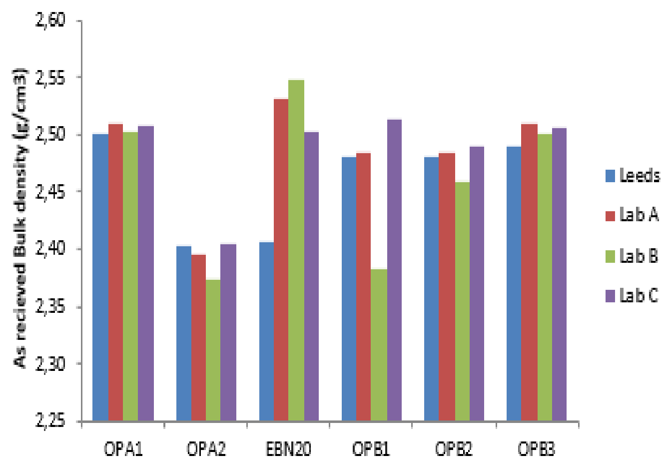

Figure 4.1: As-received Bulk Density results from round robin test.

The bulk density results between the different labs seem to resemble. Outliers are the results from laboratory B, which are lower than average for most of the samples, especially sample OPB1. The external labs have not revealed explicitly how the material is tested. The bulk density results from Leeds come from mercury injection (Olson & Grigg, 2008).

Table 4.2: Dry grain density results from round robin test.

	Leeds [g/cm^3]	Lab A [g/cm^3]	Lab B [g/cm^3]	Lab C [g/cm^3]
OPA1	2.74	2.73	2.70	2.71
OPA2	2.68	2.67	2.63	2.68
EBN20	2.66	2.70	2.71	2.68
OPB1	2.59	2.63	2.57	2.64
OPB2	2.64	2.65	2.61	2.64
OPB3	2.68	2.69	2.66	2.67

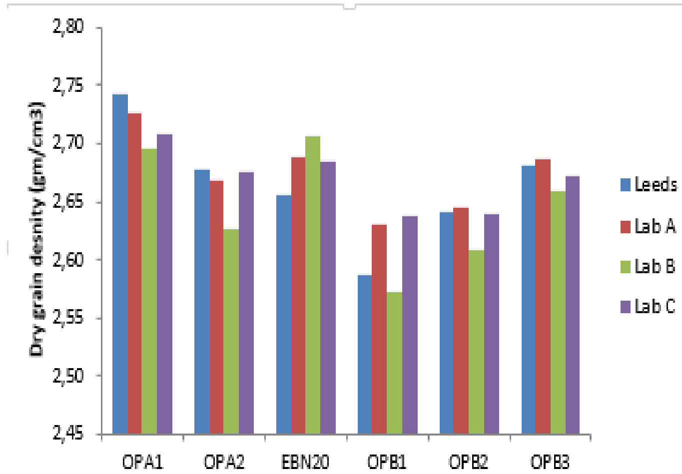

Figure 4.2: Dry grain density results from round robin test.

The grain density results are more or less aligned between the different institutions, just as the bulk density results. Laboratory B has a lower grain density, which explains the lower bulk density in Figure 4.1. Just as the bulk density results, the grain density results from Leeds are computed from mercury injection experiments.

Table 4.3: Dry matrix porosity results from round robin test.

	Leeds [-]	Lab A [-]	Lab B [-]	Lab C [-]
OPA1	8.1	8.7	7.3	8.3
OPA2	11.1	11.1	10.0	11.2
EBN20	7.8	6.9	6.4	8.3
OPB1	6.4	6.9	8.3	6.4
OPB2	7.3	7.4	6.0	7.5
OPB3	7.1	7.5	6.5	7.5

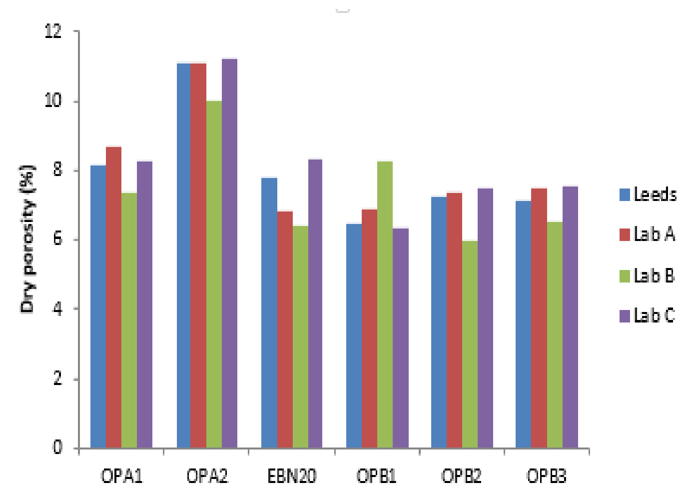

Figure 4.3: Dry matrix porosity results from round robin test.

The dry porosity measurements resemble very well between the different laboratories. The dry matrix porosity results from Leeds come from crushed shale experiments with a single porosity model. The results from laboratory B are not aligned with the rest of the results, because they used retort analysis, while the others used Dean Stark measurements (Handwerger, et al., 2012).

Table 4.4: Dry matrix permeability results from round robin test.

	Leeds [mD]	Lab A [mD]	Lab B [mD]	Lab C [mD]
OPA1	3.3E-06	3.3E-04	5.3E-04	3.4E-05
OPA2	1.7E-05	4.4E-04	1.6E-04	2.5E-04
EBN20	3.9E-06	1.1E-04	4.6E-05	1.6E-03
OPB1	5.1E-04	8.3E-05	1.6E-04	6.0E-06
OPB2	2.7E-05	1.4E-04	3.0E-04	2.6E-05
OPB3	4.1E-05	1.6E-04	5.6E-05	1.5E-03

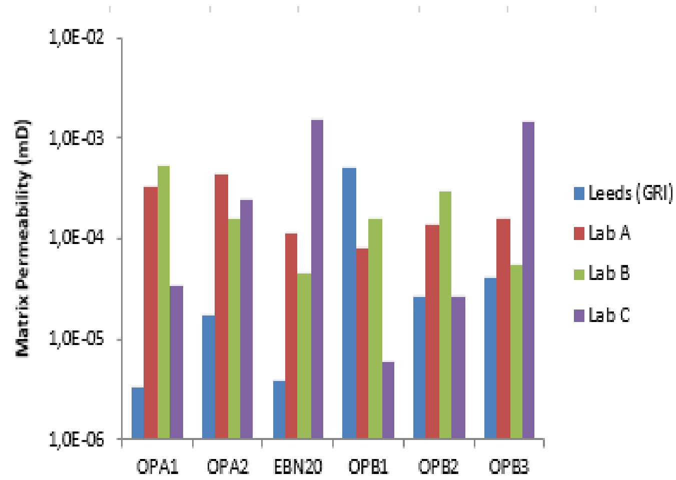

Figure 4.4: Dry matrix permeability results from round robin test.

The matrix permeability measurements between the different institutions are not aligned. The spread of results per sample may exceed several orders of magnitude. It is clear that there is a problem with the measurement of this property. The dry matrix permeability results from Leeds come from the crushed shale GRI experiments with a single porosity model.

4.1.2. Variations on Leeds' results in round robin test

In order to increase understanding of matrix porosity and matrix permeability measurements, numerous experimental variations and different ways of simulation on the same sample have been executed.

The range of experimental techniques is varied – as described in the previous chapter – between crushed shales, the GRI set-up and a confined test in the modified pulse decay set-up. The experiments were performed for different pressure pulses and the full core plugs were tested by letting gas expand in the core plug, these samples are either drilled parallel or perpendicular to their lamination. The last experimental variation is that all full core tests were performed with and without a axial hole through the plug.

The way the data is history matched also consisted of a series of alterations. The base case is a homogeneous modelled sample and a variety of alternative scenarios were calculated. They consist of modelling a high permeability streak through the core and taking into account the Klinkenberg gas slippage correction factor on permeability in tight porous media (Ziarani & Aguilera, 2012). The crushed shale experiments have been simulated with a multiple porosity system and full core plugs have also been examined with a fixed matrix porosity, which is derived from the crushed results.

The largest amount of data comes from samples EBN20 and OPA2. About 40% of all the data comes from sample EBN20 and more than 20% from sample OPA2 (Figure 4.5). The variations will therefore be explained on the basis of the experiments conducted on the core plugs from these samples, unless stated otherwise. The overview of all results can be found in appendix E.

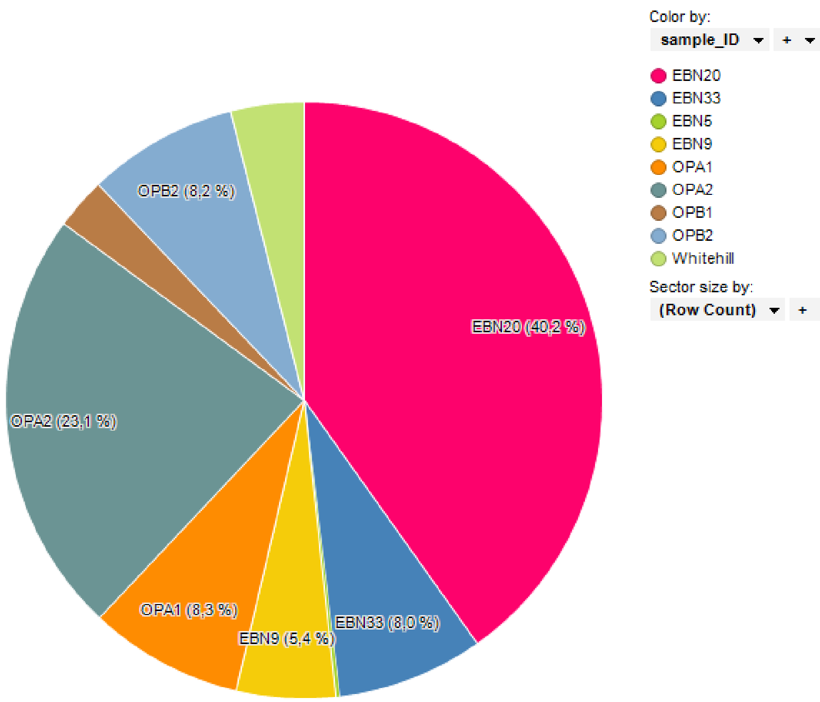

Figure 4.5: A pie chart which shows how the generated data is distributed amongst the different samples.

4.1.2.1. Results verification

Quality control was a crucial part of this study and is performed in multiple ways. This section describes when data points were qualified as usable data and when results were not included in the total data set. For both MPD and GRI results, the measured data had to reach steady state. If from the measured data it was clear that the system had not reached equilibrium, the results were disregarded. It is hard to see if the experiment equilibrated. If the experiment did not last long enough, the pressure is still falling in the upstream chamber (Figure 4.6). In case of prolonged experimental time, there are is more chance that leakage and temperature effects will affect the outcome of the results. An example is Figure 4.7a, where it seems that the data has equilibrated after about 100 seconds, but after that the pressure decay curve seems to drop further (leakage effect) and becomes irregular (temperature effect). All simulated data from curves that had a non-standard shape were not included in the end results. Examples of experiments that seem to have equilibrated are shown in Figure 4.6b and Figure 4.7b.

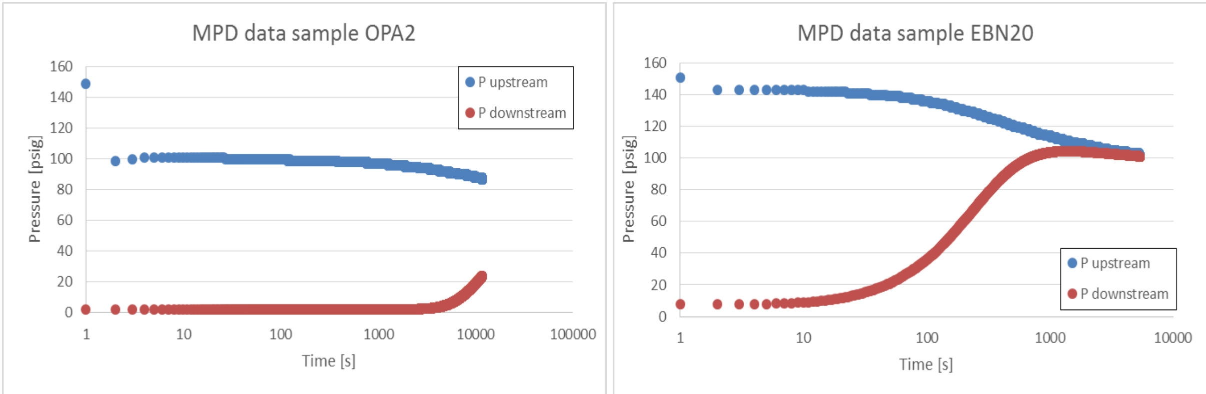

Figure 4.6a and b: The results of a MPD test which is not equilibrated (left) and the results of a MPD test that seem to be equilibrated (right).

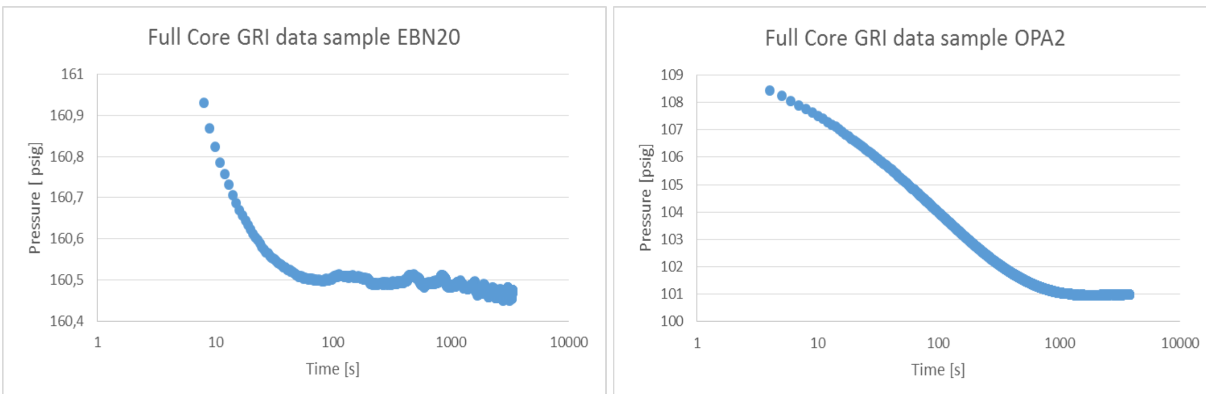

Figure 4.7a and b: The results of a full core GRI test where temperature effects seem to have taken overhand(left) and the results of a MPD test that seems to be equilibrated (right).

Another aspect of the quality control was to check if the initial pressure drop could be calculated using a material balance based on the ideal gas law ($P_1V_1 = P_2V_2$). That material balance could be used to calculate the initial downstream volume just after opening the valve, because the sizes of the containers, the sample dimensions, used calibration balls and the pressure in the upstream volume were calibrated and known. If the results mismatched severely, these results were not included in the dataset.

4.1.2.2. Matrix porosity variations

Calculating the matrix porosity and permeability of the heterogeneous shales has to be done with great care. Results can greatly vary due to different experimental set-ups and simulation input parameters. For the two samples on which most experiments were executed, an overview of all the different inverted matrix porosities can be found in Figure 4.8.

Figure 4.8: The overview of the inverted averaged porosity for the different pressure steps for all the different experimental set-ups.

Figure 4.8 shows that there is a relatively large range of matrix porosities for both the samples. In the sections below, the clearest example for each case is used to explain the effect of the variation to the base case. The base case is defined as a homogeneous linear full core plug without correction for the Klinkenberg effect. The difference in size of the data points shows the upstream pressure unless stated otherwise.

The explained trends from the data qualitatively support the theories discussed. The quantitative differences in the results read from the axes is less significant, because the results between samples vary considerably. Additionally, the same experiments should be performed multiple times to be able to discuss the uncertainty between similar tests, because the experiments and inversions are prone to errors.

4.1.2.1.1. Set-up variation

The difference in matrix porosity between the full core GRI method, where the sample is unstressed, and the MPD set-up, where the sample is confined, is depicted in Figure 4.9. In the full core GRI experiment the expanded gas has more surface area to penetrate than in the MPD set-up. In the MPD setup the gas has to follow a more or less fixed path from the upstream chamber to the downstream chamber through the sample. Additionally, the confining pressure will compress the sample, causing certain pore spaces to minimize. Therefore more gas is expanded in the downstream volume of the full core GRI set-up than the MPD resulting in a higher matrix porosity, because certain parts of the sample will not be accessed by the expanded gas.

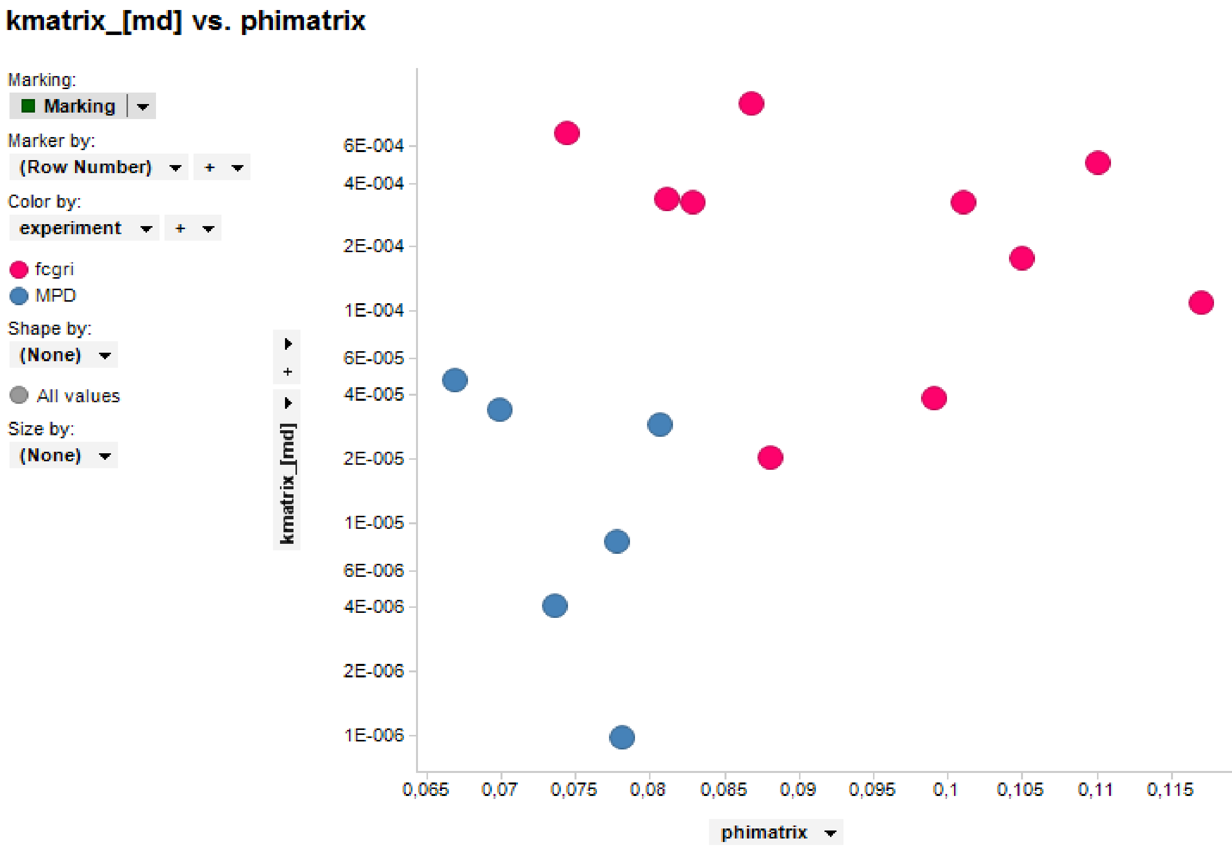

Figure 4.9: The dependency of the matrix porosity of the sample OPA2 on a confined or unstressed set-up.

4.1.2.1.2. Lamination effect

The core plugs for each sample were drilled perpendicular and parallel to their lamination when there was enough sample material, see Table 3.1 for an overview of the used samples in this dataset. Figure 4.10 shows that the matrix porosity is dependent on the way the plugs are drilled. The data points shown are all from the MPD set-up on samples EBN20 and OPA2. With this experiment the lamination effect is enhanced, because the gas has to penetrate through all subsequent layers in the perpendicular drilled plugs. In the sample drilled parallel to its lamination, the expanded gas will be able to flow along the higher permeable pathways of the parallel lamination of the shale plug. This thought experiment is verified by the data plotted in the figure below.

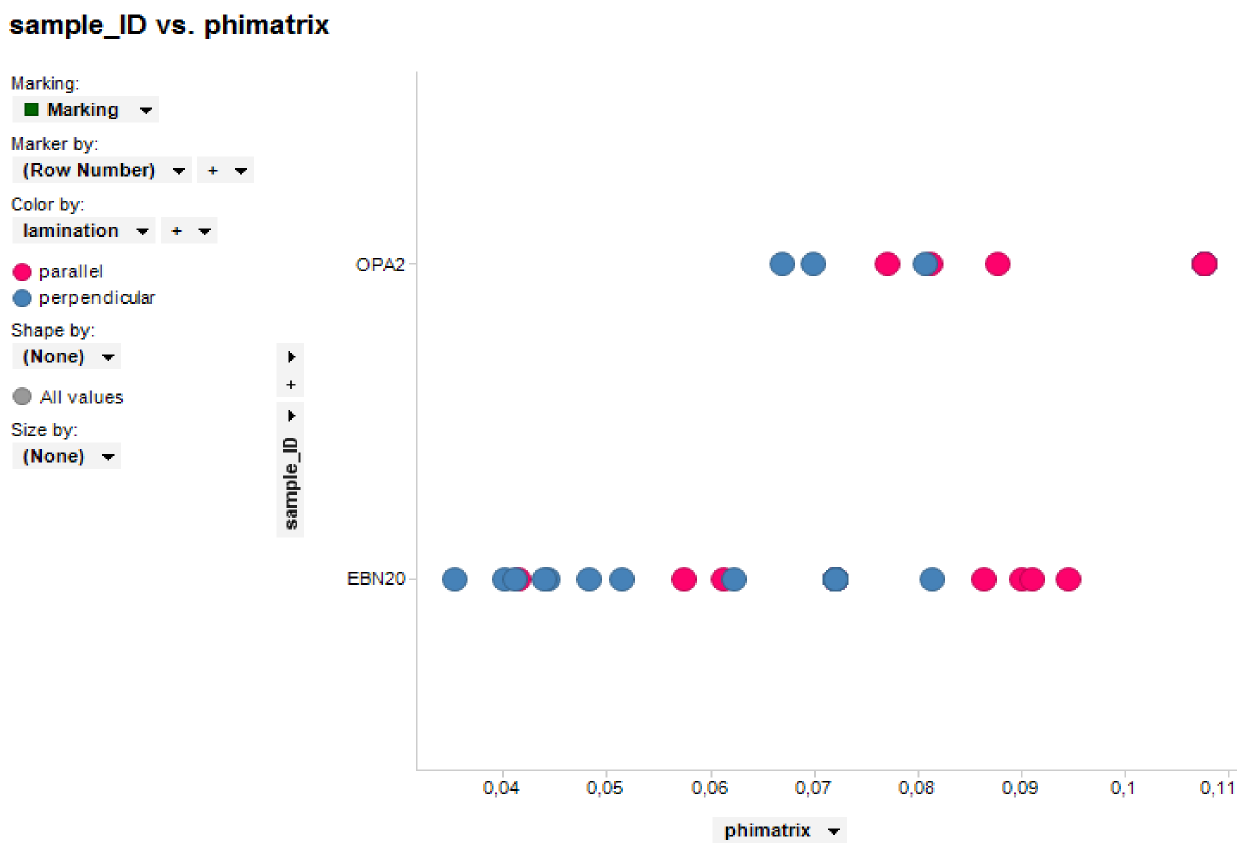

Figure 4.10: The effect of the drilled orientation of the plug compared to the lamination on the matrix porosity of the samples EBN20 and OPA2.

4.1.2.1.3. Effect of radial drilled core plug

The effect of drilling an axial hole in the core plug increases the surface area the expanded gas can penetrate. Therefore, history matched porosity with a single porosity-permeability model is expected to be higher in the radial samples than in the linear core plugs and this is also what the data shows in Figure 4.11. The reason is that there will be parts of the sample that will not be flooded by the expanded gas.

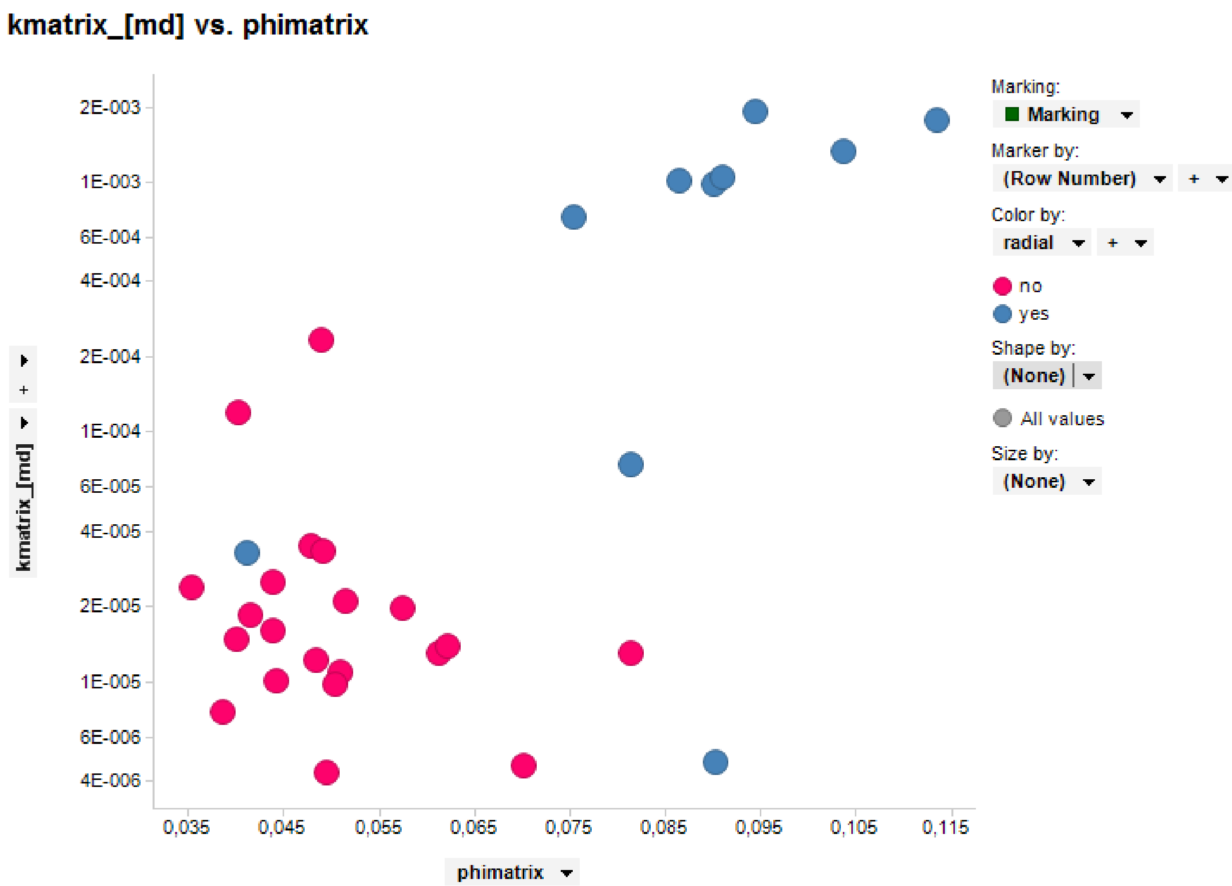

Figure 4.11: The dependency of the matrix porosity of the sample EBN20 on linear and radial flow, drilled either perpendicular or parallel to the lamination.

4.1.2.1.4. Effect of high permeability streak

The experimental set-up has played a significant role in the results. However, the way the measured data are inverted is at least as important to attain reliable results.

The matrix porosity becomes significantly lower when a high permeability streak is added in the model than when this high permeable path is excluded, Figure 4.12 shows this for the Whitehill sample. This is in line with expectations, because the total inverted matrix porosity is an average of the sample with the homogeneous model. Hence the total porosity is averaged out between the high-permeability-zone-porosity and matrix porosity in the rest of the sample. Including this high-permeability-zone – which is likely to have a high porosity as well – causes the lowering of the matrix porosity compared to the matrix porosity of the homogeneous sample without the high-permeability-zone.

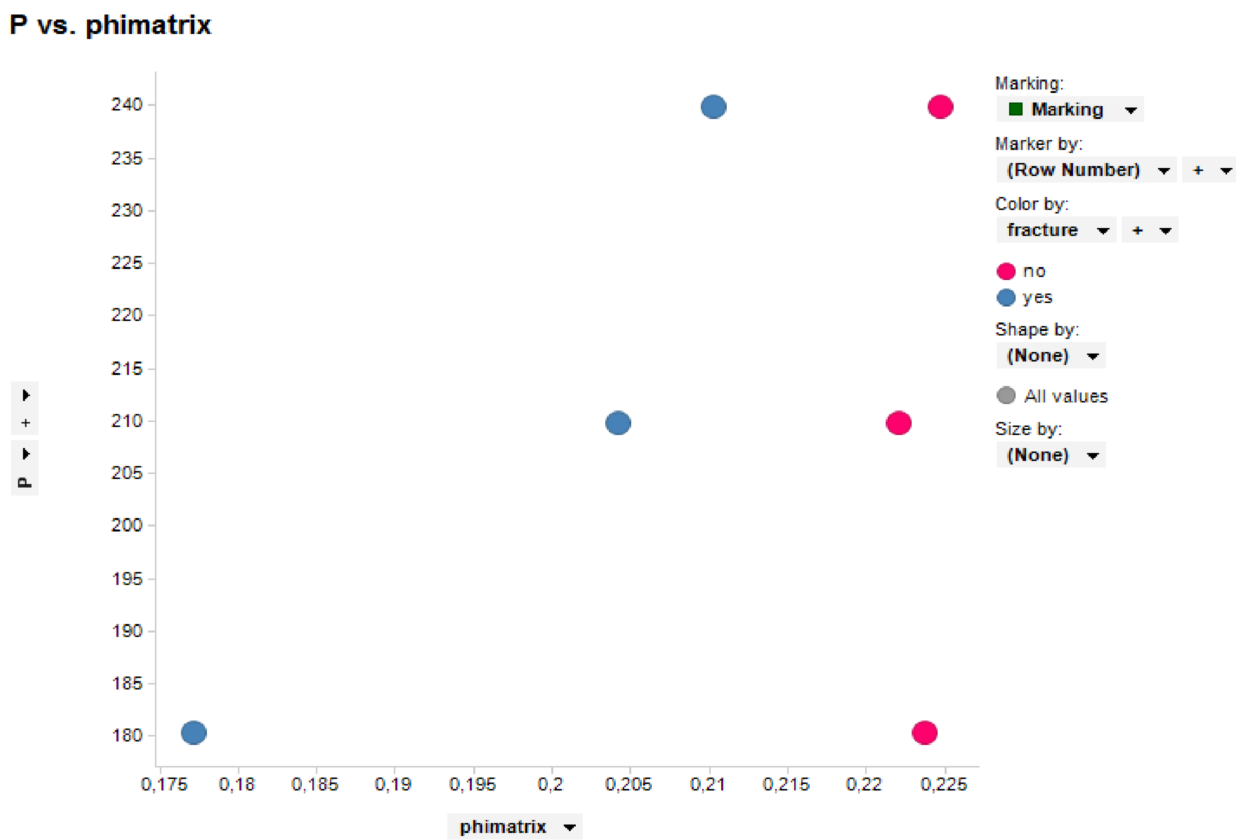

Figure 4.12: The dependency of the matrix porosity of the Whitehill sample on a high permeability streak.

4.1.2.1.5. Effect of Klinkenberg factor

The other variation computed for all samples is including the slippage correction factor in the simulation. Figure 4.13 shows that including the b-factor increases the matrix porosity.

The matrix porosity modelled with the Klinkenberg factor, has to be higher than without this effect. The reason is that when the permeability is lowered – in this case by the b-factor – another factor has to compensate for this effect, because the observed data for both simulations is the same. So when matrix permeability is lowered, the simulator assumes that it is harder for the gas to penetrate the sample. However, the same amount of gas still penetrates the sample, so the matrix porosity compensates for the lower permeability effect and the result is that the matrix porosity increases.

The Klinkenberg gas slippage factor is pressure dependent (see equation 3). The correction can become significant with low pressures, but at high pressures this effect will only be marginal. Figure 4.13 shows that for a higher pressure, the effect on porosity reduces, because the Klinkenberg factor is lowered and the matrix porosity has to compensate less than with a high gas slippage correction factor.

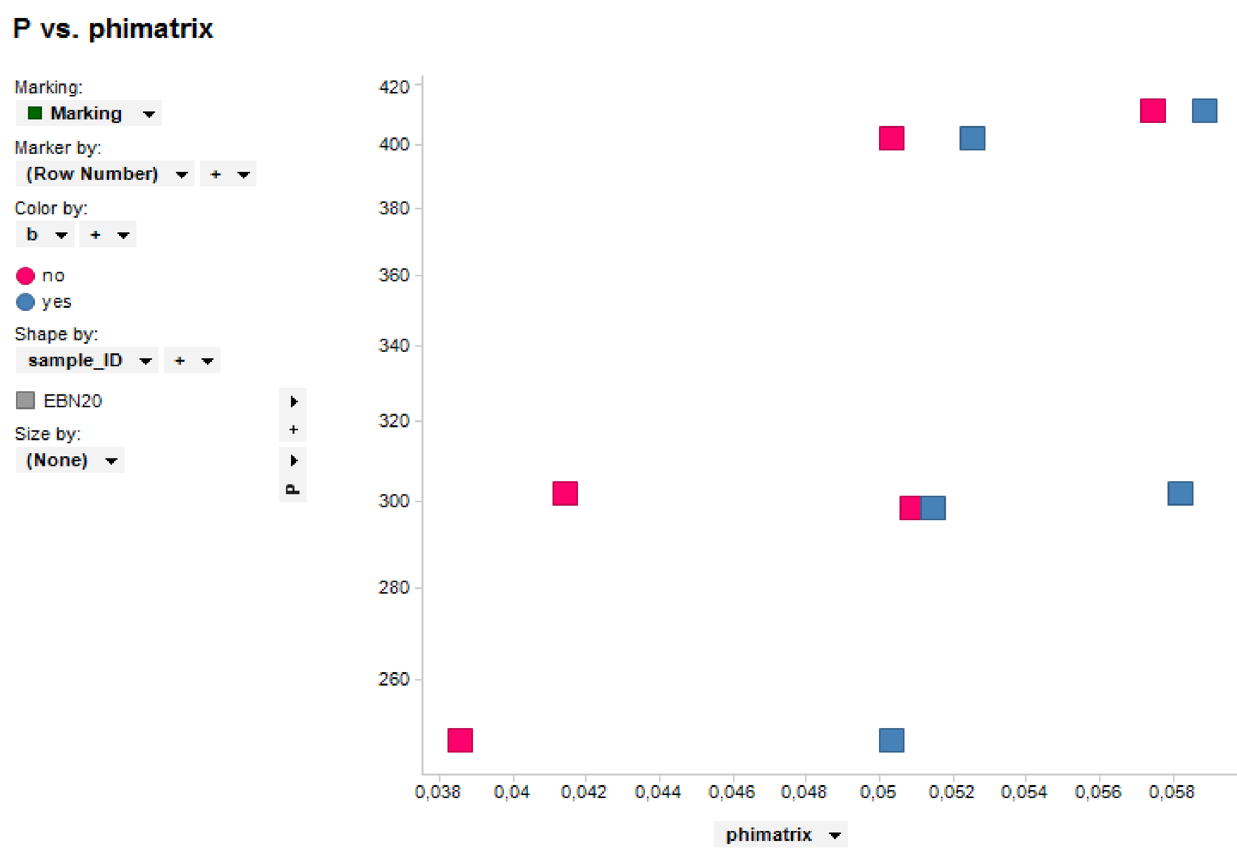

Figure 4.13: The dependency of the matrix porosity of sample EBN20 on the Klinkenberg slippage correction factor.

4.1.2.3. Matrix permeability variations

To show the effects of matrix permeability variations, the model with a fixed matrix porosity as an input parameter is used. This fixed matrix porosity is the result from the crushed shale GRI experiments with a single porosity-permeability model.

4.1.2.3.1. Set-up variation

The difference in matrix permeability between a confined core plug in the MPD and the unstressed measurements in the full core GRI measurements can be seen in Figure 4.14. The results coincide with what is expected. The unstressed core plug has more surface area available for the expanded gas to penetrate than in the MPD set-up. In the MPD set-up, the gas has to penetrate the sample through an almost fixed path, while in the GRI experiment the gas can penetrate the sample in more ways. This is also the reason the MPD experiments take longer to calibrate.

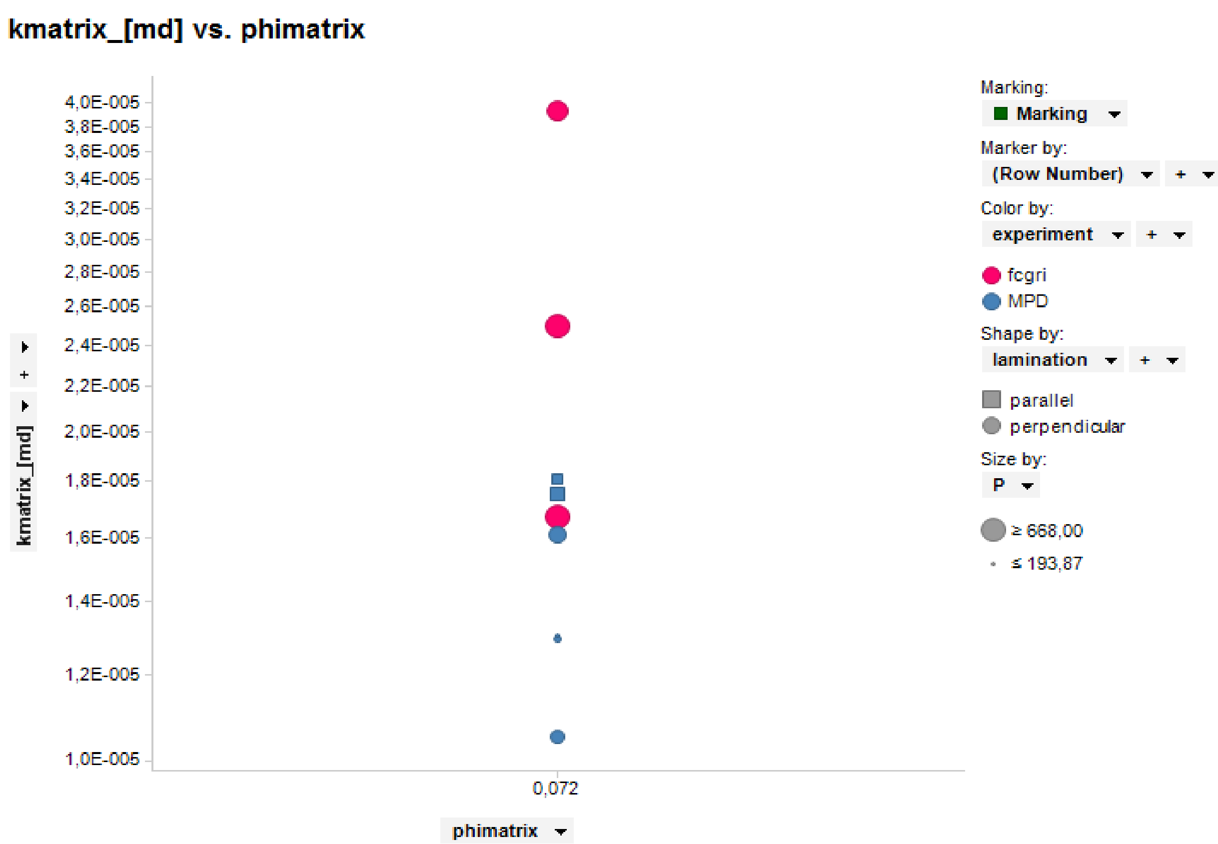

Figure 4.14: The effect of the difference of a confined or a unconfined set-up on the matrix permeability of the sample EBN20.

4.1.2.3.2. Lamination effect

In line with the variation in set-up, the effect of how the plugs are drilled is also important for matrix permeability. The plugs drilled perpendicular to their lamination cause subsequent permeability differences depending on the properties of each layer. In the parallel drilled samples, the expanded gas will have multiple routes. These tests are inverted with a single porosity-permeability model, so the resulting average matrix permeability for perpendicular drilled samples is lower than when the plugs are drilled parallel to their lamination.

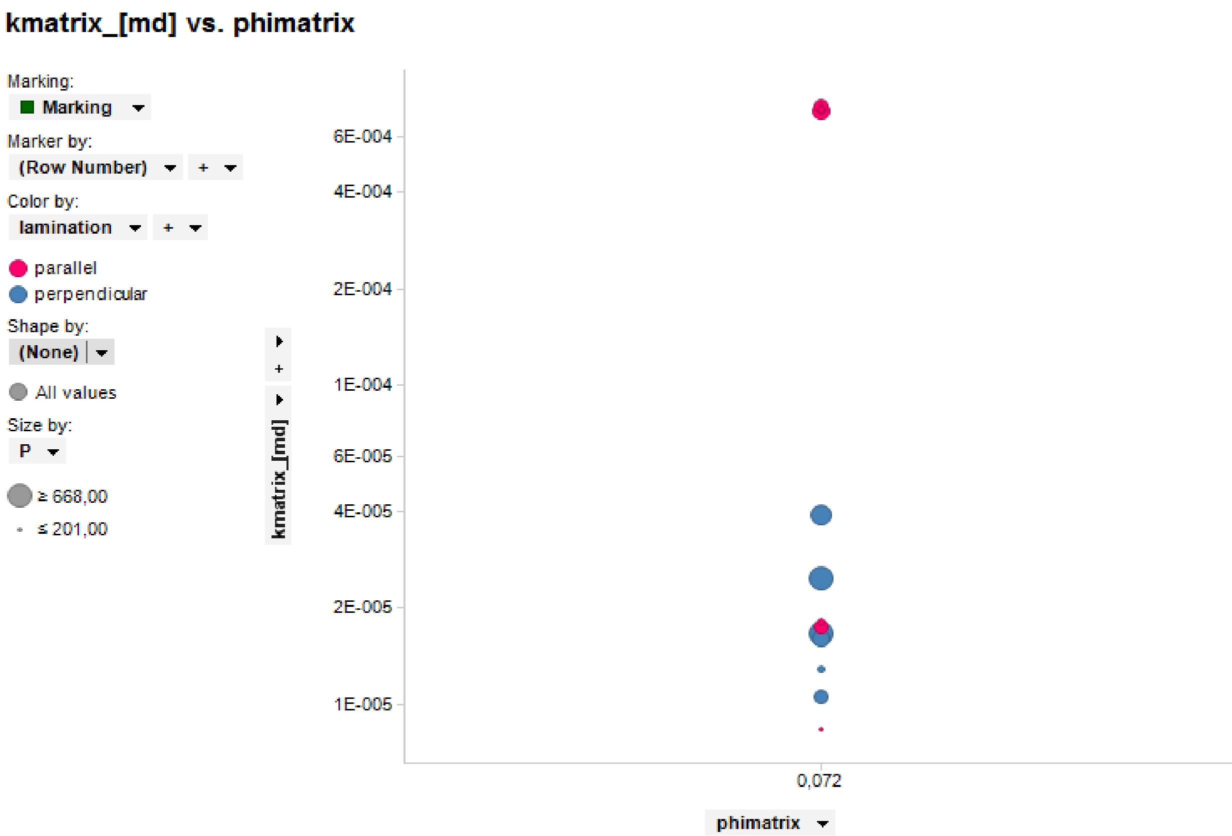

Figure 4.15: The effect of the drilled orientation of the plug compared to the lamination on the matrix permeability of the sample EBN20.

4.1.2.3.3. Effect of radial drilled core plug

In a radial plug the matrix appears to be more permeable than a linear plug, because there is more surface area for the expanded gas to penetrate. A larger volume of the core plug is reached by the expanded gas. This effect is clearly noticed in Figure 4.16. Additionally, the upstream and downstream volumes instantly reach the same pressure, which makes the MPD curve resemble the pressure decay curve of the GRI measurement. As a result the equilibrium will also be reached faster.

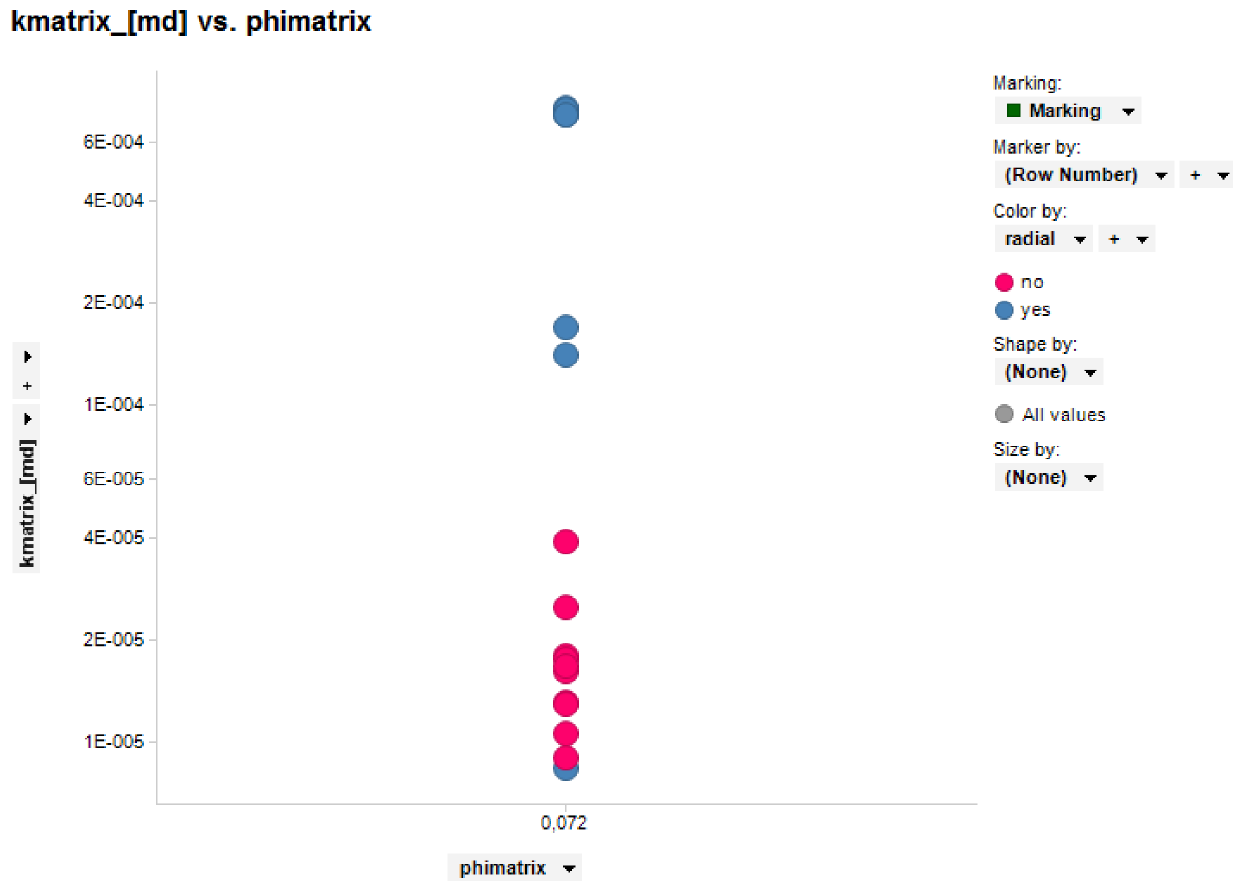

Figure 4.16: The effect of radial flow on the matrix permeability of the sample EBN20.

4.1.2.3.4. Effect of high permeability streak

When inverting with a single porosity-permeability model, adding a high permeability zone means that the matrix permeability in the rest of the sample will decrease. This is the same effect as discussed in the section on the impact of the matrix porosity (4.1.2.1.4). The inversions of sample EBN20 are shown in Figure 4.17 as an example.

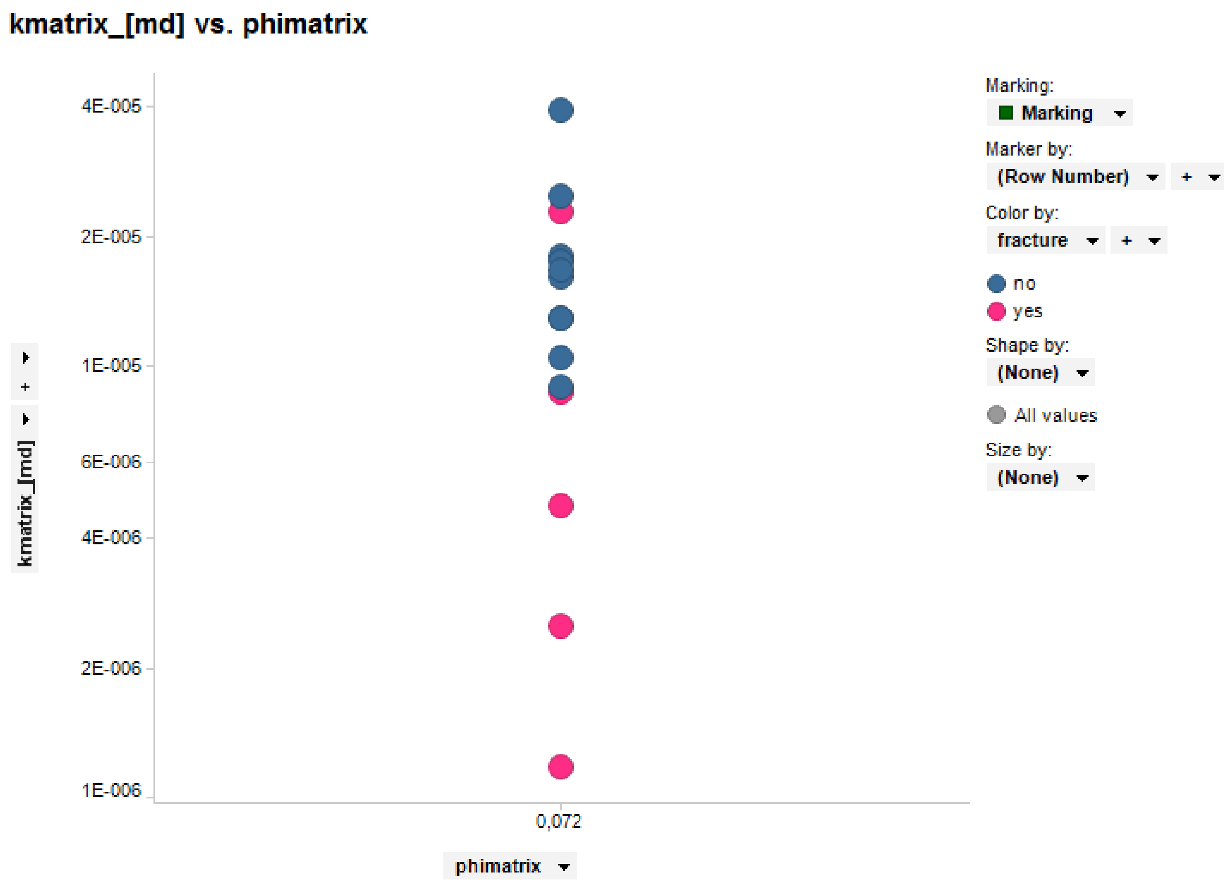

Figure 4.17: The effect of a high permeability streak on the matrix permeability on the sample EBN20.

4.1.2.3.5. Effect of Klinkenberg factor

As described in 4.1.2.1.5, the Klinkenberg factor is dependent on pressure and is a control factor for permeability. Hence, by including the b-factor the matrix will seem (or will appear) less permeable in the simulation than without, this can be seen in Figure 4.18.

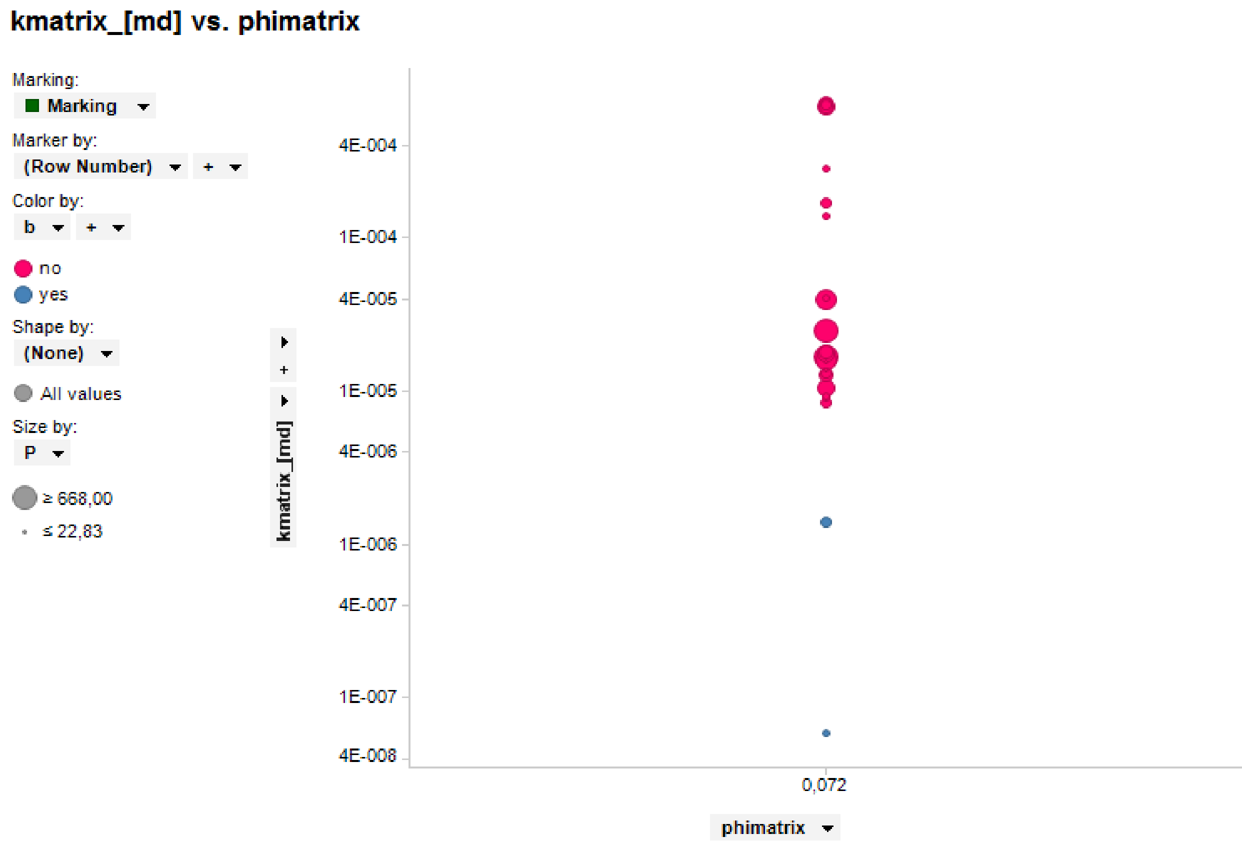

Figure 4.18: The effect of using a Klinkenberg slippage correction factor on matrix permeability for the sample EBN20.

4.2. Xenon expansion

The results of the scans after expansion of xenon do not show a clear signal of the gas. The differences are very subtle at best on helical and axial scans taken from the CT scan. Therefore, it is dangerous to draw conclusions from the images. It is hard to say anything about the samples from these images, because the sample – inside the black ring – and the surroundings give more or less the same image, with only a few larger minerals standing out (Figure 4.19).

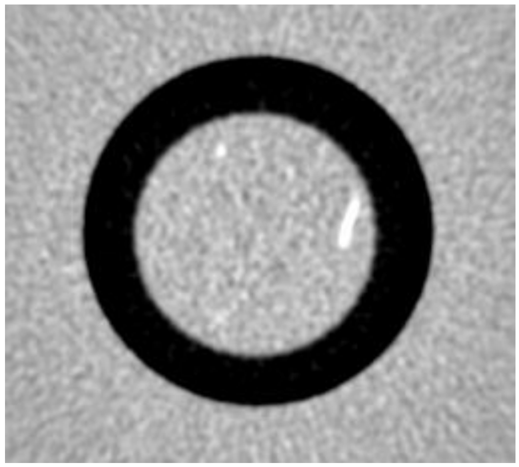

Figure 4.19: EBN20 linear core after Xenon flooding

However, after some editing of the images with the ImageJ software, some of the scans give relevant information about their properties. The artifacts in the core plugs are visible for some of the samples. The EBN20 linear plug in Figure 4.19 shows the lighting up of some of the larger minerals. The OPA2 sample images in Figure 4.20 indicate that these samples are drilled parallel to the lamination of the sample.

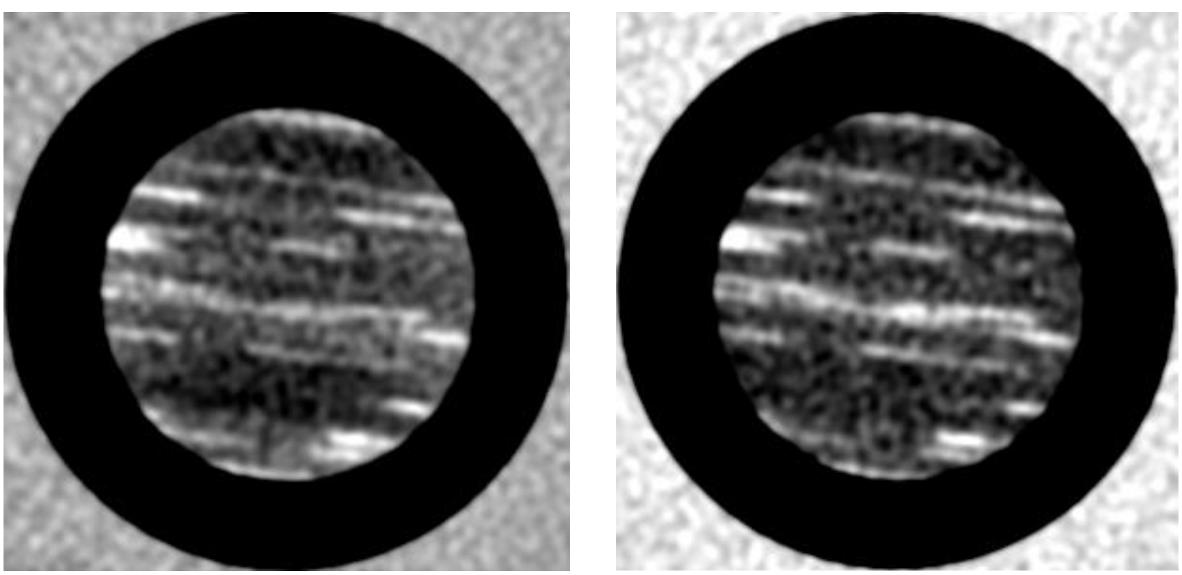

Figure 4.20: The OPA2 sample before and after the xenon expansion. The cross section is taken halfway the core plug.

It is not possible to tell the free mean path of the xenon by looking at the differences of the slices before and after flooding. Figure 4.20 shows a scan halfway the OPA2 sample filled with air on the left – that is before the expansion. The right image is a cross section flooded with xenon for a day. No clear distinction can be made between the pictures or their subtraction. Although the contrast seems to be a bit higher in the picture on the right hand side, it is too inaccurate to jump to conclusions. These cross-sections have been made at various locations and in appendix F more of the processed images can be found.

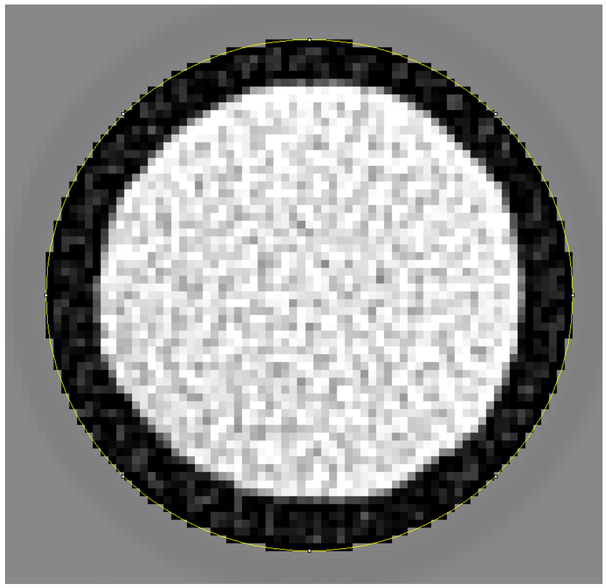

Figure 4.21: The Whitehill sample after xenon flooding.

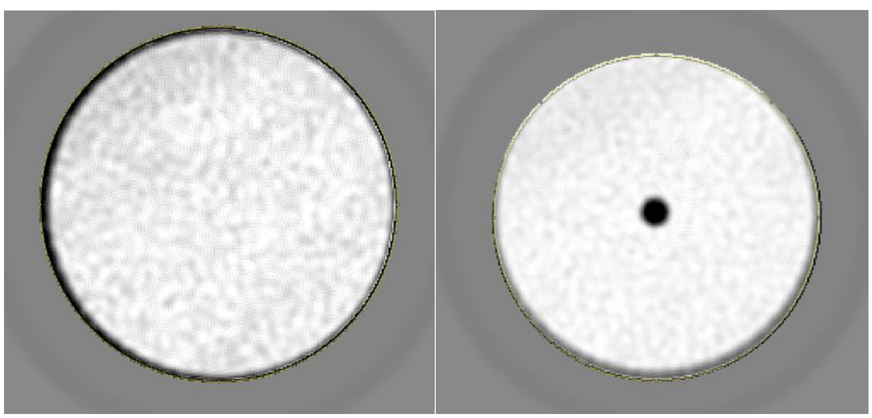

Figure 4.22: Two slices from the EBN5 sample, which has a axial hole halfway through the sample. This results in a combination of linear flow and radial flow.

In other plugs, such as EBN5 and the Whitehill sample (Figure 4.21 and Figure 4.22), even after processing and enhancing the contrast, it does not look as if it is possible to draw conclusions. Subtracting the results after xenon flooding with the starting scan filled with air (Figure 4.23) gives no clear outcome. The only object that stands out on the images inside the rubber sleeve is the drilled hole in samples EBN5 and EBN20 radial.

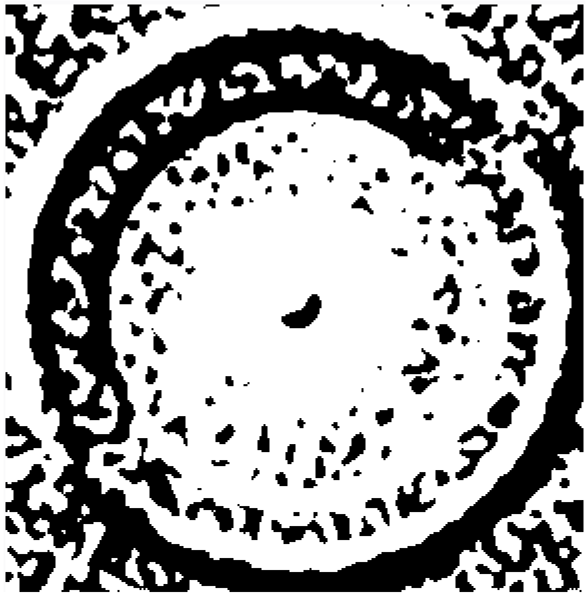

Figure 4.23: The radial sample EBN20 processed by subtracting the results after the xenon flooding with the starting scan.

ImageJ does however possess a function which measures the amount of CT units within a selected region. In Figure 4.24 the results of the radial EBN20 sample can be found. In appendix F more results can be found. The starting data curve denotes the CT results in Hounsfield Units (HU) of a sample filled with air. The end points signifies the result of the core plug filled with xenon over the length of the sample. On the right hand side (Figure 4.24b) the difference between the two is plotted. It clearly shows that the sample has not been fully saturated with the gas yet, because that would result in a straight line.

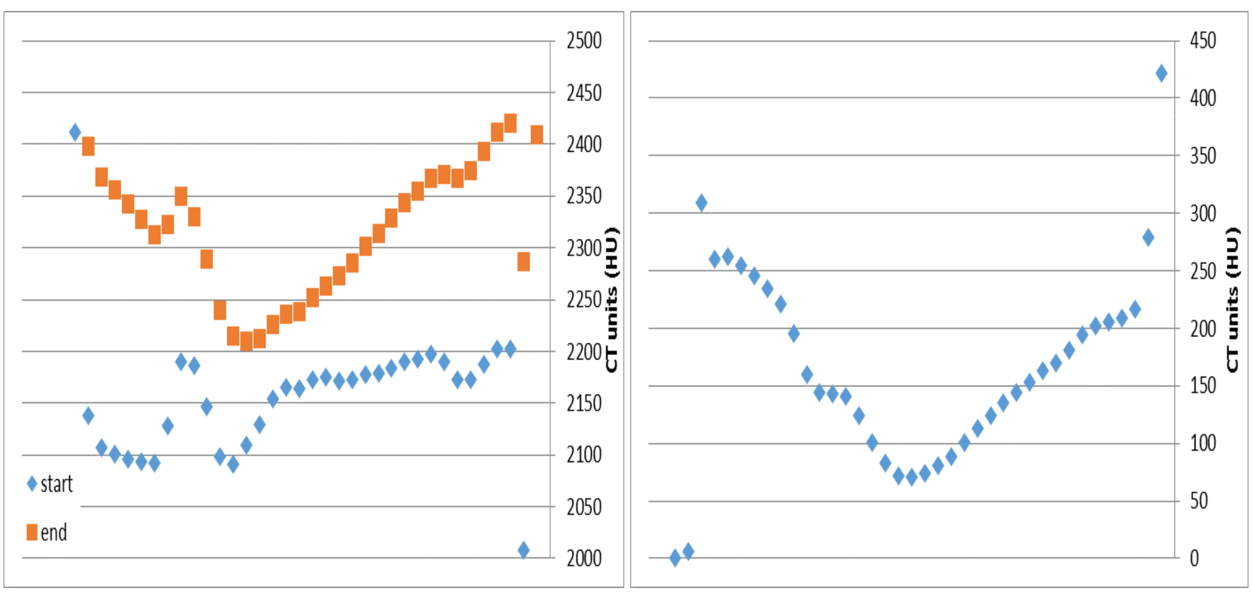

Figure 4.24a (left): Plot of the CT measurements of EBN20 radial, with the results before and after flooding with xenon. 4.25b (right): Plot of the difference after and before the flooding. Both are displayed over the length of the core with the expanded xenon entering on the left hand side of both figures.

4.3. Sorption effects: Methane expansion

This section discusses the results when helium is replaced by methane as the expanded gas. The main point that will be discussed are the sorption effects and what role they play on the matrix porosity.

For the methane samples, the same is true as discussed in the round robin section (4.1.1). With the crushed GRI test it is not possible to derive a consistent permeability value for the measured samples. This will therefore not be discussed in the crushed results section.

For the full core experiments, the inversions are conducted using Enable software. For this study the sorption effects are not taken into consideration in the model. That means that the model only describes free gas flow and not boundary flow of the absorbed gas. That means that there will already be an uncertainty factor on the matrix porosity. Therefore, permeability results from the history matches with the methane expansion are rather ambiguous. These results will not be discussed in the same amount of detail as the matrix porosity results.

4.3.1. Crushed results

First of all the results of the Langmuir experiment will be discussed. Results of the experiment on all samples tested in the round robin experiments are plotted in Figure 4.26. Although the isotherm for the sample EBN20 continues to increase, all samples represent Langmuir Type 1 sorption behavior, meaning they converge and reach a plateau in the end (Perry & Chilton, 1973).

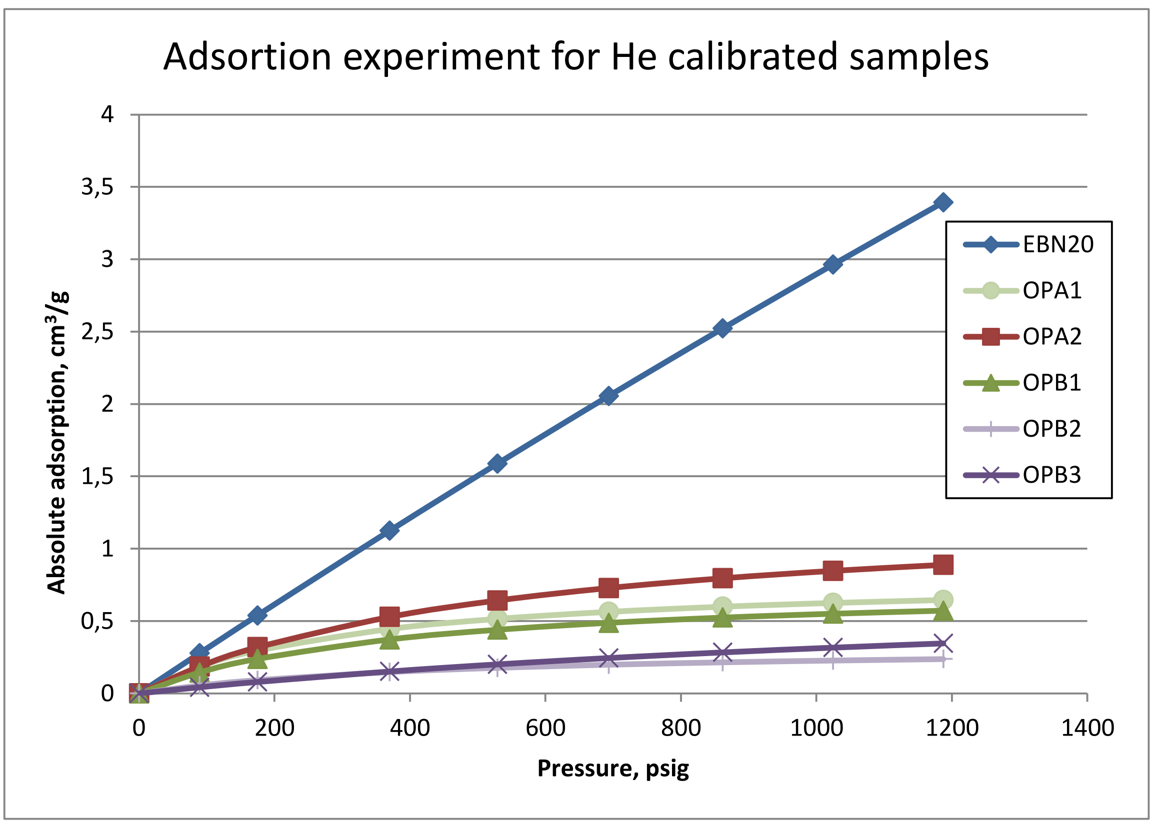

Figure 4.26: Langmuir curves for methane calibrated with helium of the tested round robin samples.

Among helium calibrated samples, EBN20A showed continuously increasing adsorption behavior with pressure, attaining a maximum value of 3.67 cm^3/g at the pressure of 1200 psig (Figure 4.27a). It can be seen that some of the graphs are showing decline (Figure 4.28). However, that is ignored in calculations (Table 4.5).

Among krypton calibrated samples, EBN20B again showed the highest adsorption value: 1.26 cm^3/g at a pressure of 1200 psig, whereas OPB1 exhibited the lowest adsorption value of 0.22 cm^3/g at the same pressure.

Table 4.5: Summary of the experimental results of the Langmuir curve experiment and calculated parameters.

Sample	Exp. Cal. He Density, g/cm^3	Exp. Cal. Kr Density, g/cm^3	Max. Exp. Pressure, psig	Max. Abs Ads, cm^3/g	V_L, cm^3/g	P_L, kPa	TOC
EBN20	2.67	N/A	1256	3.67	39.56	87226	5.67
OPA1	2.70	N/A	1194	0.56	0.81	2101	2.54
OPA2	2.73	N/A	1196	0.78	1.29	3655	4.43
OPB1	2.73	2.64	1243	0.59	0.75	2609	3.27
OPB2	2.62	N/A	1063	0.18	0.33	3106	3.21
OPB3	2.75	2.63	1190	0.34	0.82	11315	2.01

After adsorption, the desorption is also recorded. In Figure 4.27 the difference between adsorption and desorption, hysteresis, can be seen for two samples. In the appendix all plots are available. Samples OPB1 and OPB3 show differences between adsorption and desorption (Figure 4.27b), while the other samples show little or no hysteresis, as can be seen for sample EBN20 in Figure 4.27a.

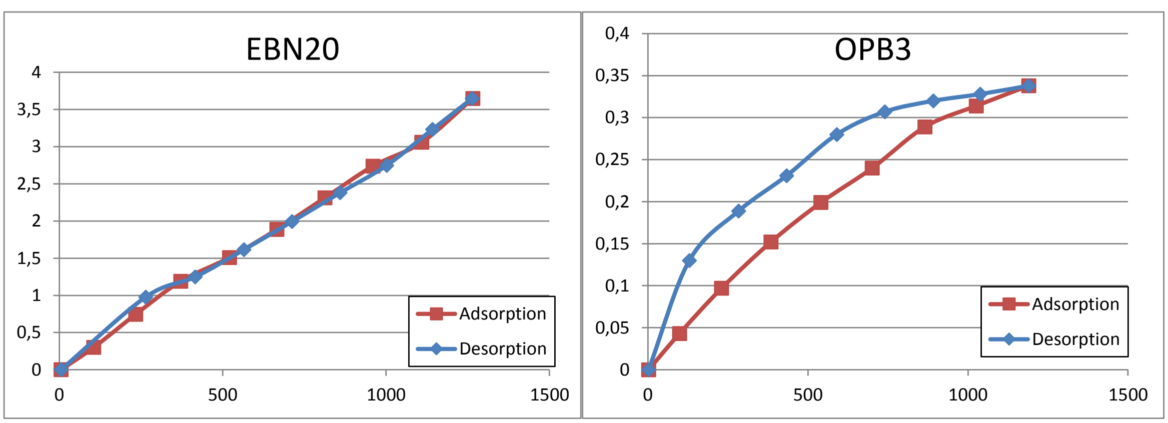

Figure 4.27a and b: the Langmuir adsorption and desorption curves for the samples EBN20 and OPB3, both calibrated with helium.

The effect of the two different gases used for the calibration process on the obtained adsorption values can be seen in Figure 4.28 for sample OPB2. Calibration with helium results in lower adsorption values than calibration with krypton. The explanation for this phenomena is the difference in the molecular size of the gases, as explained in earlier sections. Krypton has a molecular diameter of 40nm, more than 1.5 times larger than helium.

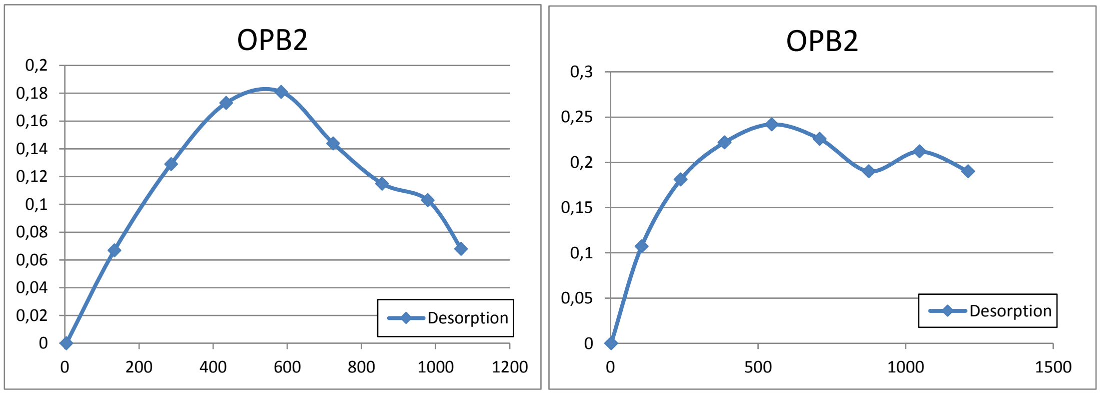

Figure 4.28a and b: Langmuir curve desorption curves for sample OPB2 calibrated with helium (left) and krypton (right).

Table 4.6 and Table 4.7 show the derived results of the samples at the different pressures conducted on the crushed samples during the crushed GRI experiments for both gasses in the Wolfson Laboratory.

Table 4.6: The GRI results for the different gases for the sample EBN20.
Source: Rybalcenko & Leeftink (2015 in press.)

Gas	Pressure step, psig	adsorb vol, cm3/g	porosity from test, frac	Porous vol, cm3/g	PV corrected porous vol, cm3/g	overall porous volume, cm3	real/real poro ratio CH4/He	theoretical/ real ratio CH4/He	theoretical/ real ratio CH4/CH4
He	176.63	N/A	0.071	0.028	0.368	21.07	0.84	2.86	3.57
He	114.73	N/A	0.073	0.029	0.257	14.76	1.75	5.29	2.59
He	210.46	N/A	0.070	0.028	0.430	24.65	0.62	2.28	4.26
CH4	72.21	0.74	0.131	0.052	0.310	17.79	N/A	N/A	N/A
CH4	123.74	0.91	0.112	0.048	0.451	25.85	N/A	N/A	N/A
CH4	63.69	0.71	0.123	0.050	0.268	15.37	N/A	N/A	N/A

Table 4.7: The GRI results for the different gases for the sample OPA2.
Source: Rybalcenko & Leeftink (2015 in press.).

Gas	Pressure step, psig	adsorb vol, cm3/g	porosity from test, frac	Porous vol, cm3/g	PV corrected porous vol, cm3/g	overall porous volume, cm3	real/real poro ratio CH4/He	theoretical/ real ratio CH4/He	theoretical/ real ratio CH4/CH4
He	68.54	N/A	0.142	0.059	0.334	21.18	1.59	1.94	1.68
He	119.83	N/A	0.131	0.055	0.501	31.72	1.52	1.95	3.11
He	161.36	N/A	0.124	0.052	0.619	39.19	1.24	1.58	3.10
He	197.79	N/A	0.131	0.055	0.789	50.02	0.92	0.82	1.67
He	197.79	N/A	0.120	0.050	0.723	45.78	0.68	1.36	3.09
CH4	63.62	0.12	0.240	0.100	0.533	33.76	0.74	1.96	3.08
CH4	115.55	0.22	0.206	0.086	0.762	48.26	1.06	1.58	N/A
CH4	115.55	0.22	0.207	0.086	0.765	48.43	0.86	2.93	N/A

A graphical comparison of porosities obtained using methane and helium is shown in Figure 4.29 and Figure 4.30. The porosity results are derived using Boyle's Law. It can be seen that the porosity values obtained with the crushed GRI experiment differ considerably between helium and methane. To explain the differences mass balance equations were computed. First, the obtained porosities were converted into porous volume per gram of the sample using the density values from Table 4.5. After that the obtained result was corrected according to the ideal gas equation ($P_1V_1 = P_2V_2$).

The obtained value represents the adsorbed amount of gas per sample per gram at each pressure. After multiplying it by the corresponding experimental weight, the overall adsorbed amount of gas was obtained for each pressure and gas. Ratios shown by the column "real/real poro ratio" of these values were made to compare the difference between each gas. Although, as shown in Table 4.6, the values that were obtained from measurements with much higher experimental pressures compared to the rest of the measurements have a higher amount of helium in the sample than methane. That shows theoretically expected behavior of methane showing higher value. For the OPA2 sample a couple of similar outliers can be seen, caused by high experimental pressures (Table 4.7). Therefore it would be better to perform and compare the experiments at the same pressures.

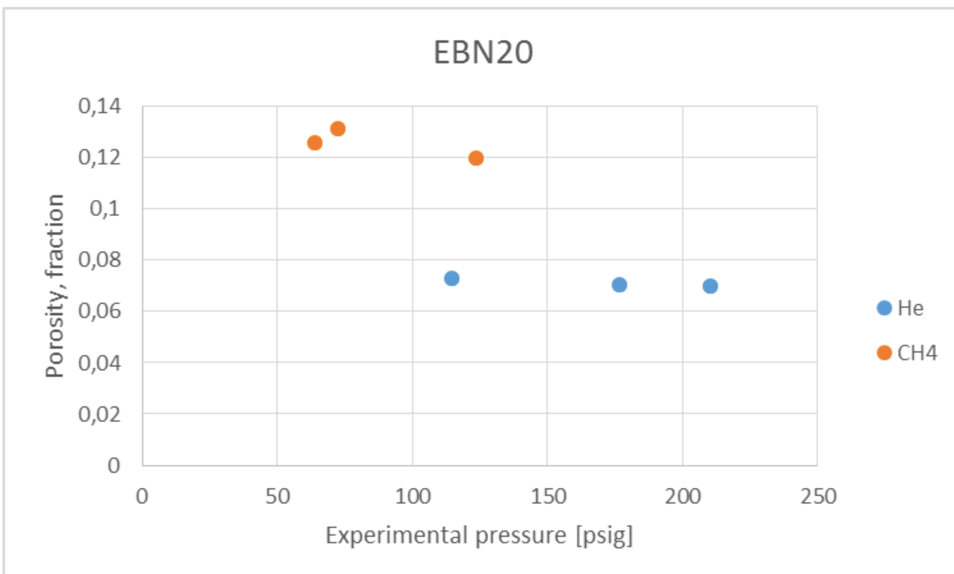

Figure 4.29: The porosity difference between helium and methane in the crushed GRI measurements for the EBN20 sample, calculated using Boyle's law.

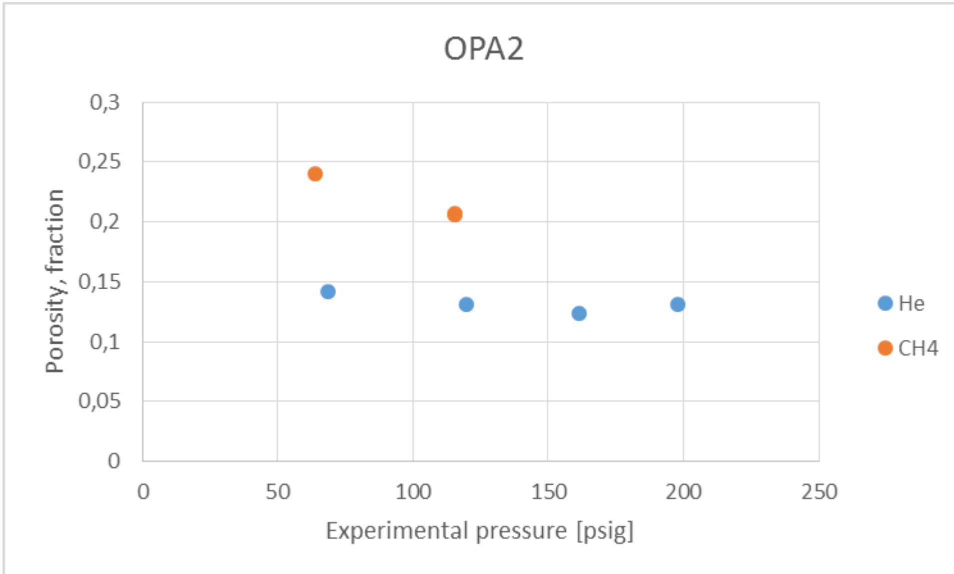

Figure 4.30: The porosity difference between helium and methane in the crushed GRI measurements for the OPA2 sample, calculated using Boyle's law.

Another value for EBN20 in Table 4.6 shows the experimental difference between helium and methane sample volumes of about 1.7 times, whereas the actual theoretical volume due to adsorption should be around 5.3 times higher. It can be said that the sample during the methane experiment did not reach equilibrium and the experiment was stopped too early. Hence, the methane did not have enough time to flood the sample completely. Figure 4.31 shows that the pressure decay curve has not reached equilibrium yet.

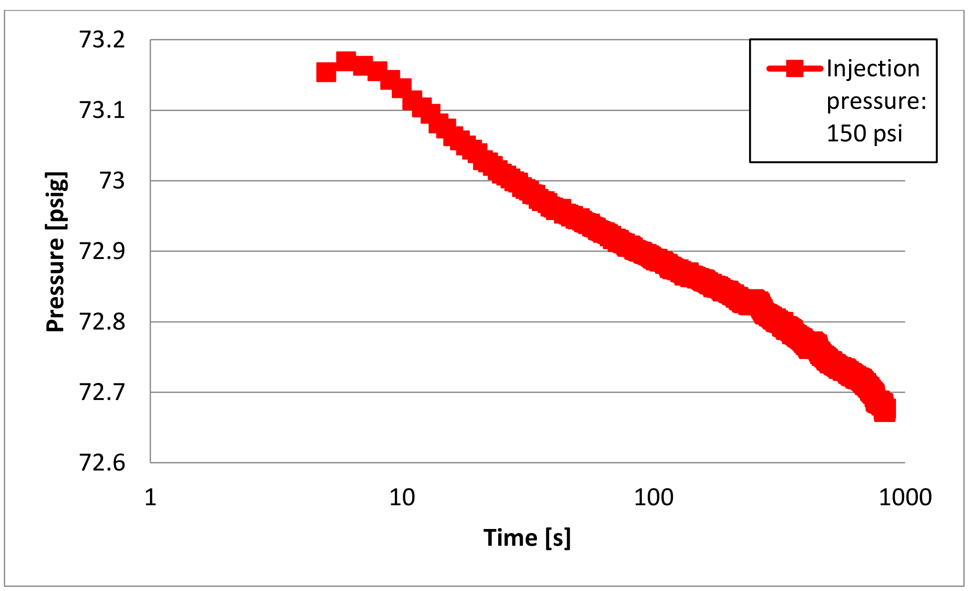

Figure 4.31: Pressure decay curve of expanded methane on crushed shale GRI experiment of EBN20 that has not yet reached equilibrium.

The OPA2 sample, on the other hand, shows much more consistent ratios between the actual experimental and theoretical porous volumes: around 1.5 and 1.9 respectively. Timing of the methane experiment was also probably not long enough. The shape of the pressure decay curve for OPA2 is more or less the same as Figure 4.31, but the ratios are more similar than for EBN20.

If the experiments would have run for a longer period of time, the full potential sample volume shown by methane experiments could prove to be larger. The ratios of full methane adsorption values to the actual methane experiment results are shown in the last columns of Table 4.6 and Table 4.7. It can be seen that potentially sample volume could have been around 3 times higher for both EBN20 and OPA2. The reason that these values were not reached might be caused by insufficient time span of the experiment or that the samples were not crushed in small enough particles. The last effect could be an important point of focus as for the Langmuir experiment, the shale sample was crushed to smaller particles (d<0.40mm) than for the GRI experiment (0.5mm<d<0.85mm).

4.3.2. Core plug results

The matrix porosity of the crushed samples has been calculated with Boyle's Law, while the full core results have been derived differently. These results have been calculated using the same algorithm used for the helium, except that the properties of the expanded gas were changed. This means that the Eclipse simulation does not include the sorption effect of methane. Due to adsorption more gas is ventilated into the downstream volume, the simulator will see this as free gas and hence overestimate the derived matrix porosity.

From the methane expansion experiments it can be seen that the full core results of the matrix porosity are significantly lower than the crushed results (Figure 4.32). This can partly be explained by the sorption effects, because more organic content is accessed by the expanded gas with the crushed experiment, than with the full core experiments. Hence, more gas could be adsorbed by the organic content. This results in a higher matrix porosity with the single porosity-permeability model for the crushed GRI test (Figure 4.32), as it does not account for sorption effects.

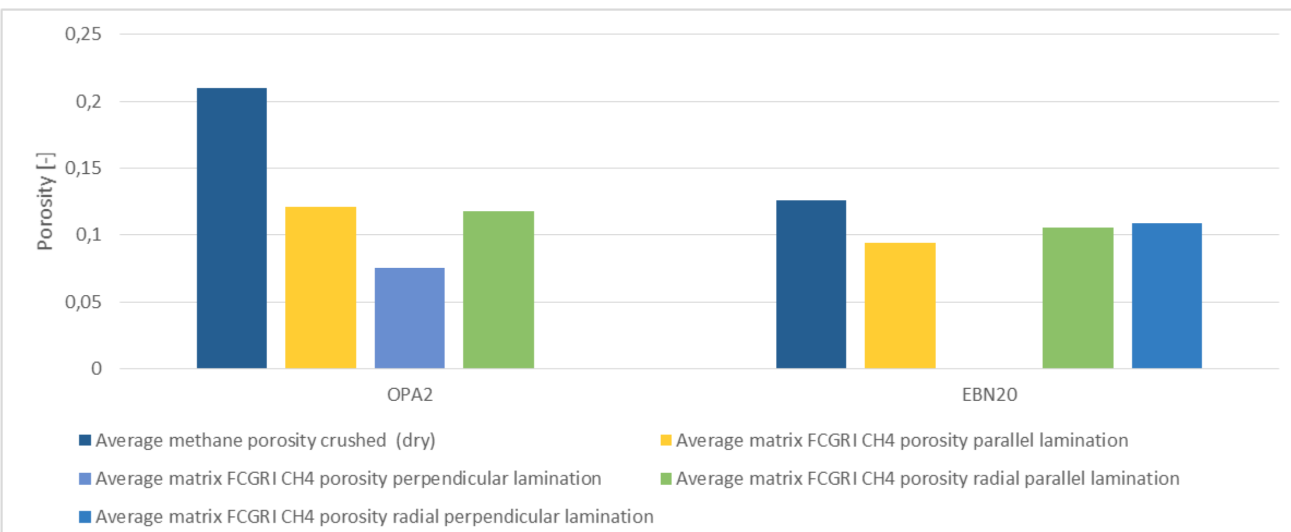

Figure 4.32: The matrix porosity differences between the full core and crushed experiments for the samples OPA2 and EBN20.

When looking at the matrix porosity differences for the variations described in the helium section, more or less the same observations can be seen as described in section 4.1.2.2. Figure 4.32 shows that the samples drilled parallel to their lamination have a higher porosity. However, the lamination effect is less significant than shown in the helium section. The reason is that the samples for methane expansion have not been measured under confined conditions. That means that the difference in experimental set-up is not tested.

Other variations in the set-up, show the same conclusions as discussed in the helium expansion section. This means that the matrix porosity is higher for the radial drilled samples than the linear samples. The same accounts for the simulations. When the samples that were measured with the methane expansion experiment are computed with a high permeability streak or take into account the gas slippage correction – their matrix porosity results are lower – than when these variations are disregarded.

Figure 4.33 shows that the matrix porosity of the samples flooded with methane give higher results than when helium is expanded. Therefore the same trend is observed as the crushed material, which could be seen in Figure 4.29 and Figure 4.30.

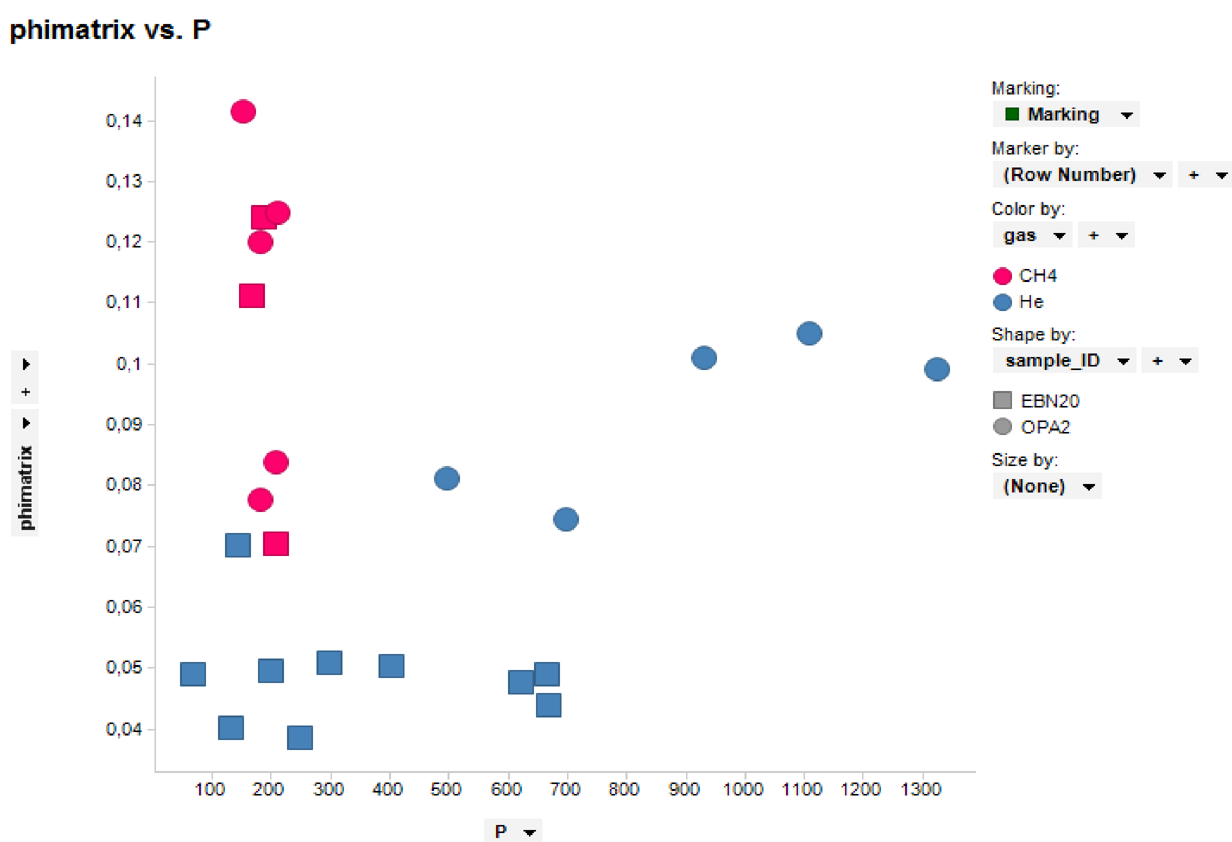

Figure 4.33: In full core GRI measurements, the matrix porosity is higher when samples are flooded with methane than with helium.

The matrix porosity derived from crushed GRI tests is taken as a fixed input parameter in the history matching model. Using this fixed value for the matrix porosity makes it easier to assess the results of the derived matrix permeability. Figure 4.34 shows that matrix permeability results for the methane samples are about half an order of magnitude higher. However, it must be questioned how realistic the matrix permeability results are, derived with the current algorithm. In the script of the model, it does not include adsorption and therefore it does not regard other flows than free gas flow, such as boundary dominated flow (Mengal, 2010). Next to that, the matrix porosity has also probably been overestimated, as discussed in the introduction of 4.3. Matrix porosity is used as an input parameter for the calculation of matrix permeability, therefore it is likely that there will be an overestimation in this parameter on its turn.

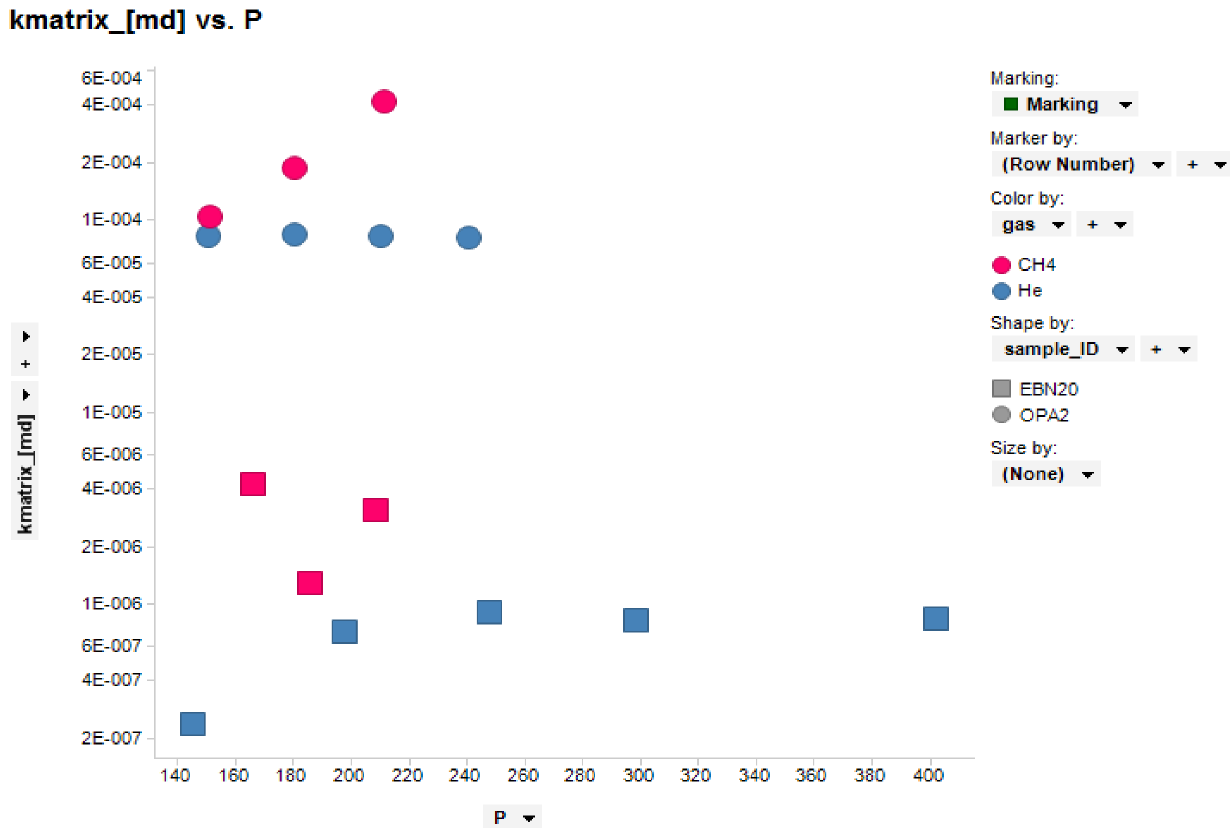

Figure 4.34: In full core GRI measurements, matrix permeability is higher when samples are flooded with methane than with helium. The results depicted are the samples EBN20 and OPA2 with fixed matrix porosities from the crushed GRI tests.

5. Evaluation

In this section the main findings from the discussed results will be combined to evaluate the most important outcomes for the scope of this work.

5.1. Crushed shale tests only consistently measure porosity, not permeability

When the round robin results are evaluated and compared for permeability results in Table 4.4 and Figure 4.4, the differences in permeability between the different laboratories stand out. Several orders of magnitude is the difference in matrix permeability for the same sample.

The main reason for this difference is that the measured volume has no internal structure after crushing. That makes it impossible to accurately compute permeability from the measurements of the crushed shale tests. Even after trying to invert the data with multiple porosity-permeability models the results differ orders of magnitude (Figure 5.1). There is also little consistency in the results when the same experiment is performed multiple times.

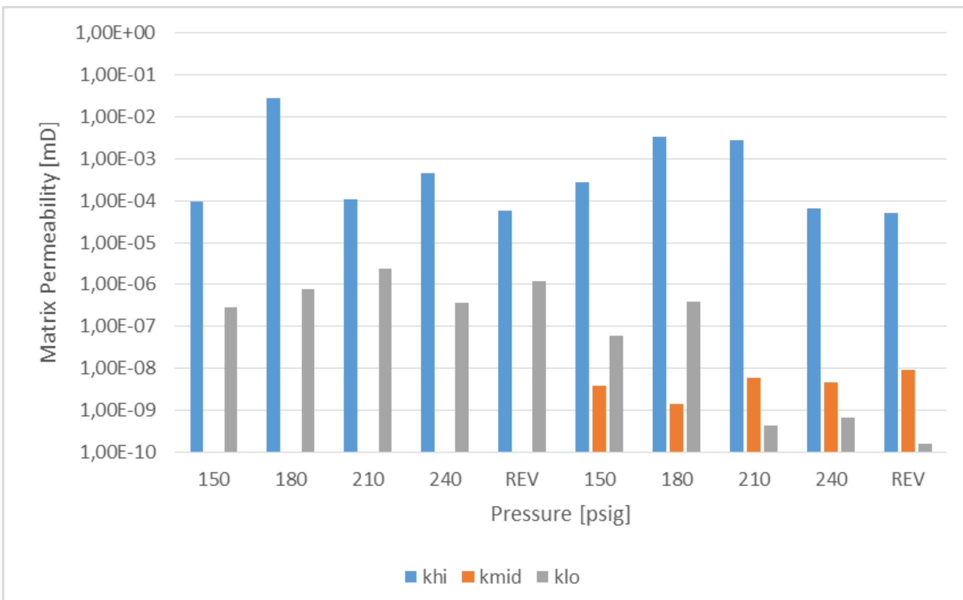

Figure 5.1: Matrix permeability measurements of dried crushed shale test on OPA2 with a double and triple porosity-permeability model. Khi, kmid and klo stand for the three regions in the multiple porosity-permeability model. With a double porosity-permeability model, there is no data for kmid as this second region is combined with the third region. See 3.2.1.1 for more information on what these regions characterize.

The crushed GRI tests do give an aligned matrix porosity between different laboratories (Figure 4.3 and Table 4.3).

The computed matrix porosity from full core measurements has a larger scatter for various tests and pressure steps than the results of the crushed GRI test (Figure 4.8). Therefore it is opted to use the porosity derived from the crushed experiment as an input value for the full core model. This would decrease the uncertainty of the inversion. It removes one of the unknown parameters in the history matching. An additional advantage is that the crushed test takes shorter to equilibrate than the full core experiments. Therefore, with less parameters to compute, the results are less prone to measurement errors. All in all, the matrix permeability can be derived with greater consistency using the porosity from the crushed measurements as an input parameter for the inversion of the full core experiments.

5.2. Combination of experiments yield best results

Two distinct sets of results are derived when a single porosity-permeability model for the inversion of the measurements is used. These data points are grouped in two areas on a matrix porosity-permeability chart. The cloud of data points on the top right of the graph have a relatively high porosity and permeability, while the other cloud has a relatively low porosity and permeability.

Two results for the permeability and the porosity are derived, when using a double porosity-permeability model. In an earlier section this model is described in more depth (3.2.1.1). The high end of the porosity and permeability results describe the initial settling of the free gas in and around the grains of the full core plugs. The low end of the results resemble the long time tail behavior (Figure 5.2).

A single porosity-permeability model also can describes these two phenomena, but the results are dependent on the experimental set-up.

The lower porosity-permeability relation is derived from the core plugs that give the highest resistance to flow of the expanded gas. This results in a plug which is drilled perpendicular to its lamination and is confined in the MDP to give the best results for the lowest production region. With these experiments, the expanded gas is forced through the most difficult flow paths (bottom left of Figure 5.3).

The high porosity-permeability zone is best characterized by the experiment where the core plug has the least boundaries to flow. Therefore the full core GRI measurement on a radial core plug where the prevailing lamination direction is parallel to the flow gives results in top right section of the graph. In this set-up, the expanded gas has the most surface contact of all experiments done (top right of Figure 5.3).

In Figure 5.4 the results of the single porosity-permeability models of the two most extreme experiments explained above are plotted and compared to the results of the double porosity-permeability model. Both the matrix permeability and the matrix porosity align very well.

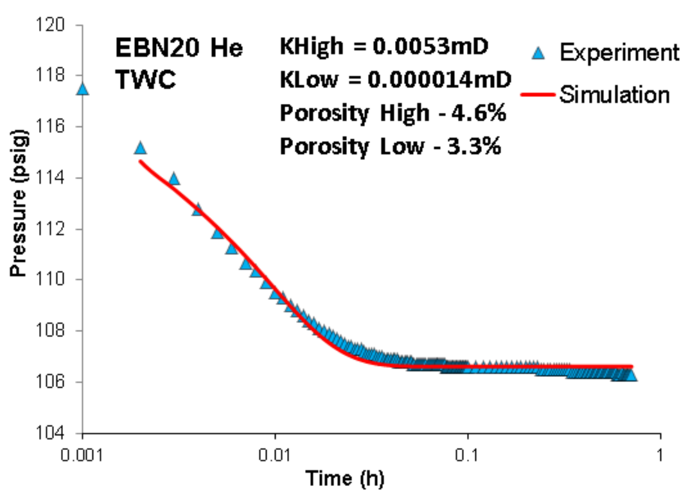

Figure 5.2: The simulated results with a multiple porosity-permeability model overlap the experimental results for a MPD test on a radial perpendicular drilled core of EBN20

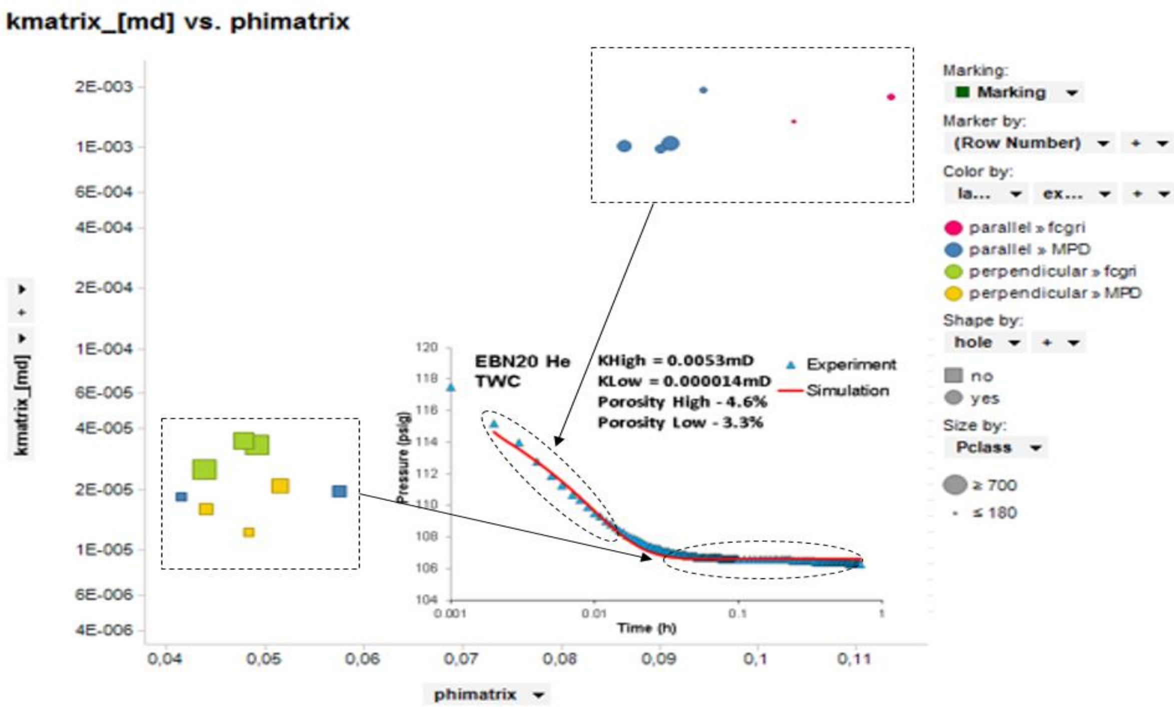

Figure 5.3: The multiple porosity-permeability model explained by different experiments on the EBN20 sample.

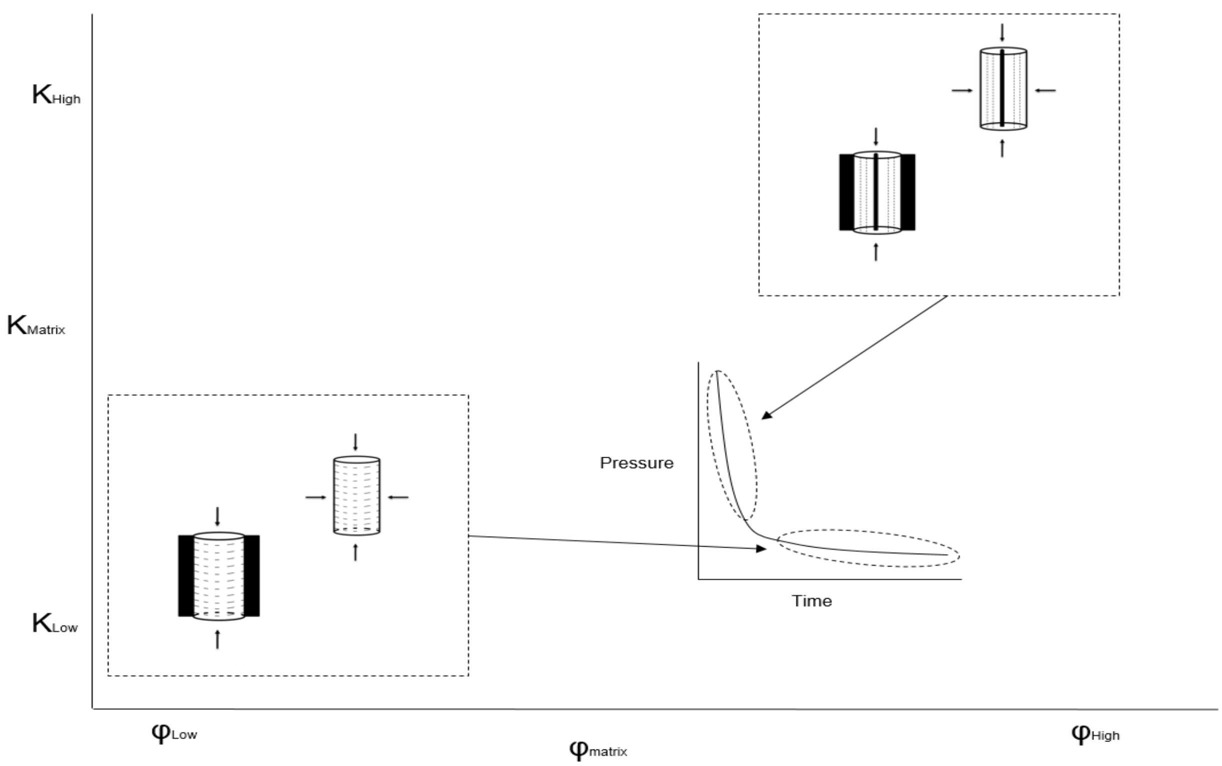

Figure 5.4: A schematic overview of the multiple porosity-permeability model explained by a schematic overview of the different experiments.

All other experiments (described in 3.1) are combinations of the high- and low-end configurations mentioned above. These experimental set-up combinations give porosity and permeability results that are situated on the trend line between the minimum and maximum set-up configurations.

Figure 5.4 depicts that the results of the full core GRI test on a linear plug drilled perpendicular to its lamination give higher porosity and permeability results than the same plug in the MPD, both are on the bottom left hand side of the graph. At the other end of the spectrum, a confined radial sample drilled parallel to the lamination gives a lower porosity and permeability than the configuration yielding the highest results, both are situated at the top right part of the graph. In Figure 5.5 the experiments are ordered by increasing matrix permeability. Plotted porosity is the derived porosity from the crushed experiments. A logical sequence from low to high permeability can be seen. The more surface area available to penetrate for the expanded gas, the higher the permeability.

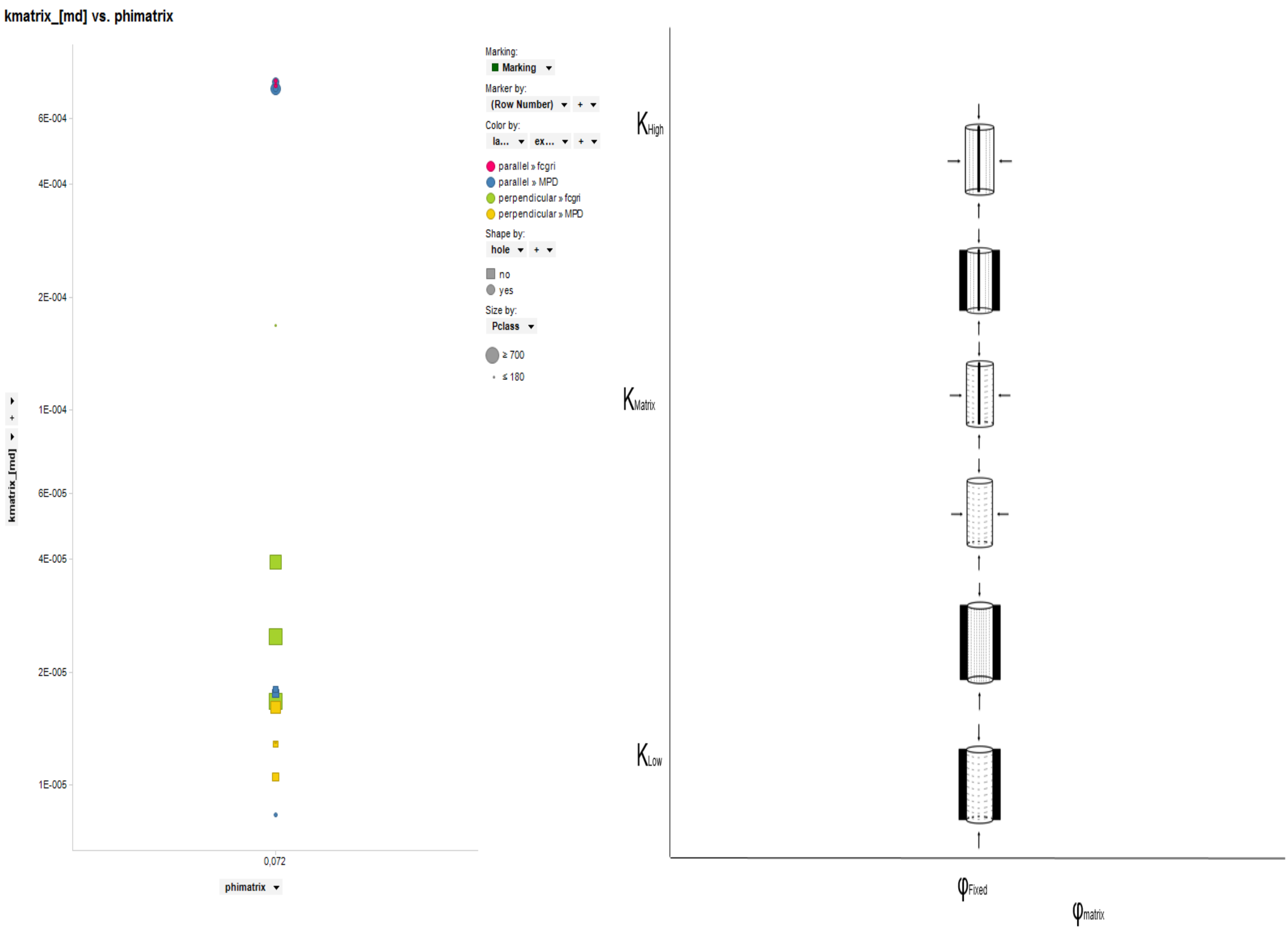

Figure 5.5a (left): The matrix permeability inversions from the different experiments with a fixed porosity of the EBN20 sample and 5.6b (right): a schematic overview of the order of results in permeability of those experiments.

5.3. Outcomes of using helium versus methane as expansion gas

When looking at the results of the Langmuir experiment, a strong positive correlation between adsorption value and TOC value can be seen in Table 5.1.

Table 5.1: Relation between TOC and adsorption of the tested round robin samples.

Sample	TOC	Max. Abs/Ads, cm^3/g
EBN20	5.67	3.67
OPA2	4.43	0.78
OPB1	3.37	0.59
OPA1	2.54	0.56
OPB3	2.01	0.34

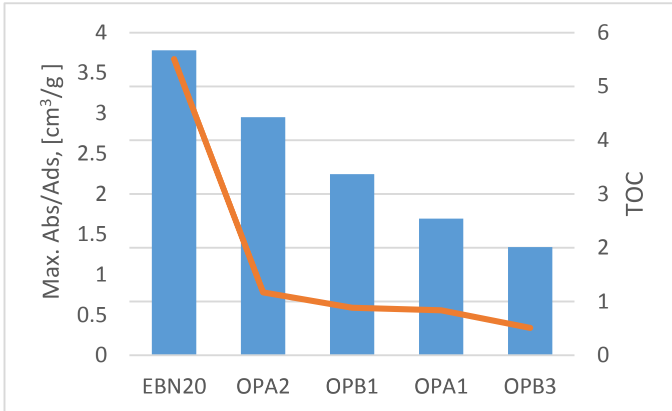

Figure 5.7: Relation TOC and adsorption of the tested round robin samples.

One should note that these experiments have been conducted at a fixed temperature of 30˚C and at relatively low pressures compared to reservoir conditions. As known from literature, the temperature and pressure play a significant effect on adsorption. Therefore it becomes harder to predict how significant these adsorption results are under subsurface conditions. The recorded Langmuir curves all show Type 1 sorption behavior, so pressure effects will probably not change the absolute adsorption after the plateau at a high pressure (>1000psig) is reached. The apparent porosity difference between helium and methane probably will become smaller at the higher temperatures present in a reservoir, because adsorption decreases under increasing temperature (Freundlich, 1906). However, there is no argument against the observed trend that more is adsorbed when the formation has a higher TOC.

5.4. The effect of the Klinkenberg factor on matrix permeability

The effect of pressure on the Klinkenberg correction factor and matrix permeability as a function of pressure is clearly seen in Figure 5.8. The lower the pressure, the more dependent the gas becomes on the slippage factor. This correction can significantly decreases the matrix permeability. The results plotted in Figure 5.8 therefore compare well with literature (Profice, et al., 2011) and Equation 5.

What this would mean for the subsurface conditions of the shale plays is hard to say, because pressures are considerably higher in subsurface conditions than in these experiments. The Klinkenberg correction factor will be greatly reduced when the trend of Figure 5.8 is extrapolated to reservoir pressures.

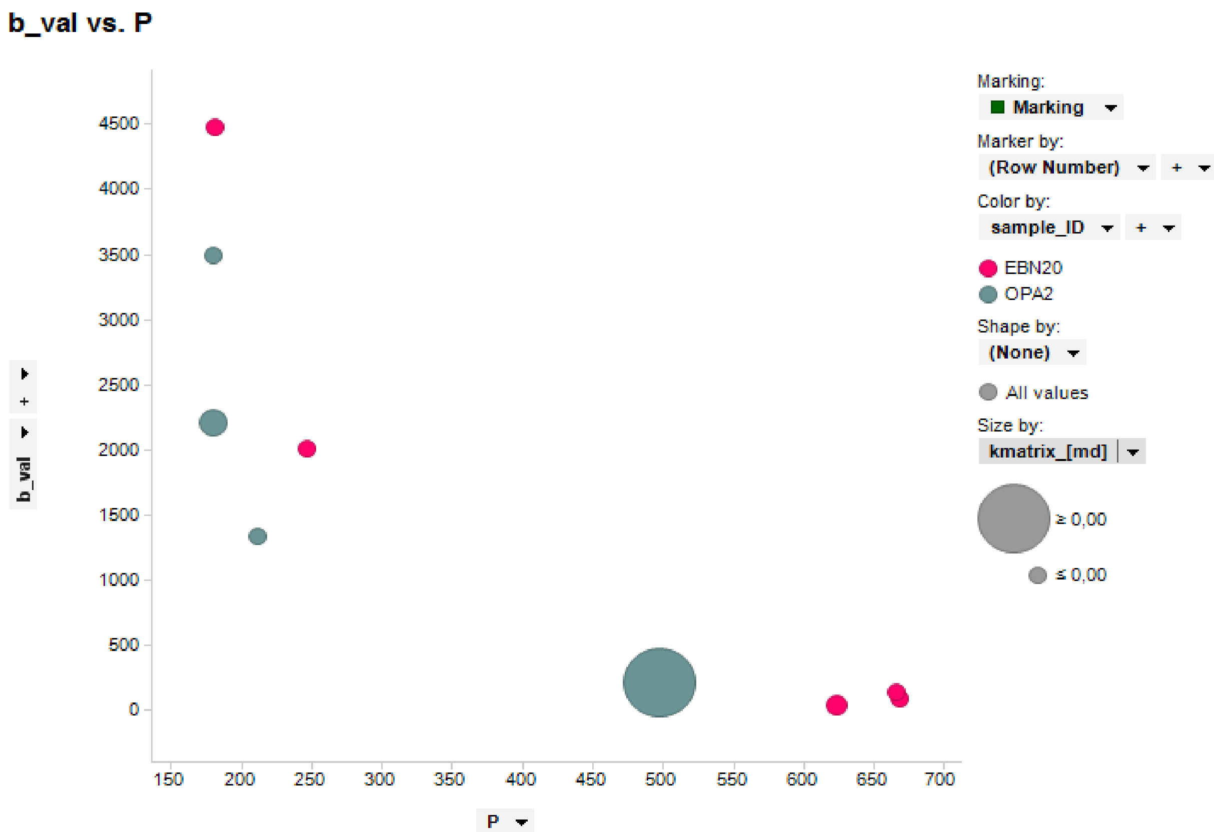

Figure 5.8: The dependency between b factor and pressure for the samples EBN20 and OPA2. The matrix permeability is increasing with the size of the points.

The trend of the results computed with the Klinkenberg factor correspond more or less with a large dataset of tight reservoirs (Figure 5.9). The scatter is mainly due to uncertainties caused by the ultra-low permeabilities and other composition of shales compared to tight sandstones.

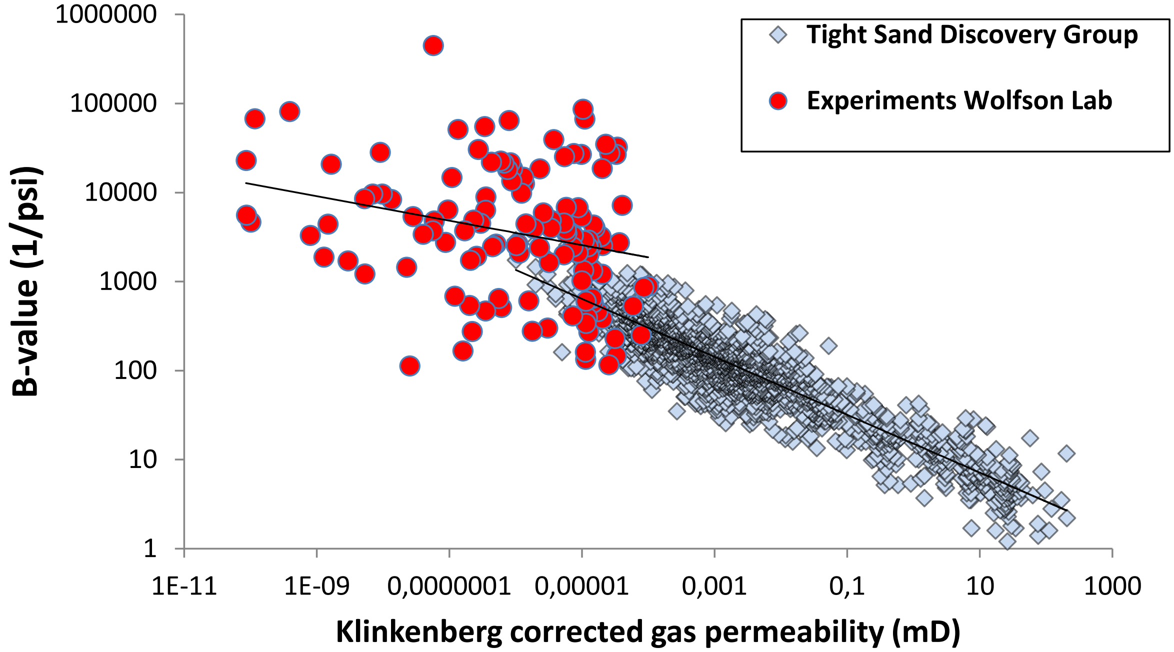

Figure 5.9: A comparison between a set of tight sands modelled with the Klinkenberg gas slippage factor and the experiments conducted in the Wolfson Lab for the purpose of this study.

Figure 5.10 is a more detailed plot of the simulated data shown above. The results of matrix permeability versus gas slippage correction factor from different samples correspond more or less with the trend line from Figure 5.9. However, when zoomed in, two clear relations can be seen; one between the linear samples of EBN20 and OPB2 and the other between the radial tests on the EBN20 sample and linear test on the OPB1 sample. These two trend lines of the different samples are also more or less parallel to each other. What exactly causes this shift and why the data is so aligned needs further investigation.

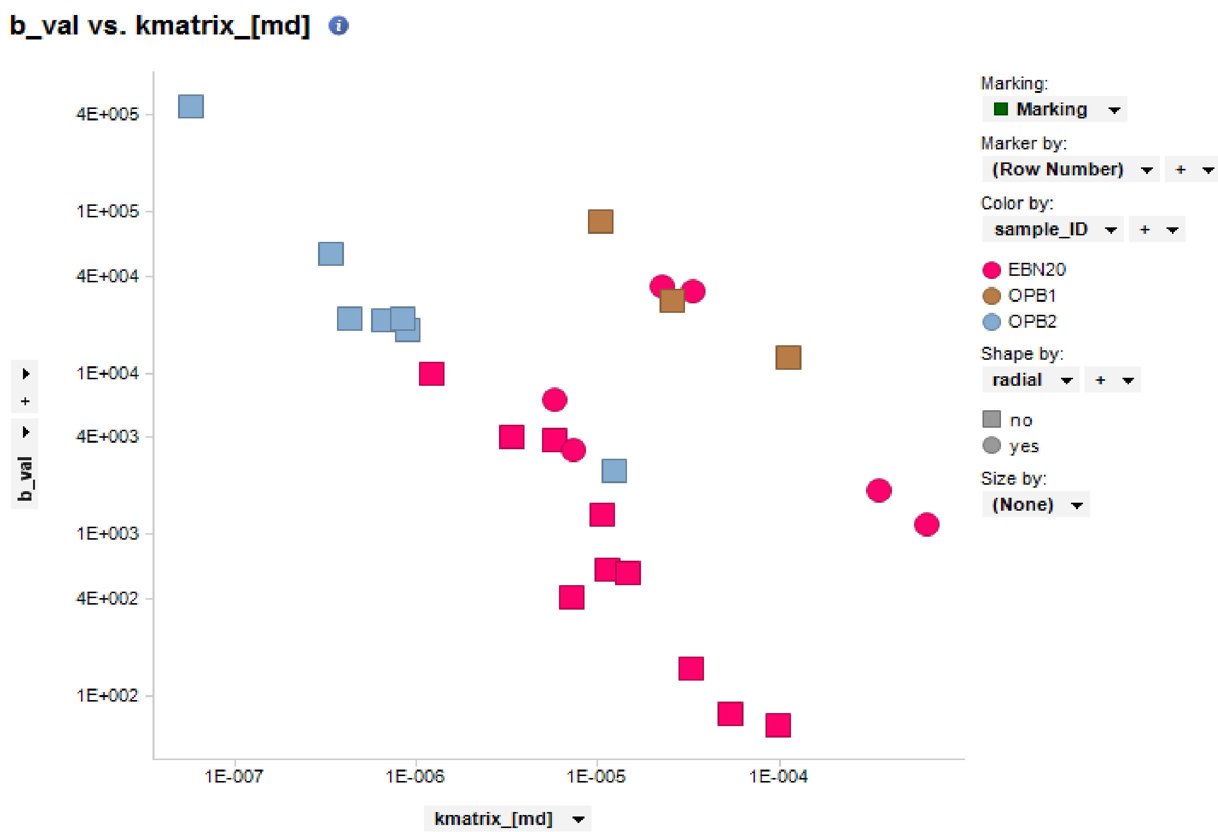

Figure 5.10: A relation between matrix permeability, Klinkenberg correction factor and pressure seems to be the same for multiple samples.

6. Conclusions

In this thesis alternative methods were studied to improve the understanding of the petrophysical properties of shale for hydrocarbon production. Currently, there are no industry standards for the measurements of these heterogeneous formations. That this provides problems is especially signified when the permeability values of multiple samples were tested in a round robin test between renowned laboratories. For the same sample the permeability differs several orders of magnitude. This study compares several experimental set-ups and various ways of history matching the measured data to compute porosity and permeability values for the tested samples. The basis of the conclusions come from a large dataset built up during the SHAPE project, broadened with all the experimental and inverted results done during this study. Even though the data is quality checked on multiple fronts, it should be noted that the uncertainties in these shale samples are relatively high. This is due to the fact that the formations, where the samples are taken from, are extremely heterogeneous. Secondly, as the shale has extremely low permeability (nano- to picoDarcy) every irregularity, such as leaks, a change in temperature or a too short equilibration time, will affect the generated data enormously.

By expanding different gases in the tested core plugs, different petrophysical properties are monitored. Helium gas was used to compare the widest range of the different experimental set-ups and core preparations. The effect these alterations have on the computed porosity and permeability has been studied. Xenon was expanded under a CT-scan in order to study the propagation of the gas through the sample. Methane was expanded on a range of samples prepared differently to study the sorption behavior of these black shales.

The round robin experiment was performed by all labs on crushed shale material. The results of this test clearly show that deriving matrix permeability with crushed shale tests is unreliable. Even if the same experiment is performed multiple times in the same set-up, results differ by orders of magnitude. However, the crushed GRI tests do give a relatively reliable outcome of matrix porosity. Hence, this study opts to only use the matrix porosity results from the crushed shale test and derive the matrix permeability from the full core experiments.

By performing a couple of relatively short tests and history matches, a swift insight on the formation's porosity and permeability can be obtained. A double porosity-permeability model can provide these results. That result can be verified with the outcomes computed with a single porosity-permeability model from a confined set-up for a linear plug and an unconfined experimental set-up for a radial plug. By coarsely calibrating the result in this way, these results give a more reliable outcome than the current techniques used. The combination of these various tests could be seen as a new standard of measuring these properties. Additional advantages are that the core holders used for these tests are easy transportable and the tests and inversions are relatively quick. Therefore they could even be used next to the drill site, although temperature variations may alter results.

Xenon expansion in shales under a CT scan gives some insights of the studied sample. However, the resolution remains too low to clearly see the path of the gas on the CT scan cross sections. Using data analysis tools, propagation of the xenon over time can be monitored when measured data is extracted from these images. More information on when steady state is reached can be derived, because the density of the gas in the pores in all cross sections can be measured.

Even though methane has a larger molecular diameter than helium, the computed matrix porosity of methane is higher in both crushed and full core experiments. These calculations are based on Boyle's Law and a history match model, which do not include sorption effects. The results from a Langmuir experiment on crushed shale of the round robin samples show that the adsorption and absorption are a crucial part of understanding the gas trapped in these nano- to picoDarcy formations. The amount of organic content is important for the amount of sorption (Figure 5.7). Tested samples with the highest TOC also had the highest maximum adsorption and the samples with the lowest TOC value adsorbed the least gas.

The gas in these shales which consist of small pore throats approach the mean free path of the gas, therefore a gas slippage correction factor on permeability is implied in one of the simulation variations. This Klinkenberg factor reduces with increased pressure along the same trend for multiple samples. If this trend is extrapolated to reservoir conditions where pressure is even higher, this effect reduces significantly.

7. Recommendations

In order to align all results, it would be better to take fresh sample material and redo the most important tests discussed in this study. As there is no log or history record available of what tests have been performed on the used samples, it is unclear how they were damaged. Known is that the EBN samples are over 40 years old, so at least all saturations will be altered. What also is known is that all samples have been tested with high pressure mercury injection, before these gas expansion tests. This probably has changed the pore network and (micro) fractures within the core plugs. Probably these are not the only modifications these samples have gone through.

If new fresh material is obtained, it would be advised to maintain those cores under reservoir conditions. Especially the difference in pressure between (in-situ) subsurface and standard conditions can change the properties of the shale significantly. Due to the relaxing of the stress on the sample, (micro) fractures can be formed. These thoroughly change the petrophysical properties of the core plug, as can be seen from the simulations when a high permeability streak is incorporated in the model.

The model used to history match the experiments has numerous assumptions. Studying these closely and enhancing the model would give more realistic results. A couple of the important assumptions that should need reconsideration are including saturation and relative permeabilities in the sample, homogeneity of the sample and interaction of the expanded gas with the grains of the sample.

Additional research is recommended to investigate the xenon expansion under a CT scan. After measuring the images before and after the flooding, a clear increase in Hounsfield units is obtained. During the timeframe of this thesis, there was not enough time to learn the details of an image processing software. Therefore, a lot can still be improved in optimizing the processing of the images. This could explain a lot about the flow behavior of the gas. Further analysis on the difference in density of the gas in the pores before and after the experiment and a comparison with the pressure data of the experiments could also show what parts of the sample are not reached by the gas within the time the experiment lasts.

This would give a more realistic image. Adding to that, the larger artifacts that are spotted on the images could also be included to the model as different property zones to make the model less homogeneous and more realistic.

The measurements on these extremely low permeable samples gives a lot of room for error. Quality control on the obtained data is essential. This also means that a lot of the data from performed experiments is not included in the dataset where conclusions were drawn from. The data set is still sufficiently large. Nevertheless, more measurements would mean more data and therefore more proof of the trends discussed. Adding to that, performing the same experiments multiple times would contribute to enhance the data set, which would increase the understanding. Secondly, the uncertainty could be quantified in greater detail of both the measurements and the inversions.

Although the data was quality checked, it cannot be excluded that the used data contains small errors. From the xenon figure it is clear that a complete steady state of the gas in the sample is not obtained within the period of measurement, therefore there are areas within the sample that the expanded gas did not reach and result in a difference in inverted porosity and permeability between experiments.

The inversion of the methane expansion should be studied more closely. The inversion model used in this thesis did not include sorption effects. An option could be to try to include the coal bed methane option in Eclipse in the model or insert the found correlations from the Langmuir curve experiment in the model.

It is advised to study the sorption effect of methane during the measurements under different temperature conditions. Known from literature is that the adsorption is not only dependent on pressure, but also decreases with increasing temperature. Hence it would be interesting to see by how much the amount of adsorbed gas will change when temperature is increased and approaches reservoir conditions.

When the data is modelled including the Klinkenberg factor, the permeability reduces with increased pressure along the same trend for multiple samples (Figure 5.10) and in line with other tight formations (Figure 5.9). This is an interesting trend that needs closer attention. By adding more data points at different pressures for these samples, probably a lot more can already be said. It would be interesting to perform these experiments under reservoir pressures to study the (diminished) effect of the permeability correction.

The proposed experiment in this study to measure samples with greater accuracy is based on a relatively small amount of data. Apart from testing this statement to a larger dataset, different samples within the same formation should be measured. Shales are very heterogeneous, so the ultimate goal is to upscale these findings to judge if a formation is prolific enough to extract hydrocarbons from. The following step would be to test the accuracy of the set-up, so it can be brought to the drill location.

Acknowledgments

I would heartily to thank everyone who helped and supported me during my thesis work.

Firstly I would like to thank Stefan Luthi who helped me with setting up this project and all parties involved. Next to that I would like to thank him for the guidance and support throughout my project.

Secondly, I would like to give my deepest gratitude to Quentin Fisher who made this thesis work possible by organizing all required facets in a very limited time frame. He has enriched me with his commitment, scientific experience and knowledge.

Enormous appreciation goes out to Konstantin Rybalcenko who has helped me a lot during my visits in Leeds, but especially assisted me from Leeds when I got back to the Netherlands. I would also like to thank all the other staff of the School of Earth and Environment at the University of Leeds who have helped me through the course of this work. Especially I would like to thank Sam Allshorn and Carlos Grattoni who helped me with setting up the experiments and discussing them. I also would like to extend a warm word to Ida Shafagh, helping with other measurements, and the rest of the department.

All this would not have been possible without EBN. I would very much like to thank them for all the advice and financial support they provided me with during the eight months I spend at the Daalsesingel and the contribution I could deliver to the SHAPE project. Michiel Harings helped me a lot as a supervisor. Jan Lutgert and Guido Hoetz assisted me enormously with setting up the project and were great sounding boards during my time at EBN. I would like to thank all the other colleagues and student (foosball) interns as well for their hospitality, they helped to bring my skills to a higher level.

Last, but certainly not least, I want to give a very warm thank word to my family, Lies and all my friends who have supported me during this project and the rest of my studies.

T.N. Leeftink

8. References

Billiotte, J., Yang, D. & Su, K., 2008. Experimental Study on Gas Permeability of Mudstones. *Physics and Chemistry of the Earth, Parts A/B/C, Vol 33, Supplement 1,* pp. S231-S236.

Bourbie, T. & Walls, J., 1982. Pulse Decay Permeability: Analytical Solution and Experimental Test. *9744-PA SPE Journal Paper.*

Bouw, S. & Lutgert, J., 2012. Shale Plays in the Netherlands. *SPE-152644-MS.*

Brace, W., Walsh, B. & Frangos, W., 1968. Permeability of granite under high pressure. *Journal of Geophysical Research,* 73(6), pp. 2225-2236.

Bustin, R. et al., 2008. Shale Gas Opportunities and Challenges. *Conference Paper at AAPG Annual Convention, San Antonio, Texas.*

Carl W. Kammeyer, D. R. W., 1972. Quantum Mechanical Calculation of Molecular Radii. Hydrides of Elements of Periodic Groups IV to VII. *The Journal of Chemical Physics, Vol 56, No. 9.*

Chaudhary, A., Ehlig-Economides, C. & Watterbarger, R., 2011. Shale Oil Production Performance From a Stimulated Reservoir Volume. *SPE 147596.*

Chere, N., Boot, P., de Wit, M. & Schultz, H., 2013. Shale Gas Potential of Permian Black Shales in the Karoo Basin. *Thesis Paper, Nelson Mandela Metropolitan University, South Africa.*

Christou, C., Dadzie & Kokou, S., 2015. Direct Simulation Monete Carlo Method in Porous Media with Varying Knudsen Number. *SPE-173314-MS.*

Civan, F., Rai, C. & Sondergeld, C., 2011. Shale Permeability Determined by Simulataneous Analysis of Multiple Pressure-Pulse Measurements Obtained under Different Conditions. *SPE-144253-MS.*

Civan, F., Rai, C. & Sondergeld, C., 2011. Shale-Gas Permeability and Diffusivity Inferred by Improved Formulation of Relevant Retention and Transport Mechanisms. *Transport in Porous Media Vol. 86,* pp. 925-944.

Cluff, R., Shanley, K. & Miller, M., 2007. Three things we thought we understood about shale gas, but were afraid to ask.... *AAPG.*

Crook, T., 2014. Implementation and Validation of a MKodel for Gas Flow in Low Porosity Shale. *University of Leeds paper.*

Cui, X. & Bustin, A., 2009. Measurements of gas permeability and diffusivity of tight reservoir rocks: different approaches and their applications. *Geofluids 9,* pp. 208-223.

East, B., 2011. Porosity - Core Plug Measurements Perspective. *Conference presentation FESM.*

Fisher, Q. & Rybalcenko, K., 2014. Modellig Laboratory Experiments using Eclipse and Enable. *University of Leeds paper.*

Florence, F., Rushing, J., Newsham, K. & Blasingame, T., 2007. Improved Permeability Prediction Relations for Low-Permeability Sands. *SPE 107954.*

Freundlich, H., 1906. Über die Adsorption in Lösungen. *Z Phys Chem 57(A),* pp. 385-470.

Guarnieri, R., 2012. Measurement of Gas Permeability on Crushed Gas Shale. *Thesis Paper, Utrecht University.*

Guidry, K., Luffel, D. & Curtis, J., 1995. Development of Laboratory and Petrophysical Techniques for Evaluating Shale Reservoirs - Final Technical Report. *GRI-95/0496.*

Handwerger, D., Suarez-Rivera, R., Vaughn, K. & Keller, J., 2011. Improved Petrophysical Core Measurements on Tight Shale Reservoirs Using Retort and Crushed Samples. *SPE 147456.*

Handwerger, D. et al., 2012. Reconciling Retort versus Dean Stark Measurements on Tight Shales. *SPE 159976.*

Hudson, J. et al., 2012. Modeling Multple-Porosity Transport in Gas-Bearing Shale Formations. *SPE-153535-PP.*

Kee, L., 2010. Onshore Shale Gas Potential of the Lower Jurassic Altena Group in the West Netherlands Basin and Roer Valley Graben. *Thesis Paper Utrecht University,* pp. 10-17.

Lorinczi, P. et al., 2013. Finite Volume Modelling of Gas Flow in Shale: Forward and Inverse Applications. *University of Leeds paper.*

Loucks, R. et al., 2009. Mrophology, Genesis, and Distribution of Nanometer-Scale Pores in Siliceous Mudstones of the Mississippian Barnett Shale. *Journal of Sedimentary Research v.79,* pp. 848-861.

Luffel, D., Hopkins, C. & Schettler, P., 1993. Matrix Permeability Measurement of Gas Productive Shales. *SPE 26633,* p. 263.

Mallon, A. & Swarbrick, R., 2007. How Should Permeability be Measured in Fine-Grained Lithologies? Evidence from the Chalk. *Geofluids, Volume 8, Issue 1,* pp. 35-45.

Mengal, S., 2010. Accounting for Adsorbed gas and Its effect on Production Behavior of Shale Gas Reservoirs. *MSc. thesis Petroleum Engineering Texas A&M University.*

Mezger, W., 2014. The Shale Oil Potential of the Posidonia Formation in the Netherlands. *Thesis paper Delft University of Technology,* pp. 12-22.

Noordoven, Q., 2011. Characterization of Stimulated Potential in Jurassic and Carboniferous Shale plays of the Netherlands. *Thesis Paper, Delft University of Technology,* pp. 15-21.

Olson, R. & Grigg, M., 2008. Mercury Injection Capillary Pressure (MICP) - A Usefull Tool for Improved Understanding of Porosity and Matrix Permeability Distributions in Shale Reservoirs. *AAPG Annual Convention, San Antonio, Texas, USA; Article 40322.*

Perry, R. & Chilton, C., 1973. In: *Chemical Engineers Handbook.* Kogakusha: s.n.

Profice, S. et al., 2011. *Permeability, Porosity and Klinkenberg Coefficient Determination on Crushed Porous Media.* Austin, Texas, s.n., pp. 1-12.

Rickman, R. et al., 2008. A Practical Use of Shale Petrophysics for Stimulation Design Optimization: All Shale Plays Are Not Clones of the Barnett Shale. *SPE-115258-MS.*

Rybalcenko, K. & Leeftink, T., 2015. Unpublished manuscript.

Sakhaee-Pour, A. & Bryant, S., 2012. Gas Permeability of Shale. *SPE-146944-PA.*

Segawa, H. et al., 1983. Computed Tomographic Measurement of Local Cerebral Blood Flow by Xenon Enhancement. *Stroke, Vol 14, No. 3,* pp. 356-362.

Soeder, D., 1988. Porosity and Permeability of Eastern Devonian Gas Shale. *SPEFE,* pp. 116-124.

Wang, D., Butler, R., Liu, H. & Ahmed, S., 2010. Flow Rate Behavior in Shale Rock. *SPE-138521-MS.*

Ziarani, A. & Aguilera, R., 2012. Knudsen's Permeability Correction for Tight Porous Media. *Transport in Porous Media Volume 91, Issue 1*, January, pp. 239-260.

APPENDIX A: Sample Dimensions and Weight

In the table below the dimensions and weight of the used core plugs can be found.

Sample ID	Lamination	Length Sample [cm]	Diameter Sample [cm]	Length Hole [cm]	Diameter Hole [cm]	Weight Sample [g]	Grain Density [g/cm^3]
EBN5	Perpendicular	5.06	3.79	2.00	0.32	153.13	2.65
EBN9	Parallel	2.62	3.38	-	-	75.06	2.55
EBN20	Parallel	7.22 / 3.01	3,81 / 3.74	- / 3.01	- / 0.37	203.29	2.50
	Perpendicular	2.23	3.74	2.23	0.37	59.07	2.50
EBN33	Perpendicular	3.11	3.83	3.11	0.46	71.48	2.08
OPA1	Perpendicular	4.25	3.74	4.25	0.37	117.19	2.51
OPA2	Parallel	5.32	3.78	5.32	0.46	157.66	2.38
	Perpendicular	3.23	3.77	-	-	51.89	2.38
OPB1	Perpendicular	2.80	3.74	-	-	90.57	2.42
Whitehill	Perpendicular	2.77	3.78	-	-	72.49	2.65

APPENDIX B: Calibration

Calibration of the pots is essential for good measurements and a correct history match. The calibration is based on Boyle's Law: $P_1\,V_1 = P_2\,V_2$. The pressures in both pots can be measured and the exact size of the inserted calibration balls are known. By performing the test for a range of pressures and with different amount of balls, multiple equations with only two unknowns are derived. Hence the upstream and downstream volume can be calibrated accurately.

For GRI set-up G2 and G3 a selection of points can be seen in the graphs below:

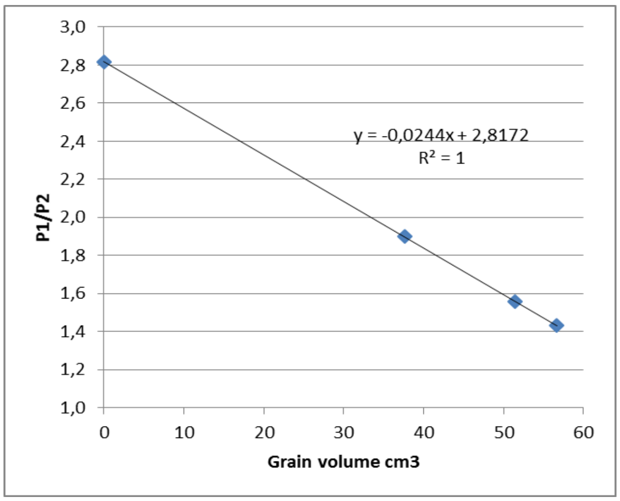

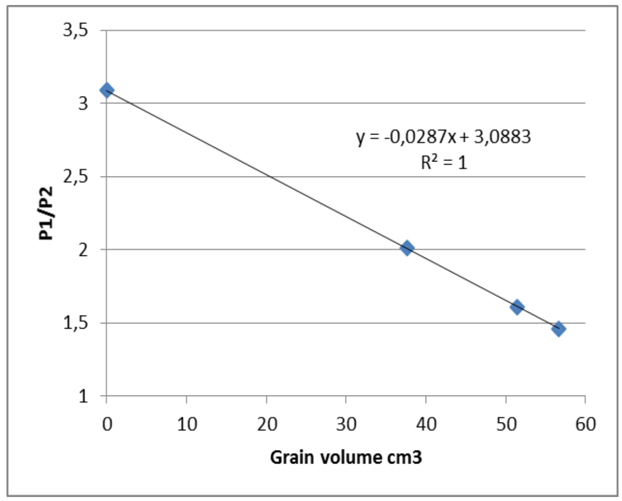

When more balls are inserted in the downstream volume, the measurements are less prone to errors and will equilibrate substantially quicker. The mean reason is that there is less gas in the system which can be affected by temperature, collisions of the molecules or other inaccuracies.

In the figure below the equilibration of an empty pot and the same pot, G3, filled with a couple of calibration balls is shown. Hence, it can is clearly observed that the pot with the balls reaches a steady state substantially quicker than the empty pot.

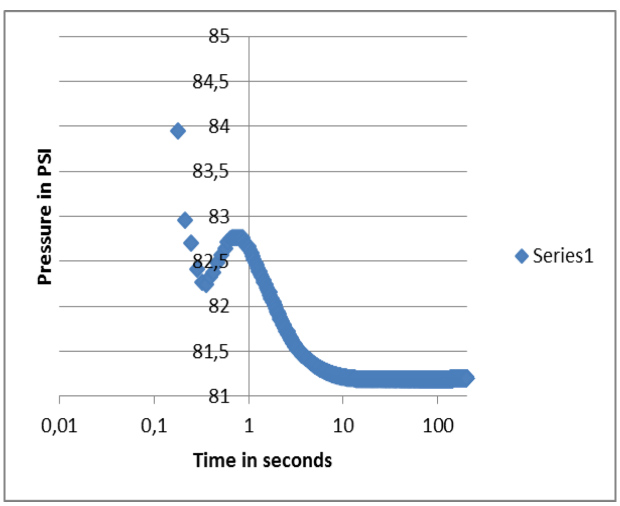

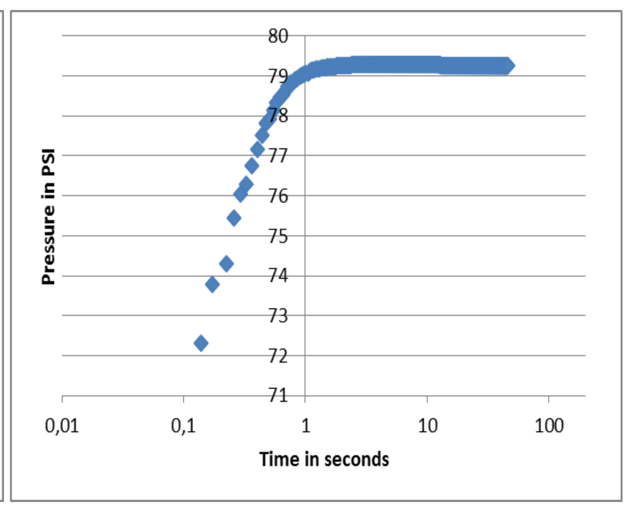

The sizes of the pots and balls used are as follows:

	Upstream volume (cm^3)	Downstream volume (cm^3)
G2	41.07	65.96
G3	34.94	64.24
GRI Silver	44.60	92.60

	Upstream Volume 1 (cm^3)	Upstream Volume 2 (cm^3)	Downstream Volume (cm^3)
MPD	10.90	4.75	1.83

	Volume (cm^3)
Small calibration ball	2.10
Medium calibration ball	7.08
Large calibration ball	16.79

APPENDIX C: History Match Script

The history matching of the performed experiments was conducted with Tempest Enable software, which had an Eclipse back-end simulator. The script was varied slightly depending on the input parameters, but it roughly was made up as follows:

```
------------------------------------------------------------------------
-- Model to estimate a full core GRI
-- Quentin Fisher 10th May 2013
-- Tom Leeftink, Konstantin Rybalcenko 3rd December 2014
-- SAMPLE Chevron-3
------------------------------------------------------------------------
RUNSPEC
TITLE
            Full core GRI
METRIC
-- Maximum well/connection/group values
--    #wells  #cons/w  #grps  #wells/grp
--    ------  -------  -----  ----------
WELLDIMS
       1      3      1      1 /
RADIAL
GAS
DIMENS
23 2 140 /
 --WELLDIMS
--1 2 1 10 /
 START
 1 'JAN' 2011 /

ROCKCOMP
```

```
REVERS 1 /

UNIFOUT

GRID

--=====================================================================

-------- IN THIS SECTION , THE GEOMETRY OF THE SIMULATION GRID AND THE

-------- ROCK PERMEABILITIES AND POROSITIES ARE DEFINED.

----------------------------------------------------------------------

--  SPECIFY INNER RADIUS OF 1ST GRID BLOCK IN THE RADIAL DIRECTION

INRAD

  0.05 /

--  SPECIFY GRID BLOCK DIMENSIONS IN THE R DIRECTION

DRV

   1*0.05 22*0.09225  /

-- SPECIFY CELL THICKNESSES ( DZ ), RADIAL PERMEABILITIES ( PERMR )

-- AND POROSITIES ( PORO ) FOR EACH LAYER OF THE GRID. ALSO CELL TOP

-- DEPTHS ( TOPS ) FOR LAYER 1. DTHETA IS SET TO 360 DEGREES FOR EVERY

-- GRID BLOCK IN THE RESERVOIR.

--     ARRAY    VALUE  ------ BOX ------

DTHETA

6440*180   /  BOX DEFAULTS TO THE WHOLE GRID

EQUALS

DZ 0.2  1 23  1  2  1  39 /

DZ 0.0722  1 23  1  2  40  140 /

/

--
--
--


Box
```

```
1 23  1  2  1  1  /

TOPS

46*0  /

ENDBOX

PERMR

6440*1000000  /

PERMZ

6440*1000000  /

PERMTHT

6440*1000000 /

-- sample chamber poro

PORO

6440*0.84939 /

EQUALS

    PERMR   0.049  1  21  1  2  40  139  /

    PERMZ   0.049  1  21  1  2  40  139  /

    PERMTHT 0.049  1  21  1  2  40  139  /

    PORO 0.047 1  21  1  2  40  139  /

/

-- expansion vol poro
EQUALS
    PORO   0.88  1  23  1  2  1  17  /

/

-- High permeability streak characteristics
EQUALS

    PERMR   10  10  10  1  2  40  139  /

    PERMZ   10  10  10  1  2  40  139  /

    PERMTHT 10  10  10  1  2  40  139  /

    PORO 0.005 10  10  1  2  40  139  /

/
```

```
COORDSYS

2* COMP /

INIT

-------- ARRAY     FACTOR

--MULTIPLY

--       'PERMZ'     0.1    /

--/

-- OUTPUT OF CELL DIMENSIONS, PERMEABILITIES, POROSITY AND TOPS

-- DATA IS REQUESTED, AND OF THE CALCULATED PORE VOLUMES, CELL

-- CENTRE DEPTHS AND X AND Z DIRECTION TRANSMISSIBILITIES

--RPTGRID

-- 1  1  1  1  0  1  0  0  0  1  0  1  1  1  1  0  1 /

--  ============================================================

-------- THE PROPS SECTION DEFINES THE REL. PERMEABILITIES, CAPILLARY

-------- PRESSURES, AND THE PVT PROPERTIES OF THE RESERVOIR FLUIDS

----------------------------------------------------------------------

-- WATER RELATIVE PERMEABILITY AND CAPILLARY PRESSURE ARE TABULATED AS

-- A FUNCTION OF WATER SATURATION.

PROPS

-- Densities in g/cm3

--          Oil      Wat      Gas

--          ---      ---      ---

DENSITY

          0.7849   1.009   0.000165 /

-- PVT data for gas

PVDG

1                    1          0.019846

2          0.500237118     0.019849

3          0.333649491     0.019853
```

4	0.2503475	0.019856
5	0.200372848	0.01986
6	0.167061863	0.019864
7	0.143256856	0.019867
8	0.125407598	0.019871
9	0.111525568	0.019874
10	0.100420271	0.019878
15	0.067102746	0.019896
20	0.050443983	0.019913
30	0.03378522	0.019948
40	0.025455021	0.019983
50	0.020457556	0.020017
60	0.017126457	0.02005
70	0.014747428	0.020084
80	0.012962666	0.020117
90	0.01157479	0.020149
100	0.010464424	0.020181

/

EXTRAPMS

1 /

```
ROCKTAB
1	1	15.97
2	1	8.48
3	1	5.99
4	1	4.74
5	1	3.99
6	1	3.49
7	1	3.14
8	1	2.87
9	1	2.66
10	1	2.50
11	1	2.36
12	1	2.25
13	1	2.15
14	1	2.07
15	1	2.00
16	1	1.94
17	1	1.88
18	1	1.83
19	1	1.79
20	1	1.75
/
-- PVT data for water
--	P	Bw	Cw	Vis	Viscosibility
--	----	----	-----	-----	-------------
--PVTW
--	4500	1.02	3E-6	0.8	0.0 /
```

```
-- Rock compressibility
--        P          Cr
--      ----       -----
-- ROCK
--        1       1.12E-06 /
-- Water and oil rel perms & capillary pressures
--        Sg      Krg     Krw     Pc
--      -----    -----    ---    ----
--SGWFN
--        0.25        0           0.067123163     10
--0.28    0.001008998     0.056277186     20
--0.32    0.00611151      0.043927126     21
--0.34    0.01072201      0.038576778     22
--0.42    0.04627044      0.021896688     23
--0.5     0.113382112     0.011318136     24
--0.6     0.244652332     0.004099585     25
--0.7     0.425199665     0.001047553     26
--0.8     0.64476772      0.000129971     30
--0.9     0.886911322     1.28076E-06     40
--0.97    1               0           45  /
--/
SOLUTION
-- Initial equilibration conditions
--       Datum   Pi@datum    WOC    Pc@WOC
--       -----   --------   -----   ------
--EQUIL
--        1    1     700    0 /
```

```
-- Output to Restart file for t=0 (.UNRST)
--    Restart file      Graphics
--    for init cond       only
--    -------------      --------
RPTRST
       BASIC=2          /
PRESSURE
6440*1.01379 /
EQUALS
PRESSURE  11.013103  1  23  1  2  1  17  /
/
--===============================================================
SUMMARY
BPR
1 1 3 /
--10 1 4/
--23 1 1/
/
EXCEL
--===============================================================
SCHEDULE
-- Output to Restart file for t>0 (.UNRST)
--    Restart file     Graphics
--     every step        only
--    ------------      --------
RPTRST
      BASIC=2          /
```

```
/
-- Location of wellhead and pressure gauge
--     Well  Well   Location   BHP    Pref.
--     name  group   I    J   datum   phase
--     -----  ----    -    -   -----   -----
WELSPECS
     PROD   G1    1   1   1    GAS  /
/
-- Completion interval
--     Well   Location  Interval  Status          Well
--     name    I    J    K1  K2   O or S          ID
--     ----    -    -    --  --   ------         --??----
COMPDAT
     PROD    1    1    1   1    OPEN         2* 0.025 /
/
-- Production control
--  Well  Status  Control   Oil   Wat   Gas   Liq  Resv   BHP
--  name          mode     rate  rate  rate   rate  rate  limit
--  ----  ------  ------   ----  ----  ----   ----  ----  -----
WCONPROD
   PROD  OPEN    GRAT   2*    0   2*  1 /
/
-- Number and size (HOURS) of timesteps
TSTEP
100*0.0000270833
100*0.0000416667
100*0.0002083333 /
END
```

When opted to invert the measured data without a high permeability streak, the "*High permeability streak characteristics* " have to be deselected. When opted to invert the measured data with the Klinkenberg correction factor, the following script replaces the "*ROCKTAB*" table:

#intrinsic permeability

$ki=1;

#pressure values in atmos

$p1=1;

$p2=2;

$p3=3;

$p4=4;

$p5=5;

$p6=6;

$p7=7;

$p8=8;

$p9=9;

$p10=10;

$p11=11;

$p12=12;

$p13=13;

$p14=14;

$p15=15;

$p16=16;

$p17=17;

$p18=18;

$p19=19;

$p100=100;

#pvmult

$pv=1;

#pressure values in psi

```
$pp1=$p1*14.7;
$pp2=$p2*14.7;
$pp3=$p3*14.7;
$pp4=$p4*14.7;
$pp5=$p5*14.7;
$pp6=$p6*14.7;
$pp7=$p7*14.7;
$pp8=$p8*14.7;
$pp9=$p9*14.7;
$pp10=$p10*14.7;
$pp11=$p11*14.7;
$pp12=$p12*14.7;
$pp13=$p13*14.7;
$pp14=$p14*14.7;
$pp15=$p15*14.7;
$pp16=$p16*14.7;
$pp17=$p17*14.7;
$pp18=$p18*14.7;
$pp19=$p19*14.7;
$pp100=$p100*14.7;
#apparent permeability ka = ki*(1+b/pp)
$ka1=$ki*(1+ %b%/ $pp1);
$ka2=$ki*(1+ %b% / $pp2);
$ka3=$ki*(1+ %b% / $pp3);
$ka4=$ki*(1+ %b% / $pp4);
$ka5=$ki*(1+ %b% / $pp5);
$ka6=$ki*(1+ %b% / $pp6);
$ka7=$ki*(1+ %b% / $pp7);
$ka8=$ki*(1+ %b% / $pp8);
```

```
$ka9=$ki*(1+ %b% / $pp9);
$ka10=$ki*(1+ %b% / $pp10);
$ka11=$ki*(1+ %b% / $pp11);
$ka12=$ki*(1+ %b% / $pp12);
$ka13=$ki*(1+ %b% / $pp13);
$ka14=$ki*(1+ %b% / $pp14);
$ka15=$ki*(1+ %b% / $pp15);
$ka16=$ki*(1+ %b% / $pp16);
$ka17=$ki*(1+ %b% / $pp17);
$ka18=$ki*(1+ %b% / $pp18);
$ka19=$ki*(1+ %b% / $pp19);
$ka100=$ki*(1+ %b% / $pp100);
#permeability multiplier kmult
$km1=$ka1 / $ki;
$km2=$ka2 / $ki;
$km3=$ka3 / $ki;
$km4=$ka4 / $ki;
$km5=$ka5 / $ki;
$km6=$ka6 / $ki;
$km7=$ka7 / $ki;
$km8=$ka8 / $ki;
$km9=$ka9 / $ki;
$km10=$ka10 / $ki;
$km11=$ka11 / $ki;
$km12=$ka12 / $ki;
$km13=$ka13 / $ki;
$km14=$ka14 / $ki;
$km15=$ka15 / $ki;
$km16=$ka16 / $ki;
```

```
$km17=$ka17 / $ki;
$km18=$ka18 / $ki;
$km19=$ka19 / $ki;
$km100=$ka100 / $ki;
#constructing the table
$rocktab_table = "ROCKTAB\n" .
"$p1 $pv $km1 \n" .
"$p2 $pv $km2 \n" .
"$p3 $pv $km3 \n" .
"$p4 $pv $km4 \n" .
"$p5 $pv $km5 \n" .
"$p6 $pv $km6 \n" .
"$p7 $pv $km7 \n" .
"$p8 $pv $km8 \n" .
"$p9 $pv $km9 \n" .
"$p10 $pv $km10 \n" .
"$p11 $pv $km11 \n" .
"$p12 $pv $km12 \n" .
"$p13 $pv $km13 \n" .
"$p14 $pv $km14 \n" .
"$p15 $pv $km15 \n" .
"$p16 $pv $km16 \n" .
"$p17 $pv $km17 \n" .
"$p18 $pv $km18 \n" .
"$p19 $pv $km19 \n" .
"$p100 $pv $km100 \n" .
"/\n" ;
return $rocktab_table;
```

APPENDIX D: Measured pressure decay curves

The following tables contain the recorded pressure decay curves of the experiments. The first few points are excluded to give a more detailed view on the shape of the curve.

Full Core GRI - Expansion gas: Helium						
Sample	Drill direction to lamination	Step 1: 150 psi	Step 2: 180 psi	Step 3: 210 psi	Step 5: 240 psi	Step 6: High pressure
EBN20	Parallel	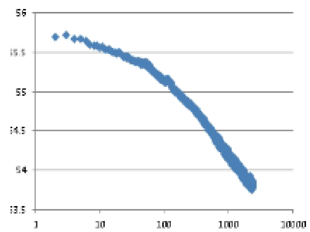	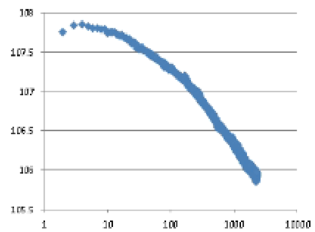	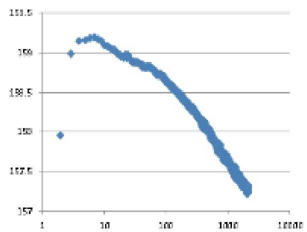	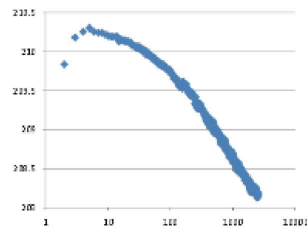	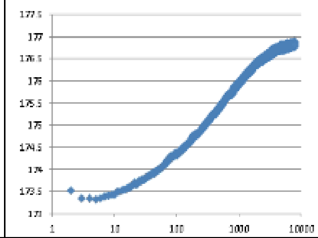
	Perpendicular	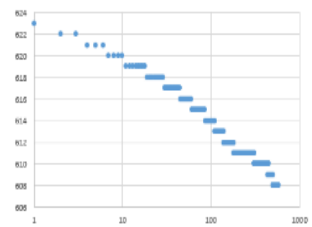	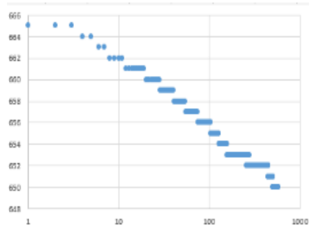	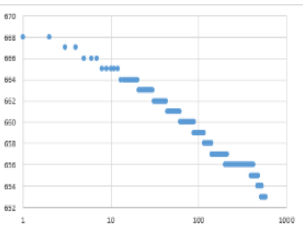		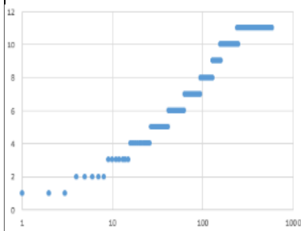
	Radial Perpendicular	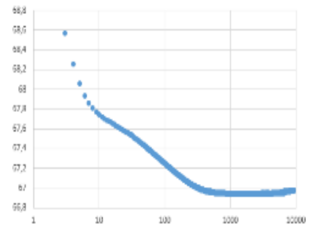	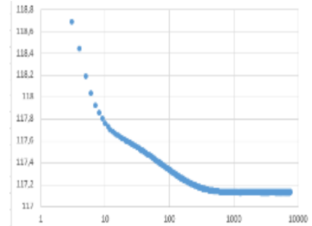			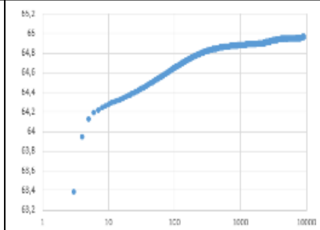
	Radial Parallel	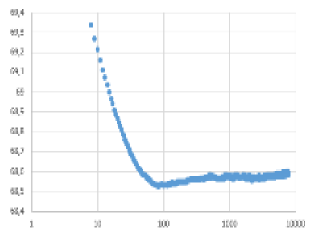	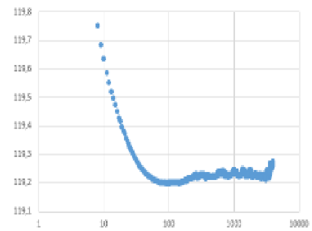	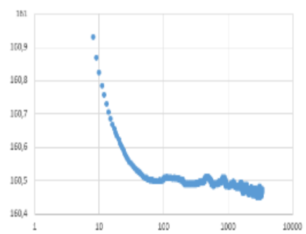	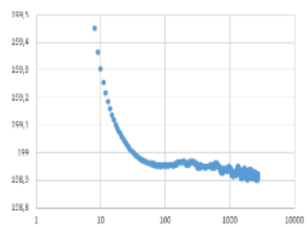	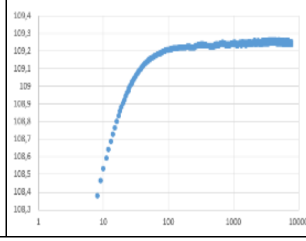

OPA2	Parallel	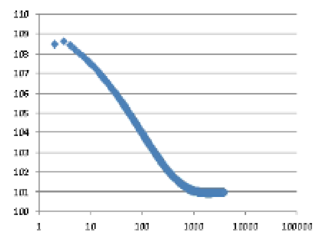	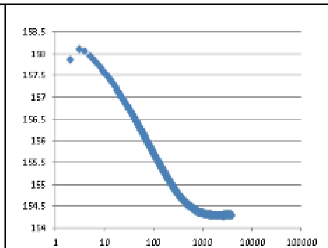	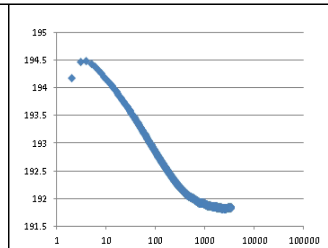	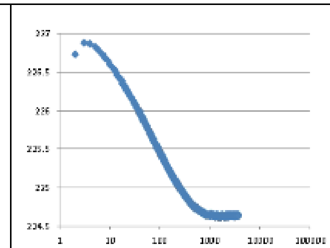	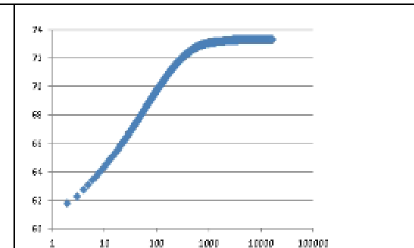
	Perpendicular	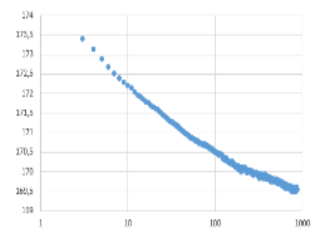	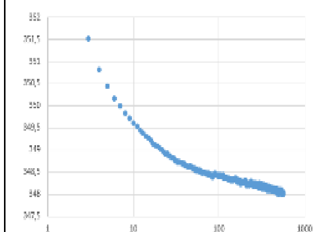	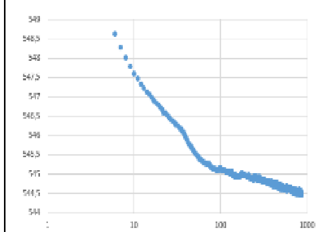	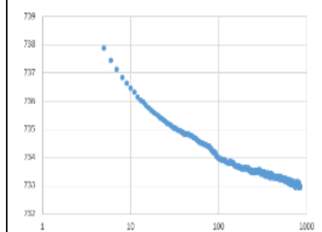	
	Radial Parallel	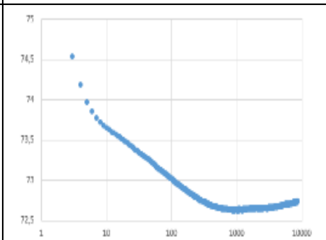	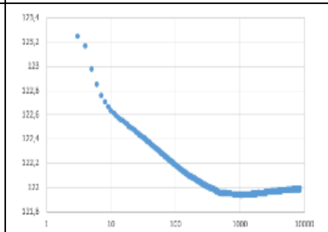			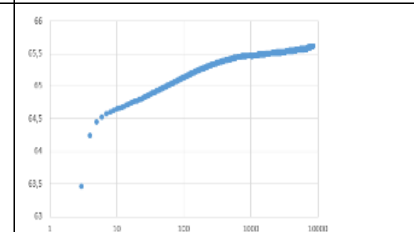
Whitehill	Perpendicular	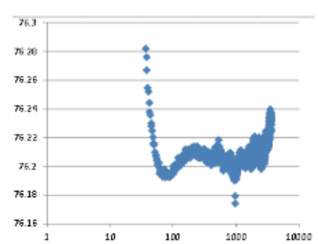	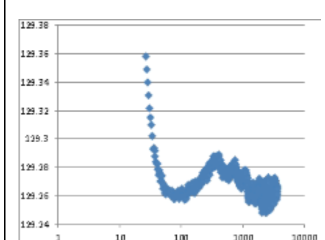	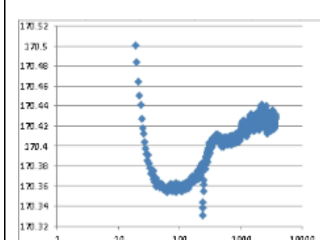	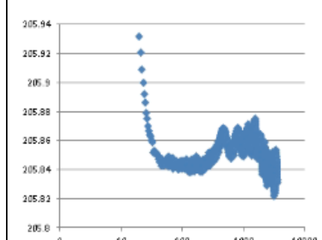	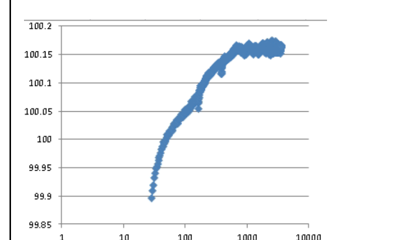
EBN9	Parallel	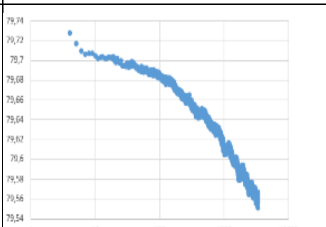	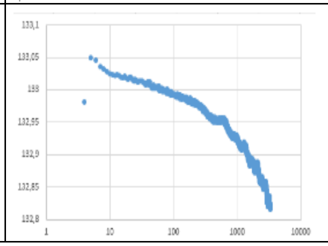	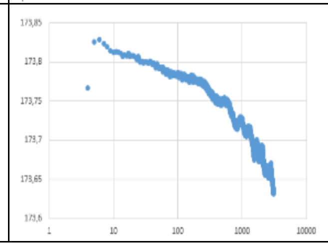	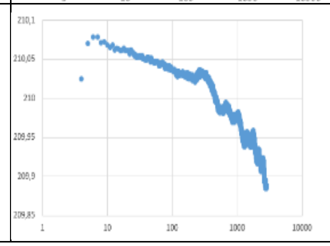	

EBN33	Parallel	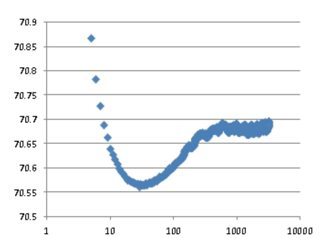	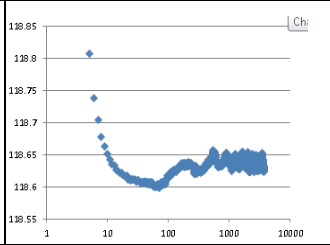	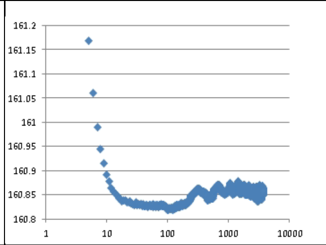	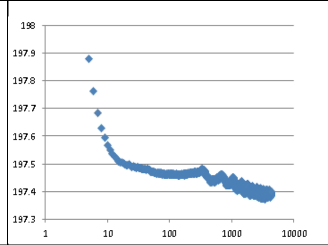	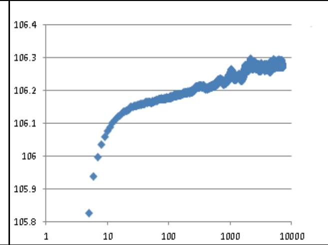
	Radial Parallel	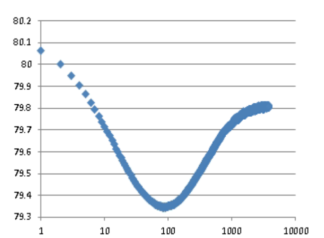	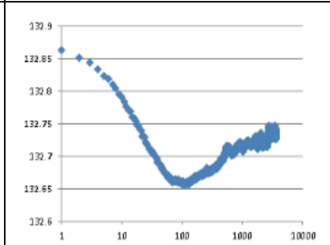	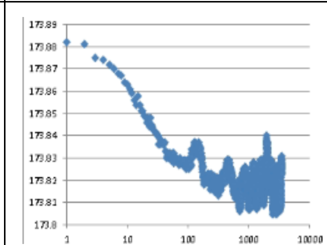	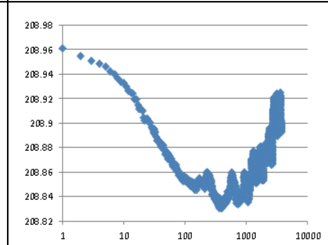	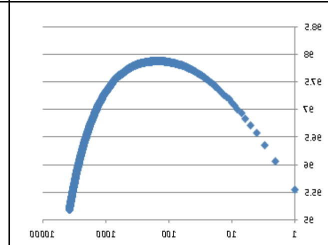
OPB1	Perpendicular	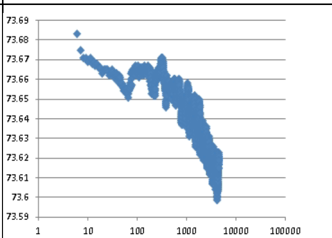	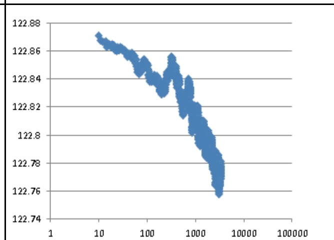	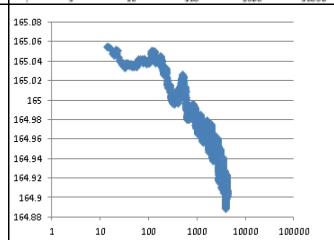	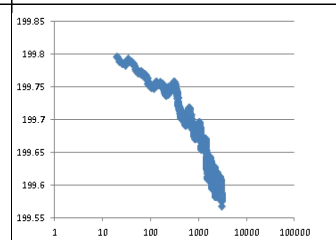	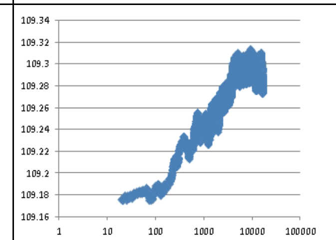
OPA1	Perpendicular	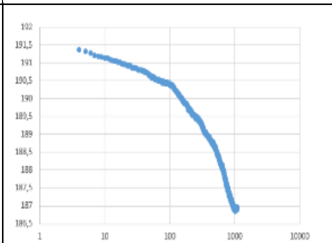	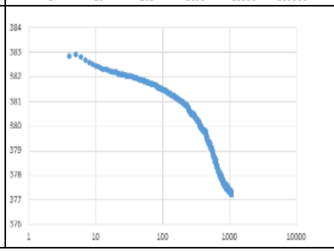	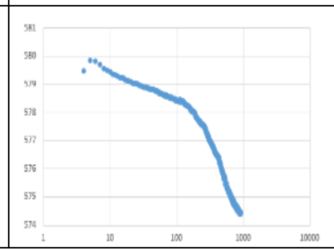	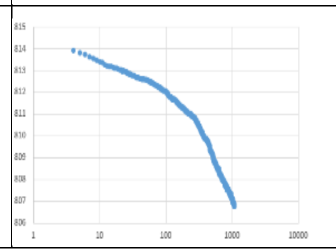	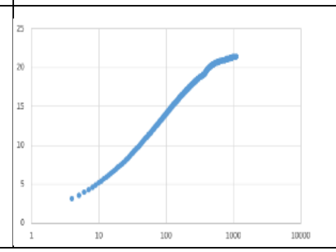

Full Core GRI - Expansion gas: Methane

Sample	Drill direction to lamination	Step 1: 150 psi	Step 2: 180 psi	Step 3: 210 psi	Step 4: Reverse 1	Step 5: Reverse 2
EBN20	Parallel	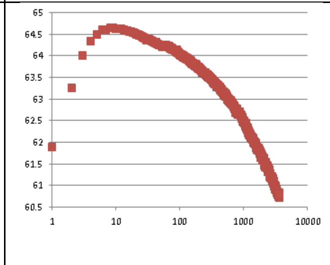	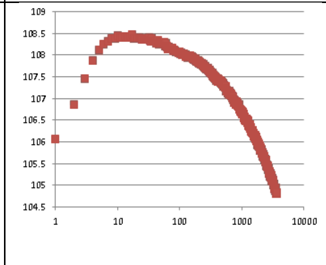	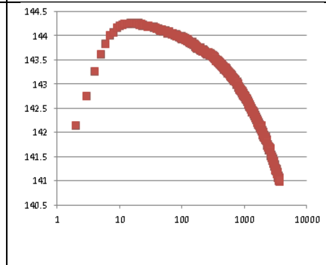	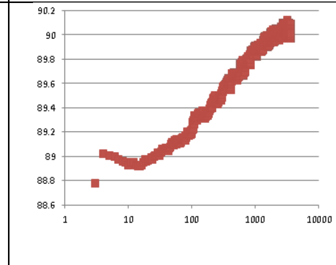	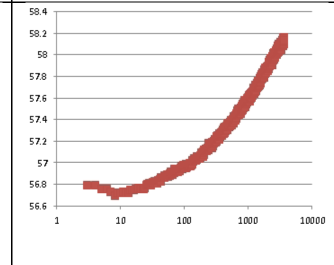
	Radial Parallel	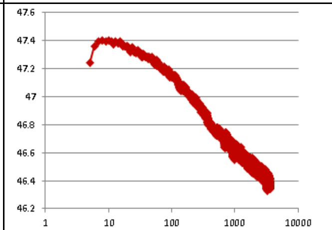	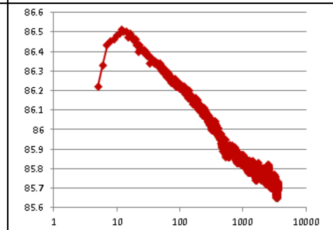	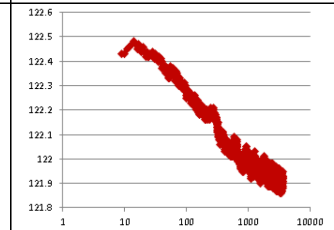	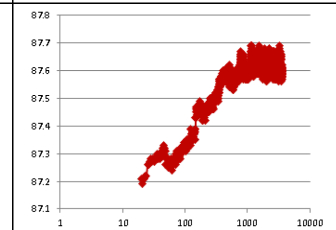	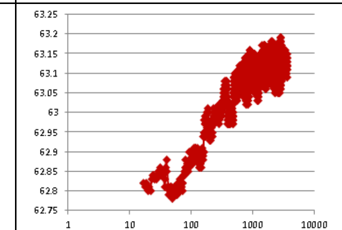
OPA2	Parallel	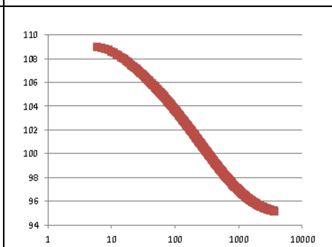	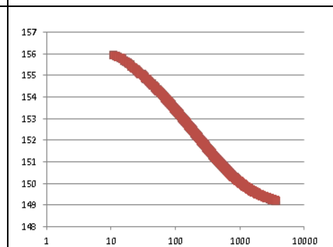	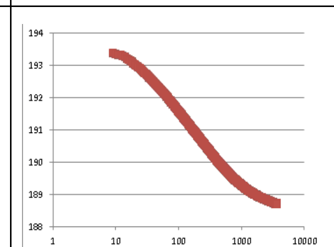	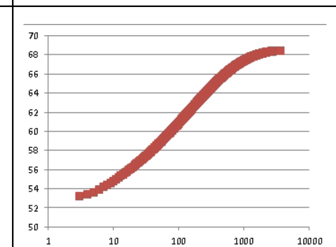	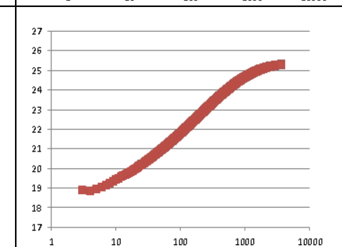
Whitehill	Perpendicular	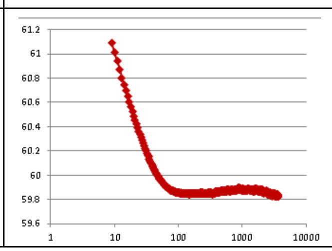	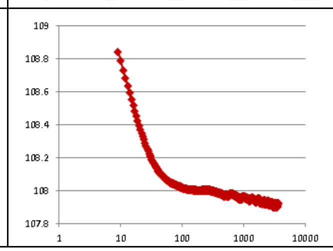	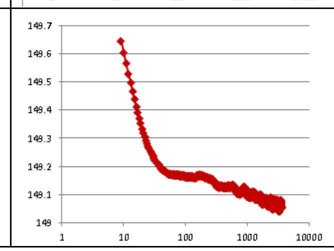	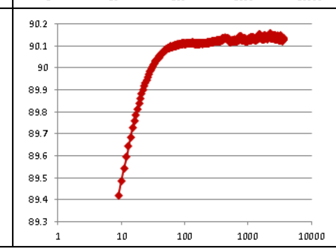	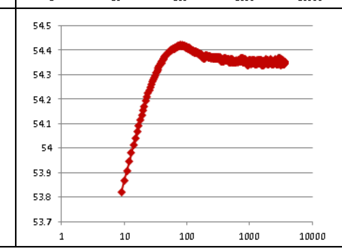

EBN9	Parallel	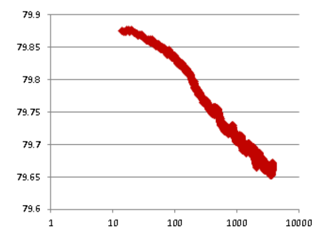			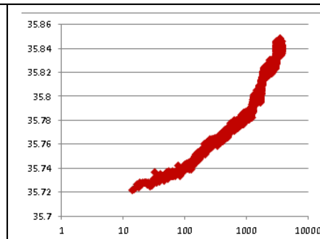	
EBN33	Parallel	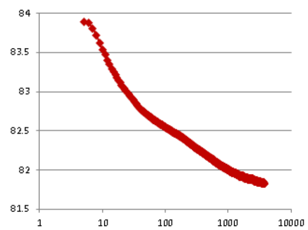	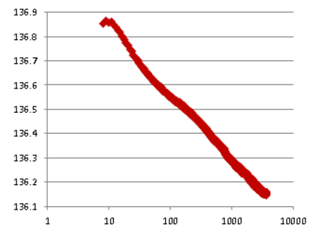	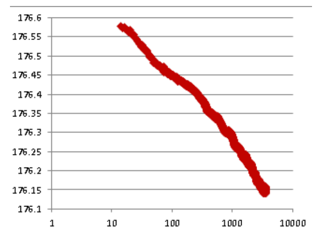	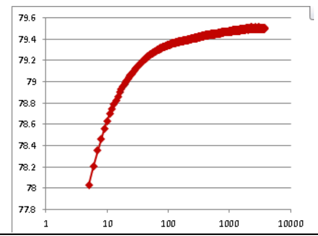	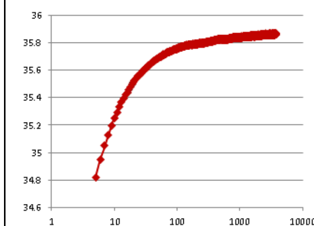
OPB1	Perpendicular	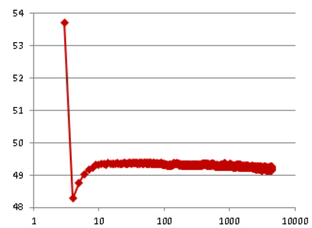	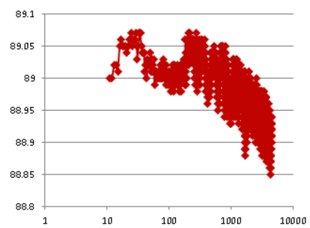	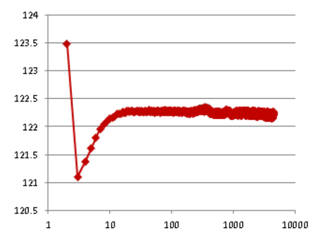	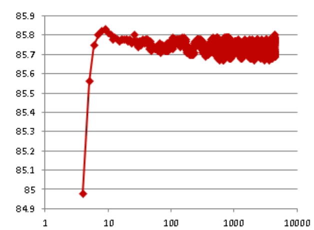	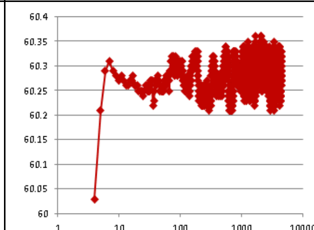
OPA1	Perpendicular	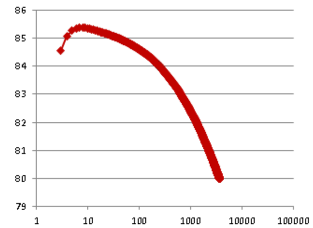			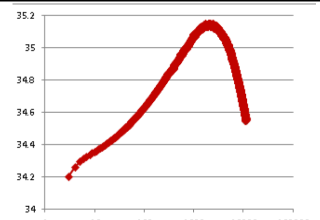	

Modified Pulse Decay – Expansion gas: Helium						
Sample	Drill direction to lamination	Step 1: 200 psi	Step 2: 300 psi	Step 3: 400 psi	Step 4: 500 psi	Step 5: Reverse
EBN20	Parallel	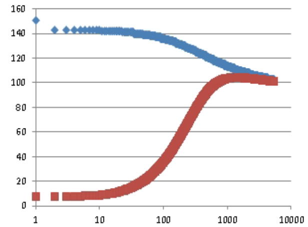	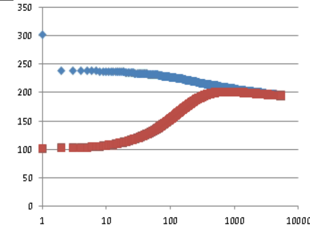	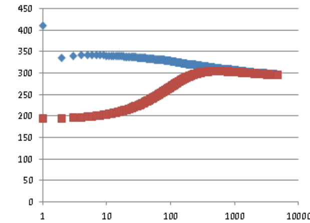		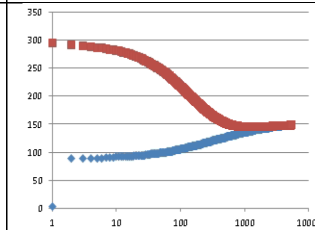
	Radial Parallel	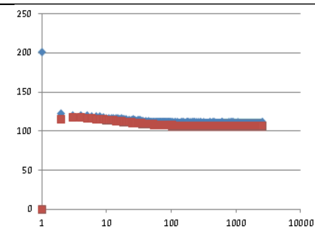	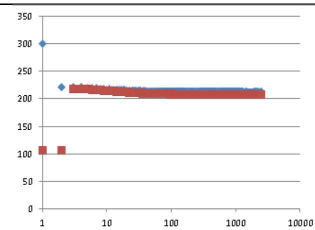	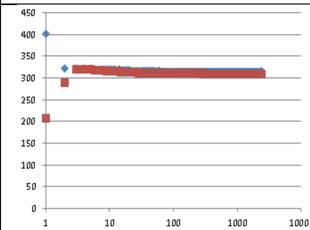	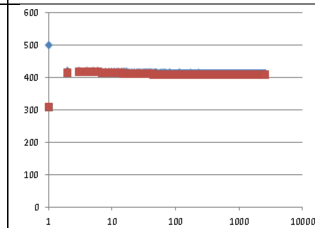	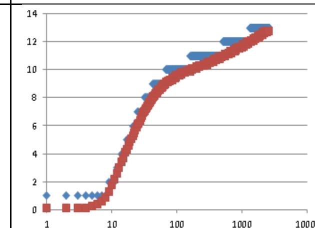
OPA2	Parallel	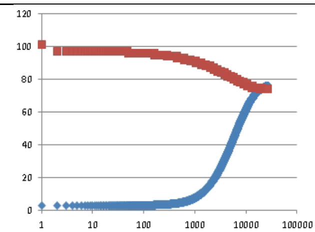	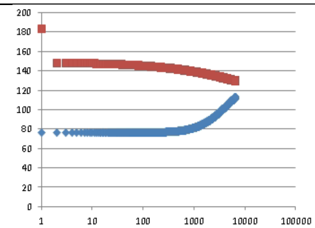	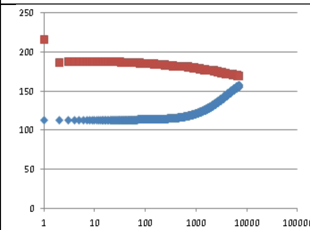		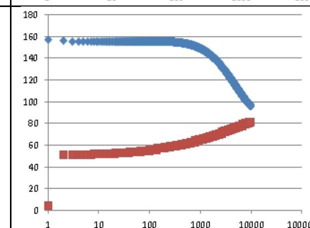
	Perpendicular	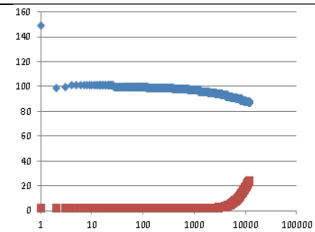	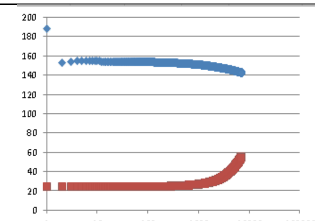	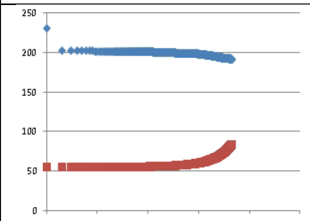		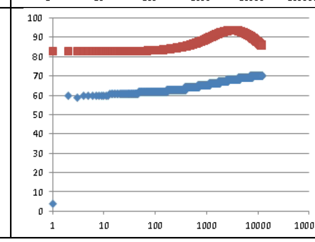

	Radial Parallel	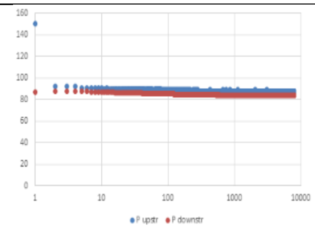				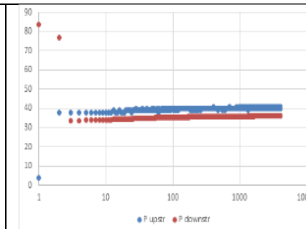
Whitehill	Perpendicular	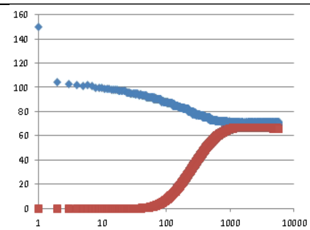	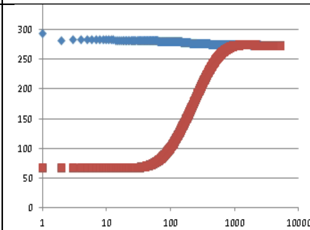	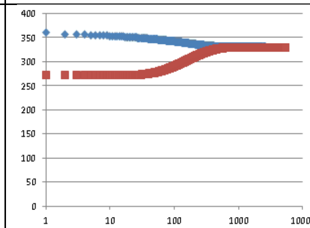		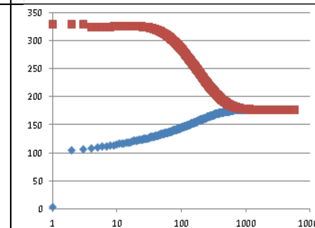
EBN9	Parallel	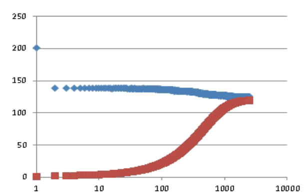	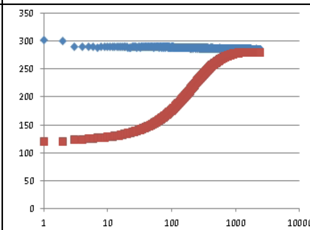	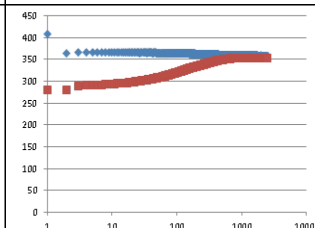	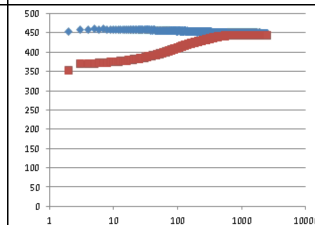	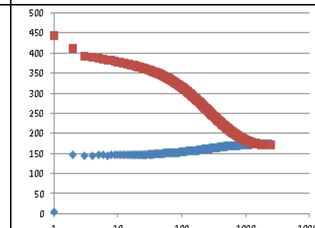
EBN33	Parallel	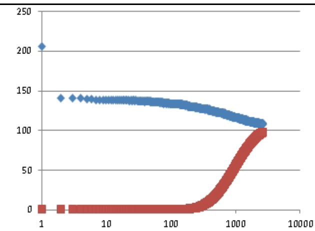	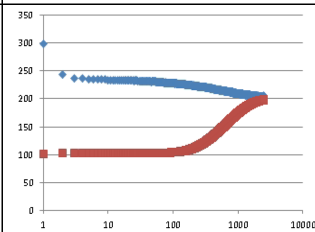	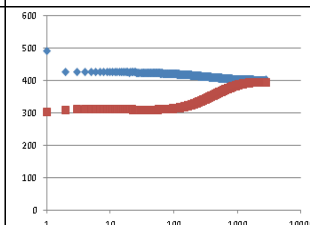	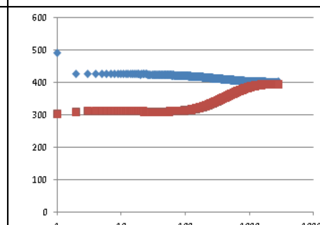	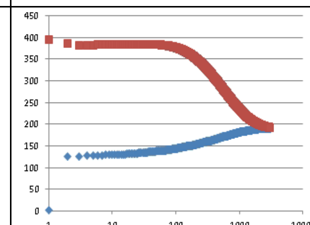
OPB1	Perpendicular	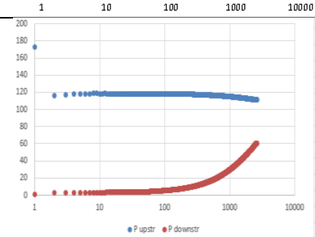				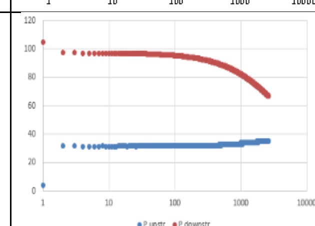

<table>
<tr><td rowspan="2">OPA1</td><td>Perpendicular</td><td>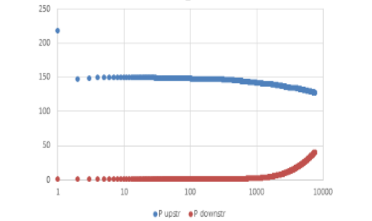</td><td>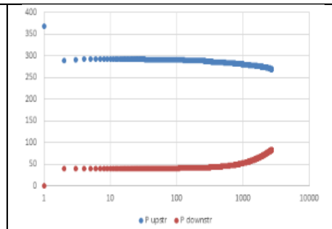</td><td>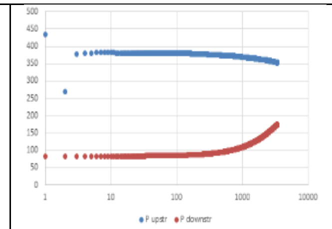</td><td>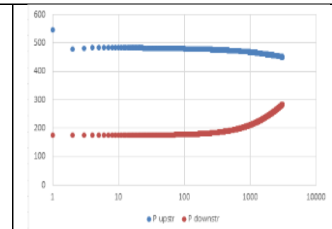</td><td>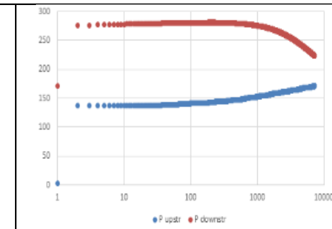</td></tr>
<tr><td>Radial Perpendicular</td><td>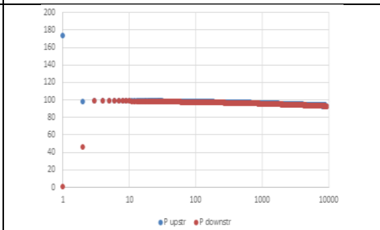</td><td></td><td></td><td></td><td>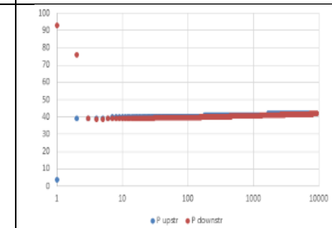</td></tr>
</table>

APPENDIX E: All history matched results

sampl	experi	gas	P	Pclass	1_div_	Peq	1_div_	lamina	hole	fractu	b	kmatrix_[	phima	kfrac_[md]	phifrac	b_val	sim_b	Pconf	REV	TOC	BET	POT	poor_	fixed_	k_app
EBN20	fcgri	He	145,2	150,0	0,0	53,8	0,0	parallel	no	yes	yes	5,11E-08	0,11	1,84E-05	0,06	6767	Tom		no	5,67	6,03	S1	WG	no	6,48E-06
EBN20	fcgri	He	197,7	210,0	0,0	106,0	0,0	parallel	no	yes	yes	4,61E-06	0,10	1,88E-03	0,09	2011	Tom		no	5,67	6,03	S1	WG	no	9,21E-05
EBN20	fcgri	He	247,7	250,0	0,0	157,3	0,0	parallel	no	yes	yes	8,92E-07	0,08	8,20E-06	0,09	921	Tom		no	5,67	6,03	S1	WG	no	6,12E-06
EBN20	fcgri	He	298,5	300,0	0,0	208,2	0,0	parallel	no	yes	yes	4,62E-08	0,10	8,10E-06	0,09	1259	Tom		no	5,67	6,03	S1	WG	no	3,26E-07
EBN20	fcgri	He	402,0	400,0	0,0	278,1	0,0	parallel	no	yes	yes	1,48E-05	0,09	1,40E-04	0,09	2218	Tom		no	5,67	6,03	S1	WG	no	1,33E-04
EBN20	fcgri	He	2,1	0,0	0,5	176,5	0,0	parallel	no	yes	yes	9,39E-08	0,07	6,84E-05	0,09	6410	Tom		yes	5,67	6,03	S1		no	3,50E-06
EBN20	fcgri	He	145,2	150,0	0,0	53,8	0,0	parallel	no	no	no	4,62E-06	0,07				Tom		no	5,67	6,03	S1	WG	no	4,62E-06
EBN20	fcgri	He	197,7	210,0	0,0	106,0	0,0	parallel	no	no	no	4,33E-06	0,05				Tom		no	5,67	6,03	S1	WG	no	4,33E-06
EBN20	fcgri	He	247,7	250,0	0,0	157,3	0,0	parallel	no	no	no	7,51E-06	0,04				Tom		no	5,67	6,03	S1	WG	no	7,51E-06
EBN20	fcgri	He	298,5	300,0	0,0	208,2	0,0	parallel	no	no	no	1,10E-05	0,05				Tom		no	5,67	6,03	S1	WG	no	1,10E-05
EBN20	fcgri	He	402,0	400,0	0,0	278,1	0,0	parallel	no	no	no	9,81E-06	0,05				Tom		no	5,67	6,03	S1	WG	no	9,81E-06
EBN20	fcgri	He	2,1	0,0	0,5	176,5	0,0	parallel	no	no	no	1,04E-05	0,05				Tom		yes	5,67	6,03	S1		no	1,04E-05
EBN20	fcgri	He	145,2	150,0	0,0	53,8	0,0	parallel	no	no	yes	5,37E-08	0,06			79283	Tom		no	5,67	6,03	S1	WG	no	7,92E-05
EBN20	fcgri	He	197,7	210,0	0,0	106,0	0,0	parallel	no	no	yes	1,23E-07	0,04			70681	Tom		no	5,67	6,03	S1	WG	no	8,24E-05
EBN20	fcgri	He	247,7	250,0	0,0	157,3	0,0	parallel	no	no	yes	3,25E-07	0,05			26662	Tom		no	5,67	6,03	S1	WG	no	5,54E-05
EBN20	fcgri	He	298,5	300,0	0,0	208,2	0,0	parallel	no	no	yes	3,30E-07	0,05			27171	Tom		no	5,67	6,03	S1	WG	no	4,33E-05
EBN20	fcgri	He	402,0	400,0	0,0	278,1	0,0	parallel	no	no	yes	3,33E-07	0,05			23207	Tom		no	5,67	6,03	S1	WG	no	2,81E-05
EBN20	fcgri	He	2,1	0,0	0,5	176,5	0,0	parallel	no	no	yes	2,71E-07	0,05			30680	Tom		yes	5,67	6,03	S1		no	4,74E-05
EBN20	fcgri	He	145,2	150,0	0,0	53,8	0,0	parallel	no	yes	no	2,37E-07	0,10	9,93E-02	0,09		Tom		no	5,67	6,03	S1	WG	no	2,37E-07
EBN20	fcgri	He	197,7	210,0	0,0	106,0	0,0	parallel	no	yes	no	1,05E-06	0,09	1,69E-04	0,09		Tom		no	5,67	6,03	S1	WG	no	1,05E-06
EBN20	fcgri	He	247,7	250,0	0,0	157,3	0,0	parallel	no	yes	no	1,29E-06	0,07	2,13E-05	0,09		Tom		no	5,67	6,03	S1	WG	no	1,29E-06
EBN20	fcgri	He	298,5	300,0	0,0	208,2	0,0	parallel	no	yes	no	2,04E-06	0,05	5,90E-06	0,06		Tom		no	5,67	6,03	S1	WG	no	2,04E-06
EBN20	fcgri	He	402,0	400,0	0,0	278,1	0,0	parallel	no	yes	no	2,34E-06	0,06	5,49E-06	0,08		Tom		no	5,67	6,03	S1	WG	no	2,34E-06
EBN20	fcgri	He	2,1	0,0	0,5	176,5	0,0	parallel	no	yes	no	3,51E-06	0,12	1,80E-03	0,09		Tom		yes	5,67	6,03	S1		no	3,51E-06
EBN20	fcgri	CH4	166,9	150,0	0,0	46,4	0,0	parallel	no	no	no	6,18E-06	0,11				Tom		no	5,67	6,03	S1	WG	no	6,18E-06
EBN20	fcgri	CH4	186,9	180,0	0,0	85,8	0,0	parallel	no	no	no	1,92E-06	0,12				Tom		no	5,67	6,03	S1	WG	no	1,92E-06
EBN20	fcgri	CH4	209,1	210,0	0,0	121,9	0,0	parallel	no	no	no	2,81E-06	0,07				Tom		no	5,67	6,03	S1	WG	no	2,81E-06
EBN20	fcgri	CH4	1,9	0,0	0,5	87,7	0,0	parallel	no	no	no	2,22E-06	0,09				Tom		yes	5,67	6,03	S1		no	2,22E-06
EBN20	fcgri	CH4	1,8	0,0	0,6	63,1	0,0	parallel	no	no	no	2,55E-06	0,08				Tom		yes	5,67	6,03	S1	WG	no	2,55E-06
EBN20	fcgri	CH4	166,9	150,0	0,0	46,4	0,0	parallel	no	no	yes	7,69E-07	0,09			3409	Tom		no	5,67	6,03	S1	WG	no	5,73E-05
EBN20	fcgri	CH4	186,9	180,0	0,0	85,8	0,0	parallel	no	no	yes	9,05E-07	0,09			3696	Tom		no	5,67	6,03	S1	WG	no	3,99E-05
EBN20	fcgri	CH4	209,1	210,0	0,0	121,9	0,0	parallel	no	no	yes	1,32E-06	0,07			2744	Tom		no	5,67	6,03	S1	WG	no	3,11E-05
EBN20	fcgri	CH4	1,9	0,0	0,5	87,7	0,0	parallel	no	no	yes	2,27E-06	0,04			2430	Tom		yes	5,67	6,03	S1		no	6,53E-05
EBN20	fcgri	CH4	1,8	0,0	0,6	63,1	0,0	parallel	no	no	yes	6,46E-07	0,08			2336	Tom		yes	5,67	6,03	S1	WG	no	2,46E-05
EBN20	fcgri	CH4	166,9	150,0	0,0	46,4	0,0	parallel	no	yes	no	4,06E-06	0,09	4,10E-04	0,11		Tom		no	5,67	6,03	S1	WG	no	4,06E-06
EBN20	fcgri	CH4	186,9	180,0	0,0	85,8	0,0	parallel	no	yes	no	1,90E-06	0,13	3,47E-05	0,12		Tom		no	5,67	6,03	S1	WG	no	1,90E-06
EBN20	fcgri	CH4	209,1	210,0	0,0	121,9	0,0	parallel	no	yes	no	4,31E-07	0,12	2,72E-03	0,13		Tom		no	5,67	6,03	S1	WG	no	4,31E-07
EBN20	fcgri	CH4	1,9	0,0	0,5	87,7	0,0	parallel	no	yes	no	8,16E-07	0,15	1,28E-04	0,08		Tom		yes	5,67	6,03	S1		no	8,16E-07
EBN20	fcgri	CH4	1,8	0,0	0,6	63,1	0,0	parallel	no	yes	no	1,17E-06	0,11	1,75E-04	0,09		Tom		yes	5,67	6,03	S1	WG	no	1,17E-06
EBN20	fcgri	CH4	166,9	150,0	0,0	46,4	0,0	parallel	no	yes	yes	1,97E-07	0,10	2,69E-05	0,10	5723	Tom		no	5,67	6,03	S1	WG	no	2,45E-05
EBN20	fcgri	CH4	186,9	180,0	0,0	85,8	0,0	parallel	no	yes	yes	4,41E-07	0,11	1,94E-04	0,10	2064	Tom		no	5,67	6,03	S1	WG	no	1,11E-05
EBN20	fcgri	CH4	209,1	210,0	0,0	121,9	0,0	parallel	no	yes	yes	1,22E-06	0,12	5,80E-06	0,09	974	Tom		no	5,67	6,03	S1	WG	no	1,09E-05
EBN20	fcgri	CH4	1,9	0,0	0,5	87,7	0,0	parallel	no	yes	yes	1,56E-05	0,08	1,29E-03	0,08	4038	Tom		yes	5,67	6,03	S1		no	7,35E-04
EBN20	fcgri	CH4	1,8	0,0	0,6	63,1	0,0	parallel	no	yes	yes	1,03E-07	0,11	9,95E-04	0,11	4676	Tom		yes	5,67	6,03	S1	WG	no	7,74E-06
EBN20	fcgri	He	153,4	150,0	0,0	68,6	0,0	parallel	yes	no	no	7,22E-04	0,08				Tom		no	5,67	6,03	G3	mbi	no	7,22E-04
EBN20	fcgri	He	181,5	180,0	0,0	119,3	0,0	parallel	yes	no	no	1,34E-03	0,10				Tom		no	5,67	6,03	G3		no	1,34E-03
EBN20	fcgri	He	211,3	210,0	0,0	160,5	0,0	parallel	yes	no	no	1,77E-03	0,11				Tom		no	5,67	6,03	G3		no	1,77E-03
EBN20	fcgri	He	246,3	250,0	0,0	198,9	0,0	parallel	yes	no	no	2,67E-03	0,19				Tom		no	5,67	6,03	G3		no	2,67E-03
EBN20	fcgri	He	-0,1	0,0	-7,1	109,2	0,0	parallel	yes	no	no	2,76E-03	0,13				Tom		yes	5,67	6,03	G3	mbi	no	2,76E-03
EBN20	fcgri	He	153,4	150,0	0,0	68,6	0,0	parallel	yes	no	yes	1,05E-05	0,09			29920	Tom		no	5,67	6,03	G3	mbi	no	4,58E-03
EBN20	fcgri	He	181,5	180,0	0,0	119,3	0,0	parallel	yes	no	yes	9,69E-06	0,08			27048	Tom		no	5,67	6,03	G3		no	2,21E-03
EBN20	fcgri	He	211,3	210,0	0,0	160,5	0,0	parallel	yes	no	yes	2,01E-05	0,08			18663	Tom		no	5,67	6,03	G3		no	2,35E-03
EBN20	fcgri	He	246,3	250,0	0,0	198,9	0,0	parallel	yes	no	yes	1,26E-05	0,09			2010	Tom		no	5,67	6,03	G3		no	1,40E-04
EBN20	fcgri	He	-0,1	0,0	-7,1	109,2	0,0	parallel	yes	no	yes	1,84E-05	0,09			20897	Tom		yes	5,67	6,03	G3	mbi	no	3,53E-03
EBN20	MPD	He	151,0	150,0	0,0	102,0	0,0	parallel	no	yes	yes	3,32E-06	0,09	1,59E-05	0,07	821	Tom		no	5,67	6,03	MPD	mbi	no	3,01E-05

EBN20	MPD	He	302,0	300,0	0,0	195,0	0,0	parallel	no	yes	yes	2,01E-07	0,13	3,00E-05	0,04	542	Tom		no	5,67	6,03	MPD		no	7,58E-07
EBN20	MPD	He	411,0	400,0	0,0	295,0	0,0	parallel	no	yes	yes	6,08E-07	0,12	2,87E-05	0,04	512	Tom		no	5,67	6,03	MPD		no	1,66E-06
EBN20	MPD	He	4,0	0,0	0,3	149,0	0,0	parallel	no	yes	yes	5,95E-09	0,14	5,17E-03	0,04	6	Tom		yes	5,67	6,03	MPD		no	6,18E-09
EBN20	MPD	He	151,0	150,0	0,0	102,0	0,0	parallel	no	yes	no	2,30E-08	0,09	1,35E-05	0,07		Tom		no	5,67	6,03	MPD	mbi	no	2,30E-08
EBN20	MPD	He	302,0	300,0	0,0	195,0	0,0	parallel	no	yes	no	1,82E-05	0,12	9,03E-05	0,08		Tom		no	5,67	6,03	MPD		no	1,82E-05
EBN20	MPD	He	411,0	400,0	0,0	295,0	0,0	parallel	no	yes	no	2,11E-05	0,09	2,24E-05	0,08		Tom		no	5,67	6,03	MPD		no	2,11E-05
EBN20	MPD	He	4,0	0,0	0,3	149,0	0,0	parallel	no	yes	no	1,61E-03	0,08	1,73E-03	0,06		Tom		yes	5,67	6,03	MPD		no	1,61E-03
EBN20	MPD	He	151,0	150,0	0,0	102,0	0,0	parallel	no	no	yes	4,79E-06	0,06			2844	Tom		no	5,67	6,03	MPD	mbi	no	1,38E-04
EBN20	MPD	He	302,0	300,0	0,0	195,0	0,0	parallel	no	no	yes	9,92E-05	0,06			66	Tom		no	5,67	6,03	MPD		no	1,33E-04
EBN20	MPD	He	411,0	400,0	0,0	295,0	0,0	parallel	no	no	yes	1,05E-05	0,06			1340	Tom		no	5,67	6,03	MPD		no	5,81E-05
EBN20	MPD	He	4,0	0,0	0,3	149,0	0,0	parallel	no	no	yes	1,48E-05	0,04			4331	Tom		yes	5,67	6,03	MPD		no	4,45E-04
EBN20	MPD	He	151,0	150,0	0,0	102,0	0,0	parallel	no	no	no	1,31E-05	0,06				Tom		no	5,67	6,03	MPD	mbi	no	1,31E-05
EBN20	MPD	He	302,0	300,0	0,0	195,0	0,0	parallel	no	no	no	1,86E-05	0,04				Tom		no	5,67	6,03	MPD		no	1,86E-05
EBN20	MPD	He	411,0	400,0	0,0	295,0	0,0	parallel	no	no	no	1,96E-05	0,06				Tom		no	5,67	6,03	MPD		no	1,96E-05
EBN20	MPD	He	4,0	0,0	0,3	149,0	0,0	parallel	no	no	no	8,41E-05	0,04				Tom		yes	5,67	6,03	MPD		no	8,41E-05
EBN20	MPD	He	102,0	80,0	0,0	65,3	0,0	perpendi	no	yes	yes	1,76E-06	0,05	8,60E-04	0,09	279	Tom		no	5,67	6,03	MPD		no	9,28E-06
EBN20	MPD	He	193,9	180,0	0,0	148,1	0,0	perpendi	no	yes	yes	3,01E-06	0,04	8,52E-04	0,08	303	Tom		no	5,67	6,03	MPD		no	9,17E-06
EBN20	MPD	He	300,1	300,0	0,0	249,9	0,0	perpendi	no	yes	yes	1,19E-05	0,04	6,28E-04	0,11	396	Tom		no	5,67	6,03	MPD		no	3,09E-05
EBN20	MPD	He	407,2	400,0	0,0	357,3	0,0	perpendi	no	yes	yes	2,03E-05	0,06	3,81E-05	0,10	383	Tom		no	5,67	6,03	MPD		no	4,21E-05
EBN20	MPD	He	522,0	500,0	0,0	447,0	0,0	perpendi	no	yes	yes	1,68E-07	0,05	1,15E-04	0,08	3739	Tom		no	5,67	6,03	MPD		no	1,58E-06
EBN20	MPD	He	108,8	80,0	0,0	201,4	0,0	perpendi	no	yes	yes	1,35E-06	0,04	5,73E-06	0,08	12697	Tom		no	5,67	6,03	MPD		no	8,65E-05
EBN20	MPD	He	39,9	80,0	0,0	92,2	0,0	perpendi	no	yes	yes	1,34E-07	0,05	4,38E-06	0,07	51481	Tom		no	5,67	6,03	MPD		no	7,49E-05
EBN20	MPD	He	22,8	80,0	0,0	40,0	0,0	perpendi	no	yes	yes	8,65E-06	0,09	9,29E-06	0,05	2120	Tom		no	5,67	6,03	MPD		no	4,67E-04
EBN20	MPD	He	102,0	80,0	0,0	65,3	0,0	perpendi	no	yes	no	4,10E-07	0,08	4,57E-04	0,08		Tom		no	5,67	6,03	MPD		no	4,10E-07
EBN20	MPD	He	193,9	180,0	0,0	148,1	0,0	perpendi	no	yes	no	2,28E-06	0,06	4,61E-04	0,08		Tom		no	5,67	6,03	MPD		no	2,28E-06
EBN20	MPD	He	300,1	300,0	0,0	249,9	0,0	perpendi	no	yes	no	1,52E-05	0,05	7,15E-05	0,09		Tom		no	5,67	6,03	MPD		no	1,52E-05
EBN20	MPD	He	407,2	400,0	0,0	357,3	0,0	perpendi	no	yes	no	1,62E-05	0,06	3,99E-05	0,08		Tom		no	5,67	6,03	MPD		no	1,62E-05
EBN20	MPD	He	522,0	500,0	0,0	447,0	0,0	perpendi	no	yes	no	2,74E-06	0,06	4,98E-04	0,10		Tom		no	5,67	6,03	MPD		no	2,74E-06
EBN20	MPD	He	108,8	80,0	0,0	201,4	0,0	perpendi	no	yes	no	3,35E-06	0,06	7,56E-04	0,10		Tom		no	5,67	6,03	MPD		no	3,35E-06
EBN20	MPD	He	39,9	80,0	0,0	92,2	0,0	perpendi	no	yes	no	8,67E-07	0,05	5,77E-04	0,08		Tom		no	5,67	6,03	MPD		no	8,67E-07
EBN20	MPD	He	22,8	80,0	0,0	40,0	0,0	perpendi	no	yes	no	8,32E-06	0,06	3,96E-04	0,04		Tom		no	5,67	6,03	MPD		no	8,32E-06
EBN20	MPD	He	102,0	80,0	0,0	65,3	0,0	perpendi	no	no	yes	5,41E-05	0,05			78	Tom		no	5,67	6,03	MPD		no	1,19E-04
EBN20	MPD	He	193,9	180,0	0,0	148,1	0,0	perpendi	no	no	yes	1,14E-05	0,05			608	Tom		no	5,67	6,03	MPD		no	5,81E-05
EBN20	MPD	He	300,1	300,0	0,0	249,9	0,0	perpendi	no	no	yes	3,29E-05	0,05			147	Tom		no	5,67	6,03	MPD		no	5,23E-05
EBN20	MPD	He	407,2	400,0	0,0	357,3	0,0	perpendi	no	no	yes	1,47E-05	0,04			578	Tom		no	5,67	6,03	MPD		no	3,84E-05
EBN20	MPD	He	522,0	500,0	0,0	447,0	0,0	perpendi	no	no	yes	1,22E-06	0,03			9900	Tom		no	5,67	6,03	MPD		no	2,83E-05
EBN20	MPD	He	108,8	80,0	0,0	201,4	0,0	perpendi	no	no	yes	5,74E-06	0,04			3852	Tom		no	5,67	6,03	MPD		no	1,15E-04
EBN20	MPD	He	39,9	80,0	0,0	92,2	0,0	perpendi	no	no	yes	3,37E-06	0,04			4007	Tom		no	5,67	6,03	MPD		no	1,50E-04
EBN20	MPD	He	22,8	80,0	0,0	40,0	0,0	perpendi	no	no	yes	7,19E-06	0,13			415	Tom		no	5,67	6,03	MPD		no	8,17E-05
EBN20	MPD	He	102,0	80,0	0,0	65,3	0,0	perpendi	no	no	no	1,00E-05	0,04				Tom		no	5,67	6,03	MPD		no	1,00E-05
EBN20	MPD	He	193,9	180,0	0,0	148,1	0,0	perpendi	no	no	no	1,30E-05	0,08				Tom		no	5,67	6,03	MPD		no	1,30E-05
EBN20	MPD	He	300,1	300,0	0,0	249,9	0,0	perpendi	no	no	no	1,23E-05	0,05				Tom		no	5,67	6,03	MPD		no	1,23E-05
EBN20	MPD	He	407,2	400,0	0,0	357,3	0,0	perpendi	no	no	no	1,60E-05	0,04				Tom		no	5,67	6,03	MPD		no	1,60E-05
EBN20	MPD	He	522,0	500,0	0,0	447,0	0,0	perpendi	no	no	no	2,10E-05	0,05				Tom		no	5,67	6,03	MPD		no	2,10E-05
EBN20	MPD	He	108,8	80,0	0,0	201,4	0,0	perpendi	no	no	no	2,39E-05	0,04				Tom		no	5,67	6,03	MPD		no	2,39E-05
EBN20	MPD	He	39,9	80,0	0,0	92,2	0,0	perpendi	no	no	no	1,48E-05	0,04				Tom		no	5,67	6,03	MPD		no	1,48E-05
EBN20	MPD	He	22,8	80,0	0,0	40,0	0,0	perpendi	no	no	no	1,39E-05	0,06				Tom		no	5,67	6,03	MPD		no	1,39E-05
EBN20	MPD	He	201,0	210,0	0,0	111,0	0,0	parallel	yes	yes	yes	4,02E-05	0,08	3,91E-03	0,15	7240	Tom		no	5,67	6,03	MPD		no	2,66E-03
EBN20	MPD	He	301,0	300,0	0,0	210,0	0,0	parallel	yes	yes	yes	4,14E-04	0,09	1,99E-03	0,12	1376	Tom		no	5,67	6,03	MPD		no	3,13E-03
EBN20	MPD	He	402,0	400,0	0,0	310,0	0,0	parallel	yes	yes	yes	1,88E-04	0,09	2,92E-04	0,14	3352	Tom		no	5,67	6,03	MPD		no	2,22E-03
EBN20	MPD	He	501,0	500,0	0,0	410,0	0,0	parallel	yes	yes	yes	3,64E-04	0,09	2,57E-03	0,20	1552	Tom		no	5,67	6,03	MPD		no	1,74E-03
EBN20	MPD	He	201,0	210,0	0,0	111,0	0,0	parallel	yes	yes	no	1,08E-05	0,09	1,98E-05	0,22		Tom		no	5,67	6,03	MPD		no	1,08E-05
EBN20	MPD	He	301,0	300,0	0,0	210,0	0,0	parallel	yes	yes	no	1,09E-03	0,11	6,07E-02	0,21		Tom		no	5,67	6,03	MPD		no	1,09E-03
EBN20	MPD	He	402,0	400,0	0,0	310,0	0,0	parallel	yes	yes	no	8,14E-04	0,07	1,05E-03	0,14		Tom		no	5,67	6,03	MPD		no	8,14E-04

EBN20	MPD	He	501,0	500,0	0,0	410,0	0,0	parallel	yes	yes	no	1,19E-03	0,09	1,33E-03	0,15		Tom		no	5,67	6,03	MPD		no	1,19E-03
EBN20	MPD	He	201,0	210,0	0,0	111,0	0,0	parallel	yes	no	no	1,93E-03	0,09				Tom		no	5,67	6,03	MPD		no	1,93E-03
EBN20	MPD	He	301,0	300,0	0,0	210,0	0,0	parallel	yes	no	no	9,84E-04	0,09				Tom		no	5,67	6,03	MPD		no	9,84E-04
EBN20	MPD	He	402,0	400,0	0,0	310,0	0,0	parallel	yes	no	no	1,01E-03	0,09				Tom		no	5,67	6,03	MPD		no	1,01E-03
EBN20	MPD	He	501,0	500,0	0,0	410,0	0,0	parallel	yes	no	no	1,04E-03	0,09				Tom		no	5,67	6,03	MPD		no	1,04E-03
EBN20	MPD	He	201,0	210,0	0,0	111,0	0,0	parallel	yes	no	yes	2,27E-05	0,12			34988	Tom		no	5,67	6,03	MPD		no	7,16E-03
EBN20	MPD	He	301,0	300,0	0,0	210,0	0,0	parallel	yes	no	yes	3,37E-05	0,11			32440	Tom		no	5,67	6,03	MPD		no	5,24E-03
EBN20	MPD	He	402,0	400,0	0,0	310,0	0,0	parallel	yes	no	yes	3,57E-04	0,08			1902	Tom		no	5,67	6,03	MPD		no	2,55E-03
EBN20	MPD	He	501,0	500,0	0,0	410,0	0,0	parallel	yes	no	yes	6,51E-04	0,10			1171	Tom		no	5,67	6,03	MPD		no	2,51E-03
EBN20	MPD	He	71,6	80,0	0,0	66,0	0,0	perpendi	yes	no	yes	7,31E-06	0,06			3365	Tom		no	5,67	6,03	MPD		no	3,80E-04
EBN20	MPD	He	23,2	80,0	0,0	26,3	0,0	perpendi	yes	no	yes	5,77E-06	0,04			6855	Tom		no	5,67	6,03	MPD		no	1,51E-03
EBN20	MPD	He	71,6	80,0	0,0	66,0	0,0	perpendi	yes	no	no	3,31E-05	0,04				Tom		no	5,67	6,03	MPD		no	3,31E-05
EBN20	MPD	He	23,2	80,0	0,0	26,3	0,0	perpendi	yes	no	no	1,31E-06	0,16				Tom		no	5,67	6,03	MPD		no	1,31E-06
EBN20	fcgri	He	68,0	80,0	0,0	66,6	0,0	perpendi	no	yes	yes	1,57E-06	0,05	4,95E-05	0,08	609	Tom		no	5,67	6,03	S1		no	1,59E-05
EBN20	fcgri	He	0,0	0,0	3600,0	1,0	1,0	perpendi	no	yes	yes	1,46E-09	0,12	3,60E-03	0,13	4443	Tom		yes	5,67	6,03	S1		no	6,37E-06
EBN20	fcgri	He	132,2	150,0	0,0	130,9	0,0	perpendi	no	yes	yes	9,95E-06	0,04	4,00E-01	0,06	1022	Tom		no	5,67	6,03	S1		no	8,77E-05
EBN20	fcgri	He	623,0	600,0	0,0	608,0	0,0	perpendi	no	yes	yes	1,47E-05	0,04	4,70E+01	0,04	60	Tom		no	5,67	6,03	S1		no	1,61E-05
EBN20	fcgri	He	1,0	0,0	1,0	10,0	0,1	perpendi	no	yes	yes	3,00E-06	0,04	1,06E+00	0,06	3107	Tom		yes	5,67	6,03	S1	WG	no	9,36E-04
EBN20	fcgri	He	665,0	700,0	0,0	650,0	0,0	perpendi	no	yes	yes	4,61E-05	0,05	7,59E-01	0,05	44	Tom		no	5,67	6,03	S1		no	4,92E-05
EBN20	fcgri	He	1,0	0,0	1,0	11,0	0,1	perpendi	no	yes	yes	6,75E-05	0,05	2,75E+00	0,06	4	Tom		yes	5,67	6,03	S1	WG	no	9,05E-05
EBN20	fcgri	He	668,0	700,0	0,0	653,0	0,0	perpendi	no	yes	yes	1,02E-06	0,04	1,80E+00	0,09	2547	Tom		no	5,67	6,03	S1		no	4,99E-06
EBN20	fcgri	He	1,0	0,0	1,0	11,0	0,1	perpendi	no	yes	yes	1,74E-06	0,04	1,07E+01	0,09	3283	Tom		yes	5,67	6,03	S1	WG	no	5,22E-04
EBN20	fcgri	He	68,0	80,0	0,0	66,6	0,0	perpendi	no	yes	no	2,29E-04	0,05	6,73E-03	0,12		Tom		no	5,67	6,03	S1		no	2,29E-04
EBN20	fcgri	He	0,0	0,0	3600,0	1,0	1,0	perpendi	no	yes	no	2,79E-06	0,10	3,30E-02	0,12		Tom		yes	5,67	6,03	S1	WG	no	2,79E-06
EBN20	fcgri	He	132,2	150,0	0,0	130,9	0,0	perpendi	no	yes	no	6,86E-05	0,04	1,34E-04	0,11		Tom		no	5,67	6,03	S1		no	6,86E-05
EBN20	fcgri	He	623,0	600,0	0,0	608,0	0,0	perpendi	no	yes	no	4,63E-05	0,05	1,29E-04	0,11		Tom		no	5,67	6,03	S1		no	4,63E-05
EBN20	fcgri	He	1,0	0,0	1,0	10,0	0,1	perpendi	no	yes	no	6,81E-05	0,05	3,40E-03	0,08		Tom		yes	5,67	6,03	S1	WG	no	6,81E-05
EBN20	fcgri	He	665,0	700,0	0,0	650,0	0,0	perpendi	no	yes	no	2,43E-05	0,04	1,88E-04	0,06		Tom		no	5,67	6,03	S1		no	2,43E-05
EBN20	fcgri	He	668,0	700,0	0,0	653,0	0,0	perpendi	no	yes	no	1,16E-05	0,04	8,72E-02	0,12		Tom		no	5,67	6,03	S1		no	1,16E-05
EBN20	fcgri	He	1,0	0,0	1,0	11,0	0,1	perpendi	no	yes	no	4,43E-05	0,05	1,35E-02	0,05		Tom		yes	5,67	6,03	S1	WG	no	4,43E-05
EBN20	fcgri	He	68,0	80,0	0,0	66,6	0,0	perpendi	no	no	yes	5,32E-06	0,04			2002	Tom		no	5,67	6,03	S1		no	1,65E-04
EBN20	fcgri	He	0,0	0,0	3600,0	1,0	1,0	perpendi	no	no	yes	1,33E-08	0,12			8417	Tom		yes	5,67	6,03	S1		no	1,10E-04
EBN20	fcgri	He	132,2	150,0	0,0	130,9	0,0	perpendi	no	no	yes	1,42E-05	0,04			655	Tom		no	5,67	6,03	S1		no	8,52E-05
EBN20	fcgri	He	623,0	600,0	0,0	608,0	0,0	perpendi	no	no	yes	3,64E-05	0,06			41	Tom		no	5,67	6,03	S1		no	3,88E-05
EBN20	fcgri	He	1,0	0,0	1,0	10,0	0,1	perpendi	no	no	yes	6,79E-05	0,05			8	Tom		yes	5,67	6,03	S1	WG	no	1,20E-04
EBN20	fcgri	He	665,0	700,0	0,0	650,0	0,0	perpendi	no	no	yes	1,13E-05	0,05			135	Tom		no	5,67	6,03	S1		no	1,37E-05
EBN20	fcgri	He	1,0	0,0	1,0	11,0	0,1	perpendi	no	no	yes	5,59E-05	0,05			4	Tom		yes	5,67	6,03	S1	WG	no	7,71E-05
EBN20	fcgri	He	668,0	700,0	0,0	653,0	0,0	perpendi	no	no	yes	1,77E-05	0,05			87	Tom		no	5,67	6,03	S1		no	2,00E-05
EBN20	fcgri	He	1,0	0,0	1,0	11,0	0,1	perpendi	no	no	yes	2,72E-05	0,05			257	Tom		yes	5,67	6,03	S1	WG	no	6,62E-04
EBN20	fcgri	He	68,0	80,0	0,0	66,6	0,0	perpendi	no	no	no	2,33E-04	0,05				Tom		no	5,67	6,03	S1		no	2,33E-04
EBN20	fcgri	He	0,0	0,0	3600,0	1,0	1,0	perpendi	no	no	no	6,51E-06	0,05				Tom		yes	5,67	6,03	S1		no	6,51E-06
EBN20	fcgri	He	132,2	150,0	0,0	130,9	0,0	perpendi	no	no	no	1,20E-04	0,04				Tom		no	5,67	6,03	S1		no	1,20E-04
EBN20	fcgri	He	623,0	600,0	0,0	608,0	0,0	perpendi	no	no	no	3,50E-05	0,05				Tom		no	5,67	6,03	S1		no	3,50E-05
EBN20	fcgri	He	1,0	0,0	1,0	10,0	0,1	perpendi	no	no	no	8,36E-05	0,05				Tom		yes	5,67	6,03	S1	WG	no	8,36E-05
EBN20	fcgri	He	665,0	700,0	0,0	650,0	0,0	perpendi	no	no	no	3,36E-05	0,05				Tom		no	5,67	6,03	S1		no	3,36E-05
EBN20	fcgri	He	1,0	0,0	1,0	11,0	0,1	perpendi	no	no	no	8,52E-05	0,05				Tom		yes	5,67	6,03	S1	WG	no	8,52E-05
EBN20	fcgri	He	668,0	700,0	0,0	653,0	0,0	perpendi	no	no	no	2,52E-05	0,04				Tom		no	5,67	6,03	S1		no	2,52E-05
EBN20	fcgri	He	1,0	0,0	1,0	11,0	0,1	perpendi	no	no	no	8,79E-05	0,05				Tom		yes	5,67	6,03	S1	WG	no	8,79E-05
EBN20	fcgri	CH4	155,1	150,0	0,0	46,4	0,0	parallel	yes	yes	yes	1,66E-05	0,13				Tom		no	5,67	6,03	S1	WG	no	1,66E-05
EBN20	fcgri	CH4	182,0	180,0	0,0	85,8	0,0	parallel	yes	yes	yes	2,76E-05	0,13				Tom		no	5,67	6,03	S1	WG	no	2,76E-05
EBN20	fcgri	CH4	210,4	210,0	0,0	121,9	0,0	parallel	yes	yes	yes	1,63E-05	0,10				Tom		no	5,67	6,03	S1	WG	no	1,63E-05
EBN20	fcgri	CH4	1,9	0,0	0,5	87,7	0,0	parallel	yes	yes	yes	3,36E-05	0,09				Tom		yes	5,67	6,03	S1	mbi	no	3,36E-05
EBN20	fcgri	CH4	2,0	0,0	0,5	63,1	0,0	parallel	yes	yes	yes	2,30E-05	0,09				Tom		yes	5,67	6,03	S1	mbi	no	2,30E-05
EBN20	fcgri	CH4	155,1	150,0	0,0	46,4	0,0	parallel	yes	yes	no	4,81E-06	0,13			816	Tom		no	5,67	6,03	S1	WG	no	4,81E-06

EBN20	fcgri	CH4	182,0	180,0	0,0	85,8	0,0	parallel	yes	yes	no	4,88E-06	0,11			1066	Tom		no	5,67	6,03	S1	WG	no	4,88E-06
EBN20	fcgri	CH4	210,4	210,0	0,0	121,9	0,0	parallel	yes	yes	no	2,93E-06	0,09			1920	Tom		no	5,67	6,03	S1	WG	no	2,93E-06
EBN20	fcgri	CH4	1,9	0,0	0,5	87,7	0,0	parallel	yes	yes	no	4,95E-06	0,09			2176	Tom		yes	5,67	6,03	S1	mbi	no	4,95E-06
EBN20	fcgri	CH4	2,0	0,0	0,5	63,1	0,0	parallel	yes	yes	no	3,22E-06	0,10			2016	Tom		yes	5,67	6,03	S1	mbi	no	3,22E-06
EBN20	fcgri	CH4	155,1	150,0	0,0	46,4	0,0	parallel	yes	yes	no	1,64E-05	0,14	1,22E-04	0,14		Tom		no	5,67	6,03	S1	WG	no	1,64E-05
EBN20	fcgri	CH4	182,0	180,0	0,0	85,8	0,0	parallel	yes	yes	no	1,90E-05	0,12	7,54E-05	0,13		Tom		no	5,67	6,03	S1	WG	no	1,90E-05
EBN20	fcgri	CH4	210,4	210,0	0,0	121,9	0,0	parallel	yes	yes	no	1,67E-05	0,10	5,20E-05	0,14		Tom		no	5,67	6,03	S1	WG	no	1,67E-05
EBN20	fcgri	CH4	1,9	0,0	0,5	87,7	0,0	parallel	yes	yes	no	2,75E-05	0,09	1,96E-05	0,14		Tom		yes	5,67	6,03	S1	mbi	no	2,75E-05
EBN20	fcgri	CH4	2,0	0,0	0,5	63,1	0,0	parallel	yes	yes	no	1,18E-05	0,10	7,26E-02	0,09		Tom		yes	5,67	6,03	S1	mbi	no	1,18E-05
EBN20	fcgri	CH4	155,1	150,0	0,0	46,4	0,0	parallel	yes	no	no	1,15E-06	0,13	2,81E-04	0,15	2227	Tom		no	5,67	6,03	S1	WG	no	1,15E-06
EBN20	fcgri	CH4	182,0	180,0	0,0	85,8	0,0	parallel	yes	no	no	3,51E-06	0,12	1,21E-05	0,14	1782	Tom		no	5,67	6,03	S1	WG	no	3,51E-06
EBN20	fcgri	CH4	210,4	210,0	0,0	121,9	0,0	parallel	yes	no	no	1,96E-06	0,10	9,85E-06	0,14	2491	Tom		no	5,67	6,03	S1	WG	no	1,96E-06
EBN20	fcgri	CH4	1,9	0,0	0,5	87,7	0,0	parallel	yes	no	no	3,30E-06	0,09	4,53E-06	0,12	2754	Tom		yes	5,67	6,03	S1	mbi	no	3,30E-06
EBN20	fcgri	CH4	2,0	0,0	0,5	63,1	0,0	parallel	yes	no	no	2,23E-06	0,11	2,70E-06	0,09	4286	Tom		yes	5,67	6,03	S1	mbi	no	2,23E-06
EBN20	MPD	He	69,0	80,0	0,0	46,9	0,0	parallel	no	yes	no	1,20E-04	0,05	4,00E-09	0,05		Konstantin		no	5,67	6,03	MPD		no	1,20E-04
EBN20	MPD	He	158,2	150,0	0,0	115,3	0,0	parallel	no	yes	no	8,00E-05	0,05	4,00E-09	0,05		Konstantin		no	5,67	6,03	MPD		no	8,00E-05
EBN20	MPD	He	281,4	300,0	0,0	225,9	0,0	parallel	no	yes	no	2,00E-05	0,05	4,00E-09	0,05		Konstantin		no	5,67	6,03	MPD		no	2,00E-05
EBN20	MPD	He	101,2	80,0	0,0	136,7	0,0	parallel	no	yes	no	4,00E-05	0,05	4,00E-09	0,05		Konstantin		no	5,67	6,03	MPD		no	4,00E-05
EBN20	MPD	He	69,0	80,0	0,0	46,9	0,0	parallel	no	yes	yes	1,26E-05	0,04	5,70E-05	0,02	272	Konstantin		no	5,67	6,03	MPD		no	8,57E-05
EBN20	MPD	He	158,2	150,0	0,0	115,3	0,0	parallel	no	yes	yes	3,11E-05	0,12	8,88E-03	0,01	231	Konstantin		no	5,67	6,03	MPD		no	9,36E-05
EBN20	MPD	He	281,4	300,0	0,0	225,9	0,0	parallel	no	yes	yes	2,52E-05	0,08	7,40E-06	0,01	117	Konstantin		no	5,67	6,03	MPD		no	3,81E-05
EBN20	fcgri	N2	124,5	150,0	0,0	113,9	0,0	parallel	no	no	no	3,00E-04	0,08				Konstantin		no	5,67	6,03	X		no	3,00E-04
EBN20	fcgri	N2	0,0	0,0	100,0	6,9	0,1	parallel	no	no	no	2,50E-04	0,05				Konstantin		yes	5,67	6,03	X		no	2,50E-04
EBN20	fcgri	He	145,2	150,0	0,0	53,8	0,0	parallel	no	no	no	2,38E-07	0,07				Tom		no	5,67	6,03	S1	WG	yes	2,38E-07
EBN20	fcgri	He	197,7	210,0	0,0	106,0	0,0	parallel	no	no	no	7,27E-07	0,07				Tom		no	5,67	6,03	S1	WG	yes	7,27E-07
EBN20	fcgri	He	247,7	250,0	0,0	157,3	0,0	parallel	no	no	no	9,04E-07	0,07				Tom		no	5,67	6,03	S1	WG	yes	9,04E-07
EBN20	fcgri	He	298,5	300,0	0,0	208,2	0,0	parallel	no	no	no	8,23E-07	0,07				Tom		no	5,67	6,03	S1	WG	yes	8,23E-07
EBN20	fcgri	He	402,0	400,0	0,0	278,1	0,0	parallel	no	no	no	8,50E-07	0,07				Tom		no	5,67	6,03	S1	WG	yes	8,50E-07
EBN20	fcgri	He	2,1	0,0	0,5	176,5	0,0	parallel	no	no	no	3,46E-07	0,07				Tom		yes	5,67	6,03	S1		yes	3,46E-07
EBN20	MPD	He	151,0	150,0	0,0	102,0	0,0	parallel	no	no	no	9,93E-06	0,07				Tom		no	5,67	6,03	MPD	mbi	yes	9,93E-06
EBN20	MPD	He	302,0	300,0	0,0	195,0	0,0	parallel	no	no	no	1,81E-05	0,07				Tom		no	5,67	6,03	MPD		yes	1,81E-05
EBN20	MPD	He	411,0	400,0	0,0	295,0	0,0	parallel	no	no	no	1,76E-05	0,07				Tom		no	5,67	6,03	MPD		yes	1,76E-05
EBN20	MPD	He	4,0	0,0	0,3	149,0	0,0	parallel	no	no	no	4,36E-05	0,07				Tom		yes	5,67	6,03	MPD		yes	4,36E-05
EBN20	MPD	He	151,0	150,0	0,0	102,0	0,0	parallel	no	yes	no	3,58E-06	0,07	1,22E-05	0,09		Tom		no	5,67	6,03	MPD	mbi	yes	3,58E-06
EBN20	MPD	He	302,0	300,0	0,0	195,0	0,0	parallel	no	yes	no	2,29E-05	0,07	5,23E-05	0,04		Tom		no	5,67	6,03	MPD		yes	2,29E-05
EBN20	MPD	He	411,0	400,0	0,0	295,0	0,0	parallel	no	yes	no	2,58E-04	0,07	1,74E-05	0,04		Tom		no	5,67	6,03	MPD		yes	2,58E-04
EBN20	MPD	He	4,0	0,0	0,3	149,0	0,0	parallel	no	yes	no	8,48E-06	0,07	1,42E-03	0,04		Tom		yes	5,67	6,03	MPD		yes	8,48E-06
EBN20	fcgri	He	153,4	150,0	0,0	68,6	0,0	parallel	yes	no	no	7,21E-04	0,07				Tom		no	5,67	6,03	G3	mbi	yes	7,21E-04
EBN20	fcgri	He	181,5	180,0	0,0	119,3	0,0	parallel	yes	no	no	7,41E-04	0,07				Tom		no	5,67	6,03	G3		yes	7,41E-04
EBN20	fcgri	He	211,3	210,0	0,0	160,5	0,0	parallel	yes	no	no	7,57E-04	0,07				Tom		no	5,67	6,03	G3		yes	7,57E-04
EBN20	fcgri	He	246,3	250,0	0,0	198,9	0,0	parallel	yes	no	no	7,34E-04	0,07				Tom		no	5,67	6,03	G3		yes	7,34E-04
EBN20	fcgri	He	-0,1	0,0	-7,1	109,2	0,0	parallel	yes	no	no	1,05E-05	0,07				Tom		yes	5,67	6,03	G3	mbi	yes	1,05E-05
EBN20	MPD	He	201,0	210,0	0,0	111,0	0,0	parallel	yes	no	no	8,35E-06	0,07				Tom		no	5,67	6,03	MPD		yes	8,35E-06
EBN20	MPD	He	301,0	300,0	0,0	210,0	0,0	parallel	yes	no	no	7,22E-04	0,07				Tom		no	5,67	6,03	MPD		yes	7,22E-04
EBN20	MPD	He	402,0	400,0	0,0	310,0	0,0	parallel	yes	no	no	7,50E-04	0,07				Tom		no	5,67	6,03	MPD		yes	7,50E-04
EBN20	MPD	He	501,0	500,0	0,0	410,0	0,0	parallel	yes	no	no	7,19E-04	0,07				Tom		no	5,67	6,03	MPD		yes	7,19E-04
EBN20	fcgri	CH4	165,9	150,0	0,0	59,8	0,0	parallel	no	no	no	4,21E-06	0,13				Tom		no	5,67	6,03	S1	WG	yes	4,21E-06
EBN20	fcgri	CH4	185,9	180,0	0,0	103,8	0,0	parallel	no	no	no	1,29E-06	0,13				Tom		no	5,67	6,03	S1	WG	yes	1,29E-06
EBN20	fcgri	CH4	208,1	210,0	0,0	140,0	0,0	parallel	no	no	no	3,12E-06	0,13				Tom		no	5,67	6,03	S1	WG	yes	3,12E-06
EBN20	MPD	He	102,0	80,0	0,0	65,3	0,0	perpendi	no	yes	no	2,57E-06	0,07	3,14E-04	0,15		Tom		no	5,67	6,03	MPD		yes	2,57E-06
EBN20	MPD	He	193,9	180,0	0,0	148,1	0,0	perpendi	no	yes	no	2,50E-06	0,07	3,37E-04	0,17		Tom		no	5,67	6,03	MPD		yes	2,50E-06
EBN20	MPD	He	300,1	300,0	0,0	249,9	0,0	perpendi	no	yes	no	8,76E-06	0,07	1,94E-04	0,13		Tom		no	5,67	6,03	MPD		yes	8,76E-06
EBN20	MPD	He	407,2	400,0	0,0	357,3	0,0	perpendi	no	yes	no	4,76E-06	0,07	4,22E-04	0,11		Tom		no	5,67	6,03	MPD		yes	4,76E-06
EBN20	MPD	He	522,0	500,0	0,0	447,0	0,0	perpendi	no	yes	no	1,18E-06	0,07	7,32E-04	0,10		Tom		no	5,67	6,03	MPD		yes	1,18E-06

EBN20	MPD	He	108,8	80,0	0,0	201,4	0,0	perpendi	no	yes	no	2,40E-06	0,07	5,49E-04	0,08		Tom		no		5,67	6,03	MPD		yes	2,40E-06
EBN20	MPD	He	39,9	80,0	0,0	92,2	0,0	perpendi	no	yes	no	5,59E-07	0,07	3,95E-04	0,06		Tom		no		5,67	6,03	MPD		yes	5,59E-07
EBN20	MPD	He	22,8	80,0	0,0	40,0	0,0	perpendi	no	yes	no	3,64E-06	0,07	4,13E-04	0,07		Tom		no		5,67	6,03	MPD		yes	3,64E-06
EBN20	MPD	He	102,0	80,0	0,0	65,3	0,0	perpendi	no	no	no	9,31E-06	0,07				Tom		no		5,67	6,03	MPD		yes	9,31E-06
EBN20	MPD	He	193,9	180,0	0,0	148,1	0,0	perpendi	no	no	no	1,30E-05	0,07				Tom		no		5,67	6,03	MPD		yes	1,30E-05
EBN20	MPD	He	300,1	300,0	0,0	249,9	0,0	perpendi	no	no	no	1,29E-05	0,07				Tom		no		5,67	6,03	MPD		yes	1,29E-05
EBN20	MPD	He	407,2	400,0	0,0	357,3	0,0	perpendi	no	no	no	1,05E-05	0,07				Tom		no		5,67	6,03	MPD		yes	1,05E-05
EBN20	MPD	He	522,0	500,0	0,0	447,0	0,0	perpendi	no	no	no	1,61E-05	0,07				Tom		no		5,67	6,03	MPD		yes	1,61E-05
EBN20	MPD	He	108,8	80,0	0,0	201,4	0,0	perpendi	no	no	no	4,04E-05	0,07				Tom		no		5,67	6,03	MPD		yes	4,04E-05
EBN20	MPD	He	39,9	80,0	0,0	92,2	0,0	perpendi	no	no	no	1,38E-05	0,07				Tom		no		5,67	6,03	MPD		yes	1,38E-05
EBN20	MPD	He	22,8	80,0	0,0	40,0	0,0	perpendi	no	no	no	1,57E-05	0,07				Tom		no		5,67	6,03	MPD		yes	1,57E-05
EBN20	fcgri	He	68,0	80,0	0,0	66,6	0,0	perpendi	no	no	no	2,81E-04	0,07				Tom		no		5,67	6,03	S1		yes	2,81E-04
EBN20	fcgri	He	0,0	0,0	3600,0	1,0	1,0	perpendi	no	no	no	3,01E-06	0,07				Tom		yes		5,67	6,03	S1		yes	3,01E-06
EBN20	fcgri	He	132,2	150,0	0,0	130,9	0,0	perpendi	no	no	no	9,00E-06	0,07				Tom		no		5,67	6,03	S1		yes	9,00E-06
EBN20	fcgri	He	623,0	600,0	0,0	608,0	0,0	perpendi	no	no	no	3,93E-05	0,07				Tom		no		5,67	6,03	S1		yes	3,93E-05
EBN20	fcgri	He	1,0	0,0	1,0	10,0	0,1	perpendi	no	no	no	8,37E-06	0,07				Tom		yes		5,67	6,03	S1		yes	8,37E-06
EBN20	fcgri	He	665,0	700,0	0,0	650,0	0,0	perpendi	no	no	no	1,67E-05	0,07				Tom		no		5,67	6,03	S1		yes	1,67E-05
EBN20	fcgri	He	1,0	0,0	1,0	11,0	0,1	perpendi	no	no	no	1,52E-05	0,07				Tom		yes		5,67	6,03	S1		yes	1,52E-05
EBN20	fcgri	He	668,0	700,0	0,0	653,0	0,0	perpendi	no	no	no	2,49E-05	0,07				Tom		no		5,67	6,03	S1		yes	2,49E-05
EBN20	fcgri	He	1,0	0,0	1,0	11,0	0,1	perpendi	no	no	no	3,25E-05	0,07				Tom		yes		5,67	6,03	S1		yes	3,25E-05
EBN20	fcgri	He	152,0	150,0	0,0	67,0	0,0	perpendi	yes	no	no	1,40E-04	0,07				Tom		no		5,67	6,03	G2		yes	1,40E-04
EBN20	fcgri	He	180,6	180,0	0,0	117,1	0,0	perpendi	yes	no	no	1,69E-04	0,07				Tom		no		5,67	6,03	G2		yes	1,69E-04
EBN20	fcgri	He	-0,1	0,0	-10,0	64,8	0,0	perpendi	yes	no	no	7,50E-05	0,07				Tom		yes		5,67	6,03	G2	WG	yes	7,50E-05
EBN20	fcgri	He	152,0	150,0	0,0	67,0	0,0	perpendi	yes	no	no	7,40E-05	0,08				Tom		no		5,67	6,03	G2		no	7,40E-05
EBN20	fcgri	He	180,6	180,0	0,0	117,1	0,0	perpendi	yes	no	no	4,76E-06	0,09				Tom		no		5,67	6,03	G2		no	4,76E-06
EBN20	fcgri	He	-0,1	0,0	-10,0	64,8	0,0	perpendi	yes	no	no	5,35E-05	0,10				Tom		yes		5,67	6,03	G2	WG	no	5,35E-05
EBN20	fcgri	CH4	157,2	150,0	0,0	74,2	-100,0	perpendi	yes	no	no	2,33E-04	0,12				Tom		no		5,67	6,03	G2		no	2,33E-04
EBN20	fcgri	CH4	0,0	0,0	-100,0	39,1	0,0	perpendi	yes	no	no	2,84E-04	0,10				Tom		yes		5,67	6,03	G2		no	2,84E-04
EBN20	fcgri	He	152,0	150,0	0,0	67,0	0,0	perpendi	yes	no	yes	5,87E-08	0,07			4820	Tom		no		5,67	6,03	G2		yes	4,28E-06
EBN20	fcgri	He	180,6	180,0	0,0	117,1	0,0	perpendi	yes	no	yes	1,41E-06	0,07			4479	Tom		no		5,67	6,03	G2		yes	5,53E-05
EBN20	fcgri	He	-0,1	0,0	-10,0	64,8	0,0	perpendi	yes	no	yes	3,95E-06	0,07			6465	Tom		yes		5,67	6,03	G2	WG	yes	3,98E-04
EBN20	fcgri	CH4	157,2	150,0	0,0	74,2	-100,0	perpendi	yes	no	yes	8,51E-05	0,08			861	Tom		no		5,67	6,03	G2		no	1,07E-03
EBN20	fcgri	CH4	0,0	0,0	-100,0	39,1	0,0	perpendi	yes	no	yes	1,20E-04	0,09			1798	Tom		yes		5,67	6,03	G2		no	5,65E-03
EBN20	fcgri	He	152,0	150,0	0,0	67,0	0,0	perpendi	yes	yes	no	1,33E-04	0,07	9,71E-04	0,16		Tom		no		5,67	6,03	G2		yes	1,33E-04
EBN20	fcgri	He	180,6	180,0	0,0	117,1	0,0	perpendi	yes	yes	no	1,22E-04	0,07	1,43E-04	0,06		Tom		no		5,67	6,03	G2		yes	1,22E-04
EBN20	fcgri	He	-0,1	0,0	-10,0	64,8	0,0	perpendi	yes	yes	no	8,95E-05	0,07	1,26E-04	0,06		Tom		yes		5,67	6,03	G2	WG	yes	8,95E-05
EBN20	fcgri	CH4	152,0	150,0	0,0	67,0	0,0	perpendi	yes	yes	no	2,29E-04	0,12	4,45E-04	0,06		Tom		no		5,67	6,03	G2		no	2,29E-04
EBN20	fcgri	CH4	180,5	180,0	0,0	117,1	0,0	perpendi	yes	yes	no	5,63E-04	0,13	7,46E-04	0,08		Tom		no		5,67	6,03	G2		no	5,63E-04
EBN20	fcgri	CH4	-0,1	0,0	-10,0	64,8	0,0	perpendi	yes	yes	yes	9,84E-06	0,13	2,32E-03	0,15	5355	Tom		yes		5,67	6,03	G2		no	8,23E-04
EBN20	fcgri	CH4	152,0	150,0	0,0	67,0	0,0	perpendi	yes	yes	yes	8,72E-06	0,10	1,46E-03	0,14	6783	Tom		no		5,67	6,03	G2		no	8,92E-04
EBN20	fcgri	CH4	180,5	180,0	0,0	117,1	0,0	perpendi	yes	yes	yes	6,95E-09	0,07	7,09E-02	0,11	9671	Tom		no		5,67	6,03	G2		yes	5,81E-07
EBN20	fcgri	CH4	-0,1	0,0	-10,0	64,8	0,0	perpendi	yes	yes	yes	9,74E-04	0,07	1,25E-03	0,11	6	Tom		yes		5,67	6,03	G2		yes	1,06E-03
EBN20	fcgri	CH4	152,0	150,0	0,0	67,0	0,0	perpendi	yes	yes	yes	5,81E-05	0,07	2,10E-04	0,17	532	Tom		no		5,67	6,03	G2		yes	5,20E-04
EBN20	fcgri	CH4	180,5	180,0	0,0	117,1	0,0	parallel	yes	no	no	1,14E-03	0,13				Tom		no		5,67	6,03	G3	WG	yes	1,14E-03
EBN20	fcgri	CH4	-0,1	0,0	-10,0	64,8	0,0	parallel	yes	no	no	5,90E-05	0,13				Tom		yes		5,67	6,03	G3	mbi	yes	5,90E-05
EBN20	fcgri	CH4	155,1	150,0	0,0	46,4	0,0	perpendi	yes	no	no	1,74E-05	0,13				Tom		no		5,67	6,03	G2		yes	1,74E-05
EBN20	fcgri	CH4	182,0	180,0	0,0	85,7	0,0	perpendi	yes	no	no	2,47E-05	0,13				Tom		no		5,67	6,03	G2		yes	2,47E-05
EBN20	fcgri	CH4	210,4	210,0	0,0	121,9	0,0	perpendi	yes	no	no	2,87E-05	0,13				Tom		no		5,67	6,03	G2		yes	2,87E-05
EBN20	fcgri	CH4	1,9	0,0	0,5	87,6	0,0	perpendi	yes	no	no	4,46E-05	0,13				Tom		yes		5,67	6,03	G2		yes	4,46E-05
EBN20	fcgri	CH4	2,0	0,0	0,5	63,0	0,0	perpendi	yes	no	no	3,51E-05	0,13				Tom		yes		5,67	6,03	G2		yes	3,51E-05
EBN20	fcgri	He	152,0	150,0	0,0	67,0	0,0	perpendi	yes	yes	yes	9,65E-09	0,07	7,09E-02	0,11	9671	Tom		no		5,67	6,03	G2		yes	1,40E-06
EBN20	fcgri	He	180,6	180,0	0,0	117,1	0,0	perpendi	yes	yes	yes	9,74E-04	0,07	1,25E-03	0,11	6	Tom		no		5,67	6,03	G2		yes	1,02E-03
EBN20	fcgri	He	-0,1	0,0	-10,0	64,8	0,0	perpendi	yes	yes	yes	5,81E-05	0,07	2,10E-04	0,17	532	Tom		yes		5,67	6,03	G2	WG	yes	5,35E-04
EBN20	fcgri	He	153,4	150,0	0,0	68,6	0,0	parallel	yes	yes	no	1,08E-05	0,09	1,98E-05	0,22		Tom		no		5,67	6,03	G3	mbi	no	1,08E-05

EBN20	fcgri	He	181,5	180,0	0,0	119,3	0,0	parallel	yes	yes	no	7,66E-04	0,08	8,50E-04	0,16		Tom		no	5,67	6,03	G3		no	7,66E-04
EBN20	fcgri	He	211,3	210,0	0,0	160,5	0,0	parallel	yes	yes	no	8,14E-04	0,07	1,05E-03	0,14		Tom		no	5,67	6,03	G3		no	8,14E-04
EBN20	fcgri	He	246,3	250,0	0,0	198,9	0,0	parallel	yes	yes	no	1,19E-02	0,09	1,33E-03	0,15		Tom		no	5,67	6,03	G3		no	1,19E-02
EBN20	fcgri	He	153,4	150,0	0,0	68,6	0,0	parallel	yes	yes	yes	4,02E-05	0,08	3,91E-03	0,15	7240	Tom		no	5,67	6,03	G3	mbi	no	4,28E-03
EBN20	fcgri	He	181,5	180,0	0,0	119,3	0,0	parallel	yes	yes	yes	4,14E-04	0,09	1,99E-03	0,12	1376	Tom		no	5,67	6,03	G3		no	5,19E-03
EBN20	fcgri	He	211,3	210,0	0,0	160,5	0,0	parallel	yes	yes	yes	1,88E-04	0,09	2,92E-04	0,14	3352	Tom		no	5,67	6,03	G3		no	4,11E-03
EBN20	fcgri	He	246,3	250,0	0,0	198,9	0,0	parallel	yes	yes	yes	3,64E-04	0,09	2,57E-03	0,20	1552	Tom		no	5,67	6,03	G3		no	3,20E-03
EBN33	fcgri	He	155,1	150,0	0,0	70,7	0,0	parallel	no	no	no	1,16E-02	0,09				Tom		no	9,23	6,13	G3	mbi	no	1,16E-02
EBN33	fcgri	He	175,6	180,0	0,0	118,6	0,0	parallel	no	no	no	4,40E-03	0,10				Tom		no	9,23	6,13	G3	mbi	no	4,40E-03
EBN33	fcgri	He	210,9	210,0	0,0	160,9	0,0	parallel	no	no	no	1,17E-03	0,10				Tom		no	9,23	6,13	G3	mbi	no	1,17E-03
EBN33	fcgri	He	241,0	250,0	0,0	197,5	0,0	parallel	no	no	no	7,89E-04	0,07				Tom		no	9,23	6,13	G3	WG	no	7,89E-04
EBN33	fcgri	He	-0,2	0,0	-4,0	106,3	0,0	parallel	no	no	no	2,98E-03	0,11				Tom		yes	9,23	6,13	G3	mbi	no	2,98E-03
EBN33	fcgri	He	155,1	150,0	0,0	70,7	0,0	parallel	no	no	yes	2,60E-04	0,08			6788	Tom		no	9,23	6,13	G3	mbi	no	2,53E-02
EBN33	fcgri	He	175,6	180,0	0,0	118,6	0,0	parallel	no	no	yes	1,42E-09	0,09			703	Tom		no	9,23	6,13	G3	mbi	no	9,83E-09
EBN33	fcgri	He	210,9	210,0	0,0	160,9	0,0	parallel	no	no	yes	3,91E-06	0,09			4293	Tom		no	9,23	6,13	G3	mbi	no	1,08E-04
EBN33	fcgri	He	241,0	250,0	0,0	197,5	0,0	parallel	no	no	yes	1,63E-03	0,17			1512	Tom		no	9,23	6,13	G3	WG	no	1,42E-02
EBN33	fcgri	He	-0,2	0,0	-4,0	106,3	0,0	parallel	no	no	yes	1,23E-03	0,09			1062	Tom		yes	9,23	6,13	G3	mbi	no	1,36E-02
EBN33	fcgri	He	155,1	150,0	0,0	70,7	0,0	parallel	no	yes	yes	1,70E-04	0,09	5,51E-04	0,15	6652	Tom		no	9,23	6,13	G3	mbi	no	1,61E-02
EBN33	fcgri	He	175,6	180,0	0,0	118,6	0,0	parallel	no	yes	yes	1,80E-04	0,05	1,22E-02	0,13	4156	Tom		no	9,23	6,13	G3	mbi	no	6,48E-03
EBN33	fcgri	He	210,9	210,0	0,0	160,9	0,0	parallel	no	yes	yes	1,69E-04	0,05	1,18E-02	0,14	4218	Tom		no	9,23	6,13	G3	mbi	no	4,59E-03
EBN33	fcgri	He	241,0	250,0	0,0	197,5	0,0	parallel	no	yes	yes	9,99E-05	0,11	1,51E-03	0,07	6044	Tom		no	9,23	6,13	G3	WG	no	3,16E-03
EBN33	fcgri	He	-0,2	0,0	-4,0	106,3	0,0	parallel	no	yes	yes	4,55E-04	0,16	1,10E-03	0,13	4790	Tom		yes	9,23	6,13	G3	mbi	no	2,10E-02
EBN33	fcgri	He	155,1	150,0	0,0	70,7	0,0	parallel	no	yes	no	2,34E-03	0,04	6,39E-02	0,10		Tom		no	9,23	6,13	G3	mbi	no	2,34E-03
EBN33	fcgri	He	175,6	180,0	0,0	118,6	0,0	parallel	no	yes	no	1,60E-07	0,04	3,58E-07	0,07		Tom		no	9,23	6,13	G3	mbi	no	1,60E-07
EBN33	fcgri	He	210,9	210,0	0,0	160,9	0,0	parallel	no	yes	no	9,80E-09	0,05	5,87E-03	0,05		Tom		no	9,23	6,13	G3	mbi	no	9,80E-09
EBN33	fcgri	He	241,0	250,0	0,0	197,5	0,0	parallel	no	yes	no	6,71E-04	0,06	8,62E-03	0,13		Tom		no	9,23	6,13	G3	WG	no	6,71E-04
EBN33	fcgri	He	-0,2	0,0	-4,0	106,3	0,0	parallel	no	yes	no	4,34E-04	0,04	3,44E-03	0,14		Tom		yes	9,23	6,13	G3	mbi	no	4,34E-04
EBN33	MPD	He	206,0	210,0	0,0	104,0	0,0	parallel	no	no	no	8,14E-04	0,11				Tom		no	9,23	6,13	MPD	ne	no	8,14E-04
EBN33	MPD	He	298,0	300,0	0,0	201,0	0,0	parallel	no	no	no	1,04E-03	0,10				Tom		no	9,23	6,13	MPD	ne	no	1,04E-03
EBN33	MPD	He	409,0	400,0	0,0	305,0	0,0	parallel	no	no	no	7,17E-04	0,08				Tom		no	9,23	6,13	MPD	ne	no	7,17E-04
EBN33	MPD	He	491,0	500,0	0,0	397,0	0,0	parallel	no	no	no	7,85E-04	0,11				Tom		no	9,23	6,13	MPD		no	7,85E-04
EBN33	MPD	He	3,0	0,0	0,3	189,0	0,0	parallel	no	no	no	8,62E-04	0,10				Tom		yes	9,23	6,13	MPD		no	8,62E-04
EBN33	MPD	He	206,0	210,0	0,0	104,0	0,0	parallel	no	no	yes	2,94E-04	0,10			467	Tom		no	9,23	6,13	MPD	ne	no	1,61E-03
EBN33	MPD	He	298,0	300,0	0,0	201,0	0,0	parallel	no	no	yes	1,37E-04	0,10			1852	Tom		no	9,23	6,13	MPD	ne	no	1,40E-03
EBN33	MPD	He	409,0	400,0	0,0	305,0	0,0	parallel	no	no	yes	1,68E-04	0,09			1626	Tom		no	9,23	6,13	MPD	ne	no	1,06E-03
EBN33	MPD	He	491,0	500,0	0,0	397,0	0,0	parallel	no	no	yes	1,33E-04	0,12			1998	Tom		no	9,23	6,13	MPD		no	8,03E-04
EBN33	MPD	He	3,0	0,0	0,3	189,0	0,0	parallel	no	no	yes	1,64E-04	0,10			1967	Tom		yes	9,23	6,13	MPD		no	1,87E-03
EBN33	MPD	He	206,0	210,0	0,0	104,0	0,0	parallel	no	yes	yes	1,16E-04	0,09	1,48E-04	0,12	2334	Tom		no	9,23	6,13	MPD	ne	no	2,72E-03
EBN33	MPD	He	298,0	300,0	0,0	201,0	0,0	parallel	no	yes	yes	5,15E-05	0,06	8,15E-05	0,12	5984	Tom		no	9,23	6,13	MPD	ne	no	1,58E-03
EBN33	MPD	He	409,0	400,0	0,0	305,0	0,0	parallel	no	yes	yes	2,73E-05	0,07	2,21E-03	0,07	3661	Tom		no	9,23	6,13	MPD	ne	no	3,55E-04
EBN33	MPD	He	491,0	500,0	0,0	397,0	0,0	parallel	no	yes	yes	3,64E-05	0,08	2,50E-03	0,08	2760	Tom		no	9,23	6,13	MPD		no	2,89E-04
EBN33	MPD	He	3,0	0,0	0,3	189,0	0,0	parallel	no	yes	yes	1,92E-05	0,08	2,57E-03	0,07	3213	Tom		yes	9,23	6,13	MPD		no	3,46E-04
EBN33	MPD	He	206,0	210,0	0,0	104,0	0,0	parallel	no	yes	no	6,33E-04	0,11	1,21E-03	0,10		Tom		no	9,23	6,13	MPD	ne	no	6,33E-04
EBN33	MPD	He	298,0	300,0	0,0	201,0	0,0	parallel	no	yes	no	5,92E-04	0,10	9,89E-03	0,12		Tom		no	9,23	6,13	MPD	ne	no	5,92E-04
EBN33	MPD	He	409,0	400,0	0,0	305,0	0,0	parallel	no	yes	no	6,27E-04	0,10	6,68E-03	0,12		Tom		no	9,23	6,13	MPD	ne	no	6,27E-04
EBN33	MPD	He	491,0	500,0	0,0	397,0	0,0	parallel	no	yes	no	1,13E-02	0,10	1,96E-03	0,12		Tom		no	9,23	6,13	MPD		no	1,13E-02
EBN33	MPD	He	3,0	0,0	0,3	189,0	0,0	parallel	no	yes	no	3,38E-04	0,11	1,62E-02	0,16		Tom		yes	9,23	6,13	MPD		no	3,38E-04
EBN33	fcgri	CH4	149,3	150,0	0,0	81,8	0,0	parallel	no	no	no	1,66E-04	0,05				Tom		no	9,23	6,13	G2	WG	no	1,66E-04
EBN33	fcgri	CH4	180,5	180,0	0,0	136,2	0,0	parallel	no	no	no	3,70E-07	0,05				Tom		no	9,23	6,13	G2	WG	no	3,70E-07
EBN33	fcgri	CH4	208,8	210,0	0,0	176,4	0,0	parallel	no	no	no	5,95E-08	0,05				Tom		no	9,23	6,13	G2	WG	no	5,95E-08
EBN33	fcgri	CH4	-0,4	0,0	-2,5	79,5	0,0	parallel	no	no	no	4,52E-04	0,16				Tom		yes	9,23	6,13	G2	mbi	no	4,52E-04
EBN33	fcgri	CH4	-0,4	0,0	-2,5	35,8	0,0	parallel	no	no	no	6,90E-04	0,09				Tom		yes	9,23	6,13	G2	mbi	no	6,90E-04
EBN33	fcgri	CH4	149,3	150,0	0,0	81,8	0,0	parallel	no	no	yes	4,44E-05	0,05			1025	Tom		no	9,23	6,13	G2	WG	no	6,01E-04
EBN33	fcgri	CH4	180,5	180,0	0,0	136,2	0,0	parallel	no	no	yes	1,04E-07	0,05			1783	Tom		no	9,23	6,13	G2	WG	no	1,47E-06

EBN33	fcgri	CH4	208,8	210,0	0,0	176,4	0,0	parallel	no	no	yes	4,54E-08	0,05			1302	Tom		no	9,23	6,13	G2	WG	no	3,81E-07
EBN33	fcgri	CH4	-0,4	0,0	-2,5	79,5	0,0	parallel	no	no	yes	1,46E-04	0,18			2336	Tom		yes	9,23	6,13	G2	mbi	no	4,42E-03
EBN33	fcgri	CH4	-0,4	0,0	-2,5	35,8	0,0	parallel	no	no	yes	1,79E-04	0,08			1776	Tom		yes	9,23	6,13	G2	mbi	no	9,04E-03
EBN33	fcgri	CH4	149,3	150,0	0,0	81,8	0,0	parallel	no	yes	yes	2,27E-05	0,05	1,21E-02	0,09	1146	Tom		no	9,23	6,13	G2	WG	no	3,40E-04
EBN33	fcgri	CH4	180,5	180,0	0,0	136,2	0,0	parallel	no	yes	yes	8,34E-08	0,05	8,66E-06	0,05	2232	Tom		no	9,23	6,13	G2	WG	no	1,45E-06
EBN33	fcgri	CH4	208,8	210,0	0,0	176,4	0,0	parallel	no	yes	yes	2,63E-08	0,04	1,41E-05	0,07	281	Tom		no	9,23	6,13	G2	WG	no	6,83E-08
EBN33	fcgri	CH4	-0,4	0,0	-2,5	79,5	0,0	parallel	no	yes	yes	2,43E-05	0,13	7,67E-04	0,19	3320	Tom		yes	9,23	6,13	G2	mbi	no	1,04E-03
EBN33	fcgri	CH4	-0,4	0,0	-2,5	35,8	0,0	parallel	no	yes	yes	8,17E-05	0,08	1,10E-03	0,20	3923	Tom		yes	9,23	6,13	G2	mbi	no	9,03E-03
EBN33	fcgri	CH4	149,3	150,0	0,0	81,8	0,0	parallel	no	yes	no	2,49E-04	0,07	3,26E-04	0,06		Tom		no	9,23	6,13	G2	WG	no	2,49E-04
EBN33	fcgri	CH4	180,5	180,0	0,0	136,2	0,0	parallel	no	yes	no	4,01E-08	0,07	1,23E-05	0,09		Tom		no	9,23	6,13	G2	WG	no	4,01E-08
EBN33	fcgri	CH4	208,8	210,0	0,0	176,4	0,0	parallel	no	yes	no	1,84E-08	0,08	2,71E-07	0,16		Tom		no	9,23	6,13	G2	WG	no	1,84E-08
EBN33	fcgri	CH4	-0,4	0,0	-2,5	79,5	0,0	parallel	no	yes	no	1,63E-05	0,08	1,86E-04	0,05		Tom		yes	9,23	6,13	G2	mbi	no	1,63E-05
EBN33	fcgri	CH4	-0,4	0,0	-2,5	35,8	0,0	parallel	no	yes	no	2,01E-04	0,08	1,46E-03	0,05		Tom		yes	9,23	6,13	G2	mbi	no	2,01E-04
EBN33	fcgri	CH4	161,6	150,0	0,0	75,0	0,0	parallel	yes	no	no	2,27E-04	0,10				Tom		no	9,23	6,13	G2		no	2,27E-04
EBN5	fcgri	He	117,1	80,0	0,0	111,7	0,0	parallel	no	no	no	3,00E-07	0,07				Konstantin		no	1,71	25,7	G3		no	3,00E-07
EBN9	MPD	He	146,4	150,0	0,0	84,8	0,0	parallel	no	no	no	9,41E-05	0,04				Tom		no	4,33	5,18	MPD		no	9,41E-05
EBN9	MPD	He	239,8	250,0	0,0	138,8	0,0	parallel	no	no	no	2,05E-03	0,04				Tom		no	4,33	5,18	MPD		no	2,05E-03
EBN9	MPD	He	512,4	500,0	0,0	294,2	0,0	parallel	no	no	no	1,48E-04	0,04				Tom		no	4,33	5,18	MPD		no	1,48E-04
EBN9	MPD	He	146,4	150,0	0,0	84,8	0,0	parallel	no	no	yes	9,96E-05	0,04			895	Tom		no	4,33	5,18	MPD		no	1,15E-03
EBN9	MPD	He	239,8	250,0	0,0	138,8	0,0	parallel	no	no	yes	2,56E-04	0,04			542	Tom		no	4,33	5,18	MPD		no	1,26E-03
EBN9	MPD	He	512,4	500,0	0,0	294,2	0,0	parallel	no	no	yes	2,25E-04	0,04			1932	Tom		no	4,33	5,18	MPD		no	1,70E-03
EBN9	MPD	He	146,4	150,0	0,0	84,8	0,0	parallel	no	yes	no	4,16E-09	0,18	4,96E-03	0,11		Tom		no	4,33	5,18	MPD		no	4,16E-09
EBN9	MPD	He	239,8	250,0	0,0	138,8	0,0	parallel	no	yes	no	2,83E-09	0,13	5,56E-02	0,07		Tom		no	4,33	5,18	MPD		no	2,83E-09
EBN9	MPD	He	512,4	500,0	0,0	294,2	0,0	parallel	no	yes	no	1,56E-09	0,13	4,32E-03	0,12		Tom		no	4,33	5,18	MPD		no	1,56E-09
EBN9	fcgri	CH4	144,3	150,0	0,0	79,7	0,0	parallel	no	yes	yes	3,50E-09	0,07	3,45E-04	0,06	702	Tom		no	4,33	5,18	G2	WG	no	3,43E-08
EBN9	fcgri	CH4	-0,3	0,0	-2,9	35,9	0,0	parallel	no	yes	yes	3,58E-09	0,07	3,62E-04	0,06	711	Tom		yes	4,33	5,18	G2	WG	no	7,46E-08
EBN9	fcgri	CH4	144,3	150,0	0,0	79,7	0,0	parallel	no	yes	no	5,99E-09	0,08	2,36E-04	0,09		Tom		no	4,33	5,18	G2	WG	no	5,99E-09
EBN9	fcgri	CH4	-0,3	0,0	-2,9	35,9	0,0	parallel	no	yes	no	5,87E-09	0,08	7,46E-05	0,06		Tom		yes	4,33	5,18	G2	WG	no	5,87E-09
EBN9	fcgri	CH4	144,3	150,0	0,0	79,7	0,0	parallel	no	no	yes	2,30E-08	0,04			552	Tom		no	4,33	5,18	G2	WG	no	1,82E-07
EBN9	fcgri	CH4	-0,3	0,0	-2,9	35,9	0,0	parallel	no	no	yes	2,26E-08	0,04			561	Tom		yes	4,33	5,18	G2	WG	no	3,76E-07
EBN9	fcgri	CH4	144,3	150,0	0,0	79,7	0,0	parallel	no	no	no	5,28E-08	0,03				Tom		no	4,33	5,18	G2	WG	no	5,28E-08
EBN9	fcgri	CH4	-0,3	0,0	-2,9	35,9	0,0	parallel	no	no	no	4,58E-08	0,03				Tom		yes	4,33	5,18	G2	WG	no	4,58E-08
EBN9	fcgri	He	771,0	800,0	0,0	752,0	0,0	parallel	no	yes	yes	1,20E-07	0,09	2,97E-07	0,09	687	Tom		no	4,33	5,18	G2		no	2,30E-07
EBN9	fcgri	He	1,0	0,0	1,0	6,6	0,2	parallel	no	yes	yes	2,93E-09	0,06	2,13E-08	0,15	1720	Tom		yes	4,33	5,18	G2		no	7,71E-07
EBN9	fcgri	He	136,2	150,0	0,0	133,8	0,0	parallel	no	yes	yes	2,51E-08	0,03	3,02E-08	0,04	113	Tom		no	4,33	5,18	G2		no	4,64E-08
EBN9	fcgri	He	771,0	800,0	0,0	752,0	0,0	parallel	no	yes	no	3,47E-08	0,06	5,00E-05	0,04		Tom		no	4,33	5,18	G2		no	3,47E-08
EBN9	fcgri	He	1,0	0,0	1,0	6,6	0,2	parallel	no	yes	no	1,04E-08	0,05	1,17E-08	0,11		Tom		yes	4,33	5,18	G2		no	1,04E-08
EBN9	fcgri	He	136,2	150,0	0,0	133,8	0,0	parallel	no	yes	no	1,70E-09	0,05	3,39E-08	0,07		Tom		no	4,33	5,18	G2		no	1,70E-09
EBN9	fcgri	He	771,0	800,0	0,0	752,0	0,0	parallel	no	no	yes	2,20E-07	0,09			275	Tom		no	4,33	5,18	G2		no	3,00E-07
EBN9	fcgri	He	1,0	0,0	1,0	6,6	0,2	parallel	no	no	yes	5,29E-09	0,06			1225	Tom		yes	4,33	5,18	G2		no	9,93E-07
EBN9	fcgri	He	136,2	150,0	0,0	133,8	0,0	parallel	no	no	yes	7,94E-10	0,05			3308	Tom		no	4,33	5,18	G2		no	2,04E-08
EBN9	MPD	He	147,4	150,0	0,0	85,8	0,0	parallel	no	yes	yes	1,59E-07	0,05	2,17E-02	0,01	167	Konstantin		no	4,33	5,18	MPD		no	4,67E-07
EBN9	MPD	He	240,8	250,0	0,0	139,8	0,0	parallel	no	yes	yes	1,53E-03	0,01	1,45E-06	0,03	8	Konstantin		no	4,33	5,18	MPD		no	1,62E-03
EBN9	MPD	He	513,4	500,0	0,0	295,2	0,0	parallel	no	yes	no	9,15E-05	0,01	1,83E-03	0,01	2524	Konstantin		no	4,33	5,18	MPD		no	9,15E-05
EBN9	fcgri	He	771,0	800,0	0,0	752,0	0,0	parallel	no	no	no	5,00E-07	0,08				Konstantin		no	4,33	5,18	G2		no	5,00E-07
EBN9	fcgri	He	1,0	0,0	1,0	6,6	0,2	parallel	no	no	no	2,50E-07	0,02				Konstantin		yes	4,33	5,18	G2		no	2,50E-07
EBN9	fcgri	He	136,2	150,0	0,0	133,8	0,0	parallel	no	no	no	5,00E-06	0,04				Konstantin		no	4,33	5,18	G2		no	5,00E-06
EBN9	fcgri	N2	91,9	80,0	0,0	90,1	0,0	parallel	no	no	no	1,20E-05	0,05				Konstantin		no	4,33	5,18	G2		no	1,20E-05
EBN9	fcgri	N2	129,8	150,0	0,0	127,8	0,0	parallel	no	no	no	1,20E-05	0,04				Konstantin		no	4,33	5,18	G2		no	1,20E-05
EBN9	fcgri	N2	0,3	0,0	3,3	2,0	0,5	parallel	no	no	no	1,20E-05	0,03				Konstantin		yes	4,33	5,18	G2		no	1,20E-05
EBN9	fcgri	He	771,0	800,0	0,0	752,0	0,0	parallel	no	no	no	5,00E-07	0,08				Konstantin		no	4,33	5,18	G2		no	5,00E-07
EBN9	fcgri	He	1,0	0,0	1,0	4,0	0,3	parallel	no	no	no	2,50E-07	0,02				Konstantin		yes	4,33	5,18	G2		no	2,50E-07
EBN9	fcgri	He	136,2	150,0	0,0	133,9	0,0	parallel	no	no	no	5,00E-07	0,04				Konstantin		no	4,33	5,18	G2		no	5,00E-07
OPA1	fcgri	He	489,2	500,0	0,0	186,0	0,0	perpendi	no	no	no	2,66E-06	0,06				Tom		no	2,54	11,78	G2		no	2,66E-06

OPA1	fcgri	He	692,2	700,0	0,0	376,6	0,0	perpendi	no	no	no	3,14E-06	0,05				Tom		no	2,54	11,78	G2		no	3,14E-06
OPA1	fcgri	He	899,8	800,0	0,0	573,5	0,0	perpendi	no	no	no	1,79E-06	0,06				Tom		no	2,54	11,78	G2		no	1,79E-06
OPA1	fcgri	He	1196,0	1000,0	0,0	805,2	0,0	perpendi	no	no	no	1,86E-06	0,06				Tom		no	2,54	11,78	G2		no	1,86E-06
OPA1	fcgri	He	1326,6	1000,0	0,0	991,1	0,0	perpendi	no	no	no	2,97E-06	0,18				Tom		no	2,54	11,78	G2		no	2,97E-06
OPA1	fcgri	He	0,5	0,0	2,0	18,8	0,1	perpendi	no	no	no	9,82E-06	0,04				Tom		yes	2,54	11,78	G2		no	9,82E-06
OPA1	fcgri	He	489,2	500,0	0,0	186,0	0,0	perpendi	no	no	yes	1,14E-06	0,06			2105	Tom		no	2,54	11,78	G2		no	1,40E-05
OPA1	fcgri	He	692,2	700,0	0,0	376,6	0,0	perpendi	no	no	yes	1,07E-06	0,05			2664	Tom		no	2,54	11,78	G2		no	8,64E-06
OPA1	fcgri	He	899,8	800,0	0,0	573,5	0,0	perpendi	no	no	yes	5,30E-06	0,05			4590	Tom		no	2,54	11,78	G2		no	4,77E-05
OPA1	fcgri	He	1196,0	1000,0	0,0	805,2	0,0	perpendi	no	no	yes	4,60E-07	0,05			2522	Tom		no	2,54	11,78	G2		no	1,90E-06
OPA1	fcgri	He	1326,6	1000,0	0,0	991,1	0,0	perpendi	no	no	yes	3,50E-07	0,19			6351	Tom		no	2,54	11,78	G2		no	2,59E-06
OPA1	fcgri	He	0,5	0,0	2,0	18,8	0,1	perpendi	no	no	yes	1,85E-06	0,04			3971	Tom		yes	2,54	11,78	G2		no	3,94E-04
OPA1	fcgri	He	489,2	500,0	0,0	186,0	0,0	perpendi	no	yes	yes	2,56E-07	0,10	1,35E-06	0,12	1936	Tom		no	2,54	11,78	G2		no	2,92E-06
OPA1	fcgri	He	692,2	700,0	0,0	376,6	0,0	perpendi	no	yes	yes	8,65E-08	0,09	1,32E-03	0,11	2766	Tom		no	2,54	11,78	G2		no	7,22E-07
OPA1	fcgri	He	899,8	800,0	0,0	573,5	0,0	perpendi	no	yes	yes	3,48E-07	0,06	5,73E-04	0,12	469	Tom		no	2,54	11,78	G2		no	6,33E-07
OPA1	fcgri	He	1196,0	1000,0	0,0	805,2	0,0	perpendi	no	yes	yes	2,07E-07	0,05	7,02E-06	0,08	1744	Tom		no	2,54	11,78	G2		no	6,54E-07
OPA1	fcgri	He	1326,6	1000,0	0,0	991,1	0,0	perpendi	no	yes	yes	2,31E-07	0,19	6,69E-06	0,16	4944	Tom		no	2,54	11,78	G2		no	1,39E-06
OPA1	fcgri	He	0,5	0,0	2,0	18,8	0,1	perpendi	no	yes	yes	3,53E-07	0,04	2,70E-03	0,10	8997	Tom		yes	2,54	11,78	G2		no	1,69E-04
OPA1	fcgri	He	489,2	500,0	0,0	186,0	0,0	perpendi	no	yes	no	8,55E-07	0,09	9,12E-06	0,09		Tom		no	2,54	11,78	G2		no	8,55E-07
OPA1	fcgri	He	692,2	700,0	0,0	376,6	0,0	perpendi	no	yes	no	2,12E-07	0,09	5,86E-04	0,22		Tom		no	2,54	11,78	G2		no	2,12E-07
OPA1	fcgri	He	899,8	800,0	0,0	573,5	0,0	perpendi	no	yes	no	3,27E-07	0,09	5,54E-04	0,22		Tom		no	2,54	11,78	G2		no	3,27E-07
OPA1	fcgri	He	1196,0	1000,0	0,0	805,2	0,0	perpendi	no	yes	no	2,27E-07	0,05	9,23E-03	0,21		Tom		no	2,54	11,78	G2		no	2,27E-07
OPA1	fcgri	He	1326,6	1000,0	0,0	991,1	0,0	perpendi	no	yes	no	8,34E-07	0,14	5,63E-02	0,06		Tom		no	2,54	11,78	G2		no	8,34E-07
OPA1	fcgri	He	0,5	0,0	2,0	18,8	0,1	perpendi	no	yes	no	4,89E-06	0,04	1,86E-02	0,09		Tom		yes	2,54	11,78	G2		no	4,89E-06
OPA1	fcgri	He	490,2	500,0	0,0	187,0	0,0	perpendi	no	no	yes	1,12E-05	0,06			162	Konstantin		no	2,54	11,78	G2		no	2,08E-05
OPA1	fcgri	He	693,2	700,0	0,0	377,6	0,0	perpendi	no	no	yes	1,14E-05	0,08			342	Konstantin		no	2,54	11,78	G2		no	2,18E-05
OPA1	fcgri	He	900,8	1000,0	0,0	574,5	0,0	perpendi	no	no	yes	1,10E-05	0,08			80	Konstantin		no	2,54	11,78	G2		no	1,25E-05
OPA1	fcgri	He	1197,0	1000,0	0,0	806,2	0,0	perpendi	no	no	yes	1,73E-05	0,14			462	Konstantin		no	2,54	11,78	G2		no	2,72E-05
OPA1	fcgri	He	1327,6	1000,0	0,0	992,1	0,0	perpendi	no	no	yes	3,00E-05	0,20			60	Konstantin		no	2,54	11,78	G2		no	3,18E-05
OPA1	fcgri	He	1,5	0,0	0,7	19,8	0,1	perpendi	no	no	yes	2,50E-04	0,04			4	Konstantin		yes	2,54	11,78	G2		no	2,94E-04
OPA1	fcgri	He	490,2	500,0	0,0	187,0	0,0	perpendi	no	no	no	2,30E-06	0,07				Konstantin		no	2,54	11,78	G2		no	2,30E-06
OPA1	fcgri	He	693,2	700,0	0,0	377,6	0,0	perpendi	no	no	no	3,80E-06	0,06				Konstantin		no	2,54	11,78	G2		no	3,80E-06
OPA1	fcgri	He	900,8	1000,0	0,0	574,5	0,0	perpendi	no	no	no	1,90E-06	0,07				Konstantin		no	2,54	11,78	G2		no	1,90E-06
OPA1	fcgri	He	1197,0	1000,0	0,0	806,2	0,0	perpendi	no	no	no	2,80E-06	0,07				Konstantin		no	2,54	11,78	G2		no	2,80E-06
OPA1	fcgri	He	1327,6	1000,0	0,0	992,1	0,0	perpendi	no	no	no	6,93E-06	0,15				Konstantin		no	2,54	11,78	G2		no	6,93E-06
OPA1	fcgri	He	1,5	0,0	0,7	19,8	0,1	perpendi	no	no	no	6,90E-07	0,05				Konstantin		yes	2,54	11,78	G2		no	6,90E-07
OPA1	fcgri	He	490,2	500,0	0,0	187,0	0,0	perpendi	no	yes	no	2,04E-06	0,07	2,89E-04	0,03		Konstantin		no	2,54	11,78	G2		no	2,04E-06
OPA1	fcgri	He	693,2	700,0	0,0	377,6	0,0	perpendi	no	yes	no	2,04E-06	0,06	1,18E-02	0,04		Konstantin		no	2,54	11,78	G2		no	2,04E-06
OPA1	fcgri	He	900,8	1000,0	0,0	574,5	0,0	perpendi	no	yes	no	3,52E-06	0,07	1,92E-02	0,05		Konstantin		no	2,54	11,78	G2		no	3,52E-06
OPA1	fcgri	He	1197,0	1000,0	0,0	806,2	0,0	perpendi	no	yes	no	1,45E-06	0,07	1,14E-02	0,03		Konstantin		no	2,54	11,78	G2		no	1,45E-06
OPA1	fcgri	He	1327,6	1000,0	0,0	992,1	0,0	perpendi	no	yes	no	3,56E-06	0,14	8,95E-04	0,03		Konstantin		no	2,54	11,78	G2		no	3,56E-06
OPA1	fcgri	He	1,5	0,0	0,7	19,8	0,1	perpendi	no	yes	no	1,58E-07	0,04	1,73E-05	0,14		Konstantin		yes	2,54	11,78	G2		no	1,58E-07
OPA1	fcgri	CH4	149,3	150,0	0,0	80,0	0,0	perpendi	no	no	no	6,35E-07	0,20				Tom		no	2,54	11,78	G3		no	6,35E-07
OPA1	fcgri	CH4	-0,3	0,0	-3,9	34,6	0,0	perpendi	no	no	no	6,76E-07	0,14				Tom		yes	2,54	11,78	G3		no	6,76E-07
OPA1	fcgri	CH4	149,3	150,0	0,0	80,0	0,0	perpendi	no	yes	no	8,70E-07	0,18	3,04E-05	0,16		Tom		no	2,54	11,78	G3		no	8,70E-07
OPA1	fcgri	CH4	-0,3	0,0	-3,9	34,6	0,0	perpendi	no	yes	no	7,61E-07	0,13	2,80E-04	0,09		Tom		yes	2,54	11,78	G3		no	7,61E-07
OPA1	fcgri	CH4	149,3	150,0	0,0	80,0	0,0	perpendi	no	yes	yes	5,00E-07	0,11	4,61E-05	0,12	2656	Tom		no	2,54	11,78	G3		no	1,71E-05
OPA1	fcgri	CH4	-0,3	0,0	-3,9	34,6	0,0	perpendi	no	yes	yes	3,42E-06	0,07	1,89E-05	0,11	4882	Tom		yes	2,54	11,78	G3		no	4,86E-04
OPA1	fcgri	CH4	149,3	150,0	0,0	80,0	0,0	perpendi	no	no	yes	4,45E-07	0,13			2476	Tom		no	2,54	11,78	G3		no	1,42E-05
OPA1	fcgri	CH4	-0,3	0,0	-3,9	34,6	0,0	perpendi	no	no	yes	2,94E-07	0,06			4526	Tom		yes	2,54	11,78	G3		no	3,87E-05
OPA2	fcgri	He	150,3	150,0	0,0	101,0	0,0	parallel	no	no	no	2,41E-04	0,08				Tom		no	4,43	8,4	G2	mbi	no	2,41E-04
OPA2	fcgri	He	180,4	180,0	0,0	154,3	0,0	parallel	no	no	no	1,08E-04	0,08				Tom		no	4,43	8,4	G2	mbi	no	1,08E-04
OPA2	fcgri	He	210,4	210,0	0,0	191,8	0,0	parallel	no	no	no	1,29E-04	0,08				Tom		no	4,43	8,4	G2	mbi	no	1,29E-04
OPA2	fcgri	He	240,8	250,0	0,0	224,6	0,0	parallel	no	no	no	9,47E-05	0,07				Tom		no	4,43	8,4	G2	mbi	no	9,47E-05
OPA2	fcgri	He	150,3	150,0	0,0	101,0	0,0	parallel	no	no	yes	2,47E-06	0,09			38636	Tom		no	4,43	8,4	G2	mbi	no	9,48E-04

OPA2	fcgri	He	180,4	180,0	0,0	154,3	0,0	parallel	no	no	yes	5,01E-06	0,08			17889	Tom		no	4,43	8,4	G2	mbi	no	5,86E-04
OPA2	fcgri	He	210,4	210,0	0,0	191,8	0,0	parallel	no	no	yes	1,70E-05	0,09			7903	Tom		no	4,43	8,4	G2	mbi	no	7,18E-04
OPA2	fcgri	He	240,8	250,0	0,0	224,6	0,0	parallel	no	no	yes	3,15E-06	0,07			22171	Tom		no	4,43	8,4	G2	mbi	no	3,14E-04
OPA2	fcgri	He	-0,4	0,0	-2,4	73,3	0,0	parallel	no	no	yes	5,52E-06	0,08			19251	Tom		yes	4,43	8,4	G2	mbi	no	1,45E-03
OPA2	fcgri	He	150,3	150,0	0,0	101,0	0,0	parallel	no	yes	yes	7,99E-07	0,08	2,48E-03	0,15	3289	Tom		no	4,43	8,4	G2	mbi	no	2,68E-05
OPA2	fcgri	He	180,4	180,0	0,0	154,3	0,0	parallel	no	yes	yes	2,70E-05	0,08	3,76E-05	0,06	2792	Tom		no	4,43	8,4	G2	mbi	no	5,16E-04
OPA2	fcgri	He	210,4	210,0	0,0	191,8	0,0	parallel	no	yes	yes	6,40E-06	0,07	2,94E-05	0,11	13027	Tom		no	4,43	8,4	G2	mbi	no	4,41E-04
OPA2	fcgri	He	240,8	250,0	0,0	224,6	0,0	parallel	no	yes	yes	1,17E-05	0,08	2,93E-01	0,12	11534	Tom		no	4,43	8,4	G2	mbi	no	6,13E-04
OPA2	fcgri	He	-0,4	0,0	-2,4	73,3	0,0	parallel	no	yes	yes	8,20E-07	0,08	1,44E-03	0,08	56447	Tom		yes	4,43	8,4	G2	mbi	no	6,32E-04
OPA2	fcgri	He	150,3	150,0	0,0	101,0	0,0	parallel	no	yes	no	2,30E-04	0,08	2,91E-03	0,11		Tom		no	4,43	8,4	G2	mbi	no	2,30E-04
OPA2	fcgri	He	180,4	180,0	0,0	154,3	0,0	parallel	no	yes	no	5,69E-05	0,07	1,81E-02	0,11		Tom		no	4,43	8,4	G2	mbi	no	5,69E-05
OPA2	fcgri	He	210,4	210,0	0,0	191,8	0,0	parallel	no	yes	no	4,57E-05	0,07	6,92E-02	0,09		Tom		no	4,43	8,4	G2	mbi	no	4,57E-05
OPA2	fcgri	He	240,8	250,0	0,0	224,6	0,0	parallel	no	yes	no	4,38E-05	0,08	1,73E-01	0,08		Tom		no	4,43	8,4	G2	mbi	no	4,38E-05
OPA2	fcgri	He	-0,4	0,0	-2,4	73,3	0,0	parallel	no	yes	no	7,92E-05	0,09	3,87E-01	0,09		Tom		yes	4,43	8,4	G2	mbi	no	7,92E-05
OPA2	fcgri	CH4	151,2	150,0	0,0	94,2	0,0	parallel	no	no	no	7,70E-05	0,14				Tom		no	4,43	8,4	G2		no	7,70E-05
OPA2	fcgri	CH4	180,5	180,0	0,0	148,2	0,0	parallel	no	no	no	3,27E-05	0,12				Tom		no	4,43	8,4	G2		no	3,27E-05
OPA2	fcgri	CH4	211,4	210,0	0,0	187,7	0,0	parallel	no	no	no	3,44E-05	0,12				Tom		no	4,43	8,4	G2		no	3,44E-05
OPA2	fcgri	CH4	-0,4	0,0	-2,6	67,5	0,0	parallel	no	no	no	4,55E-05	0,12				Tom		yes	4,43	8,4	G2		no	4,55E-05
OPA2	fcgri	CH4	-0,3	0,0	-2,9	24,4	0,0	parallel	no	no	no	3,50E-05	0,12				Tom		yes	4,43	8,4	G2		no	3,50E-05
OPA2	fcgri	CH4	151,2	150,0	0,0	94,2	0,0	parallel	no	yes	yes	3,17E-06	0,14	5,52E-03	0,18	1643	Tom		no	4,43	8,4	G2		no	5,84E-05
OPA2	fcgri	CH4	180,5	180,0	0,0	148,2	0,0	parallel	no	yes	yes	1,07E-05	0,14	1,52E-05	0,15	2887	Tom		no	4,43	8,4	G2		no	2,19E-04
OPA2	fcgri	CH4	211,4	210,0	0,0	187,7	0,0	parallel	no	yes	yes	1,36E-05	0,14	2,78E-05	0,15	2472	Tom		no	4,43	8,4	G2		no	1,93E-04
OPA2	fcgri	CH4	-0,4	0,0	-2,6	67,5	0,0	parallel	no	yes	yes	1,25E-05	0,12	2,96E-05	0,11	2945	Tom		yes	4,43	8,4	G2		no	5,58E-04
OPA2	fcgri	CH4	-0,3	0,0	-2,9	24,4	0,0	parallel	no	yes	yes	7,23E-06	0,14	1,24E-04	0,10	2451	Tom		yes	4,43	8,4	G2		no	7,34E-04
OPA2	fcgri	CH4	151,2	150,0	0,0	94,2	0,0	parallel	no	yes	no	6,65E-05	0,13	5,57E-04	0,17		Tom		no	4,43	8,4	G2		no	6,65E-05
OPA2	fcgri	CH4	180,5	180,0	0,0	148,2	0,0	parallel	no	yes	no	3,47E-05	0,12	6,29E-05	0,21		Tom		no	4,43	8,4	G2		no	3,47E-05
OPA2	fcgri	CH4	211,4	210,0	0,0	187,7	0,0	parallel	no	yes	no	3,36E-05	0,11	6,85E-05	0,18		Tom		no	4,43	8,4	G2		no	3,36E-05
OPA2	fcgri	CH4	-0,4	0,0	-2,6	67,5	0,0	parallel	no	yes	no	2,15E-05	0,11	1,08E-02	0,24		Tom		yes	4,43	8,4	G2		no	2,15E-05
OPA2	fcgri	CH4	-0,3	0,0	-2,9	24,4	0,0	parallel	no	yes	no	3,58E-05	0,13	8,34E-05	0,11		Tom		yes	4,43	8,4	G2		no	3,58E-05
OPA2	fcgri	CH4	151,2	150,0	0,0	94,2	0,0	parallel	no	no	yes	7,31E-06	0,15			3302	Tom		no	4,43	8,4	G2		no	2,63E-04
OPA2	fcgri	CH4	180,5	180,0	0,0	148,2	0,0	parallel	no	no	yes	5,89E-06	0,12			3493	Tom		no	4,43	8,4	G2		no	1,45E-04
OPA2	fcgri	CH4	211,4	210,0	0,0	187,7	0,0	parallel	no	no	yes	1,43E-05	0,11			1332	Tom		no	4,43	8,4	G2		no	1,16E-04
OPA2	fcgri	CH4	-0,4	0,0	-2,6	67,5	0,0	parallel	no	no	yes	2,01E-05	0,11			1215	Tom		yes	4,43	8,4	G2		no	3,82E-04
OPA2	fcgri	CH4	-0,3	0,0	-2,9	24,4	0,0	parallel	no	no	yes	1,92E-04	0,11			59	Tom		yes	4,43	8,4	G2		no	6,58E-04
OPA2	fcgri	CH4	149,5	150,0	0,0	76,5	0,0	perpendi	no	no	yes	6,98E-06	0,08			4084	Tom		no	4,43	8,4	G3	mbi	no	3,80E-04
OPA2	fcgri	CH4	180,9	180,0	0,0	130,2	0,0	perpendi	no	no	yes	9,85E-06	0,06			2017	Tom		no	4,43	8,4	G3	WG	no	1,62E-04
OPA2	fcgri	CH4	209,0	210,0	0,0	170,9	0,0	perpendi	no	no	yes	5,51E-06	0,06			2703	Tom		no	4,43	8,4	G3	WG	no	9,26E-05
OPA2	fcgri	CH4	-0,1	0,0	-11,8	83,5	0,0	perpendi	no	no	yes	1,02E-05	0,07			4884	Tom		yes	4,43	8,4	G3	mbi	no	6,05E-04
OPA2	fcgri	CH4	-0,3	0,0	-3,9	40,8	0,0	perpendi	no	no	yes	1,35E-05	0,07			2551	Tom		yes	4,43	8,4	G3	mbi	no	8,58E-04
OPA2	fcgri	CH4	149,5	150,0	0,0	76,5	0,0	perpendi	no	no	no	3,20E-05	0,08				Tom		no	4,43	8,4	G3	mbi	no	3,20E-05
OPA2	fcgri	CH4	180,9	180,0	0,0	130,2	0,0	perpendi	no	no	no	6,28E-05	0,08				Tom		no	4,43	8,4	G3	WG	no	6,28E-05
OPA2	fcgri	CH4	209,0	210,0	0,0	170,9	0,0	perpendi	no	no	no	3,51E-05	0,08				Tom		no	4,43	8,4	G3	WG	no	3,51E-05
OPA2	fcgri	CH4	-0,1	0,0	-11,8	83,5	0,0	perpendi	no	no	no	1,16E-04	0,09				Tom		yes	4,43	8,4	G3	mbi	no	1,16E-04
OPA2	fcgri	CH4	-0,3	0,0	-3,9	40,8	0,0	perpendi	no	no	no	7,01E-05	0,09				Tom		yes	4,43	8,4	G3	mbi	no	7,01E-05
OPA2	fcgri	CH4	149,5	150,0	0,0	76,5	0,0	perpendi	no	yes	no	8,13E-06	0,08	5,64E-04	0,10		Tom		no	4,43	8,4	G3	mbi	no	8,13E-06
OPA2	fcgri	CH4	180,9	180,0	0,0	130,2	0,0	perpendi	no	yes	no	9,78E-07	0,08	1,61E-02	0,05		Tom		no	4,43	8,4	G3	WG	no	9,78E-07
OPA2	fcgri	CH4	209,0	210,0	0,0	170,9	0,0	perpendi	no	yes	no	1,17E-05	0,07	1,03E-03	0,05		Tom		no	4,43	8,4	G3	WG	no	1,17E-05
OPA2	fcgri	CH4	-0,1	0,0	-11,8	83,5	0,0	perpendi	no	yes	no	7,90E-05	0,07	7,44E-08	0,18		Tom		yes	4,43	8,4	G3	mbi	no	7,90E-05
OPA2	fcgri	CH4	-0,3	0,0	-3,9	40,8	0,0	perpendi	no	yes	no	1,06E-04	0,11	1,84E-04	0,21		Tom		yes	4,43	8,4	G3	mbi	no	1,06E-04
OPA2	fcgri	CH4	149,5	150,0	0,0	76,5	0,0	perpendi	no	yes	yes	1,90E-06	0,09	5,13E-06	0,11	2486	Tom		no	4,43	8,4	G3	mbi	no	6,37E-05
OPA2	fcgri	CH4	180,9	180,0	0,0	130,2	0,0	perpendi	no	yes	yes	8,75E-07	0,08	1,91E-04	0,07	2251	Tom		no	4,43	8,4	G3	WG	no	1,60E-05
OPA2	fcgri	CH4	209,0	210,0	0,0	170,9	0,0	perpendi	no	yes	yes	1,54E-05	0,08	2,55E-05	0,11	647	Tom		no	4,43	8,4	G3	WG	no	7,39E-05
OPA2	fcgri	CH4	-0,1	0,0	-11,8	83,5	0,0	perpendi	no	yes	yes	1,60E-07	0,08	9,75E-06	0,15	4480	Tom		yes	4,43	8,4	G3	mbi	no	8,74E-06
OPA2	fcgri	CH4	-0,3	0,0	-3,9	40,8	0,0	perpendi	no	yes	yes	2,58E-05	0,09	4,52E-05	0,12	2242	Tom		yes	4,43	8,4	G3	mbi	no	1,44E-03

OPA2	fcgri	He	150,3	150,0	0,0	101,0	0,0	parallel	no	no	no	2,41E-04	0,08				Konstantin		no	4,43	8,4	G2	mbi	no	2,41E-04
OPA2	fcgri	He	180,4	180,0	0,0	154,3	0,0	parallel	no	no	no	1,08E-04	0,09				Konstantin		no	4,43	8,4	G2	mbi	no	1,08E-04
OPA2	fcgri	He	210,4	210,0	0,0	191,8	0,0	parallel	no	no	no	1,29E-04	0,08				Konstantin		no	4,43	8,4	G2	mbi	no	1,29E-04
OPA2	fcgri	He	240,8	250,0	0,0	224,6	0,0	parallel	no	no	no	9,47E-05	0,07				Konstantin		no	4,43	8,4	G2	mbi	no	9,47E-05
OPA2	fcgri	He	150,3	150,0	0,0	101,0	0,0	parallel	no	yes	no	2,30E-04	0,08	2,90E-03	0,11		Konstantin		no	4,43	8,4	G2	mbi	no	2,30E-04
OPA2	fcgri	He	180,4	180,0	0,0	154,3	0,0	parallel	no	yes	no	5,69E-05	0,07	1,81E-02	0,11		Konstantin		no	4,43	8,4	G2	mbi	no	5,69E-05
OPA2	fcgri	He	210,4	210,0	0,0	191,8	0,0	parallel	no	yes	no	4,57E-05	0,07	6,92E-02	0,09		Konstantin		no	4,43	8,4	G2	mbi	no	4,57E-05
OPA2	fcgri	He	240,8	250,0	0,0	224,6	0,0	parallel	no	yes	no	4,37E-05	0,07	1,73E-01	0,08		Konstantin		no	4,43	8,4	G2	mbi	no	4,37E-05
OPA2	fcgri	He	496,6	500,0	0,0	169,6	0,0	perpendi	no	no	yes	6,00E-04	0,12			220	Konstantin		no	4,43	8,4	G2		no	1,38E-03
OPA2	fcgri	He	697,2	700,0	0,0	348,0	0,0	perpendi	no	no	yes	3,26E-05	0,11			27048	Konstantin		no	4,43	8,4	G2		no	2,56E-03
OPA2	fcgri	He	930,7	1000,0	0,0	544,0	0,0	perpendi	no	no	yes	2,30E-06	0,08			18498	Konstantin		no	4,43	8,4	G2		no	8,05E-05
OPA2	fcgri	He	1106,8	1000,0	0,0	733,0	0,0	perpendi	no	no	yes	5,40E-06	0,12			25339	Konstantin		no	4,43	8,4	G2		no	1,92E-04
OPA2	fcgri	He	1323,9	1000,0	0,0	929,8	0,0	perpendi	no	no	yes	7,90E-07	0,11			64803	Konstantin		no	4,43	8,4	G2		no	5,59E-05
OPA2	fcgri	He	496,6	500,0	0,0	169,6	0,0	perpendi	no	no	no	3,38E-04	0,08				Konstantin		no	4,43	8,4	G2		no	3,38E-04
OPA2	fcgri	He	697,2	700,0	0,0	348,0	0,0	perpendi	no	no	no	6,89E-04	0,07				Konstantin		no	4,43	8,4	G2		no	6,89E-04
OPA2	fcgri	He	930,7	1000,0	0,0	544,0	0,0	perpendi	no	no	no	3,27E-04	0,10				Konstantin		no	4,43	8,4	G2		no	3,27E-04
OPA2	fcgri	He	1106,8	1000,0	0,0	733,0	0,0	perpendi	no	no	no	1,79E-04	0,11				Konstantin		no	4,43	8,4	G2		no	1,79E-04
OPA2	fcgri	He	1323,9	1000,0	0,0	929,8	0,0	perpendi	no	no	no	3,90E-05	0,10				Konstantin		no	4,43	8,4	G2		no	3,90E-05
OPA2	fcgri	He	496,6	500,0	0,0	169,6	0,0	perpendi	no	yes	no	3,27E-04	0,08	8,28E-03	0,03		Konstantin		no	4,43	8,4	G2		no	3,27E-04
OPA2	fcgri	He	697,2	700,0	0,0	348,0	0,0	perpendi	no	yes	no	9,54E-04	0,09	6,20E-05	0,01		Konstantin		no	4,43	8,4	G2		no	9,54E-04
OPA2	fcgri	He	930,7	1000,0	0,0	544,0	0,0	perpendi	no	yes	no	5,00E-04	0,11	1,00E-05	0,09		Konstantin		no	4,43	8,4	G2		no	5,00E-04
OPA2	fcgri	He	1106,8	1000,0	0,0	733,0	0,0	perpendi	no	yes	no	1,09E-04	0,12	5,35E+01	0,09		Konstantin		no	4,43	8,4	G2		no	1,09E-04
OPA2	fcgri	He	1323,9	1000,0	0,0	929,8	0,0	perpendi	no	yes	no	2,05E-05	0,09	2,58E+00	0,01		Konstantin		no	4,43	8,4	G2		no	2,05E-05
OPA2	fcgri	He	496,6	500,0	0,0	169,6	0,0	perpendi	no	yes	yes	7,46E-06	0,10	4,88E-05	0,06	27626	Konstantin		no	4,43	8,4	G2		no	1,22E-03
OPA2	fcgri	He	697,2	700,0	0,0	348,0	0,0	perpendi	no	yes	yes	1,09E-05	0,10	6,00E-05	0,06	67064	Konstantin		no	4,43	8,4	G2		no	2,11E-03
OPA2	fcgri	He	930,7	1000,0	0,0	544,0	0,0	perpendi	no	yes	yes	3,74E-06	0,11	2,99E-04	0,00	39630	Konstantin		no	4,43	8,4	G2		no	2,76E-04
OPA2	fcgri	He	1106,8	1000,0	0,0	733,0	0,0	perpendi	no	yes	yes	8,99E-03	0,11	6,33E-03	0,05	64458	Konstantin		no	4,43	8,4	G2		no	8,00E-01
OPA2	fcgri	He	1323,9	1000,0	0,0	929,8	0,0	perpendi	no	yes	yes	5,90E-07	0,08	3,12E-04	0,05	22762	Konstantin		no	4,43	8,4	G2		no	1,50E-05
OPA2	MPD	He	101,0	80,0	0,0	74,0	0,0	parallel	no	yes	yes	2,04E-06	0,08	1,31E-03	0,09	1525	Tom	2000	no	4,43	8,4	MPD	mbi	no	4,41E-05
OPA2	MPD	He	183,0	180,0	0,0			parallel	no	yes	yes	2,31E-06	0,09	3,67E-03	0,15	830	Tom	2000	no	4,43	8,4	MPD	ne	no	#DIV/0!
OPA2	MPD	He	216,0	210,0	0,0			parallel	no	yes	yes	2,31E-06	0,09	3,67E-03	0,15	800	Tom	2000	no	4,43	8,4	MPD	ne	no	#DIV/0!
OPA2	MPD	He	4,0	0,0	0,3			parallel	no	yes	yes	9,37E-05	0,10	3,14E-03	0,13	340	Tom	2000	yes	4,43	8,4	MPD	ne	no	#DIV/0!
OPA2	MPD	He	101,0	80,0	0,0	74,0	0,0	parallel	no	yes	no	2,01E-04	0,07	3,95E-04	0,08		Tom	2000	no	4,43	8,4	MPD	mbi	no	2,01E-04
OPA2	MPD	He	183,0	180,0	0,0			parallel	no	yes	no	1,01E-04	0,07	1,21E-02	0,04		Tom	2000	no	4,43	8,4	MPD	ne	no	1,01E-04
OPA2	MPD	He	216,0	210,0	0,0			parallel	no	yes	no	3,58E-04	0,07	5,35E-04	0,19		Tom	2000	no	4,43	8,4	MPD	ne	no	3,58E-04
OPA2	MPD	He	4,0	0,0	0,3			parallel	no	yes	no	2,23E-04	0,07	1,64E-03	0,08		Tom	2000	yes	4,43	8,4	MPD	ne	no	2,23E-04
OPA2	MPD	He	101,0	80,0	0,0	74,0	0,0	parallel	no	no	no	2,00E-04	0,08				Tom	2000	no	4,43	8,4	MPD	mbi	no	2,00E-04
OPA2	MPD	He	183,0	180,0	0,0			parallel	no	no	no	4,26E-04	0,08				Tom	2000	no	4,43	8,4	MPD	ne	no	4,26E-04
OPA2	MPD	He	216,0	210,0	0,0			parallel	no	no	no	2,79E-04	0,09				Tom	2000	no	4,43	8,4	MPD	ne	no	2,79E-04
OPA2	MPD	He	4,0	0,0	0,3			parallel	no	no	no	2,32E-04	0,07				Tom	2000	yes	4,43	8,4	MPD	ne	no	2,32E-04
OPA2	MPD	He	101,0	80,0	0,0	74,0	0,0	parallel	no	no	yes	1,49E-05	0,08			3194	Tom	2000	no	4,43	8,4	MPD	mbi	no	6,57E-04
OPA2	MPD	He	183,0	180,0	0,0			parallel	no	no	yes	1,77E-05	0,09			7585	Tom	2000	no	4,43	8,4	MPD	ne	no	#DIV/0!
OPA2	MPD	He	216,0	210,0	0,0			parallel	no	no	yes	3,00E-05	0,09			2929	Tom	2000	no	4,43	8,4	MPD	ne	no	#DIV/0!
OPA2	MPD	He	4,0	0,0	0,3			parallel	no	no	yes	9,73E-06	0,09			7458	Tom	2000	yes	4,43	8,4	MPD	ne	no	#DIV/0!
OPA2	MPD	He	149,0	150,0	0,0			perpendi	no	yes	yes	1,90E-06	0,09	5,13E-06	0,11	2486	Tom	2000	no	4,43	8,4	MPD	NE	no	#DIV/0!
OPA2	MPD	He	188,0	180,0	0,0			perpendi	no	yes	yes	8,75E-07	0,08	1,91E-04	0,07	2251	Tom	2000	no	4,43	8,4	MPD	NE	no	#DIV/0!
OPA2	MPD	He	231,0	250,0	0,0			perpendi	no	yes	yes	1,44E-05	0,09	5,31E-05	0,09	659	Tom	2000	no	4,43	8,4	MPD	NE	no	#DIV/0!
OPA2	MPD	He	4,0	0,0	0,3			perpendi	no	yes	yes	2,15E-06	0,11	2,45E-06	0,13	1954	Tom	2000	yes	4,43	8,4	MPD	NE	no	#DIV/0!
OPA2	MPD	He	149,0	150,0	0,0			perpendi	no	yes	no	8,14E-06	0,08	5,64E-04	0,10		Tom	2000	no	4,43	8,4	MPD	NE	no	8,14E-06
OPA2	MPD	He	188,0	180,0	0,0			perpendi	no	yes	no	9,78E-07	0,08	1,61E-03	0,05		Tom	2000	no	4,43	8,4	MPD	NE	no	9,78E-07
OPA2	MPD	He	231,0	250,0	0,0			perpendi	no	yes	no	4,07E-06	0,07	9,13E-04	0,05		Tom	2000	no	4,43	8,4	MPD	NE	no	4,07E-06
OPA2	MPD	He	4,0	0,0	0,3			perpendi	no	yes	no	1,87E-04	0,08	4,39E-04	0,08		Tom	2000	yes	4,43	8,4	MPD	NE	no	1,87E-04
OPA2	MPD	He	149,0	150,0	0,0			perpendi	no	no	no	2,92E-05	0,08				Tom	2000	no	4,43	8,4	MPD	NE	no	2,92E-05
OPA2	MPD	He	188,0	180,0	0,0			perpendi	no	no	no	4,71E-05	0,07				Tom	2000	no	4,43	8,4	MPD	NE	no	4,71E-05

OPA2	MPD	He	231,0	250,0	0,0			perpendi	no	no	no	3,46E-05	0,07				Tom	2000	no	4,43	8,4	MPD	NE	no	3,46E-05
OPA2	MPD	He	4,0	0,0	0,3			perpendi	no	no	no	2,22E-05	0,07				Tom	2000	yes	4,43	8,4	MPD	NE	no	2,22E-05
OPA2	MPD	He	149,0	150,0	0,0			perpendi	no	no	yes	2,71E-06	0,09			1898	Tom	2000	no	4,43	8,4	MPD	NE	no	#DIV/0!
OPA2	MPD	He	188,0	180,0	0,0			perpendi	no	no	yes	2,80E-06	0,10			5868	Tom	2000	no	4,43	8,4	MPD	NE	no	#DIV/0!
OPA2	MPD	He	231,0	250,0	0,0			perpendi	no	no	yes	6,76E-06	0,10			1257	Tom	2000	no	4,43	8,4	MPD	NE	no	#DIV/0!
OPA2	MPD	He	4,0	0,0	0,3			perpendi	no	no	yes	9,38E-06	0,11			679	Tom	2000	yes	4,43	8,4	MPD	NE	no	#DIV/0!
OPA2	fcgri	He	150,3	150,0	0,0	101,0	0,0	parallel	no	no	no	8,30E-05	0,11				Tom		no	4,43	8,4	G2	mbi	yes	8,30E-05
OPA2	fcgri	He	180,4	180,0	0,0	154,3	0,0	parallel	no	no	no	8,43E-05	0,11				Tom		no	4,43	8,4	G2	mbi	yes	8,43E-05
OPA2	fcgri	He	210,4	210,0	0,0	191,8	0,0	parallel	no	no	no	8,30E-05	0,11				Tom		no	4,43	8,4	G2	mbi	yes	8,30E-05
OPA2	fcgri	He	240,8	250,0	0,0	224,6	0,0	parallel	no	no	no	8,09E-05	0,11				Tom		no	4,43	8,4	G2	mbi	yes	8,09E-05
OPA2	fcgri	He	-0,4	0,0	-2,4	73,3	0,0	parallel	no	no	no	1,09E-04	0,11				Tom		yes	4,43	8,4	G2	mbi	yes	1,09E-04
OPA2	MPD	He	101,0	80,0	0,0	74,0	0,0	parallel	no	no	no	3,75E-04	0,11				Tom		no	4,43	8,4	MPD	mbi	yes	3,75E-04
OPA2	MPD	He	183,0	180,0	0,0			parallel	no	no	no	4,68E-04	0,11				Tom		no	4,43	8,4	MPD	ne	yes	4,68E-04
OPA2	MPD	He	216,0	210,0	0,0			parallel	no	no	no	3,46E-04	0,11				Tom		no	4,43	8,4	MPD	ne	yes	3,46E-04
OPA2	MPD	He	4,0	0,0	0,3			parallel	no	no	no	4,10E-04	0,11				Tom		yes	4,43	8,4	MPD	ne	yes	4,10E-04
OPA2	MPD	He	101,0	80,0	0,0	74,0	0,0	parallel	no	yes	no	3,48E-04	0,11	2,47E-05	0,13		Tom		no	4,43	8,4	MPD	mbi	yes	3,48E-04
OPA2	MPD	He	183,0	180,0	0,0			parallel	no	yes	no	3,87E-04	0,11	4,44E-09	0,13		Tom		no	4,43	8,4	MPD	ne	yes	3,87E-04
OPA2	MPD	He	216,0	210,0	0,0			parallel	no	yes	no	3,55E-04	0,11	4,09E-04	0,10		Tom		no	4,43	8,4	MPD	ne	yes	3,55E-04
OPA2	MPD	He	4,0	0,0	0,3			parallel	no	yes	no	2,33E-04	0,11	5,86E-03	0,05		Tom		yes	4,43	8,4	MPD	ne	yes	2,33E-04
OPA2	MPD	He	149,0	150,0	0,0			perpendi	no	no	no	2,23E-05	0,11				Tom	2000	no	4,43	8,4	MPD	NE	yes	2,23E-05
OPA2	MPD	He	188,0	180,0	0,0			perpendi	no	no	no	3,20E-05	0,11				Tom	2000	no	4,43	8,4	MPD	NE	yes	3,20E-05
OPA2	MPD	He	231,0	250,0	0,0			perpendi	no	no	no	5,18E-05	0,11				Tom	2000	no	4,43	8,4	MPD	NE	yes	5,18E-05
OPA2	MPD	He	4,0	0,0	0,3			perpendi	no	no	no	6,37E-05	0,11				Tom	2000	yes	4,43	8,4	MPD	NE	yes	6,37E-05
OPA2	fcgri	CH4	151,2	150,0	0,0	94,2	0,0	parallel	no	no	no	1,05E-04	0,21				Tom		no	4,43	8,4	G2		yes	1,05E-04
OPA2	fcgri	CH4	180,5	180,0	0,0	148,2	0,0	parallel	no	no	no	1,86E-04	0,21				Tom		no	4,43	8,4	G2		yes	1,86E-04
OPA2	fcgri	CH4	211,4	210,0	0,0	187,7	0,0	parallel	no	no	no	4,17E-04	0,21				Tom		no	4,43	8,4	G2		yes	4,17E-04
OPA2	fcgri	CH4	-0,4	0,0	-2,6	67,5	0,0	parallel	no	no	no	1,85E-04	0,21				Tom		yes	4,43	8,4	G2		yes	1,85E-04
OPA2	fcgri	CH4	-0,3	0,0	-2,9	24,4	0,0	parallel	no	no	no	1,45E-04	0,21				Tom		yes	4,43	8,4	G2		yes	1,45E-04
OPA2	fcgri	CH4	149,5	150,0	0,0	76,5	0,0	perpendi	no	no	no	6,98E-04	0,21				Tom		no	4,43	8,4	G3	mbi	yes	6,98E-04
OPA2	fcgri	CH4	180,9	180,0	0,0	130,2	0,0	perpendi	no	no	no	3,40E-04	0,21				Tom		no	4,43	8,4	G3	WG	yes	3,40E-04
OPA2	fcgri	CH4	209,0	210,0	0,0	170,9	0,0	perpendi	no	no	no	4,18E-04	0,21				Tom		no	4,43	8,4	G3	WG	yes	4,18E-04
OPA2	fcgri	CH4	-0,1	0,0	-11,8	83,5	0,0	perpendi	no	no	no	6,13E-04	0,21				Tom		yes	4,43	8,4	G3	mbi	yes	6,13E-04
OPA2	fcgri	CH4	-0,3	0,0	-3,9	40,8	0,0	perpendi	no	no	no	1,32E+00	0,21				Tom		yes	4,43	8,4	G3	mbi	yes	1,32E+00
OPA2	MPD	He	149,0	150,0	0,0			perpendi	no	yes	no	9,60E-06	0,11	1,84E-04	0,08		Tom	2000	no	4,43	8,4	MPD	NE	yes	9,60E-06
OPA2	MPD	He	188,0	180,0	0,0			perpendi	no	yes	no	1,07E-05	0,11	9,47E-04	0,12		Tom	2000	no	4,43	8,4	MPD	NE	yes	1,07E-05
OPA2	MPD	He	231,0	250,0	0,0			perpendi	no	yes	no	1,28E-06	0,11	1,71E-04	0,13		Tom	2000	no	4,43	8,4	MPD	NE	yes	1,28E-06
OPA2	MPD	He	4,0	0,0	0,3			perpendi	no	yes	no	3,29E-05	0,11	5,00E-04	0,16		Tom	2000	yes	4,43	8,4	MPD	NE	yes	3,29E-05
OPA2	MPD	He	150,0	150,0	0,0	83,8	0,0	parallel	yes	no	no	2,80E-07	0,11				Tom		no	4,43	8,4	MPD		yes	2,80E-07
OPA2	MPD	He	4,0	0,0	0,3	36,1	0,0	parallel	yes	no	no	2,13E-08	0,11				Tom		yes	4,43	8,4	MPD		yes	2,13E-08
OPA2	fcgri	CH4	154,9	150,0	0,0	65,0	0,0	parallel	yes	no	no	4,33E-05	0,14				Tom		no	4,43	8,4	G2		no	4,33E-05
OPA2	fcgri	CH4	0,0	0,0	-100,0	37,8	0,0	parallel	yes	no	no	3,83E-05	0,10				Tom		yes	4,43	8,4	G2		no	3,83E-05
OPA2	fcgri	He	158,3	150,0	0,0	72,7	0,0	parallel	yes	no	no	5,48E-03	0,11				Tom		no	4,43	8,4	G2	mbi	yes	5,48E-03
OPA2	fcgri	He	179,9	180,0	0,0	122,0	0,0	parallel	yes	no	no	2,63E-03	0,11				Tom		no	4,43	8,4	G2		yes	2,63E-03
OPA2	fcgri	He	-0,5	0,0	-2,1	65,7	0,0	parallel	yes	no	no	1,39E-03	0,11				Tom		yes	4,43	8,4	G2	mbi	yes	1,39E-03
OPA2	fcgri	He	158,3	150,0	0,0	72,7	0,0	parallel	yes	no	yes	9,23E-05	0,11			2027	Tom		no	4,43	8,4	G2	mbi	yes	2,66E-03
OPA2	fcgri	He	179,9	180,0	0,0	122,0	0,0	parallel	yes	no	yes	1,07E-04	0,11			2211	Tom		no	4,43	8,4	G2		yes	2,05E-03
OPA2	fcgri	He	-0,5	0,0	-2,1	65,7	0,0	parallel	yes	no	yes	9,21E-05	0,11			3305	Tom		yes	4,43	8,4	G2	mbi	yes	4,73E-03
OPA2	fcgri	CH4	154,9	150,0	0,0	65,0	0,0	parallel	yes	no	yes	2,59E-06	0,14			5949	Tom		no	4,43	8,4	G2		no	2,40E-04
OPA2	fcgri	CH4	0,0	0,0	-100,0	37,8	0,0	parallel	yes	no	yes	2,02E-05	0,15			2552	Tom		yes	4,43	8,4	G2		no	1,39E-03
OPA2	MPD	He	150,0	150,0	0,0	83,8	0,0	parallel	yes	no	yes	3,98E-08	0,11			3410	Tom		no	4,43	8,4	MPD		yes	1,66E-06
OPA2	MPD	He	4,0	0,0	0,3	36,1	0,0	parallel	yes	no	yes	5,56E-08	0,11			3731	Tom		yes	4,43	8,4	MPD		yes	5,80E-06
OPA2	fcgri	He	158,3	150,0	0,0	72,7	0,0	parallel	yes	yes	no	1,59E-07	0,11	4,48E-02	0,22		Tom		no	4,43	8,4	G2	mbi	yes	1,59E-07
OPA2	fcgri	He	179,9	180,0	0,0	122,0	0,0	parallel	yes	yes	no	4,13E-08	0,11	1,30E-04	0,28		Tom		no	4,43	8,4	G2		yes	4,13E-08
OPA2	fcgri	He	-0,5	0,0	-2,1	65,7	0,0	parallel	yes	yes	no	2,55E-08	0,11	1,44E-03	0,31		Tom		yes	4,43	8,4	G2	mbi	yes	2,55E-08

OPA2	fcgri	He	158,3	150,0	0,0	72,7	0,0	parallel	yes	yes	yes	2,63E-05	0,11	1,09E-04	0,06	6282	Tom		no	4,43	8,4	G2	mbi	yes	2,30E-03
OPA2	fcgri	He	179,9	180,0	0,0	122,0	0,0	parallel	yes	yes	yes	7,72E-05	0,11	4,12E-04	0,11	252	Tom		no	4,43	8,4	G2		yes	2,37E-04
OPA2	fcgri	He	-0,5	0,0	-2,1	65,7	0,0	parallel	yes	yes	yes	7,01E-06	0,11	1,50E-01	0,04	6973	Tom		yes	4,43	8,4	G2	mbi	yes	7,51E-04
OPA2	fcgri	CH4	151,2	150,0	0,0	94,2	0,0	parallel	no	yes	no	1,78E-04	0,21	1,32E-03	0,12		Tom		no	4,43	8,4	G2		yes	1,78E-04
OPA2	fcgri	CH4	180,5	180,0	0,0	148,2	0,0	parallel	no	yes	no	1,35E-04	0,21	3,74E-03	0,16		Tom		no	4,43	8,4	G2		yes	1,35E-04
OPA2	fcgri	CH4	211,4	210,0	0,0	187,7	0,0	parallel	no	yes	no	5,89E-05	0,21	1,91E-07	0,16		Tom		no	4,43	8,4	G2		yes	5,89E-05
OPA2	fcgri	CH4	-0,4	0,0	-2,6	67,5	0,0	parallel	no	yes	no	2,94E-05	0,21	7,75E-02	0,24		Tom		yes	4,43	8,4	G2		yes	2,94E-05
OPA2	fcgri	CH4	-0,3	0,0	-2,9	24,4	0,0	parallel	no	yes	no	2,00E-07	0,21	1,15E-06	0,13		Tom		yes	4,43	8,4	G2		yes	2,00E-07
OPA2	fcgri	CH4	149,5	150,0	0,0	76,5	0,0	perpendi	no	yes	no	9,60E-06	0,21	1,84E-04	0,08		Tom		no	4,43	8,4	G3	mbi	yes	9,60E-06
OPA2	fcgri	CH4	180,9	180,0	0,0	130,2	0,0	perpendi	no	yes	no	1,07E-05	0,21	9,47E-04	0,12		Tom		no	4,43	8,4	G3	WG	yes	1,07E-05
OPA2	fcgri	CH4	209,0	210,0	0,0	170,9	0,0	perpendi	no	yes	no	1,28E-06	0,21	1,71E-04	0,13		Tom		no	4,43	8,4	G3	WG	yes	1,28E-06
OPA2	fcgri	CH4	-0,1	0,0	-11,8	83,5	0,0	perpendi	no	yes	no	2,82E-05	0,21	2,27E-03	0,25		Tom		yes	4,43	8,4	G3	mbi	yes	2,82E-05
OPB1	MPD	He	524,0	500,0	0,0	321,0	0,0	perpendi	no	yes	no	1,00E-09	0,06	7,21E-03	0,08		Konstantin		no	3,27	4,79	MPD		no	1,00E-09
OPB1	MPD	He	641,0	600,0	0,0	513,3	0,0	perpendi	no	yes	no	2,66E-09	0,05	1,08E-01	0,05		Konstantin		no	3,27	4,79	MPD		no	2,66E-09
OPB1	MPD	He	748,0	700,0	0,0	652,0	0,0	perpendi	no	yes	no	2,67E-07	0,10	1,62E-03	0,10		Konstantin		no	3,27	4,79	MPD		no	2,67E-07
OPB1	MPD	He	850,0	800,0	0,0	769,0	0,0	perpendi	no	yes	no	3,00E-08	0,05	2,95E-03	0,10		Konstantin		no	3,27	4,79	MPD		no	3,00E-08
OPB1	MPD	He	524,0	500,0	0,0	321,0	0,0	perpendi	no	yes	yes	1,16E-10	0,08	3,82E-03	0,09	67516	Konstantin		no	3,27	4,79	MPD		no	2,45E-08
OPB1	MPD	He	641,0	600,0	0,0	513,3	0,0	perpendi	no	yes	yes	8,64E-11	0,06	6,51E-03	0,02	5612	Konstantin		no	3,27	4,79	MPD		no	1,03E-09
OPB1	MPD	He	748,0	700,0	0,0	652,0	0,0	perpendi	no	yes	yes	8,52E-11	0,09	3,13E-04	0,10	22977	Konstantin		no	3,27	4,79	MPD		no	3,09E-09
OPB1	MPD	He	850,0	800,0	0,0	769,0	0,0	perpendi	no	yes	yes	3,87E-10	0,10	4,20E-07	0,06	81719	Konstantin		no	3,27	4,79	MPD		no	4,15E-08
OPB1	MPD	He	524,0	500,0	0,0	321,0	0,0	perpendi	no	no	no	2,22E-03	0,01				Konstantin		no	3,27	4,79	MPD		no	2,22E-03
OPB1	MPD	He	641,0	600,0	0,0	513,3	0,0	perpendi	no	no	no	3,18E-03	0,01				Konstantin		no	3,27	4,79	MPD		no	3,18E-03
OPB1	MPD	He	748,0	700,0	0,0	652,0	0,0	perpendi	no	no	no	3,54E-03	0,02				Konstantin		no	3,27	4,79	MPD		no	3,54E-03
OPB1	MPD	He	524,0	500,0	0,0	321,0	0,0	perpendi	no	no	yes	2,60E-05	0,02			27850	Konstantin		no	3,27	4,79	MPD		no	2,28E-03
OPB1	MPD	He	641,0	600,0	0,0	513,3	0,0	perpendi	no	no	yes	1,13E-04	0,02			12655	Konstantin		no	3,27	4,79	MPD		no	2,90E-03
OPB1	MPD	He	748,0	700,0	0,0	652,0	0,0	perpendi	no	no	yes	1,03E-05	0,02			87007	Konstantin		no	3,27	4,79	MPD		no	1,38E-03
OPB2	MPD	He	509,0	500,0	0,0	327,0	0,0	perpendi	no	no	no	3,25E-05	0,02				Konstant	1500	no	3,21	5,77	MPD		no	3,25E-05
OPB2	MPD	He	620,0	600,0	0,0	491,0	0,0	perpendi	no	no	no	2,69E-05	0,03				Konstant	1500	no	3,21	5,77	MPD		no	2,69E-05
OPB2	MPD	He	727,0	700,0	0,0	629,0	0,0	perpendi	no	no	no	4,90E-06	0,04				Konstant	1500	no	3,21	5,77	MPD		no	4,90E-06
OPB2	MPD	He	509,0	500,0	0,0	327,0	0,0	perpendi	no	no	yes	5,70E-08	0,03			450959	Konstant	1500	no	3,21	5,77	MPD		no	7,87E-05
OPB2	MPD	He	620,0	600,0	0,0	491,0	0,0	perpendi	no	no	yes	1,23E-05	0,02			2476	Konstant	1500	no	3,21	5,77	MPD		no	7,42E-05
OPB2	MPD	He	727,0	700,0	0,0	629,0	0,0	perpendi	no	no	yes	5,69E-04	0,06			41520	Konstant	1500	no	3,21	5,77	MPD		no	3,81E-02
OPB2	MPD	He	509,0	500,0	0,0	327,0	0,0	perpendi	no	yes	no	2,20E-07	0,07	3,60E-03	0,09		Konstant	1500	no	3,21	5,77	MPD		no	2,20E-07
OPB2	MPD	He	620,0	600,0	0,0	491,0	0,0	perpendi	no	yes	no	4,89E-07	0,06	3,60E-03	0,09		Konstant	1500	no	3,21	5,77	MPD		no	4,89E-07
OPB2	MPD	He	509,0	500,0	0,0	327,0	0,0	perpendi	no	yes	yes	1,08E-07	0,03	6,36E-05	0,07	14782	Konstant	1500	no	3,21	5,77	MPD		no	4,99E-06
OPB2	MPD	He	620,0	600,0	0,0	491,0	0,0	perpendi	no	yes	yes	5,22E-09	0,04	1,47E-04	0,02	8580	Konstant	1500	no	3,21	5,77	MPD		no	9,64E-08
OPB2	MPD	He	727,0	700,0	0,0	629,0	0,0	perpendi	no	yes	yes	2,26E-08	0,06	4,00E-05	0,01	1450	Konstant	1500	no	3,21	5,77	MPD		no	7,47E-08
OPB2	MPD	He	532,0	500,0	0,0	339,0	0,0	perpendi	no	no	no	1,84E-05	0,02				Konstant	2000	no	3,21	5,77	MPD		no	1,84E-05
OPB2	MPD	He	626,0	600,0	0,0	516,0	0,0	perpendi	no	no	no	1,26E-05	0,04				Konstant	2000	no	3,21	5,77	MPD		no	1,26E-05
OPB2	MPD	He	735,0	700,0	0,0	636,0	0,0	perpendi	no	no	no	1,58E-05	0,02				Konstant	2000	no	3,21	5,77	MPD		no	1,58E-05
OPB2	MPD	He	821,0	800,0	0,0	742,0	0,0	perpendi	no	no	no	1,26E-05	0,06				Konstant	2000	no	3,21	5,77	MPD		no	1,26E-05
OPB2	MPD	He	4,0	0,0	0,3	250,0	0,0	perpendi	no	no	no	1,30E-05	0,02				Konstant	2000	yes	3,21	5,77	MPD		no	1,30E-05
OPB2	MPD	He	3,0	0,0	0,3	93,0	0,0	perpendi	no	no	no	1,09E-05	0,01				Konstant	2000	yes	3,21	5,77	MPD		no	1,09E-05
OPB2	MPD	He	532,0	500,0	0,0	339,0	0,0	perpendi	no	no	yes	8,90E-07	0,02			18709	Konstant	2000	no	3,21	5,77	MPD		no	5,00E-05
OPB2	MPD	He	626,0	600,0	0,0	516,0	0,0	perpendi	no	no	yes	6,56E-07	0,03			21522	Konstant	2000	no	3,21	5,77	MPD		no	2,80E-05
OPB2	MPD	He	735,0	700,0	0,0	636,0	0,0	perpendi	no	no	yes	3,40E-07	0,01			55260	Konstant	2000	no	3,21	5,77	MPD		no	2,99E-05
OPB2	MPD	He	821,0	800,0	0,0	742,0	0,0	perpendi	no	no	yes	8,30E-07	0,03			21741	Konstant	2000	no	3,21	5,77	MPD		no	2,51E-05
OPB2	MPD	He	4,0	0,0	0,3	250,0	0,0	perpendi	no	no	yes	7,50E-07	0,01			18308	Konstant	2000	yes	3,21	5,77	MPD		no	5,57E-05
OPB2	MPD	He	3,0	0,0	0,3	93,0	0,0	perpendi	no	no	yes	8,68E-07	0,01			13569	Konstant	2000	yes	3,21	5,77	MPD		no	1,28E-04
OPB2	MPD	He	532,0	500,0	0,0	339,0	0,0	perpendi	no	yes	no	9,00E-08	0,07	6,12E-04	0,02		Konstant	2000	no	3,21	5,77	MPD		no	9,00E-08
OPB2	MPD	He	626,0	600,0	0,0	516,0	0,0	perpendi	no	yes	no	2,56E-09	0,04	7,39E-04	0,02		Konstant	2000	no	3,21	5,77	MPD		no	2,56E-09
OPB2	MPD	He	735,0	700,0	0,0	636,0	0,0	perpendi	no	yes	no	1,18E-05	0,02	1,14E-04	0,04		Konstant	2000	no	3,21	5,77	MPD		no	1,18E-05
OPB2	MPD	He	821,0	800,0	0,0	742,0	0,0	perpendi	no	yes	no	1,25E-05	0,06	7,32E-05	0,03		Konstant	2000	no	3,21	5,77	MPD		no	1,25E-05
OPB2	MPD	He	4,0	0,0	0,3	250,0	0,0	perpendi	no	yes	no	1,69E-08	0,04	5,00E-04	0,05		Konstant	2000	yes	3,21	5,77	MPD		no	1,69E-08

OPB2	MPD	He	3,0	0,0	0,3	93,0	0,0	perpendi	no	yes	no	2,00E-08	0,03	4,63E-04	0,06		Konstant	2000	yes	3,21	5,77	MPD		no	2,00E-08
OPB2	MPD	He	532,0	500,0	0,0	339,0	0,0	perpendi	no	yes	yes	5,47E-07	0,03	4,98E-04	0,07	650	Konstant	2000	no	3,21	5,77	MPD		no	1,60E-06
OPB2	MPD	He	626,0	600,0	0,0	516,0	0,0	perpendi	no	yes	yes	1,30E-06	0,03	2,20E-06	0,03	14951	Konstant	2000	no	3,21	5,77	MPD		no	3,90E-05
OPB2	MPD	He	735,0	700,0	0,0	636,0	0,0	perpendi	no	yes	yes	9,00E-09	0,03	2,40E-05	0,06	28427	Konstant	2000	no	3,21	5,77	MPD		no	4,11E-07
OPB2	MPD	He	821,0	800,0	0,0	742,0	0,0	perpendi	no	yes	yes	1,64E-09	0,06	4,00E-05	0,04	20859	Konstant	2000	no	3,21	5,77	MPD		no	4,77E-08
OPB2	MPD	He	4,0	0,0	0,3	250,0	0,0	perpendi	no	yes	yes	1,00E-10	0,02	1,22E-04	0,05	4683	Konstant	2000	yes	3,21	5,77	MPD		no	1,97E-09
OPB2	MPD	He	3,0	0,0	0,3	93,0	0,0	perpendi	no	yes	yes	1,27E-09	0,02	1,89E-04	0,04	1897	Konstant	2000	yes	3,21	5,77	MPD		no	2,72E-08
OPB2	MPD	He	516,0	500,0	0,0	346,0	0,0	perpendi	no	no	no	6,70E-06	0,08				Konstant	2500	no	3,21	5,77	MPD		no	6,70E-06
OPB2	MPD	He	619,0	600,0	0,0	513,0	0,0	perpendi	no	no	no	8,54E-06	0,01				Konstant	2500	no	3,21	5,77	MPD		no	8,54E-06
OPB2	MPD	He	715,0	700,0	0,0	623,0	0,0	perpendi	no	no	no	8,00E-06	0,02				Konstant	2500	no	3,21	5,77	MPD		no	8,00E-06
OPB2	MPD	He	516,0	500,0	0,0	346,0	0,0	perpendi	no	yes	no	6,80E-05	0,03	2,49E-04	0,04		Konstant	2500	no	3,21	5,77	MPD		no	6,80E-05
OPB2	MPD	He	516,0	500,0	0,0	346,0	0,0	perpendi	no	no	yes	4,28E-07	0,03			22018	Konstant	2500	no	3,21	5,77	MPD		no	2,77E-05
OPB2	MPD	He	516,0	500,0	0,0	346,0	0,0	perpendi	no	yes	yes	2,80E-08	0,07	4,13E-05	0,07	5403	Konstant	2500	no	3,21	5,77	MPD		no	4,65E-07
Whitehill	fcgri	He	150,1	150,0	0,0	76,2	0,0	perpendi	no	no	no	1,13E-03	0,18				Tom		no	5,56		G2		no	1,13E-03
Whitehill	fcgri	He	180,4	180,0	0,0	129,3	0,0	perpendi	no	no	no	2,10E-03	0,22				Tom		no	5,56		G2		no	2,10E-03
Whitehill	fcgri	He	209,9	210,0	0,0	170,4	0,0	perpendi	no	no	no	3,30E-03	0,22				Tom		no	5,56		G2		no	3,30E-03
Whitehill	fcgri	He	239,9	250,0	0,0	205,8	0,0	perpendi	no	no	no	3,35E-03	0,22				Tom		no	5,56		G2		no	3,35E-03
Whitehill	fcgri	He	-0,4	0,0	-2,4	100,2	0,0	perpendi	no	no	no	4,22E-03	0,26				Tom		yes	5,56		G2		no	4,22E-03
Whitehill	fcgri	He	150,1	150,0	0,0	76,2	0,0	perpendi	no	no	yes	3,53E-03	0,14			34	Tom		no	5,56		G2		no	5,11E-03
Whitehill	fcgri	He	180,4	180,0	0,0	129,3	0,0	perpendi	no	no	yes	3,25E-03	0,16			187	Tom		no	5,56		G2		no	7,95E-03
Whitehill	fcgri	He	209,9	210,0	0,0	170,4	0,0	perpendi	no	no	yes	1,41E-03	0,17			1458	Tom		no	5,56		G2		no	1,35E-02
Whitehill	fcgri	He	239,9	250,0	0,0	205,8	0,0	perpendi	no	no	yes	6,80E-03	0,18			148	Tom		no	5,56		G2		no	1,17E-02
Whitehill	fcgri	He	-0,4	0,0	-2,4	100,2	0,0	perpendi	no	no	yes	7,22E-04	0,20			3810	Tom		yes	5,56		G2		no	2,82E-02
Whitehill	fcgri	He	150,1	150,0	0,0	76,2	0,0	perpendi	no	yes	yes	7,79E-05	0,18	2,06E-04	0,16	9886	Tom		no	5,56		G2		no	1,02E-02
Whitehill	fcgri	He	180,4	180,0	0,0	129,3	0,0	perpendi	no	yes	yes	6,72E-05	0,17	7,85E-05	0,15	10000	Tom		no	5,56		G2		no	5,26E-03
Whitehill	fcgri	He	209,9	210,0	0,0	170,4	0,0	perpendi	no	yes	yes	1,72E-04	0,16	2,39E-03	0,22	9726	Tom		no	5,56		G2		no	1,00E-02
Whitehill	fcgri	He	239,9	250,0	0,0	205,8	0,0	perpendi	no	yes	yes	7,49E-05	0,07	6,41E-04	0,12	5184	Tom		no	5,56		G2		no	1,96E-03
Whitehill	fcgri	He	-0,4	0,0	-2,4	100,2	0,0	perpendi	no	yes	yes	1,65E-05	0,05	2,08E-02	0,17	670	Tom		yes	5,56		G2		no	1,27E-04
Whitehill	fcgri	He	150,1	150,0	0,0	76,2	0,0	perpendi	no	yes	no	5,47E-04	0,12	1,26E-03	0,04		Tom		no	5,56		G2		no	5,47E-04
Whitehill	fcgri	He	180,4	180,0	0,0	129,3	0,0	perpendi	no	yes	no	1,20E-03	0,18	1,98E-02	0,04		Tom		no	5,56		G2		no	1,20E-03
Whitehill	fcgri	He	209,9	210,0	0,0	170,4	0,0	perpendi	no	yes	no	3,12E-03	0,20	3,26E-03	0,17		Tom		no	5,56		G2		no	3,12E-03
Whitehill	fcgri	He	239,9	250,0	0,0	205,8	0,0	perpendi	no	yes	no	2,57E-03	0,21	3,62E-03	0,17		Tom		no	5,56		G2		no	2,57E-03
Whitehill	fcgri	He	-0,4	0,0	-2,4	100,2	0,0	perpendi	no	yes	no	1,16E-06	0,15	1,34E-01	0,15		Tom		yes	5,56		G2		no	1,16E-06
Whitehill	fcgri	CH4	150,1	150,0	0,0	59,8	0,0	perpendi	no	no	no	4,26E-03	0,17				Tom		no	5,56		G3		no	4,26E-03
Whitehill	fcgri	CH4	179,8	180,0	0,0	107,9	0,0	perpendi	no	no	no	3,27E-04	0,10				Tom		no	5,56		G3		no	3,27E-04
Whitehill	fcgri	CH4	210,0	210,0	0,0	149,0	0,0	perpendi	no	no	no	1,45E-04	0,05				Tom		no	5,56		G3		no	1,45E-04
Whitehill	fcgri	CH4	-0,2	0,0	-6,1	90,1	0,0	perpendi	no	no	no	1,86E-03	0,17				Tom		yes	5,56		G3		no	1,86E-03
Whitehill	fcgri	CH4	-0,3	0,0	-3,8	54,3	0,0	perpendi	no	no	no	2,84E-03	0,28				Tom		yes	5,56		G3		no	2,84E-03
Whitehill	fcgri	CH4	150,1	150,0	0,0	59,8	0,0	perpendi	no	no	yes	1,46E-04	0,11			2278	Tom		no	5,56		G3		no	5,70E-03
Whitehill	fcgri	CH4	179,8	180,0	0,0	107,9	0,0	perpendi	no	no	yes	4,14E-05	0,05			1102	Tom		no	5,56		G3		no	4,64E-04
Whitehill	fcgri	CH4	210,0	210,0	0,0	149,0	0,0	perpendi	no	no	yes	7,33E-05	0,04			974	Tom		no	5,56		G3		no	5,52E-04
Whitehill	fcgri	CH4	-0,2	0,0	-6,1	90,1	0,0	perpendi	no	no	yes	1,65E-04	0,10			3109	Tom		yes	5,56		G3		no	5,85E-03
Whitehill	fcgri	CH4	-0,3	0,0	-3,8	54,3	0,0	perpendi	no	no	yes	3,89E-07	0,11			1117	Tom		yes	5,56		G3		no	8,38E-06
Whitehill	fcgri	CH4	150,1	150,0	0,0	59,8	0,0	perpendi	no	yes	yes	7,79E-05	0,18	2,06E-04	0,16	9886	Tom		no	5,56		G3		no	1,30E-02
Whitehill	fcgri	CH4	179,8	180,0	0,0	107,9	0,0	perpendi	no	yes	yes	6,72E-05	0,17	7,85E-05	0,15	10000	Tom		no	5,56		G3		no	6,29E-03
Whitehill	fcgri	CH4	210,0	210,0	0,0	149,0	0,0	perpendi	no	yes	yes	1,72E-04	0,16	2,39E-03	0,22	9726	Tom		no	5,56		G3		no	1,14E-02
Whitehill	fcgri	CH4	-0,2	0,0	-6,1	90,1	0,0	perpendi	no	yes	yes	7,49E-05	0,07	6,41E-04	0,12	5184	Tom		yes	5,56		G3		no	4,39E-03
Whitehill	fcgri	CH4	-0,3	0,0	-3,8	54,3	0,0	perpendi	no	yes	yes	1,65E-05	0,05	2,08E-02	0,17	670	Tom		yes	5,56		G3		no	2,20E-04
Whitehill	fcgri	CH4	150,1	150,0	0,0	59,8	0,0	perpendi	no	yes	no	1,18E-04	0,08	6,61E-04	0,18		Tom		no	5,56		G3		no	1,18E-04
Whitehill	fcgri	CH4	179,8	180,0	0,0	107,9	0,0	perpendi	no	yes	no	6,72E-04	0,05	6,72E-04	0,15		Tom		no	5,56		G3		no	6,72E-04
Whitehill	fcgri	CH4	210,0	210,0	0,0	149,0	0,0	perpendi	no	yes	no	1,85E-04	0,06	2,55E-03	0,13		Tom		no	5,56		G3		no	1,85E-04
Whitehill	fcgri	CH4	-0,2	0,0	-6,1	90,1	0,0	perpendi	no	yes	no	4,32E-04	0,08	1,87E-03	0,14		Tom		yes	5,56		G3		no	4,32E-04
Whitehill	fcgri	CH4	-0,3	0,0	-3,8	54,3	0,0	perpendi	no	yes	no	5,87E-04	0,16	6,08E-02	0,11		Tom		yes	5,56		G3		no	5,87E-04

APPENDIX F: Images of expanded xenon under a CT scan and results

All studied samples have been recorded with a set of axial scans and helical scans. The helical scans only scan two-thirds of the core at one position and then move on. That makes these images less accurate to compare over time than the axial scans who have been shot at exactly the same position every time.

Sample: OPA2

Distance from start core plug	Filled with air – before flooding	Filled with Xenon – after flooding
0.95 cm	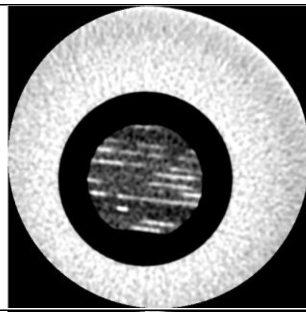	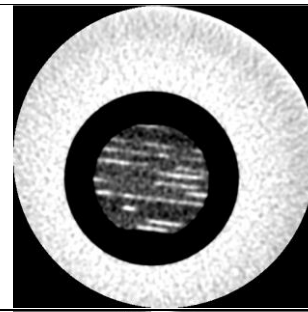
3.3 cm	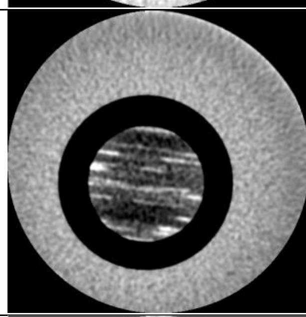	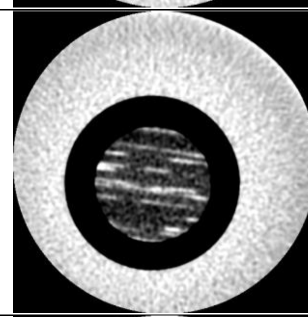
5.3 cm	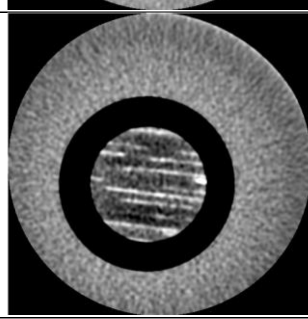	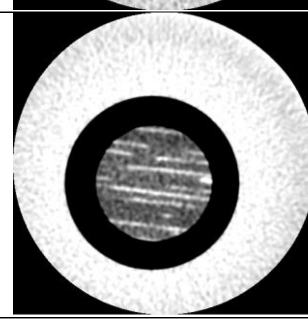
Response	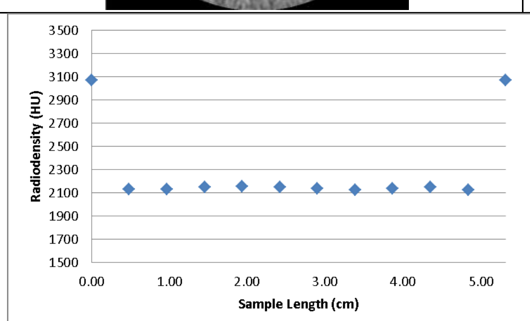	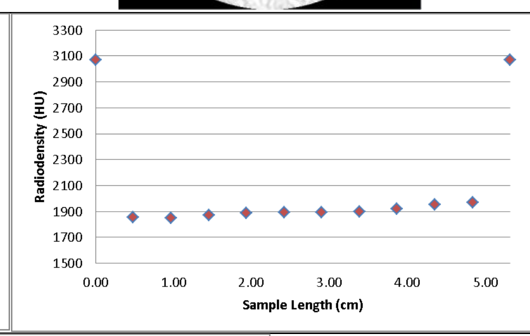
Difference	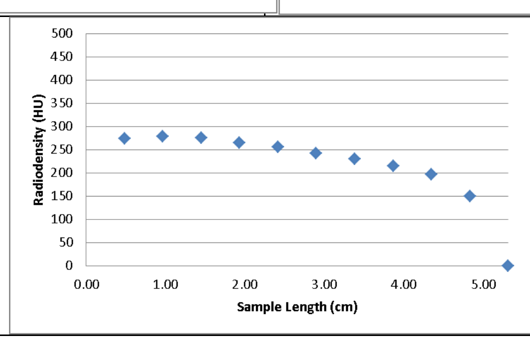	

Sample: Whitehill

<table>
<tr><td>Distance from start core plug</td><td>Filled with air – before flooding</td><td>Filled with Xenon – after flooding</td></tr>
<tr><td>0.3 cm</td><td>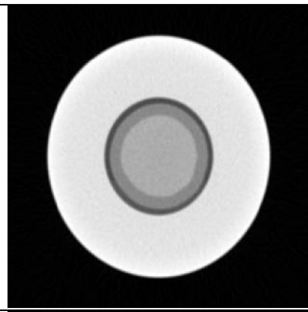</td><td>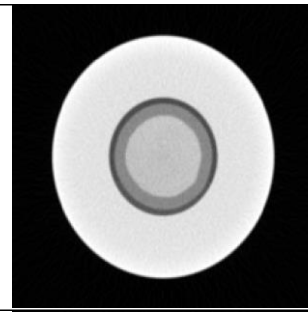</td></tr>
<tr><td>1.5 cm</td><td>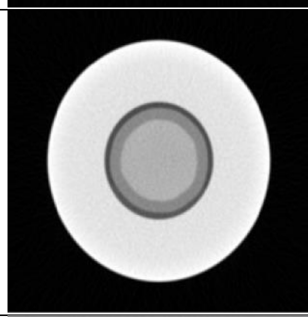</td><td>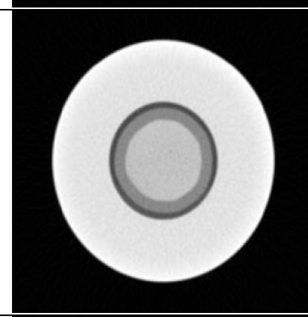</td></tr>
<tr><td>2.7 cm</td><td>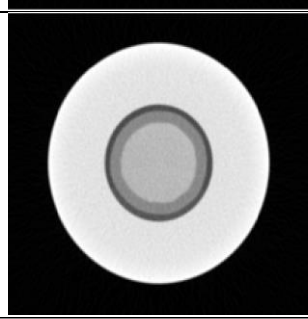</td><td>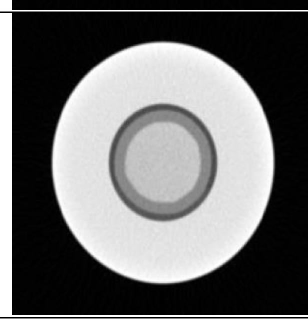</td></tr>
<tr><td>Response</td><td>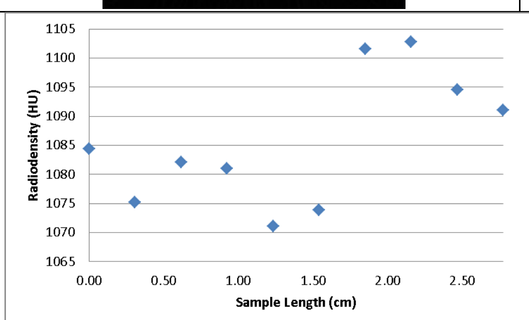
</td><td>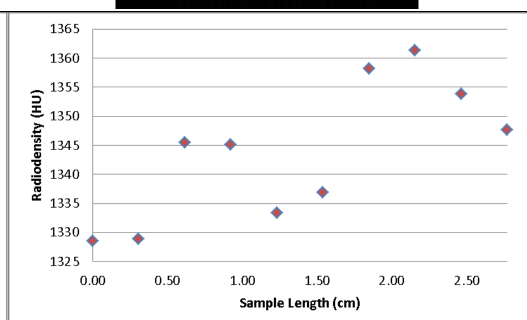
</td></tr>
<tr><td>Difference</td><td colspan="2">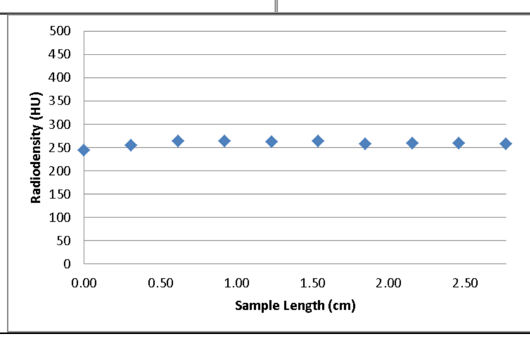
</td></tr>
</table>

Sample: EBN5

Distance from start core plug	Filled with air – before flooding	Filled with Xenon – after flooding
0.5 cm	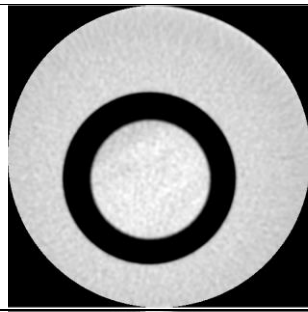	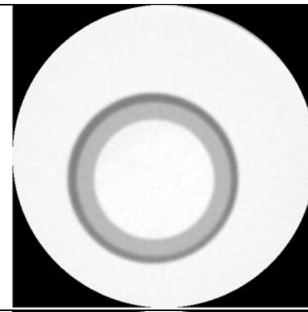
2.5 cm	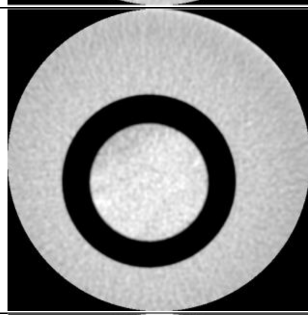	
4.5 cm		
Response	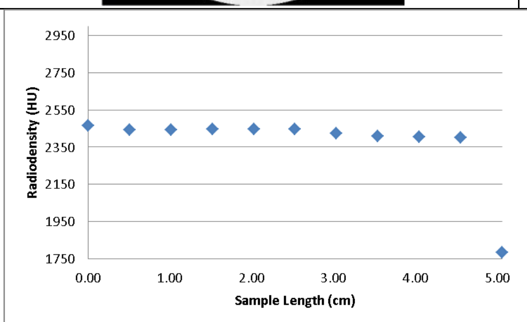	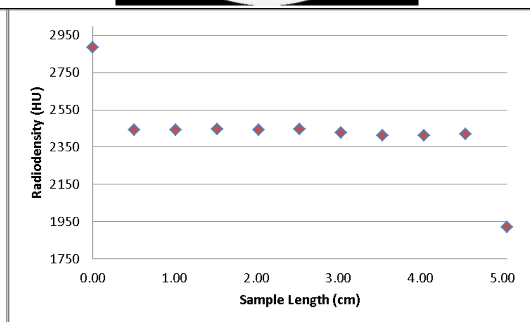
Difference	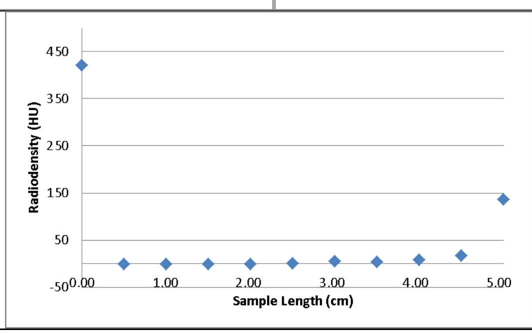	

Sample: EBN20 linear

Distance from start core plug	Filled with air – before flooding	Filled with Xenon – after flooding
0.5 cm	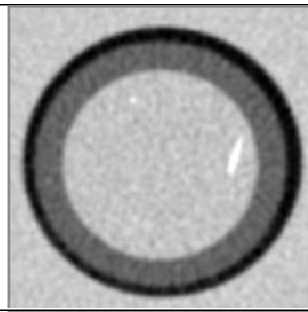	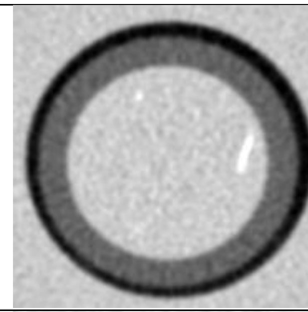
4.2 cm	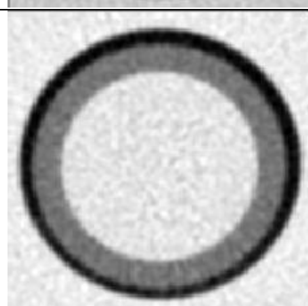	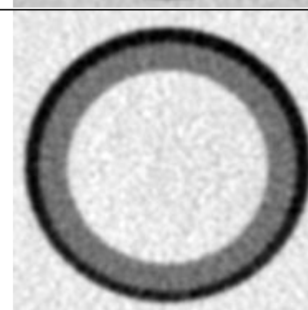
7.2 cm	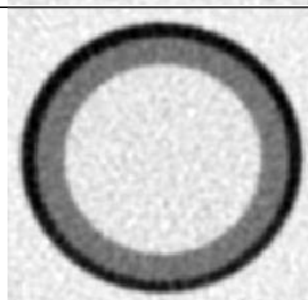	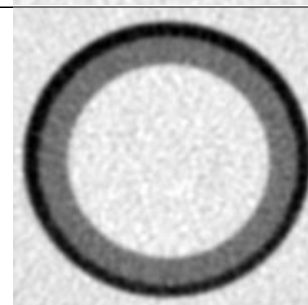
Response	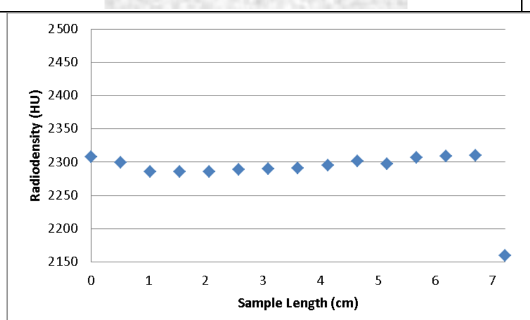	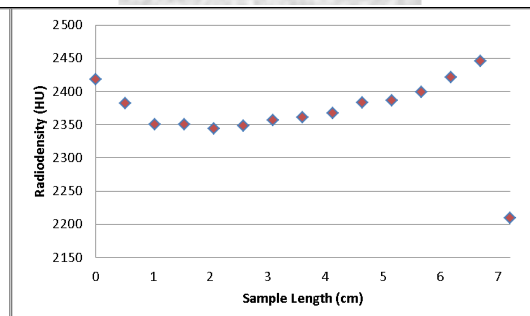
Difference	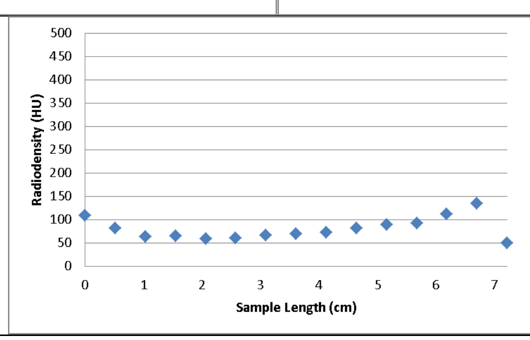	

Sample: EBN20 radial

Distance from start core plug	Filled with air – before flooding	Filled with Xenon – after flooding
0.5 cm	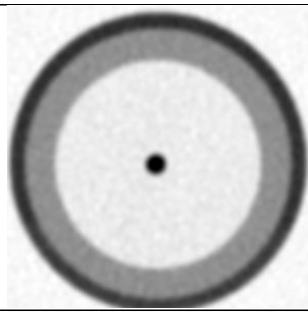	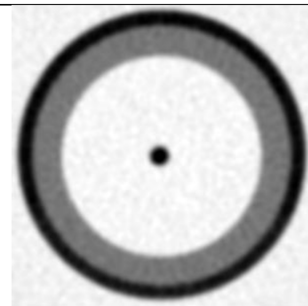
1.5 cm	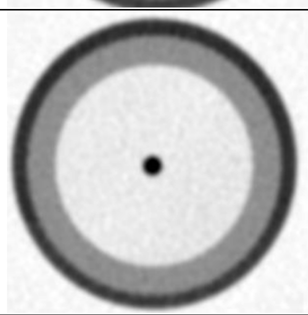	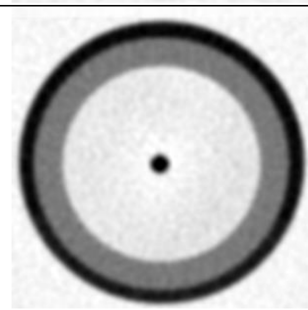
2.9 cm	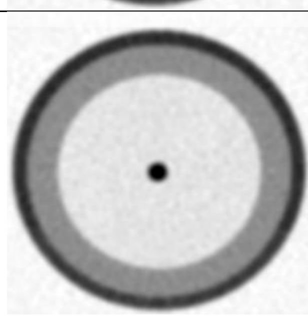	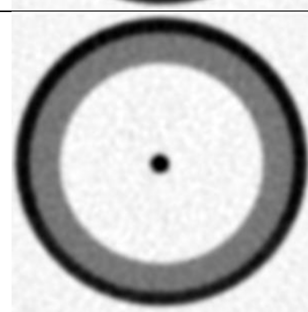
Response	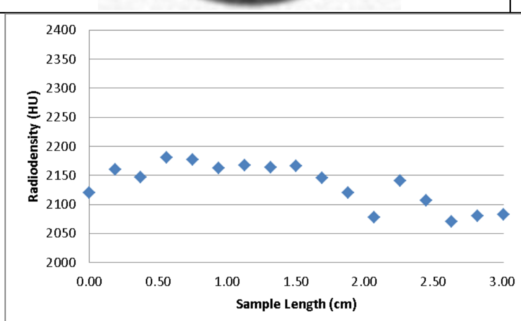	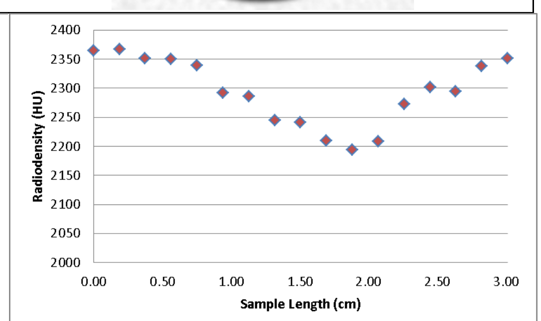
Difference	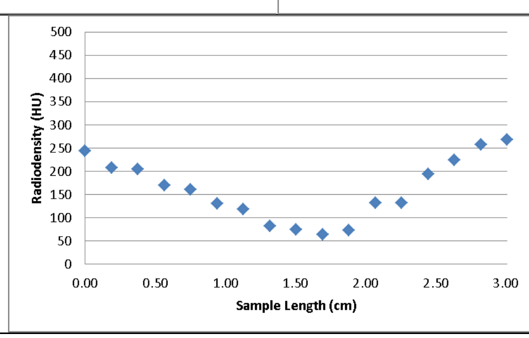	

APPENDIX G: Langmuir Sorption Curves

The figures of the Langmuir adsorption and desorption curves per sample can be found in the following table of figures. In the last column the possible hysteresis can be monitored.

<table>
<tr><th>Sample</th><th>Adsorption and Absorption curve</th><th>Desorption curve</th><th>Combination</th></tr>
<tr><td>OPA1</td><td>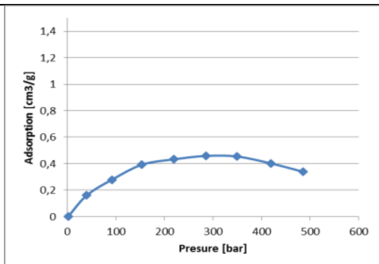</td><td>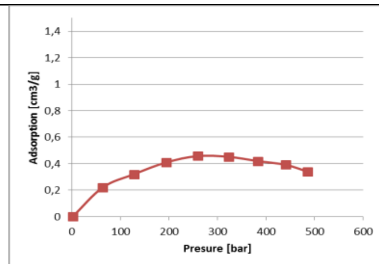</td><td>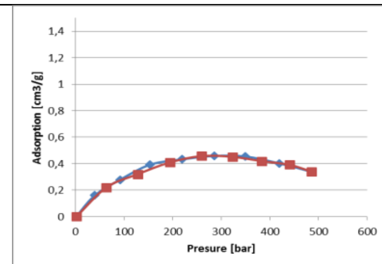</td></tr>
<tr><td>OPA2</td><td>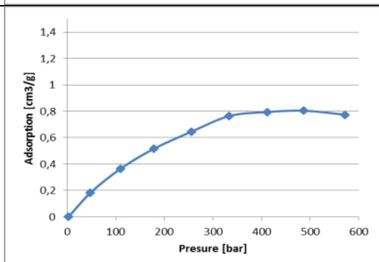</td><td>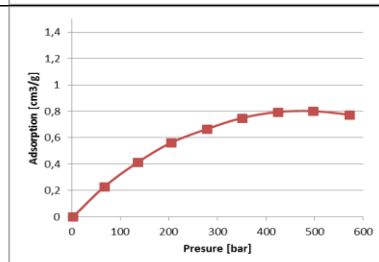</td><td>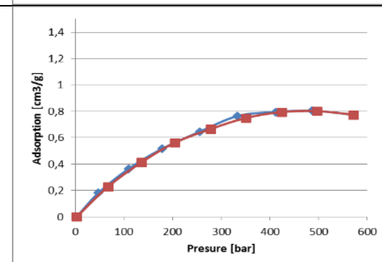</td></tr>
<tr><td>EBN20</td><td>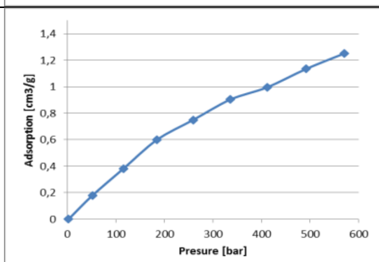</td><td>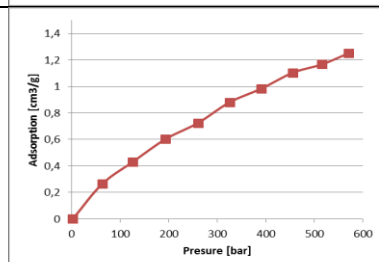</td><td>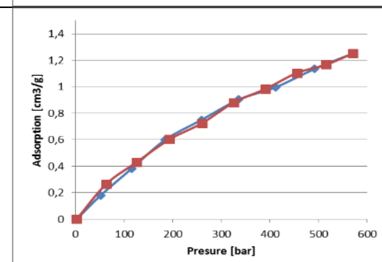</td></tr>
<tr><td>OPB1</td><td>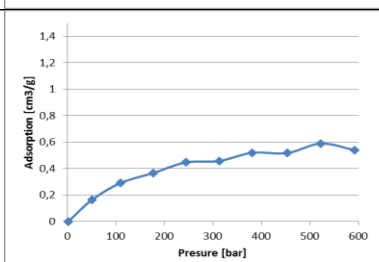</td><td>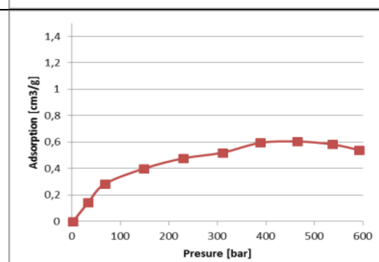</td><td>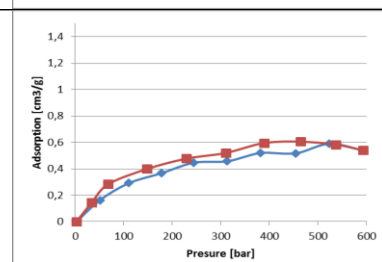</td></tr>
<tr><td>OPB2</td><td>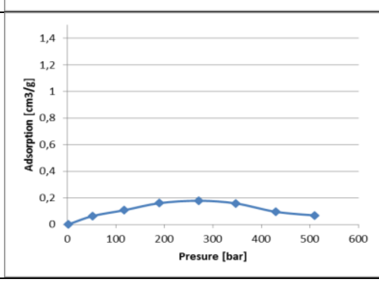</td><td>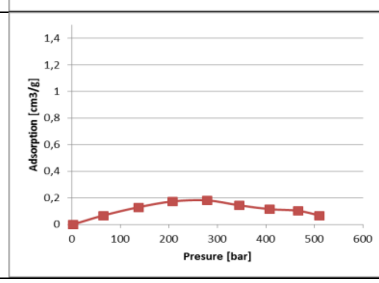</td><td>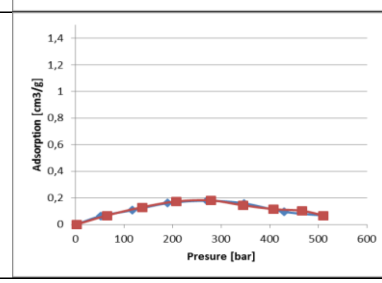</td></tr>
</table>

OPB3	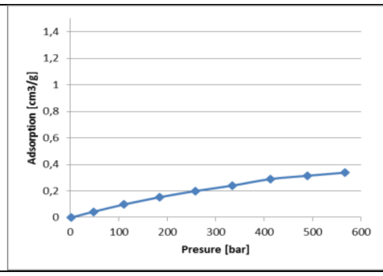Adsorption [cm3/g] Presure [bar] 0 0,2 0,4 0,6 0,8 1 1,2 1,4 0 100 200 300 400 500 600	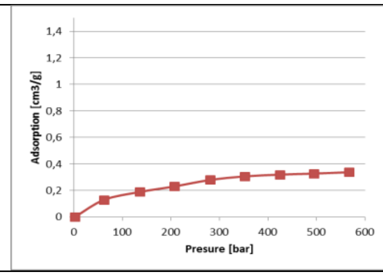Adsorption [cm3/g] Presure [bar] 0 0,2 0,4 0,6 0,8 1 1,2 1,4 0 100 200 300 400 500 600	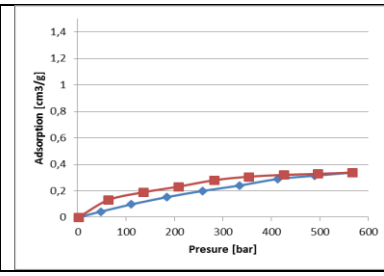Adsorption [cm3/g] Presure [bar] 0 0,2 0,4 0,6 0,8 1 1,2 1,4 0 100 200 300 400 500 600